CHALMERS
UNIVERSITY OF TECHNOLOGY

SCIENTIFIC REPORT

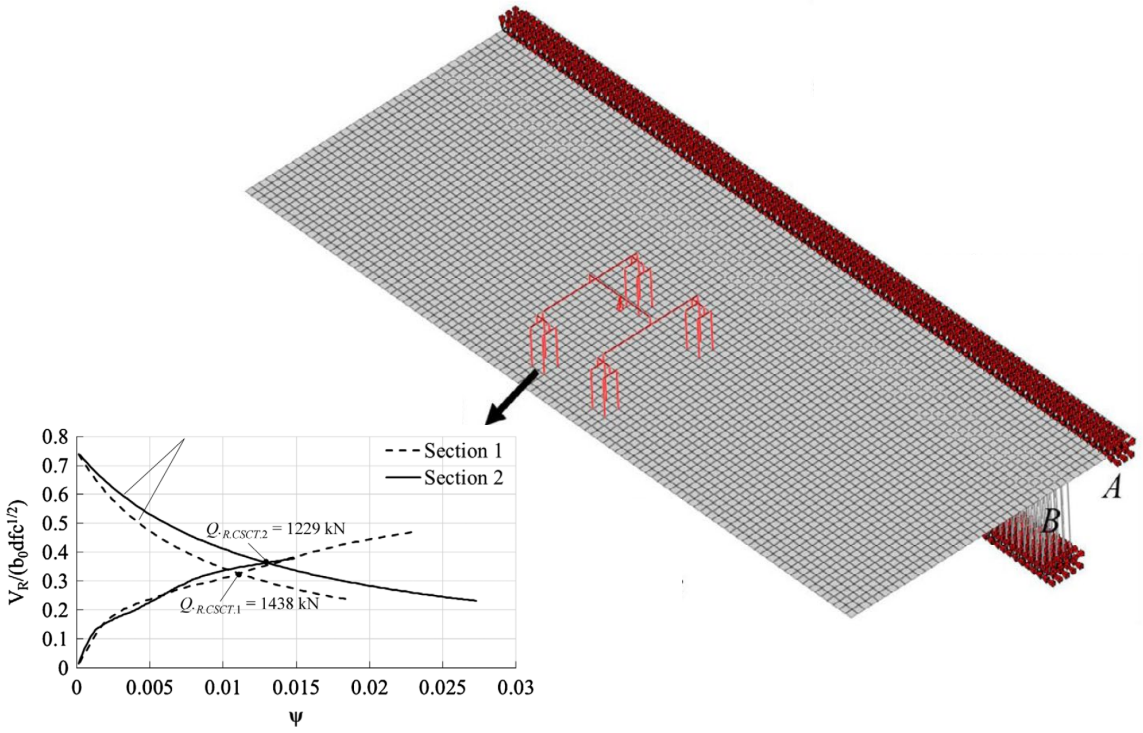

Recommendations for Assessment of Reinforced Concrete Slabs

Enhanced structural analysis with the finite element method

Mario Plos, Morgan Johansson, Kamyab Zandi, Jiangpeng Shu

DEPARTMENT OF ARCHITECTURE AND CIVIL ENGINEERING
Division of Structural Engineering
Concrete Structures

CHALMERS UNIVERSITY OF TECHNOLOGY
Report ACE 2021:3
Gothenburg, Sweden 2021
www.chalmers.se

REPORT ACE 2021:3

Recommendations for Assessment of Reinforced Concrete Slabs

Enhanced structural analysis with the finite element method

MARIO PLOS
MORGAN JOHANSSON
KAMYAB ZANDI
SHU JIANGPENG

Department of Architecture and Civil Engineering
Division of Structural Engineering
Concrete Structures
CHALMERS UNIVERSITY OF TECHNOLOGY
Göteborg, Sweden 2021

Recommendations for Assessment of Reinforced Concrete Slabs
Enhanced structural analysis with the finite element method

MARIO PLOS

MORGAN JOHANSSON

KAMYAB ZANDI

SHU JIANGPENG

© MARIO PLOS, MORGAN JOHANSSON, KAMYAB ZANDI, SHU JIANGPENG, 2021

Report ACE 2021:3
Institutionen för arkitektur och samhällsbyggnadsteknik
Chalmers tekniska högskola, 2021

Department of Architecture and Civil Engineering
Division of Structural Engineering
Concrete Structures
Chalmers University of Technology
SE-412 96 Göteborg
Sweden
Telephone: + 46 (0)31-772 1000

Cover:
Example of Structural assessment of a bridge cantilever slab using non-linear shell finite element analysis and higher level-of-approximation punching resistance model.
Department of Architecture and Civil Engineering
Göteborg, Sweden, 2021

Recommendations for Assessment of Reinforced Concrete Slabs

Enhanced structural analysis with the finite element method

MARIO PLOS, MORGAN JOHANSSON, KAMYAB ZANDI, SHU JIANGPENG

Department of Architecture and Civil Engineering
Division of Structural Engineering, Concrete Structures
Chalmers University of Technology

ABSTRACT

Reinforced concrete structures show a pronounced non-linear response, with cracking of concrete for service loads and reinforcement yielding and concrete crushing at ultimate load. With non-linear finite element (FE) analysis, the structural response can be captured, and such analyses have shown great potential to reveal higher load carrying capacity compared to simplified and linear analysis methods. A multi-level structural assessment strategy, developed in previous research, provides a framework for more advanced, successively improved analysis of reinforced concrete slabs.

This report provides recommendations for practicing structural engineers on structural assessment using FE analysis. The focus is on enhanced assessment with non-linear FE analysis, and the scope is reinforced concrete slabs with limited membrane effects. The intention is to facilitate the use of non-linear analysis in engineering practice by providing detailed recommendations on how such analyses can be made to provide increased understanding of the structural behaviour and reliable estimations of the load-carrying capacity of concrete slabs. However, the framework presented is general, and the approach can in many aspects also be used for other types of reinforced concrete structures. The recommendations given here are based on previous research performed by the authors, information from literature and engineering judgement based on practical experience. They are intended to give conservative estimates of the load-carrying capacity, fulfilling the required safety level.

The report includes a thorough description of the assessment strategy. The global safety format recommended for non-linear analysis is presented and its application for different assessment levels is described. Furthermore, recommendations on how to take deterioration into account are given. Non-linear FE analysis of concrete structures is presented together with general advices for its application. Furthermore, general recommendations are presented for simplified and linear analysis, corresponding to today's practice.

For assessment with non-linear FE analysis, detailed recommendations for use in engineering practice are presented. Advices are given on idealization of the structure, choice of material models, determination of material parameters, modelling and analysis. Furthermore, the evaluation of structural response, determination of load carrying capacity and response under service conditions are described. For non-linear analysis with shell elements, resistance models on higher *Level-of-Approximation* according to Model Code 2010 are used. Finally, examples are showing the application of the strategy on two slabs tested in laboratory and one bridge deck slab.

Key words: Structural assessment, Reinforced concrete slab, Non-linear finite element analysis, Load carrying capacity, Global safety format, Deterioration, Frost, Corrosion.

Rekommendationer för utvärdering av armerade betongplattor

Förbättrade strukturanalyser med finit elementmetod

MARIO PLOS, MORGAN JOHANSSON, KAMYAB ZANDI, SHU JIANGPENG

Institutionen för arkitektur och samhällsbyggnadsteknik
Avdelningen för Konstruktionsteknik, Betongbyggnad
Chalmers tekniska högskola

SAMMANFATTNING

Armerade betongkonstruktioner uppvisar ett olinjärt beteende vid belastning, med uppsprickning av betong för brukslaster och plasticering av armering och krossning av betong för brottlaster. Med icke-linjär finit elementanalys (FE-analys) kan konstruktionens respons beskrivas på ett korrekt sätt och därigenom ge bättre förståelse för verkningssättet. Sådana analyser har också visat stor potential för att påvisa högre bärförmåga jämfört med traditionella förenklade och linjära analysmetoder. En strategi för bärighetsberäkningar, som utvecklats inom tidigare forskning, erbjuder en strukturerad metodik för hur mer avancerade och successivt noggrannare analysmetoder kan användas för att utvärdera armerade betongplattor.

I denna rapport ges rekommendationer för praktisk bärighetsutvärdering med FE-analys. Fokus är på förbättrad strukturanalys med icke-linjär FE-analys, och tillämpningen är armerade betongplattor med begränsad membranverkan. Avsikten är att underlätta användningen av icke-linjär FE-analys i praktiskt ingenjörsarbete genom detaljerade rekommendationer för hur sådana analyser kan utföras. Även om tillämpningen är armerade betongplattor är den presenterade metodiken generell, och kan i flera avseenden därför även användas för andra typer av konstruktioner. Rekommendationerna som ges i denna rapport baseras på författarnas tidigare forskning, på information i litteraturen och på ingenjörsmässiga bedömningar baserade på praktisk erfarenhet. Avsikten är att ge konservativa uppskattningar av bärförmågan, vilka uppfyller aktuell säkerhetsnivå.

Rapporten innehåller en noggrann beskrivning av strategin för bärighetsberäkningar. Det globala säkerhetsformat som rekommenderas för icke-linjära beräkningar presenteras, och rekommendationer ges för hur det kan tillämpas på olika nivåer i strategin. Rekommendationer ges även för hur effekten av nedbrytning kan beaktas i analyserna. Icke-linjär FE-analys av betongkonstruktioner behandlas i ett eget kapitel och generella råd ges för tillämpningen. Vidare ges generella rekommendationer för utvärdering med förenklade beräkningar och linjära analyser enligt dagens praxis.

För utvärdering med icke-linjär FE-analys ges detaljerade rekommendationer för praktisk tillämpning. Råd ges för val av strukturmodell och materialmodeller, bestämning av materialparametrar, modellering och genomförande av analys. Vidare beskrivs utvärdering av konstruktionens respons baserat på analysresultaten, bestämning av bärförmåga och kontroll av respons i bruksgränstillstånd. För icke-linjär analys med skalelement används modeller på högre appoximationsnivå från Model Code 2010 för bestämning av lokal bärförmåga. Slutligen visas tillämpningen av strategin på exempel bestående av två plattor provade i laboratorium och en brobaneplatta.

Nyckelord: Bärighet, utvärdering, bärförmåga, armerad betong, platta, icke-linjär finit element analys, Globalt säkerhetsformat, nedbrytning, frost, korrosion.

Contents

Preface

This report was written within a project at the division of Structural Engineering at Chalmers. The project was financed by the Swedish Transport Administration (Trafikverket), Chalmers University of Technology, Norconsult and the home organisations and companies of the reference group. This support is gratefully acknowledged.

The purpose was to provide practical recommendations for structural engineers on the use of non-linear finite element analyses of concrete structures. Detailed recommendations are given for assessment of reinforced concrete slabs, but the framework and much of the content is general and applicable also for other types of concrete structures. The authors hope that this work will contribute to more resource efficient and sustainable bridge management, and lead to economical savings and lower carbon footprint.

The authors want to express their gratitude to the members of the reference group, who have contributed with valuable input to the report:

- Ebbe Rosell (Bridge Specialist, Swedish Transport Administration),
- Mikael Hallgren, (Adj. Professor, Royal Institute of Technology / Tyréns),
- Costin Pacoste (Adj. Professor, Royal Institute of Technology / ELU Konsult)
- Thomas Darholm (Tech. Dir., COWI)
- Max Hendriks (Professor, Norwegian University of Science and Technology / TU Delft)
- Karin Lundgren (Professor, Chalmers University of Technoogy)

The work with the report was performed mainly during a period from spring 2018 to summer 2020 by a working group consisting of:

- Mario Plos, Professor, Chalmers
- Morgan Johansson, Adjunct Professor, Chalmers / Norconsult
- Kamyab Zandi, Associate Professor, Chalmers
- Jiangpeng Shu, Ph.D., Chalmers / Zhejiang University

Acknowledgements: This report is derived in part from an article published in *Structure and Infrastructure Engineering*, see Plos *et al.* (2017), published online 12 April 2016, copyright Taylor & Francis, available online: http://www.tandfonline.com/doi/full/10.1080/15732479.2016.1162177. In particular, Sections 2.2, 2.3, 7.1 and 7.2 are based on this article.

In addition, Section 7.3 is largely derived from an article published in *Engineering Structures*, see Shu *et al.* (2019), published December 2019, available online: https://doi.org/10.1016/j.engstruct.2019.109666.

The computations made for the examples were enabled by resources provided by the Swedish National Infrastructure for Computing (SNIC) at Chalmers Centre for Computational Science and Engineering (C3SE).

Notations

Roman upper case letters

$A_{element}$	Area of a (2D) finite element
A_s	Reinforcement cross-section area
$A_{s,eff}$	Effective reinforcement cross-section area
$A_{s,mod}$	Modelled (effective) reinforcement cross-section area
$C_{Rd,c}$	Factor (in calculation of shear resistance)
E_c	Young's modulus for concrete
E_{ck}	Young's modulus for concrete, characteristic value
E_{cm}	Young's modulus for concrete, mean value
E_s	Young's modulus for steel reinforcement
E_{sh}	Strain hardening modulus for steel reinforcement
E_{sk}	Young's modulus for steel reinforcement, characteristic value
E_{sm}	Young's modulus for steel reinforcement, mean value
F	Force
F_d	Force or action, design value
F_{sE}	Reinforcement force, action effect
F_{sR}	Reinforcement force resistance
G_{Ck}	Fracture energy for concrete in compression, characteristic value
G_{Cm}	Fracture energy for concrete in compression, mean value
$G_{c,uncracked}$	Shear modulus of uncracked concrete
$G_{c,cracked}$	Shear modulus of cracked concrete
G_F	Fracture energy for concrete in tension
G_{Fk}	Fracture energy for concrete in tension, characteristic value
G_{Fm}	Fracture energy for concrete in tension, mean value
L	Length
L_c	Characteristic span length
M	Bending moment
M_E	Bending moment, action effect
M_R	Bending moment resistance
N	Normal force
N_{cr}	Normal force at cracking
N_E	Normal force, action effect
N_y	Normal force at (reinforcement) yielding
P	Point load
$P_{u,\exp}$	Ultimate point load from experiment
Q_E	Global structural action effect
Q_R	Global structural resistance

Q_u	Load carrying capacity
$Q_{u,\exp}$	Ultimate total failure load from experiment
R	Structural resistance
R_d	Structural resistance, design value
R_k	Structural resistance, characteristic value
R_{kc}	Structural resistance, determined with characteristic concrete compression strength (mean values for other parameters)
R_{kct}	Structural resistance, determined with characteristic concrete tension strength (mean values for other parameters)
R_{ks}	Structural resistance, determined with characteristic steel reinforcement strength (mean values for other parameters)
V_E	Shear force, action effect
V_R	Shear force resistance, Coefficient of variation for resistance
$V_{Rd,c}$	Shear resistance attributed to concrete, design value
$V_{Rk,c}$	Shear resistance attributed to concrete, characteristic value
$V_{Rm,c}$	Shear resistance attributed to concrete, mean value
V_f	Coefficient of variation for material uncertainty
V_{fc}	Coefficient of variation for concrete material parameters
V_{fs}	Coefficient of variation for steel reinforcement material parameters
V_g	Coefficient of variation for geometrical uncertainty
V_θ	Coefficient of variation for modelling uncertainty

Roman lower case letters

a	Support width
a_{nom}	geometrical parameter, nominal value
a_v	shear span length
b	width of a concentrated load, parallel to support
b_0	length of shear resisting control section for punching
b_w	width of control section for (one-way) shear
c	width of a concentrated load, perpendicular to support
c_1, c_2	Parameters
c_{clear}	Clear distance between ribs on reinforcement bar
d	Effective height of cross-section
d_g	Aggregate size
$f_{0.2}$	0.2% proof stress of steel reinforcement
f_c	Concrete compression strength
f_{ck}	Concrete compression strength, characteristic value
$f_{ck,cube}$	Cube compression strength of concrete, characteristic value

f_{cm}	Concrete compression strength, mean value
f_{ctk}	Concrete tensile strength, characteristic value
$f_{ctk,\min}$	Concrete tensile strength, lower bound characteristic value
$f_{ctk,\max}$	Concrete tensile strength, upper bound characteristic value
f_{ctm}	Concrete tensile strength, mean value
f_k	Material strength, material parameter, characteristic value
f_m	Material strength or material parameter, mean value
f_{sk}	Steel reinforcement strength, characteristic value
f_{sm}	Steel reinforcement strength, mean value
f_t	Tensile strength
f_{tk}	Ultimate strength of steel reinforcement, characteristic value
f_{tm}	Ultimate strength of steel reinforcement, mean value
f_u	Ultimate strength
f_y	Yield strength of steel reinforcement
f_{yk}	Yield strength of steel reinforcement, characteristic value
f_{ym}	Yield strength of steel reinforcement, mean value
h	Height of cross-section
h_{cyl}	Height of compression test cylinder
k	Coefficient, factor
k_{dg}	Factor to take aggregate size into account
k_v	Factor for the mid-depth strain dependency (in one-way shear resistance)
k_ψ	Factor for the slab rotation dependency (in punching shear resistance)
l_b	Anchorage length
l_{cr}	Crack band width
$l_{element}$	Element length (perpendicular to crack)
m_E	Distributed moment, action effect (moment per unit width)
m_R	Distributed moment resistance (moment per unit width)
m_{rx}, m_{ry}	Reinforcement slab moment in x and y directions, respectively
$m_{rx,av}$	Average reinforcement slab moment in x direction
m_x, m_y	Bending slab moment in x and y directions, respectively
m_{xy}	Torsional slab moment
n	Distributed normal force, Factor
n_E	Distributed normal force, action effect (force per unit width)
q	Distributed load
s	Slip, Reinforcement bar distance
s_1, s_2, s_3	Slip limits for the bond-slip relation
s_{rm}	Mean crack spacing
t	Thickness of surface layer

u	Displacement
v_E	Distributed shear force, action effect (force per unit width)
v_R	Distributed shear force resistance (force per unit width)
w	Crack opening width, Redistribution width
w_u	Ultimate crack opening
x_u	Compression zone height
y_{cs}	Distance from the centre of a concentrated load to the critical cross-section
z	Inner level arm of cross-section

Greek letters

α	Angle, Constant, Factor
α_R	Sensitivity factor of the resistance
β	Reliability index, Shear retention factor, Factor
Δ	Increment of
δ	Displacement
ε	Strain
ε_c	Concrete strain
ε_{c1}	Concrete strain at maximum compressive stress
ε_{cu1}	Ultimate concrete compressive strain
ε_h	Strain at (start of) hardening of steel reinforcement
ε_{hk}	Strain at hardening of steel reinforcement, characteristic value
ε_{hm}	Strain at hardening of steel reinforcement, mean value
ε_s	Strain in steel reinforcement
ε_u	Strain at ultimate strength of steel reinforcement
$\varepsilon_{u,cr}$	Ultimate crack strain
ε_{uk}	Strain at ultimate strength of steel reinforcement, characteristic value
ε_{um}	Strain at ultimate strength of steel reinforcement, mean value
ε_x	Longitudinal mid-depth strain (in a slab)
ε_y	Yield strain for steel reinforcement
ϕ	Diameter of reinforcement bar
ϕ_{ef}	Effective bar diameter for a bundle of bar
γ_R^*	Global resistance safety factor
γ_{Rd}	Model uncertainty factor
η	Relative concrete compressive strain
μ	Factor
ν	Poisson's ratio
$\nu_{cracked}$	Poisson's ratio, cracked concrete

$\nu_{uncracked}$	Poisson's ratio, uncracked concrete
ν_s	Poisson's ratio, steel reinforcement
ρ	Reinforcement ratio
ρ_{PC}	Density, plain concrete
ρ_{RC}	Density, reinforced concrete
ρ_s	Density, steel reinforcement
ϑ	inclination, angle
θ_m	Model bias
σ	Stress
$\sigma_1, \sigma_2, \sigma_3$	Principal stresses
σ_c	Concrete stress
σ_s	Stress in steel reinforcement
τ_b	Bond stress
τ_{bf}, τ_f	Residual bond stress
$\tau_{b,\max}$	Maximum bond stress
$\tau_{b,split}$	Bond stress at concrete cover splitting
ψ	Slab rotation

Abbreviations

1D	One-dimensional
2D	Two-dimensional
3D	Three-dimensional
COV	Coefficient of variation
ECOV	Estimate of coefficient of variation (see ECOV method, Section 2.4.4)
FE	Finite element
FEM	Finite element method
LoA	Level of approximation (as used in Model Code 2010, fib 2013)
PSF	Partial safety factor (see PSF method, Section 2.4.1)
SLS	Serviceability limit state
ULS	Ultimate limit state

1 Introduction

It is of outermost importance that the huge investments made in the built environment are well managed and that existing structures can be used during their entire lifetime with respect to function and safety. When assessing existing structures, many of these shows insufficient load-carrying capacity and there are often doubts regarding the structural behaviour. However, tests on real structures as well as experience with advanced assessment methods shows that existing structures often have higher intrinsic capacity and a more complex response than shown with ordinary assessment methods.

For design and assessment of reinforced concrete structures, simplified analysis methods and code provisions are generally used. For structural analysis, the linear finite element method (FEM) is common. However, in assessment of existing structures, a greater effort with more advanced methods for structural analysis is often motivated. Research as well as experience from engineering practice has shown that non-linear FE analysis possess great possibilities of achieving better understanding of the structural response and of revealing higher load-carrying capacity. For assessment of reinforced concrete slabs, a strategy for successively improved structural analysis with non-linear FE analysis has been developed, Plos *et al.* (2017). For analysis on different levels of detailing, structural analysis methods have been developed and proven feasible for assessment of existing concrete slabs, see Shu *et al.* (2015, 2016, 2017, 2018).

This report presents recommendations for assessment of the structural response and load-carrying capacity of reinforced concrete slabs, using non-linear FE analysis. The recommendations are based on the principle of successively improved assessment. The assessment starts with simplified analysis methods and limited information of the structure and is successively improved using more advanced structural analysis methods, improved knowledge of the structure and safety formats suitable for non-linear analysis. *The Multi-Level Assessment Strategy* according to Plos *et al.* (2017) is followed, combining successively improved structural analysis with resistance models on a higher *Level-of-Approximation* according to Model Code 2010, fib (2013). Recommendations are given for the non-linear FE analysis and assessment procedure for different assessment levels. For higher levels, the load-carrying capacity is evaluated directly from the non-linear FE analysis for failure modes reflected in the analysis, without a separate resistance model. For non-linear analysis, a global resistance method is used to achieve the required safety level.

The present recommendations apply to slab and shell structures primarily subjected to out-of-plane moment and shear actions, with limited membrane effects, i.e. slab and shell structures subjected to loading in a direction normal to the plane of the structure. For higher assessment levels with non-linear FE analysis, the membrane action is reflected in the analysis and contributes to the response and load-carrying capacity, but the recommendations are not developed or verified for structures with dominant membrane forces, like e.g. high beams and domes.

The structural engineer applying these recommendations for higher assessment levels is expected to have experience from structural assessment. Knowledge in the finite element method is expected, including experience from non-linear analysis of concrete structures. Furthermore, it is expected to be familiar with the analysis models

in Eurocode 2, CEN (2004a), and Model Code 2010, fib (2013), and to have access to these documents.

Even though the authors have tried to cover the subject, there will be assessment situations not explicitly covered by the present recommendations due to the great diversity of assessment problems and the way existing structures were designed. In such situations, the structural engineers performing the assessment need to interpret and adopt these recommendations based on engineering judgement and use of additional information found in relevant literature.

These recommendations were primarily developed with typical bridge applications in mind. Nevertheless, the intention of the authors was that the recommendations should be applicable also for other types of reinforced concrete slabs.

Chapter 2 includes a thorough description of the strategy for enhanced structural assessment, based on the principle of successively improved assessment and *the Multi-Level Assessment Strategy,* Plos *et al.* (2017). Different safety formats are described, and the global safety factor methods recommended for non-linear FE analysis are presented. Advices are given on the estimation of model uncertainty and the modelling of the action (or load) history in non-linear analysis. Finally, recommendations on how to take deterioration into account are given.

Chapter 3 is treating non-linear FE analysis of concrete structures. Advices for how to make such analyses are presented, and different analysis approaches, modelling of concrete, reinforcement and their interaction, and recommendations on FE modelling and quality control are given.

Chapter 4 presents general recommendations for simplified analysis methods and 3D linear shell FE analysis corresponding to today's practice.

Chapter 5 presents detailed recommendations for 3D non-linear shell FE analysis. Advices are given on idealization of the structure, choice of material models, determination of material parameters, FE modelling and FE analysis. The evaluation of structural response and determination of load-carrying capacity and response under service conditions is described. The capacity with respect to bending moments can be evaluated directly from the results of the non-linear analysis, but for shear related failures (including punching), the analysis results are combined with resistance models on higher *Level-of-Approximation* according to Model Code 2010, fib (2013). The ECOV method is used to determine the global safety factor.

Chapter 6 presents detailed recommendations for 3D non-linear FE analysis with continuum (solid) elements. As in chapter 5 advices are given on: idealization of the structure; choice of material models; determination of material parameters; FE modelling; FE analysis; evaluation of structural response; determination of load-carrying capacity and response under service conditions. Here, both moment and shear related failures and, if the reinforcement bond is included, also anchorage failures can be evaluated directly from the analysis results. Here, the safety format according to Schlune *et al.* (2012) is recommended.

In **Chapter 7**, the assessment strategy and the analysis methods described are applied in three examples. The first two examples are on slabs tested in laboratory. They show the applicability of the assessment strategy, but also that it results in conservative estimates of the load-carrying capacity. The third example show the application to a real bridge example with hypothetic (future) deterioration. This example shows how the assessment strategy can be applied to a real deteriorated structure and includes

evaluation of design values for the load-carrying capacity using the global safety formats.

In the **Appendices**, recommendations are given for: determination of material properties for non-linear analysis of reinforced concrete; properties of frost-damaged concrete; bond of reinforcement in frost-damaged concrete; properties of concrete with corrosion cracking; and modelling of bond for corroded reinforcement.

2 Basis for enhanced structural assessment

Structural assessment refers to the evaluation and judgement of a structures' safety, capacity, function and condition. It involves gathering of information about the structure and its conditions of operation, analysis of the consequences in terms of structural response and load-carrying capacity, evaluation of its safety and judgement of which measures that need to be taken to ensure that it fulfils the requirements.

2.1 Current practice for structural assessment

Structural assessment of existing structures is usually made using basically the same calculation methods as in design of new structures. However, it is generally made for specific loads and slightly different demands specified in national regulations. The national regulations may also refer to national standards or codes specifying other calculation methods than those used for design of new structures. For example, until 2018 the code for assessment of existing bridges in Sweden referred to the old national codes for design of concrete structures, BBK04, Boverket (2004), that was superseded by Eurocode in 2010.

When performing a structural assessment, structural analyses are performed to determine the action effects in the members, normally in terms of cross-sectional forces and moments for a great number of load combinations. These are compared to corresponding (cross-sectional) capacities, determined using local resistance models. Resistance models used are typically described in Eurocode 2, CEN (2004a), ACI 318-11, ACI (2011) or national regulations.

For the structural analysis of reinforced concrete slab structures, simplified linear two-dimensional (2D) beam or frame models have traditionally been used for bridges in combination with distribution widths from handbooks such as BBK 04, Boverket (2004). For two-way floors or flat slabs in buildings, methods based on plasticity, such as the yield line method, Johansen (1972) and the strip method, Hillerborg (1996) were common. Today, linear three-dimensional (3D) FE analysis is commonly used in engineering practice, see e.g. Pacoste *et al.* (2012), Blaauwendraad (2010) and Rombach (2004). Linear analysis is generally desired since it enables to handle multiple load combinations and to simplify the analysis. Although concrete slabs have a pronounced non-linear response, the use of linear analysis can be justified in ultimate limit state since concrete slabs normally have good plastic deformation capacity, and hence are able to redistribute the forces in the slab until the force distribution assumed in the linear analysis is obtained. Theoretically, the assessment is based on the lower bound theorem of plasticity and, consequently, such an analysis will result in a conservative estimate of the capacity.

The initial assessment is commonly made based on existing documentation of the bridge. If there are doubts about the bridge condition or if the initial assessment shows insufficient capacity, detailed inspection and material characterisation from samples of the structure is often made. If the structure is deteriorated, the effect on the structural performance can be included as a change in geometry (cross-section) and material properties of the concrete, reinforcement and their interface, see e.g. Zandi *et al.* (2011a). In special cases, when the consequences of inadequate structural performance are large and the potential with improved assessment is identified,

measuring, testing or monitoring of the structure is made, or more advanced structural analysis methods or reliability-based methods are used.

2.2 The principle of successively improved assessment

The recommendations presented in this report are based on that the structural assessment is made in steps, with successively more advanced structural analysis methods, improved knowledge of the structure and its conditions of operation and with safety formats suitable for the analysis methods used, see e.g. Sustainable Bridges (2007). In Figure 2.1, a flow diagram for the assessment process is shown.

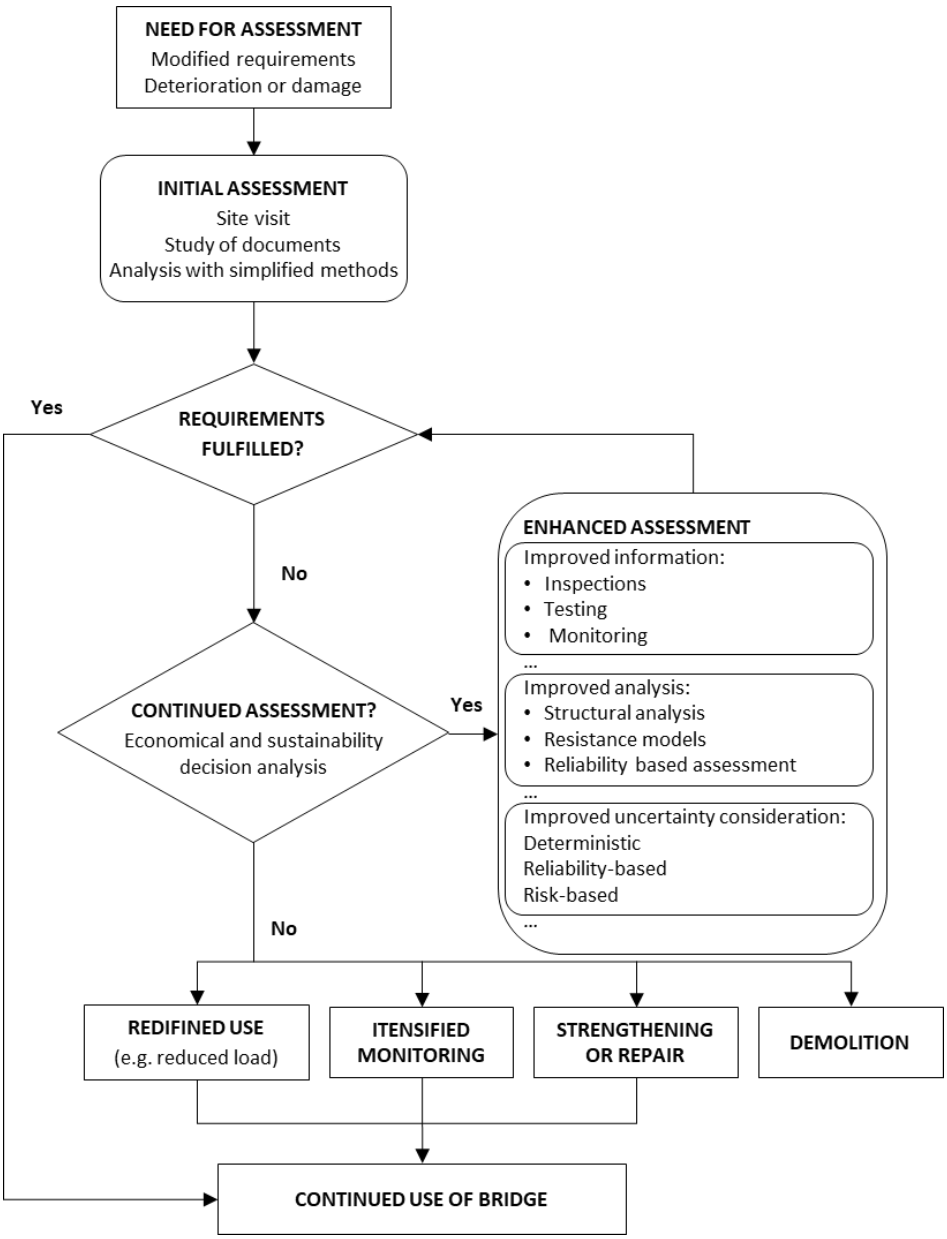

Figure 2.1 Flow diagram for structural assessment based on the principle of successively improved evaluation. Shu et al. (2018), based on Sustainable Bridges (2007).

The assessment starts with an initial assessment based on available documentation, using simplified analysis methods similar to those used in design. If the requirements are not fulfilled, it is possible to continue the assessment by an enhanced assessment. To judge if such an assessment is motivated, the economical, societal and environmental consequences of the enhanced assessment is compared to the measures needed if the assessment is terminated. A framework for decision support in structural assessment assisting the judgement is described in Shu et al. (2019).

A continued assessment can for example include:

- Improved information about the in-situ conditions of the structure and its conditions of operation, like e.g. the site-specific loads. The information can be achieved through inspections, monitoring and testing, or deeper studies of documentation.
- More advanced structural analyses and resistance models that are more accurate and reliable.
- More advanced safety formats, appropriate for the structural analysis method used.

These dimensions of enhanced assessment are also referred to as knowledge content, model sophistication and uncertainty consideration, respectively, Björnsson *et al.* (2017). However, they are not independent of each other; instead they are often strongly interconnected. For example, an enhanced structural analysis based on non-linear FEM requires improved knowledge of the material response and condition of the structure to be motivated, and a more advanced safety format is generally required. Figure 2.2 shows the concept of how an assessment may be successively enhanced through improvements in these three dimensions. In the first steps, the information and analysis methods are improved. Further on, also the safety

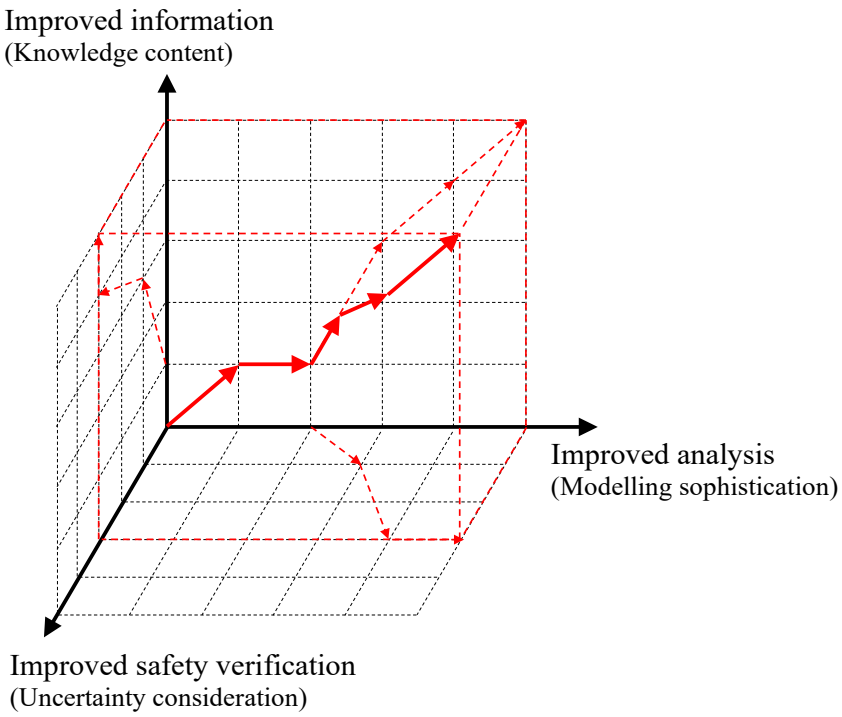

Figure 2.2 Successive improvement of an assessment through actions in three dimension, based on Björnsson et al. (2017).

verification methods are improved simultaneously. This is further treated in Section 2.4.

After performing enhanced assessment, it is again re-evaluated if the requirements are fulfilled and whether to proceed with further improved assessment, and which methods that are best to use. Finally, the assessment results in a decision whether it is possible to continue to use the structure, and if so, whether intensified monitoring, strengthening or repair is needed.

2.3 The Multi-Level Assessment Strategy

In this report, *the Multi-Level Assessment Strategy* according to Plos *et al.* (2017) is followed. It facilitates enhanced assessment through successively improved structural analysis and resistance evaluation. It also provides a structured approach to the use of non-linear FE analysis for structural assessment of RC slabs. Five different assessment levels can be distinguished, see Figure 2.3. Here, the assessment starts with traditional simplified analysis methods (Level I), followed by the currently dominating linear FE analysis method (Level II). The higher levels (Levels III – V) involves non-linear FE analysis on different levels of detailing.

A non-linear FE analysis simulates the response of the structure. It resembles the structural behaviour under successively increased loads, possibly up to and beyond the failure of the structure. This means that the load-carrying capacity can be evaluated from the non-linear analysis directly, in a one-step procedure, provided it is

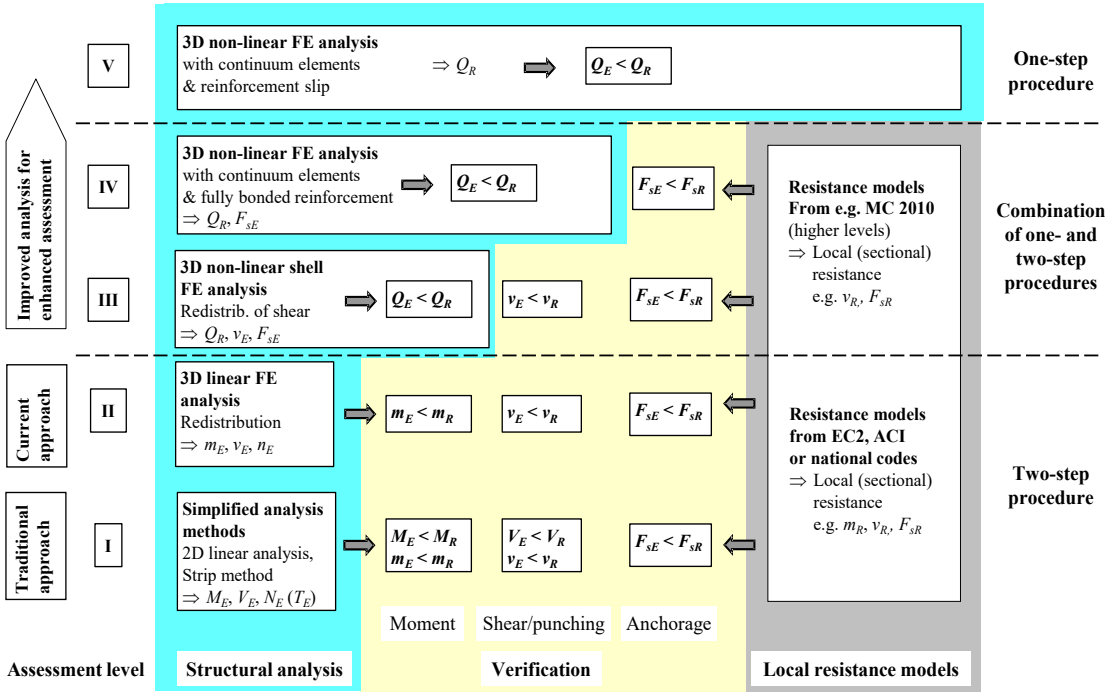

Figure 2.3 *Scheme for the Multi-Level Assessment Strategy for RC bridge deck slabs. From Plos et al. (2017). In the figure, Q refers to the global structural response while m (M), v (V), n (N), T and F_s refers to the different local responses in terms of moment, shear, normal, torsion and reinforcement force, respectively. Index E refers to the action effect and index R to the resistance.*

sufficiently detailed to reflect the governing failure mode. If all possible failure modes of interest are not reflected, the action effect from the analysis must instead be compared to corresponding local resistances for these failure modes in a two-step procedure, similarly as for Levels I and II. This is the case for some of the failure modes at Levels III and IV, see Figure 2.3. While the common resistance models from e.g. Eurocode 2 (2004a), ACI (2011) or national regulations are used at Levels I and II, higher *Level-of-Approximation* resistance models from Model Code 2010, fib (2013), are used for Levels III and IV.

If the governing failure mode is reflected in the non-linear analysis, the load-carrying capacity of the structure can be evaluated from the structural analysis directly, in a one-step procedure, without any separate resistance model. The resistance is then represented by the external load, or set of loads, applied on the structure at failure. For this situation, the partial factor method is not directly applicable for assessment of the structural reliability. Instead, global safety factor methods are suitable and recommended for use in combination with non-linear finite analyses on assessment Levels III – V. Such methods are further treated in Section 2.4.

When the structure is deteriorated due to e.g. reinforcement corrosion, frost damage or alkali-silica reaction, it is important to include the effect of this in the assessment. This is further treated in Section 2.5.

The assessment levels of *the Multi-Level Assessment Strategy* are briefly described below. In Chapters 4 to 6, they are described in more detail, and detailed recommendations are given for non-linear analysis at Levels III and IV.

Level I: Simplified analysis methods

On this level, the structural system is commonly simplified to 2D linear beam or frame models with a pre-assumed load distribution between the main directions. For a RC slab, this can be generalised to the strip method (Hillerborg, 1996). In both cases, the structural model is based on the lower bound theorem of plasticity. The analysis can be complemented with the yield line method (Johansen, 1972), giving an upper bound for the plastic load-carrying capacity. The limited plastic deformation capacity of the slab can be accounted for by limitations on the load distribution widths, e.g. BBK 04, Boverket (2004). For two-way spanning slabs, there are also tabulated solutions available in textbooks and handbooks for the distribution of load effects, e.g. Timoshenko and Woinowsky-Krieger (1959). The load effects are compared with corresponding resistances determined by local models for bending, shear, punching and anchorage of reinforcement. Common design resistance models are used, as described in e.g. the Eurocode 2, CEN (2004a), ACI 318-05, ACI (2011) or national regulations.

Level II: 3D linear FE analysis

Here, the structural analysis is made with 3D FE models, most often based on shell or bending plate theory. The analysis is made assuming linear response to be able to superimpose the effect of different loads, in order to achieve the maximum load effects in terms of cross-sectional forces and moments throughout the structure for all possible load combinations. Since both geometrical simplifications and the assumption of linear material response result in unrealistic stress concentrations, and since the reinforcement normally are arranged in strips with equal bar diameter and spacing, redistribution of the linear cross-sectional forces and moments are necessary.

Recommendations on redistribution widths for bending moments and shear forces are given in e.g. Pacoste *et al.* (2012). The load effects are compared with corresponding resistances in similar way as in Level I.

Level III: 3D non-linear shell FE analysis

On this assessment level, shell (or bending plate) finite elements are used. The reinforcement is included in the FE model but is assumed to have perfect bond to the concrete; it is preferably modelled as *embedded reinforcement* layers in the shell elements, strengthening the concrete in the direction and at the level of the reinforcement bars. In such a model, bending failures will be reflected in the analysis, while neither out-of-plane shear, punching, or anchorage failures are reflected. Instead they must be checked by local resistance models. With this level of accuracy on the structural analysis, resistance models on higher *Level-of-Approximation* according to the Model Code 2010, fib (2013) are recommended. For shear type failures, models taking into account the in-plane stress-state from the non-linear analysis are used.

Level IV: 3D non-linear FE analysis with continuum elements and fully bonded reinforcement

Here, non-linear analysis is made with 3D continuum elements representing the concrete. Similarly to Level III, the reinforcement is assumed to have perfect bond and no slip to the concrete; *embedded reinforcement* layers can be used in coarse FE meshes, while individual (embedded) bars may be preferred in dense meshes with small elements compared to the reinforcement bar distances, to better reflect the crack pattern. In such an analysis both bending and shear type failures including punching can be reflected with sufficiently dense mesh. However, anchorage failures need to be checked with separate resistance models.

Level V: 3D non-linear FE analysis with continuum elements including reinforcement bond

Compared to the Level IV analysis, the reinforcement is modelled using separate finite elements. Furthermore, the bond-slip behaviour of the interface between the reinforcement and the concrete is included. With a fine mesh, individual cracks can be studied, and anchorage failure is reflected in the analysis. With this level of accuracy of the structural analysis, the intention is that no major failure modes should be necessary to check using separate resistance models.

It should be noted that it is not only recommended, but in practice necessary that an assessment with non-linear analysis of a real structure is preceded by assessment on the lower levels, i.e. Levels I or II. In engineering practice, it is generally necessary to assess the structure for a great number of load combinations and load positions. However, in a non-linear analysis, the response is history dependent and load effects from different loads cannot be combined. Instead, a separate non-linear analysis must be made for each combination of loads. Since it is comparably much more time consuming and computationally demanding to do a non-linear analysis, it can only be used to evaluate a limited number of critical load combinations, previously identified on lower assessment levels.

2.4 Safety formats

2.4.1 Introduction

The reliability of a structure can be assessed in different ways, often referred to as different safety formats. These can be divided into three classes based on their probabilistic approach, fib (2018):

- Full probabilistic analysis
- Global safety factor methods
- Partial safety factor (PSF) methods

Often, for all safety formats, assumptions are made which allow treating the resistance and the actions of the studied structure separately. From a theoretical viewpoint, the full probabilistic analysis is the most correct method. However, it can be demanding to use in practice since it, in addition to a realistic model for the structural resistance, requires detailed information about the probabilistic parameters of the limit state function. In particular, it is difficult to combine with non-linear structural analysis since this becomes computationally very demanding.

The PSF method is suitable for traditional structural design and assessment, where the reliability is verified locally in points or cross-sections of the structure or for individual structural elements. This is also the safety format primarily used in Eurocodes, CEN (2002a). With a linear structural analysis, the action effects can be determined through superposition for all possible combinations of loads. The maximum action effects are then compared to local resistances determined with different resistance models for different possible failure modes. Consequently, the PSF method is recommended for assessment on Levels I and II in *the Multi-Level Assessment Strategy*.

A non-linear FE analysis simulates instead the behaviour of a structure for one specific load combination; the response can be studied for successively increased loads, possibly up to and beyond the failure of the structure. It can be seen as a virtual testing of the existing structure as a whole and is by its nature always a global type of assessment. A representative value of resistance is here global and not local; it can e.g. be a force, or a set of external actions applied on the structure. For this situation, the PSF method is not considered to be directly applicable. Instead, global safety factor methods are suitable. Such methods are described in fib Model Code 2010, fib (2013), and one method is given in Eurocode 2-2, CEN (2004b). In this report, global safety factor methods are recommended for use in combination with non-linear finite analyses for assessment on Levels III, IV and V in *the Multi-Level Assessment Strategy*.

If all failure modes are not captured in the non-linear analysis, these are checked using separate resistance models, as described in Section 2.3. Since the resistance is checked locally, the PSF method could be applicable. On the other hand, the resistance is evaluated for one particular load combination and can be expressed by the global load on the structure. Consequently, global safety factor methods are also applicable and in this report they are recommended for checking all failure modes when non-linear analysis is used.

2.4.2 General about global safety factor methods

Current standards and codes for design and assessment of structures are based on the generally accepted safety principles agreed by the Joint Committee of Structural Safety, JCSS (2001). They are the basis for reliability assessment according to the Eurocodes, CEN (2002a), and the partial safety factors used are derived based on these. They also form the basis for the global safety factor formats described here.

A basic assumption, both for the global and PSF methods, is that the action and resistance can be decoupled when verifying the reliability in the limit states. In this report, the safety formats described treats the resistance, while the design values for the actions are assumed to be determined separately. This can be made following the principles in e.g. Eurocodes, CEN (2002b), but with loads relevant for assessment, given in e.g. national standards and codes. Enhanced methods to determine the actions based on improved information from e.g. in-situ operation conditions are not treated here. However, application of actions in non-linear analysis is treated in Section 2.4.7. Since the response in a non-linear analysis is history dependent, the resistance depends on the order in which the actions are applied. This is generally not treated in standards or codes. The recommendations given here are instead based on experience from practical assessment with non-linear analysis and are in agreement with the general concepts in the Eurocodes, CEN (2002a).

The design condition in a global safety format can be written, following the notations in fib (2013):

$$F_d \le R_d\,, \quad R_d \le \frac{R_m}{\gamma_R^* \cdot \gamma_{Rd}} \tag{2.1}$$

where:

F_d is design value of actions
R_d is design resistance for the structure
R_m is mean value of resistance for the structure
γ^*_R is global resistance safety factor, and
γ_{Rd} is model uncertainty factor.

Here, the mean resistance is chosen as a reference for safety assessment, and the global resistance safety factor relate to the global mean resistance value. This is reasonable for assessment with non-linear FE analysis, since the purpose of the analysis is to simulate the real structural response and to determine the resistance based on the most probable response of the structure. The safety factors are then used to scale the mean resistance to a design resistance value.

The mean value of resistance is determined from a non-linear FE analysis with mean values on modelling parameters, like material properties and geometry measures. The global safety factor γ^*_R accounts for random uncertainties of the modelling parameters. The model uncertainty factor γ_{Rd} accounts for uncertainty in the model formulation. In case of non-linear FE analysis, the value of the model uncertainty factor depends on the quality of the non-linear analysis, i.e. how accurate the model can predict the resistance of the structure. To be used to determine a design resistance, the model need to be sufficiently validated. Nevertheless, the model uncertainty factor depends both on the complexity of the structural model and on the failure mode governing the resistance, Schlune *et al.* (2012).

In the following, some global safety formats are briefly described, and their advantages and drawbacks discussed. The difference between these formats is how the safety factors and the modelling parameters used to obtain the mean resistance are determined.

Global safety format according to Eurocode 2-2

This method, given in Eurocode 2-2, CEN (2004b) was originally proposed by König *et al.* (1997), and is also one of the safety formats for non-linear analysis described in Model Code 2010, fib (2013). In this method, formal values of the material strengths are used to be able to adopt one single global safety factor value, prescribed to be $\gamma^*_R \cdot \gamma_{Rd} = 1.27$, regardless if steel or concrete failure governs the resistance. This makes the method easy to use, and it requires only one non-linear analysis for each load combination studied. On the other hand, the value for model uncertainty given in given in Eurocode 2-2 is applicable for models with low uncertainties only, such as beams or frames, Schlune (2011). Furthermore, a non-linear analysis is usually made to gain improved insight into the structural behaviour; it is then preferable to use in-situ[1] values for mean material parameters to obtain a probable structural response.

Estimate of coefficient of variation (ECOV) method.

This safety formats for non-linear analysis, originally proposed by Cervenka *et al.* (2007), is described in fib Model Code 2010, fib (2013). In this method, the coefficient of variation (COV) of the global resistance is used to calculate the global resistance safety factor. The COV is estimated from mean (R_m) and characteristic (R_k) values of resistance, calculated through two different non-linear analyses with mean and characteristic values of material properties, respectively. Since realistic in-situ values of the material properties are used, the mean resistance represents a realistic and probable structural response. According to the Model Code, fib (2013), it is possible to use different model uncertainty factors for models with "low" and "high" uncertainties, respectively. However, it is questionable if these values properly account for complex structural models and failure modes that are difficult to model correctly, Schlune *et al.* (2012). With this method, two non-linear analyses are required for each load combination studied, which makes it a little more demanding than the safety format according to Eurocode 2-2. This method is further described in Section 2.4.3.

Safety format according to Schlune *et al.*

This safety format was suggested as a further development of the ECOV method, Schlune *et al.* (2011, 2012). In this method, the total global resistance factor, including model uncertainty, is calculated from a COV composed of contributions from material, geometry and model uncertainty, respectively. The COV from material uncertainty is evaluated by decreasing one material strength at a time in a separate non-linear analysis to account for alternative failure modes. For the model uncertainty, not only the COV but also the model bias[2] is taken into account. As for

[1] It is often motivated to determine in-situ values of material properties based on tests on samples from the structure. However, all material properties needed for a non-linear analysis are often not possible to test. For determination of material properties, see Appendix A.

[2] The model bias describes how well the model can predict the response in question in average. It is determined as the mean ratio of experimental to predicted resistance (when calibrating the model).

the ECOV method, in-situ values of the material properties are used, resulting in a realistic structural response and mean resistance value. If the COV of the model uncertainty and the model bias has been determined for the certain modelling method used, and type of structure and failure mode studied, it is possible to use these in the calculation of the global resistance factor. In this way, the doubts regarding the model uncertainty factors that exist for the other methods can be avoided. This method requires two or more non-linear analyses for each load combination studied and is therefore furthermore computationally demanding. This method is further described in Section 2.4.4.

2.4.3 Recommended safety formats

For assessment with *the Multi-Level Assessment Strategy*, the following safety formats are recommended for the different assessment levels:

For assessment with simplified analysis methods or 3D linear FE analysis on **Levels I and II**, the partial safety factor (PSF) method according to Eurocodes, CEN (2002a), is recommended.

For assessment with non-linear analysis on **Level III**, the ECOV method is recommended based on the considerations in Section 2.4.2. The model uncertainty factor for models with high uncertainties given in Model Code 2010, fib (2013), is recommended for this type of non-linear analysis. This is motivated since the analysis reflects bending failures in skew directions to the reinforcement and shear type failures checked by higher *Level-of-Approximation* resistance models according to Model Code 2010. If the mean (R_m) and characteristic (R_k) values of resistance are obtained for different failure modes, the ECOV method may result in an un-conservative design value of the capacity; for such cases the safety format according to Schlune *et al.* (2011, 2012) is recommended instead. The ECOV method is described more in detail in Section 2.4.4.

The global safety format according to Eurocode 2-2 is not recommended since a low model uncertainty is assumed. This approach may be reasonable for non-linear analysis of continuous beams and frames subjected to bending moments and normal forces but can be questioned for slabs assessed for bending and shear type failures.

For assessment on **Level IV and V**, the safety format according to Schlune *et al.* (2011, 2012) is recommended. Here, it is possible to use specific values of the COV of the model uncertainty and the model bias, determined for the certain modelling method used to analyse the type of structure and failure mode assessed. In cases where such specific values have not been determined, conservative values according to Schlune (2011) can be used, see Section 2.4.6. The ECOV method, as described in Model Code 2010, is not recommended for analysis on this level since the model uncertainty factors given are likely to give un-conservative estimates of the design load-carrying capacity. The global safety format according to Eurocode 2-2 is not recommended with the same motivation as for level III.

In the current revisions of the Eurocodes and the Model Code, further development of safety formats for non-linear analysis are made. For example, methods to determine the model uncertainty explicitly for the modelling method used, and the structure and failure mode studied, are being developed. Furthermore, methods to consider the possible change of failure modes when the material parameter varies, and their influence on the model uncertainty, are being further developed. Consequently, new

alternatives may become available with the coming versions of Eurocodes and Model Code, respectively, particularly for assessment Levels IV and V.

2.4.4 ECOV method

The estimate of coefficient of variation (ECOV) method, Model Code 2010, fib (2013), is based on the assumption that the random distribution of the structural resistance can be described by a lognormal distribution identified by its mean value R_m and coefficient of variation (COV) V_R. The mean value of the structural resistance, R_m, can be determined by a non-linear structural analysis with mean *in-situ* values on the material parameters, f_m, and nominal or measured values on the geometrical parameters, a_{nom}:

$$R_m = r\left(f_m, a_{nom}\right) \tag{2.2}$$

To estimate the coefficient of variation, a characteristic value of the structural resistance, R_k, is determined by an additional non-linear analysis with lower bound characteristic values on the material parameters, f_k:

$$R_k = r\left(f_k, a_{nom}\right) \tag{2.3}$$

The coefficient of variation is then estimated from:

$$V_R = \frac{1}{1.65}\ln\left(\frac{R_m}{R_k}\right) \tag{2.4}$$

The global resistance safety factor can be determined from:

$$\gamma_R^* = \exp\left(\alpha_R \beta V_R\right) \tag{2.5}$$

Where the factors can be chosen according to fib Model Code 2010, fib (2013):

$\alpha_R = 0.8$ is the sensitivity factor of the resistance, and

$\beta = 3.8$ is the reliability index corresponding to a probability of $P_f = 10^{-3}$ [3].

The sensitivity factor and the target reliability are chosen so that the global resistance can be directly compared with design value of actions determined in accordance with Eurocodes, CEN (2002a, 2002b).

In case, after a detailed inspection of the nonlinear finite element results, the values of R_m and R_k turn out to be based on different failure modes, the ECOV method should be applied with great care. In this case, the assumption that the resistance can be described by a lognormal distribution is questionable. For such cases, the Safety format according to Schlune *et al.*, Section 2.4.5, is recommended.

The design resistance is finally calculated using equation (2.1), using a model uncertainty factor according to Section 2.4.6.

[3] The reliability index may vary and are often specified by national regulations. For example, in Sweden, it is related to different safety classes, see Boverket (2019).

2.4.5 Safety format according to Schlune *et al.*

The safety format according to Schlune *et al.* (2011, 2012) may be seen as a further development of the ECOV method. As in the ECOV method, the design resistance is based on the mean structural resistance, R_m, determined by a non-linear structural analysis with mean *in situ* material parameters for the concrete, f_{cm} and f_{ctm}, and reinforcement, f_{sm}, respectively, and nominal or measured values on the geometrical parameters, a_{nom}.

$$R_m = r\left(f_{cm}, f_{ctm}, f_{sm}, a_{nom}\right) \tag{2.6}$$

A single global resistance safety factor is determined in a similar way as for the ECOV method, but here it includes also the model uncertainty. Furthermore, the possible model bias, θ_m, is also taken into account:

$$\gamma_R^* \cdot \gamma_{Rd} = \frac{\exp\left(\alpha_R \beta V_R\right)}{\theta_m} \tag{2.7}$$

With the factors $\alpha_R = 0.8$ and $\beta = 3.8$ chosen according to fib Model Code 2010 in the same way as for the ECOV method, fib (2013).

The coefficient of variation for the resistance, V_R, is calculated from the coefficients of variation to account for modelling uncertainty, V_θ, geometrical uncertainty, V_g, and material uncertainty, V_f, respectively:

$$V_R = \sqrt{V_\theta^2 + V_g^2 + V_f^2} \tag{2.8}$$

The coefficient of variation for modelling uncertainty, V_θ, and the model bias, θ_m, vary depending on the complexity of the model and failure mode studied. The determination of these values is treated in Section 2.4.6.

A reinforced concrete slab is generally insensitive to geometrical imperfections, and a relatively small coefficient of variation for geometrical uncertainty is recommended:

$$V_g = 5\% \tag{2.9}$$

The coefficient of variation for material uncertainty is determined through a sensitivity study, similarly to the ECOV method. However, instead of reducing all material strengths simultaneously in one additional FE analysis, one material strength at a time is reduced. In Schlune *et al.* (2011), a larger reduction of the mean strength than what corresponds to characteristic values was recommended but here, to make the method more easily applicable, it is recommended to use characteristic values; as shown in Schlune *et al.* the difference on the reliability index for the resistance was low. For a concrete slab, three additional FE analyses are generally needed in addition to the mean material parameters:

With characteristic concrete compression strength:

$$R_{kc} = r\left(f_{ck}, f_{ctm}, f_{sm}, a_{nom}\right) \tag{2.10}$$

With characteristic concrete tension strength:

$$R_{kct} = r\left(f_{cm}, f_{ctk}, f_{sm}, a_{nom}\right) \tag{2.11}$$

With characteristic reinforcement steel strength:

$$R_{ks} = r\left(f_{cm}, f_{ctm}, f_{sk}, a_{nom}\right) \tag{2.12}$$

In these analyses, not only the material strength value but also the corresponding material parameters are adjusted to reflect a characteristic material response. For example, if the concrete tensile strength is reduced from mean to characteristic value, also the fracture energy is reduced proportionally. Recommendations for material properties for non-linear analysis are given in Appendix A.

The coefficient of variation for material uncertainty can then be calculated as

$$V_f = \frac{1}{R_m}\sqrt{\left(\frac{R_m - R_{kc}}{f_{cm} - f_{ck}}\right)^2 \left(V_{fc} \cdot f_{cm}\right)^2 + \left(\frac{R_m - R_{kct}}{f_{ctm} - f_{ctk}}\right)^2 \left(V_{fc} \cdot f_{ctm}\right)^2 + \left(\frac{R_m - R_{ks}}{f_{sm} - f_{sk}}\right)^2 \left(V_{fs} \cdot f_{sm}\right)^2} \tag{2.13}$$

The coefficient of variation for the material parameters in Equation (2.13), V_{fc} for concrete and V_{fs} for reinforcement steel, can be chosen to correspond to the material uncertainty assumed for the partial factors in Eurocode 2 (European Concrete Platform, ASBL, 2008; Schlune *et al.* 2011):

$$V_{fc} = 15\% \tag{2.14}$$

$$V_{fs} = 4\% \tag{2.15}$$

As a simplification, the coefficient of variation for material uncertainty can instead be estimated from:

$$V_f \cong \frac{1}{R_m}\max\left\{\frac{R_m - R_{kc}}{f_{cm} - f_{ck}} \cdot \left(V_{fc} \cdot f_{cm}\right), \quad \frac{R_m - R_{kct}}{f_{ctm} - f_{ctk}} \cdot \left(V_{fc} \cdot f_{ctm}\right), \quad \frac{R_m - R_{ks}}{f_{sm} - f_{sk}} \cdot \left(V_{fs} \cdot f_{sm}\right)\right\} \tag{2.16}$$

In cases where it is obvious which failure mode that determines the failure, the number of analyses can be reduced and only characteristic analyses corresponding to governing failure mode(s) need to be included. Only minor differences were found between Equation (2.13) and (2.16) for such cases, Schlune *et al.* (2012).

When the coefficient of variation for the resistance, V_R, is determined using Equation (2.8), the design resistance for the structure can finally be calculated using Equation (2.1), by dividing the mean structural resistance, R_m (Equation (2.6), with the total global resistance safety factor, $\gamma^*_R \cdot \gamma_{Rd}$ (Equation (2.7).

2.4.6 Estimation of model uncertainty

For assessment on **Level III** in *the Multi-Level Assessment Strategy* with the ECOV method, model uncertainty factors according to Model Code 2010, fib (2013), can be used. Analyses of bending failures in slabs with varying reinforcement directions and content show a higher model uncertainty than analysis of continuous beams and frames subjected to bending, Schlune *et al.* (2012). Consequently, if not shown otherwise for the specific case, the model uncertainty factor for models with high uncertainties is applicable.

When assessing the load carrying capacity with respect to shear type failures, higher *Level-of-Approximation* resistance models from Model Code 2010, fib (20 13), is

recommended. Here, deformation results from the non-linear slab analysis are used as input. The resistance models were originally set up to give design resistances using the PSF method. The equations express conservative estimates of the resistances and thus takes the model uncertainty of the expression itself into account.

When using them in a global safety format context, they are used to estimate mean and characteristic shear and punching resistances instead. These predictions of mean and characteristic resistances can be expected to have the same degree of conservativeness, giving a global resistance factor that is unbiased by the resistance model. In the end, the model uncertainty determined by the ECOV method takes into account the model uncertainty connected with the non-linear FE analysis, while the model uncertainty connected with the resistance model is accounted for by its inherent conservativeness. This results in a final prediction of the design load-carrying capacity that is expected to be conservative.

Consequently, the model uncertainty factor is, regardless of failure mode, recommended to:

$$\gamma_{Rd} = 1.1 \tag{2.17}$$

For assessment on **Levels IV and V** in *the Multi-Level Assessment Strategy*, the model uncertainty factors given in Model Code 2010 are generally too low, at least for other failure modes than bending, Schlune *et al.* (2011, 2012). Instead, the safety format according to Schlune *et al.* is recommended, together with model uncertainty parameters for the specific modelling method used and failure mode studied. The coefficient of variation for the model uncertainty and the model bias can be determined by comparing predictions from non-linear analysis with representative experimental results in a systematic way. The model bias is here determined as the mean ratio of experimental to predicted resistance. The determination of these values for given modelling method and failure type is described in e.g. Engen *et al.* (2017).

If such values are not available for the modelling method used (and it is too demanding to determine them) the recommendations from Schlune (2011) in Table 2.1 can be used as conservative estimates. These values were determined from round robin analyses in which a variety of modelling methods were used. The results from the experiments used for comparison was not known to the analyst before making the analysis. Furthermore, there were no requirements that the capability of the modelling methods to predict the load-carrying capacity should have been verified and validated *a priori*. Consequently, the coefficients of variation for the model uncertainty given in the table might be exaggerated and may lead to an over-conservative estimation of the load carrying capacity.

2.4.7 Modelling of the action history

In a non-linear analysis, the structure is subjected to successively increasing actions to simulate the response. The non-linear response in terms of cracking, plastic deformation or damage from prior loading will influence the response of additional load increments. This means that the response in a non-linear analysis depends on the load path and that the resistance is history dependent and may be different depending on in which order the actions are applied. However, detailed rules on the order of application of actions are not given in standards or codes.

Table 2.1 Coefficients of variation for modelling uncertainty and model bias (mean ratios of experimental to predicted resistance), evaluated from round robin analysis of experiments. From Schlune (2011).

Failure type	Characteristics of the structure	Coefficient of variation V_θ [%]	Model bias (mean ratio of experimental to predicted resistance) θ_m [-]
Compression	Normal strength concrete	10 – 20	0.9 – 1.0
	High strength concrete	20 – 30	1.0
Bending	Under-reinforced	5 – 15	1.0 – 1.2
	Under-reinforced, bending reinforcement not aligned in principal moment direction	5 – 15	0.9
	Over-reinforced, normal strength concrete	10 – 15	0.9 – 1.0
	Over-reinforced, high strength concrete	20 – 30	1.0
Shear	Failure due to yielding of the reinforcement	10 – 25	0.9 – 1.0
	Failure due to crushing of concrete, Combination of compression and shear, Large members, Bending reinforcement not aligned in principal moment direction	20 – 40	0.7 – 1.0

Here, it is recommended that the actions are applied in the order the structure is likely to be subjected to them. This means that permanent actions are applied first, followed by variable actions. Each action is increased up to its design value. In case the construction sequence has a significant influence on the distribution of stresses in the structure, it should be reflected in the action history. If the variable actions have different durations, the actions with longer duration are applied first. In case failure is not reached when all actions are applied up to their design values, all or a chosen subset of the actions, e.g. the concentrated forces of a traffic load, are further increased until failure is reached.

When the load-carrying capacity of a concrete structure is assessed with non-linear analysis, it is often sufficient to assume that the structure is uncracked and undamaged before loading is applied. The influence of previous cracking due to loading in other positions can normally be neglected when evaluating the design load-carrying capacity. When evaluating the response in service conditions, previous cracking may however influence the response; this can be simulated by loading and subsequent un-loading in the non-linear analysis corresponding to previous load situations. If on-site inspections indicate deterioration this can be taken into account according to Section 2.5.

Using a global safety format, the design load-carrying capacity will have different interpretations depending on the load scheme in the final load step for which failure is

reached in the analysis. There are two main options when increasing the load above the design level:

- **All loads are increased until failure is reached.** In this case both permanent and variable loads are increased simultaneously. With this approach, a utilisation ratio can be determined for the entire structure that is comparable to the highest utilisation ratio (often) calculated for different structural members and failure modes in a conventional (two-step) assessment on lower assessment levels. A drawback is that it is more complicated to achieve stable solutions in a non-linear analysis for such a loading scheme; consequently, it may be difficult to determine reliable global resistances in the analyses. Furthermore, the global safety formats is not directly applicable if the mean and characteristic resistances are obtained under different loading schemes; this may occur if the mean resistance is obtained for a load level higher than the design load while a characteristic resistance is achieved before the design load level is reached, see Figure 2.4 (a).
- **One particular load is increased until failure is reached.** In this case only one variable load is increased while all other loads are kept constant at their design load level. This could for example be the concentrated loads from a type vehicle used in assessment of a bridge. In this case, the load carrying capacity is expressed as the design axle or bogie load for that type vehicle, provided all other loads have their design value. An advantage with this approach is that the variable load increased can be controlled more easily (using displacement control) and it is easier to determine reliable global resistances. Furthermore, since the variable load increased above the design load level normally also is the final load applied to reach the design load, the mean and characteristic resistances are normally obtained for the same loading scheme.

Figure 2.4 show examples of these different ways to apply the actions.

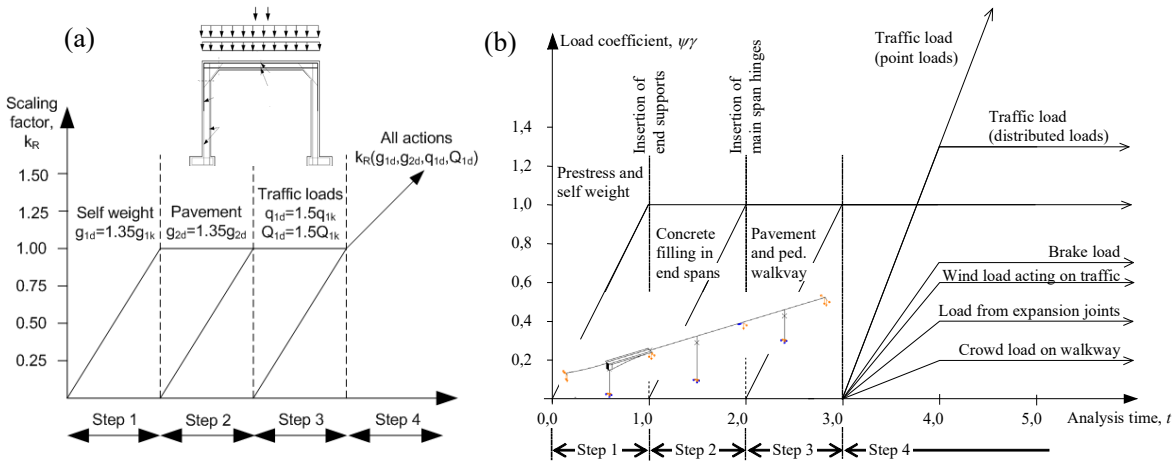

Figure 2.4 Examples of loading histories used in non-linear analyses: (a) for an assessment of a slab bridge, Schlune (2011) and (b) for an assessment of a prestressed box girder bridge built with the free cantilevering method, Plos and Gylltoft (2006)

- In (a), a bridge deck slab was first subjected to the self-weight of the structure, corresponding to the load applied at removal of the formwork. Other permanent loads were then applied, in this case from pavement and railings, followed by the variable traffic loads up to the design load level. Finally, all loads were increased simultaneously until failure was reached.
- In (b) a free cantilever bridge was assessed. The diagram shows the order in which permanent loads and supports were added to simulate the main stages of construction (step 1 – 3). All variable loads were then increased up to their design values. Finally, the point loads of the traffic load were increased until failure was reached.

The load factor at failure has quite different meaning in these two cases: In (a) all loads, including permanent loads, were magnified with the same load factor; the design resistance represents here the load factor for all loads, and its inverse is the utilisation factor for the structure. In (b) only the traffic point loads were magnified; the design resistance here represents the traffic load that the bridge can resist in addition to all other loads.

2.5 Modelling of deterioration and damages

Non-linear structural analysis has proven to be capable of describing the behaviour of deteriorated reinforced concrete structures in a comprehensive way, provided that appropriate constitutive models are adopted, see e.g. Zandi (2010). When the structure is deteriorated due to, for instance, reinforcement corrosion or frost damage, the structural effect of the deterioration needs to be counted for in structural analyses or using local resistance models. Depending on the level of assessment, the effect of such deteriorations on RC slabs can be included as a change in (a) material properties of concrete and cross-sectional area of the structural member, (b) material properties and cross-sectional area of steel reinforcement, and (c) bond properties between reinforcement and concrete. These considerations are briefly described below.

(a) The effect of concrete cracking due to a specific type of deterioration can be accounted for by adjusting material properties of concrete; this is applicable to all levels of structural analysis. It should however be noted that at analysis Levels I and II, the deterioration will affect the action effects in the structural analysis only if the stiffness of material is altered. Recommendations regarding the material properties of concrete damaged due to frost and reinforcement corrosion can be found in Appendix B and Appendix D, respectively. Spalling of concrete cover, as a result of high corrosion levels or external frost damage, can also be considered in all levels of analysis by adjusting the concrete cross-section area. Recommendations can be found in Zandi *et al.* (2011a) for corrosion-induced spalling, and in Zandi *et al.* (2011b, c) for spalling caused by external frost damage, also called surface scaling.

(b) Corrosion of steel bars will lead to a reduction of rebar area and ductility. These effects are taken into account in all levels of assessment by adjusting the cross-sectional area and martial properties of steel reinforcement in structural analyses and resistance models. The reduction in steel cross-section area due to corrosion can be calculated from the corrosion level (steel weight loss). However, in practice, it can be hard to estimate the corrosion level within an existing structure. The influence of corrosion on the ductility of

rebars is still subjected to research. Nonetheless, empirical correlations were suggested in Du *et al.* (2005) and physics-based models can be found in Fernandez *et al.* (2015) and Chen *et al.* (2020).

(c) The effect of the deterioration on bond can be accounted for in assessment on different levels.

- Assessment at Levels I and II: Simplified/engineering resistance models are used together with bond strength and available anchorage length to calculate anchorage capacity. If the effect of deterioration on bond strength is unknown, the residual capacity of the bond-slip relation can be used as a conservative assumption. See Appendix E for more detailed description and Tahershamsi *et al.* (2017) for practical examples.
- Assessment at Levels III and IV: The effect of the deterioration on bond is taken into account in resistance models using a 1D bond-slip model and a given available anchorage length. The anchorage capacity is obtained by numerically solving the 1D differential equation along the available anchorage length. See Appendix E for more detailed description and Blomfors *et al.* (2018) for practical examples.
- Assessment at Level V: the deterioration will affect the structural analysis with a pre-defined one-dimensional (1D) bond-slip relation between concrete and reinforcement. This level of modelling cannot directly take into account the splitting effects of the reinforcement slip and the expansion of corrosion products; these effects are instead accounted for by modifying the 1D bond-slip relation given as input. See Appendix E for more detailed description and Blomfors *et al.* (2018) for practical examples.

3 Non-linear FE analysis

This chapter gives a brief introduction of the concept of non-linear finite element (FE) analyses, including the numerical approach, iteration methods, tolerance measures and load application. Further, information of how to choose input data for material parameters and how to handle the non-linear response in reinforced concrete structures are treated. Several things mentioned in this chapter are valid for different types of materials and structures, but here the general focus is on reinforced concrete structures and particularly on the assessment of reinforced concrete slabs.

3.1 Introduction

Non-linear FE analysis is a powerful tool to better describe the structural response of a real structure subjected to loading. Correctly used, such analyses may provide considerable knowledge of the real structural response and may hence be used to e.g. better understand the cause of damage or failure in an existing structure, or to predict what response is to expect from a structure once loaded. Accordingly, non-linear FE analyses also have the potential to show higher capacity of a structure than what is possible using more simplified or approximate calculation methods.

Non-linear FE analyses are nowadays commonly used in research; often in combination with experimental testing to confirm that the results obtained are in line with observations made in real structures. Consequently, using such analyses one may get results that are considerably closer to reality, and hence it is also possible to e.g. show an increased load capacity compared to what would be possible using more conventional methods. However, there is a price to perform non-linear analyses; the amount of time and resources needed to prepare, carry out and process such an analysis may be considerably larger. Further, the demand on the engineer carrying out the analysis is usually also substantially increased. Consequently, the cost to carry out a non-linear analysis is higher, and therefore, such analyses are usually only carried out in special situations, e.g.:

- In research, to better understand and describe the physical response of a loaded structure, e.g. to develop simplified calculation methods that may be used in practice.
- To demonstrate a higher load carrying capacity; this is often of interest in the assessment of existing structures and is what is done in Levels III to V in *the Multi-Level Assessment Strategy*, see Section 2.3.
- Improved description and understanding of a complex load and/or structural response; e.g. where the load distribution changes due to non-linear response, to include second order effects that otherwise may be difficult to describe correctly or combine the effect of restrained forces and external loading in cracked concrete structures.

As mentioned above, the use of non-linear analysis results in higher complexity and costs, and it requires certain expertise in the subject. Some common consequences of using non-linear analysis identified are listed below and will be further discussed in Section 3.2:

Increased complexity

- Higher demands on the software used, i.e. the software must include appropriate variants of e.g. the complex material models needed to correctly model the non-linearity of interest.
- More complex input data needed to describe both the model itself (e.g. reinforcement bars in concrete) and the materials used therein.
- Additional input data related to e.g. type of load application, tolerance measures, tolerance criteria and iteration methods must be given, see Section 3.2.2.

Increased calculation time

- All loads are divided into increments. Depending on what solution method is used iterations are needed within each load increment (implicit method) or the size of the load increments have to be very small (explicit method), see Section 3.2.2.
- Risk of numerical convergence problems may result in solutions that are terminated prior to the load level of interest, i.e. it is possible that results of interest are not obtained or that it takes very long time to obtain them. If encountering numerical problems, it may be very difficult to estimate how long it takes to reach further progress with the analysis (or if it even is possible).

Increased amount of results

- Due to increased complexity, the amount of results obtained may increase substantially. This often makes the results more difficult to interpret and therefore puts higher demand on the user. This also makes it even more important for the user to correctly understand the results obtained.
- Since the complexity of the analysis also increases the risk of making errors, there is a higher risk that the analysis turns into a "black box"; i.e. a calculation tool in which things happen which the user has limited control or understanding of.

3.2 Performing non-linear FE analyses

3.2.1 Various types of non-linearity

The common practice when using FE methods in the design or assessment of structures is to use linear FE analyses, i.e. assuming linear elastic material response and neglecting the possible effects of changed structural geometry or boundary conditions due to loading. However, when performing non-linear FE analyses, some or all the effects listed below are considered in the model used, see Figure 3.1 for schematic examples:

- **Non-linear material response**, e.g. cracking of concrete or yielding of steel reinforcement.
- **Non-linear geometrical response**, e.g. second order effects of a column and rigid body movement (large deformations) or the use of different strain measures (large strains: e.g. to model necking of a steel bar in tension).

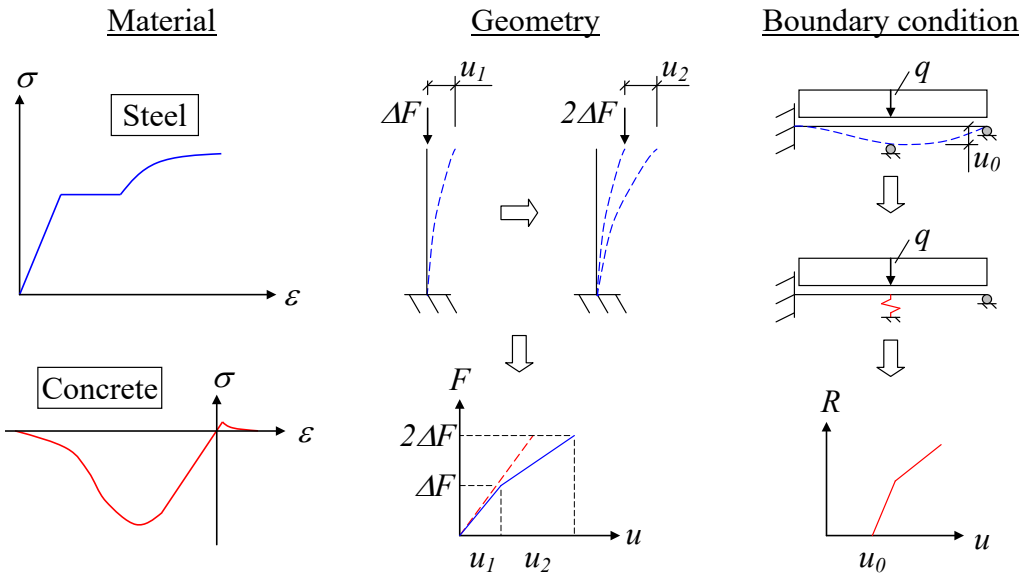

Figure 3.1 Examples of possible types of non-linearity in a FE analysis.

- **Non-linear boundary conditions**, e.g. contact with or without friction between different structural parts or removal/adding of structural parts in the model.

In the assessment of reinforced concrete slabs, the most common type of non-linearity is due to non-linear material response; hence, in this document, focus is on this aspect. For a concrete slab, though, the effect of large deformations may also be of importance to properly describe the real structural response if the deformations, in relation to the slab thickness, are large.

The complexity on non-linear material response is not limited to the non-linearity of the material´s mechanical properties, e.g. stress-strain relation, but also of how unloading and reloading of the material is handled. The conceptual difference of this response is schematically illustrated in Figure 3.2 for three different but common types of non-linearity: non-linear elastic, plastic and damage response. Here the stress-strain relation $\sigma(\varepsilon)$ is identical for all cases but the response at unloading/reloading is completely different. It is also possible to have material models that combine these types of responses, e.g. a damage plasticity model.

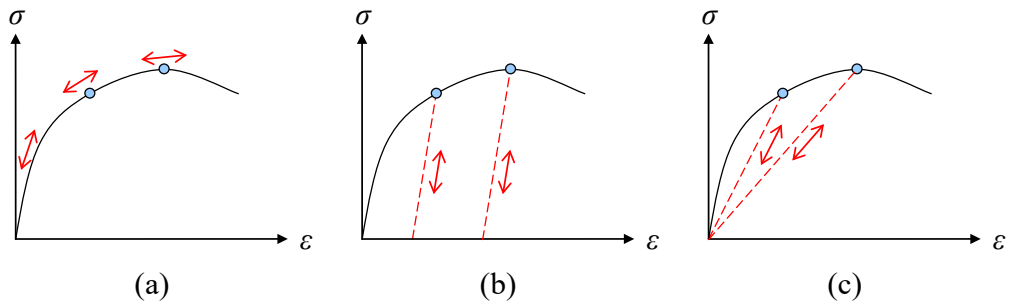

Figure 3.2 Examples of possible types of response at unloading/reloading in a non-linear material model: (a) non-linear elastic; (b) plastic; (c) damage.

In a linear elastic analysis, the need of material properties is limited to a few parameters, i.e. Young´s modulus, Poison's ratio and (if making a dynamic analysis) density. However, in an analysis making use of the non-linear response, much more information is needed, i.e. material parameters that is of no need for linear analyses now have to be specified (e.g. full mechanical properties of material until failure). Which type of material properties that is needed depends on the material models used; different material models may use different type of parameters to describe the same physical phenomenon (e.g. cracking of concrete or yielding of reinforcement). Hence, the demand on the user's knowledge of what material properties to use may increase considerably compared to that required in a linear elastic analysis.

3.2.2 Numerical approach

In a non-linear FE analysis, the relation between load and displacement becomes non-linear, and the displacement at a given stage usually depends on previous displacements. Hence, it can be said that the solution at a given load will be history dependent. This also means that, unlike a linear elastic analysis, it matters in which order various loads is applied to the structure.

To solve a non-linear system, the load is subdivided into several load increments. Depending on what type of solution method is used the treatment within each load increment differs (Bathe, 2016):

- **Implicit solution method:** Equilibrium in increment *i* is based on information in both increment *i* and previous load increments, i.e. an iteration procedure is needed to find equilibrium in each increment. The implicit solution method can be used in both static and dynamic analyses.
- **Explicit solution method:** Equilibrium in increment *i* are based solely on information in previous load increments, i.e. all information necessary to proceed the calculation is already known and an iteration procedure is not needed. The explicit solution method is used in dynamic analyses but can also be used to simulate the effect of static loading.

In the implicit solution method, a linear approximation of the stiffness, representing a linearized form of the relation between load and displacement increments, is established at each step. However, since the stiffness varies with the displacement, the internal forces of the structure are not in equilibrium with the external forces. This produces an error in the solution and if not handled this error will increase with increased loading, see Figure 3.3. Therefore, to minimise this error, an iterative solution procedure is used within each load increment and the solution is refined until a specified convergence criterion is satisfied.

When using an implicit solution method there are several different iteration methods available that can be used in the solution process. The general procedure, though, is the same for all iteration methods; the difference is in how the stiffness matrix is determined. The iterative methods can be divided roughly into three categories: the tangent stiffness method, the initial stiffness method and the secant stiffness method, see Figure 3.4. In the tangent stiffness method, the stiffness matrix is determined at each iteration, resulting in a method that often requires few iterations, but where every iteration is relatively time-consuming. In the initial stiffness method, the stiffness is determined at the beginning of each load step and it is then used throughout the whole

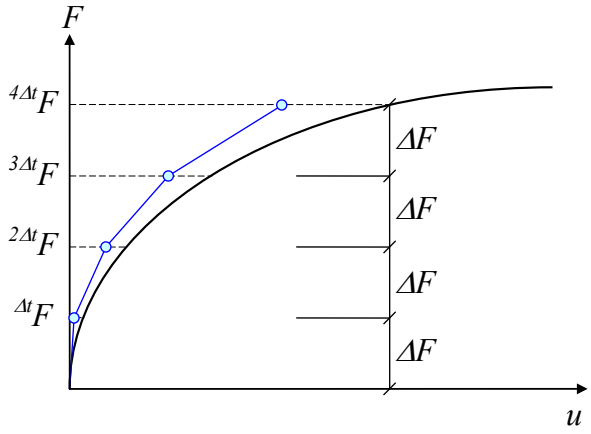

Figure 3.3 *Increasing error of the solution when using implicit incremental load method without correction, for a system with one degree of freedom.*

iteration process within an increment. This method requires more iterations to reach convergence than the tangent stiffness method but, since the same stiffness matrix is used in each iteration within the increment, every iteration is faster. The secant stiffness method uses the information from previous solutions to update the inverse stiffness matrix in each iteration, which results in a convergence rate somewhere between that of the tangent and the initial stiffness methods. Further information on iteration methods can be found in e.g. Bathe (2016).

To determine whether the solution obtained in an increment is good enough, different types of measures are used and then compared with a given tolerance. Typical measures used are force, displacement and energy, and which one to use normally depends on what type of structure and response that are modelled. Often a combined measure based on force and energy works well, while a measure based on displacements only should be avoided. Which type of iteration method that should be used and what settings to use for it (e.g. tolerance type, tolerance value and number of iterations used) depends on a combination of the problem to be solved and the material model used. In the software manuals there are usually different type of recommendations to handle this. In the examples in Chapter 7, the regular Newton-Raphson (tangent stiffness method) or quasi-Newton iteration methods (secant stiffness method) were successfully used. In Hendriks *et al.* (2017), a tolerance of 0.001 is suggested for the energy-norm and a tolerance of 0.01 is suggested for the

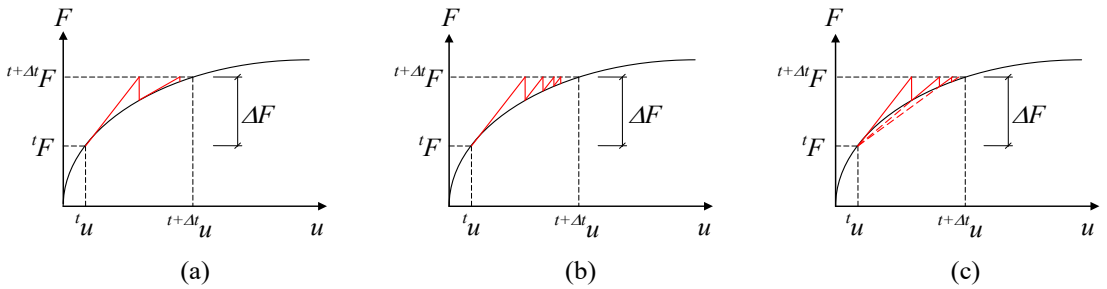

Figure 3.4 *Schematic view of different iteration methods for a system with one degree of freedom: (a) tangent stiffness method, (b) initial stiffness method, (c) secant stiffness method.*

force-norm. However, in case convergence problems are encountered, it can sometimes be worthwhile to violate those recommendations; e.g. using a different iteration method and allowing a higher number of iterations (Plos, 1995; Johansson, 2000); also see Section 3.4.4. In the two first examples in Chapter 7, consisting of comparisons to experiments, a tolerance of 0.01 was used also for the energy norm in order to achieve a stably converging analysis. This shows that a larger tolerance must sometimes be used, and that a realistic response still may be obtained. However, using smaller tolerances may also be a way to improve the overall convergence of a nonlinear analysis since it may provide an improved solution so that numerical difficulties at a later stage may be reduced or avoided all together (Malm, 2016).

In the explicit method, equilibrium is satisfied without conducting any iteration. This is possible by fulfilling dynamic equilibrium instead of a static one in which the displacements at the next increment is based on the deformations and stiffness in the previous load steps only. A disadvantage with this method, though, is that the size of the load increment (time step) must fulfil certain conditions; usually causing it to be very small. Consequently, this usually means that different types of tricks (i.e. highly increased load rate) is needed when using an explicit method to simulate quasi-static loading. Hence, using an explicit method may be an effective way to avoid numerical convergence problems but may at the same time cause the analysis to take longer time to perform and also introduce new challenges regarding load rate. Nevertheless, using explicit methods to simulate quasi-static loading may still be effectively handled, see e.g. Malm (2016) and Veganzones *et al.* (2019). Therefore, which type of solution method that is suitable to use depends on what type of structural situation is to be modelled.

3.2.3 Load application

As explained in Section 3.2.2, the structural response is history dependent in a non-linear analysis. Therefore, it is important that the load of interest is applied on the structure in the order they appear in reality, e.g. first permanent loads followed by variable loads in the positions of interest. There are three conceptually different methods available to use when applying the load:

- **Load-controlled loading:** This method means that the load is applied using a monotonic increase of forces [N] and moments [Nm]. This method is what is normally used in a linear elastic FE analysis and can be used also in a non-linear analysis.
- **Displacement-controlled loading:** In this method the load is applied using a monotonic increase of displacements [m] (velocities [m/s] and accelerations [m/s^2] are also available in a dynamic analysis).
- **Arc-length method:** This method makes use of load- and/or displacement-controlled loading but uses a special method to handle the load vector in the iteration process so that the load does not need to be monotonically applied. For more detailed information, see e.g. Bathe (2016).

In Figure 3.5 the concept of these load applications is schematically illustrated using a non-linear load-displacement relation of a given structure. The thick black line represents the true solution of a structure with a so-called snap-back response, while the dashed red line with filled circles represent the results that may be obtained when

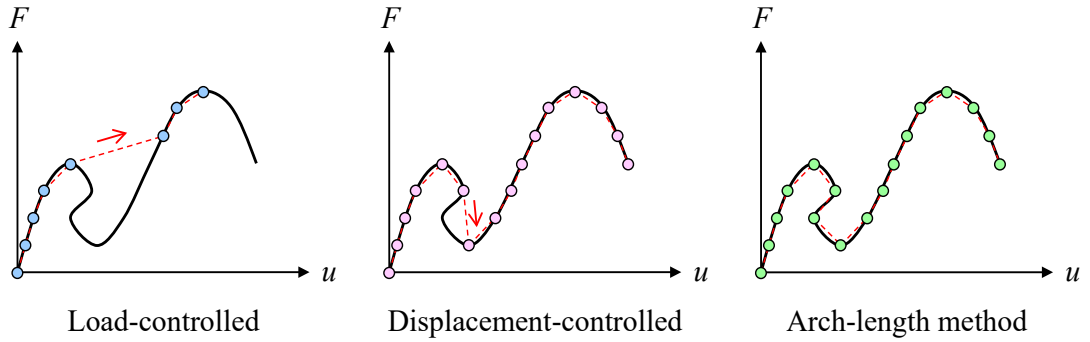

Figure 3.5 *Schematic illustration of various concepts of load application. Thick black line shows correct solution and dashed red line with filled circles represent the results obtained when using the method indicated.*

using the method indicated. Load controlled loading is the simplest method and the monotonically increase in force means that it will not be able to adequately capture the response when the force F decreases with increasing displacement u. Instead, the response obtained in the analysis will skip that part (marked with an arrow in Figure 3.5) and potentially find a new solution (fulfilling convergence in this part may be challenging) at a somewhat increased load but considerably increased displacement. In the case using displacement-controlled loading most of the response may be accurately described; only the snap-back part with decreased force and decreased displacement will be missed (jump marked with an arrow). When using the arch-length method the full response may be correctly captured in the analysis.

In non-linear analyses it is often of interest to be able to follow the structural response beyond the maximum load, i.e. to capture the descending branch of the load-displacement relation. If the response is not captured beyond the maximum load, it may be difficult to ensure that the maximum load really is reached in the analysis. Therefore, load controlled loading is often not an acceptable method to use when reaching a load level close to a possible maximum load. However, it is usually not a problem to use in an initial load stage, e.g. applying the dead weight of a bridge deck that later is also subjected to traffic load. Using displacement-controlled loading, though; it is possible to capture a correct response in most cases (the snap-back response illustrated in Figure 3.5 is not a feature in most structures, and specifically not so in a concrete slab). Therefore, this method is also widely used in non-linear FE analyses. Further, it has been found that displacement-controlled loading often may result in less numerical problems, i.e. it is easier to reach convergence in the analysis when using such a load application.

If the load of interest consists of a single point load it is easy to replace the force applied with a displacement acting in the same point and direction as the point load; the result will be the same. However, if a more complex load application is of interest, e.g. two point loads or an evenly distributed load, special measures need to be taken to use displacement controlled loading. Such more complex load cases can still be simulated using displacement-controlled loading using a system of fictitious, simply supported, beams as schematically illustrated in Figure 3.6. Here, an evenly distributed load is approximately modelled using a system of fictitious, simply supported beams. Since each beam is simply supported the forces acting in each support will be evenly distributed, and hence, the system shown will result in a

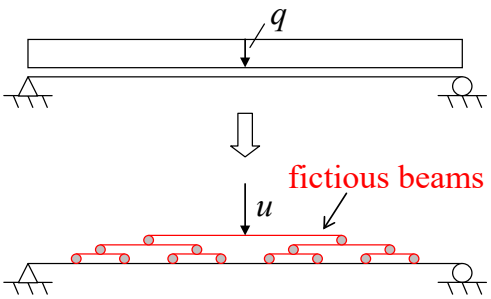

Figure 3.6 *Schematic illustration of how an evenly distributed load can be approximately modelled as displacement-controlled using a system of fictitious beams.*

distribution of eight point loads acting on the beam of interest; i.e. probably an acceptable approximation of the evenly distributed load. Using the same concept, the number of point loads acting on the beam studied could easily be increased to e.g. 16 or 32 instead. Similarly, a more complex load application could also be approximated using the same concept, see e.g. Broo *et al.* (2008) for detailed information of how to handle more complex loads such as group of vehicles.

3.3 Non-linear analysis of reinforced concrete

3.3.1 Material properties

The number of required material parameters depends highly on the material model used. The parameter values of these models should be either based on material tests from the structure assessed or on the material properties as given in e.g. Model Code 2010, fib (3013), or Eurocode 2, see Appendix A for suggested expressions. The material properties should reflect the current physical state of the structure. In Sections 3.3.2 to 3.3.6 more detailed discussions are made of concrete in tension, compression and shear, steel reinforcement and bond interaction between reinforcement and surrounding concrete.

3.3.2 Concrete in tension

The fracture mechanics models commonly used for concrete originate from studies of the initiation and propagation of a crack in a uniaxial concrete tensile test. Cracking occurs when the tensile strength of concrete is reached and a typical stress-displacement relation for such a test specimen is shown in Figure 3.7. Once a fracture zone has formed, the stress σ_c transferred through the zone depends upon the crack opening w and can be defined as $\sigma_c = \sigma_c(w)$, where $\sigma_c(w)$ is a function that describes the softening behaviour of the concrete. The area under the softening curve $\sigma_c(w)$ represents the energy release when concrete cracks and is, according to Hillerborg *et al.* (1976), the mean energy per unit area of a formed crack. This energy, denoted fracture energy G_F, is an essential concept when modelling cracking in concrete. Fracture mechanics for concrete and concrete structures in general is treated by e.g. Bazant and Oh (1983) and Jirasek and Bazant (2001).

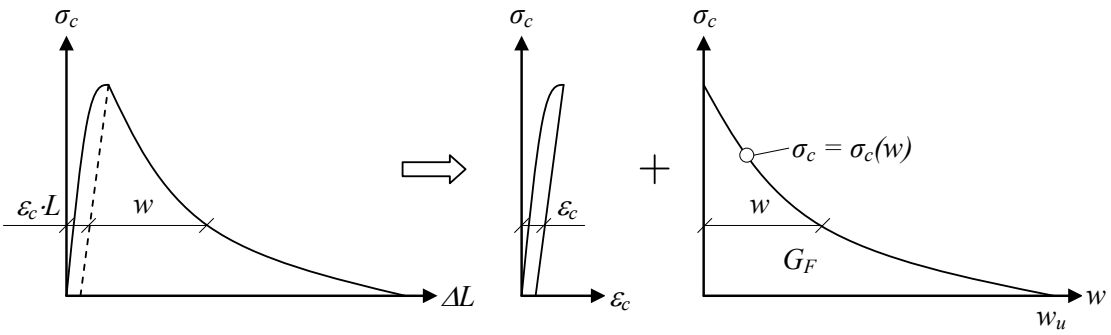

Figure 3.7 Stress-displacement relation for a uniaxial tensile test specimen. The displacement is separated into a stress-strain relation and a stress-crack opening relation. The area under the softening curve $\sigma_c(w)$ represents the fracture energy G_F.

When modelling cracked concrete there is a large amount of different methods described in the literature to do this, e.g. discrete, smeared or embedded crack approaches. However, in most non-linear FE software the smeared crack approach is available, and this method is also assumed here if nothing else is stated. This approach can in turn be divided into several types of material models that handle the position and direction of cracks in different ways, e.g. fixed cracks, rotating cracks or plasticity. These types of models may be suitable for analysis of reinforced concrete structures, provided that proper parameter values can be provided for the material model.

In the smeared crack approach, the localised non-linearity of the crack is "smeared" out over the finite element, i.e. all the material deformations, including both the crack and the uncracked concrete, are considered in the same element. This means that the crack pattern need not be taken into account in advance, making the smeared crack approach a powerful tool. Cracks may then form in each integration point within the model, and the cracked material is described with a stress-strain relation.

The smeared crack models reported in the literature can be subdivided into the following: fixed orthogonal cracks, fixed non-orthogonal cracks, rotating cracks, plasticity models and a combination of damage and plasticity models. In the first two kind of models, once a crack is initiated it is permanently fixed in a direction perpendicular to the maximum principal stress at the time of initiation. Both methods allow the formation of additional cracks at the same point. However, in a fixed orthogonal crack model such cracks may only form perpendicular to already initiated cracks. In non-orthogonal models, though, this limitation is not as harsh. Instead, the number of cracks that may form at an integration point is determined by a threshold angle chosen by the user. However, a new crack may only arise if it forms at an angle to already existing cracks that exceeds this threshold angle. Further, once initiated a fixed crack is never removed. This means that even though the crack at a later stage closes completely it will still affect the initiation of further cracks at the same integration point. Hence, as schematically shown in Figure 3.8, the principal stresses may also become larger than the tensile strength without causing a new crack. To take into account this possible stress-locking, the concept of reduced shear stiffness over the crack is introduced by the use of a so-called shear retention factor β. This means that the shear modulus $G_{c,cracked}$ of the cracked concrete is given as

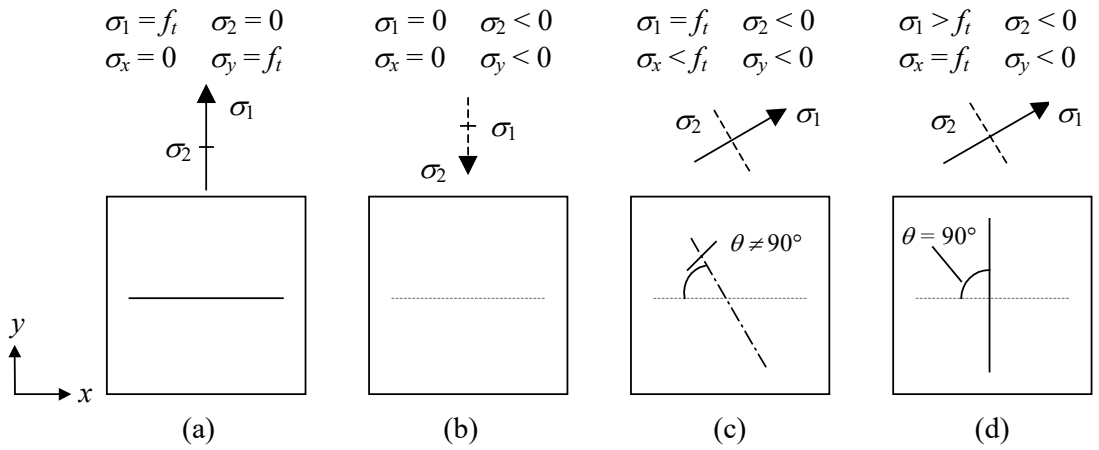

Figure 3.8 Schematic view of the initiation of a first and second cracks in a fixed orthogonal crack model: (a) initiation of horizontal crack; (b) crack closes; (c) principal stress reaches tensile strength, angle $\theta \leq 90°$, though, and a new crack cannot form; (d) second crack forms when $\sigma_x = f_t$, note that $\sigma_1 > f_t$. From Johansson (2000).

$$G_{c,cracked} = \beta \cdot G_{c,uncracked} \tag{3.1}$$

where $G_{c,\,uncracked}$ is the shear modulus of the uncracked concrete and $0 \leq \beta \leq 1$. Due to their lower restriction on secondary cracks, though, non-orthogonal models are less sensitive to such stress-locking than orthogonal models.

In this model the crack orientation follows the normal to the direction of the principal strain. However, to retain the consistency of using principal stress-strain curves to describe the cracked material response, the principal stress directions are forced to coincide with those of the principal strains. The effect can be interpreted as a single crack, whose orientation is continuously updated with respect to the present stress state. Hence, it may also be considered to act as a fixed non-orthogonal crack model in which the threshold angle is set to 0° (Rots, 1988). In a 3D continuum element, up to three orthogonal cracks may appear at the same integration point, and since the crack directions are the same as that of the principal strains there will be no shear stresses acting across the cracks. Accordingly, there is no need to use a shear retention factor for cracked concrete and the kind of stress-locking obtained in fixed crack models can be avoided (Feenstra, 1993). Crack models based on plasticity criterion have the same advantage and also show approximately the same behaviour as that of rotating crack models (Feenstra, 1993). These types of models have also proven to agree better with experimental results than does a fixed crack model; see e.g. Rots (1989), Lundgren (1999) and Shu (2017).

In the literature, there are many proposals of what the relation $\sigma_c = f(w)$ might look like, see A. Based on the relation chosen, the fracture energy G_F and tensile strength f_t are used to calculate an ultimate crack opening w_u where the post-peak stress reaches zero. However, since the input data to the crack models used are based on stress-strain relations, the stress-crack opening relation must be smeared out over a certain distance, the crack band width l_{cr}. Thereby, the ultimate crack strain $\varepsilon_{u,cr}$ used in the material model is proportional ($\propto$) to the fracture energy G_F and inversely proportional to the tensile strength f_t, i.e.

$$\varepsilon_{u,cr} = \frac{w_u}{l_{cr}} \propto \frac{G_F}{f_t l_{cr}} \tag{3.2}$$

From this expression it is clear that the value of the crack band width l_{cr} is just as important as the fracture energy G_F when determining the ultimate crack strain $\varepsilon_{u,cr}$. Evidently, the numerical response will be accurate only if the width of the softening region obtained in an analysis is equal to the assumed crack band width l_{cr}. It is therefore important to accurately determine this width prior to carrying out the analysis.

The crack patterns obtained in a FE analysis differ from case to case, depending on e.g. geometry, boundary conditions and load conditions. However, in the case of unreinforced concrete a crack usually localises within a row of elements as schematically shown in Figure 3.9a. In such a case, a correct crack band width would be to use the length of the element in which the crack localises. If using a smeared crack approach, l_{cr} is often set to $l_{element}$; i.e. the length of the element perpendicular to the crack. However, since the direction of the crack might not be known in advance it may be difficult to estimate what value on $l_{element}$ to use. In the literature, different approaches exist of how to do this, e.g. Rots (1988) that determine $l_{element}$ as

$$l_{element} = \sqrt{A_{element}} \tag{3.3}$$

where $A_{element}$ is the area of the element, when using two-dimensional elements (i.e. 2D continuum elements or shell elements). For three-dimensional continuum elements the same concept is obtained using the third root of the element's volume. Some software also make it possible to define the crack band width l_{cr} at the moment of cracking (i.e. when the crack direction is known); see e.g. Slobbe *et al.* (2013) for an overview. Further, depending on the software, the crack band width $l_{element}$ may also depend on the number of integration points used for the element, i.e. a quadratic 2D element with 2 x 2 integration points may define $l_{element}$ differently in different software. Consequently, it is very important for the user to be fully aware of the definitions in the software used.

The above reasoning presumes that the cracks localise within a single row of elements. Depending on the model used this condition may also be fulfilled in a reinforced concrete structure and one way to achieve this is to accurately include the interaction between the reinforcement and the surrounding concrete in the model. In such a case the cracks will, as schematically shown in Figure 3.9b, appear in a way like that obtained in tests. However, if perfect bond is assumed in the modelling, i.e. if the nodes used to define the reinforcement and concrete elements are locked to each other so that the strains in both materials remain the same, cracking will not localise into single element rows. Accordingly, using the element length to determine the stress-strain relation in such a case is no longer correct. Instead of crack localisation, the cracks may be partly spread out the over a distance in the elements located close to the reinforcement, as illustrated in Figure 3.9c. This smeared zone of cracks will then represent the discrete cracks observed in an experiment. Accordingly, a more satisfactory approximation of the crack band width in such a case could be to use the mean crack spacing s_{rm}; see e.g. Zandi *et al.* (2011b) and Shu *et al.* (2015).

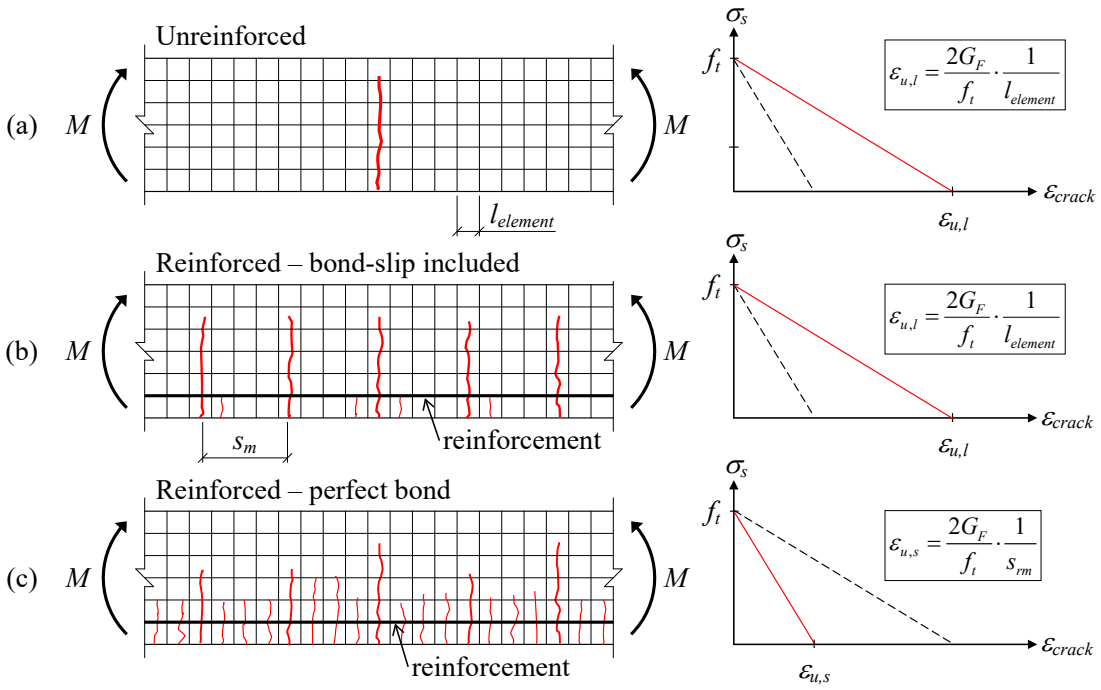

Figure 3.9 Schematic view of crack patterns obtained when modelling unreinforced and reinforced concrete. Filled line shows the stress-strain relation used; dashed lines are shown for comparison only. Based on Johansson (2000).

When the cracks propagate further into the structure, away from the reinforcement, they tend to localise in a way similar to that of unreinforced concrete, provided a sufficiently fine element mesh is used. This suggests that the approximation of the crack extension as the mean crack spacing is incorrect in these unreinforced regions. Instead, in such internal regions it may be more correct to use $l_{cr} = l_{element}$ even though perfect bond is used. To exemplify this, Figure 3.10 shows the crack pattern obtained in a reinforced concrete prism, subjected to a tensile force, when modelled using different mesh density and assuming perfect bond or a bond-slip relation, respectively, between reinforcement and surrounding concrete; see Section 3.3.6 for more information of perfect bond and bond-slip relations. When a finer mesh is used more distinct localised cracks can be seen, regardless of whether perfect bond or a bond-slip relation is used. However, it can also be seen that the cracked region close to the reinforcement is more smeared out when using perfect bond. Hence, based on this it can be argued that when assuming perfect bond, the concrete region close to the reinforcement should be modelled using $l_{cr} = s_{rm}$ but for the concrete region located a certain distance away from the reinforcement it would be more accurate to use $l_{cr} = l_{element}$.

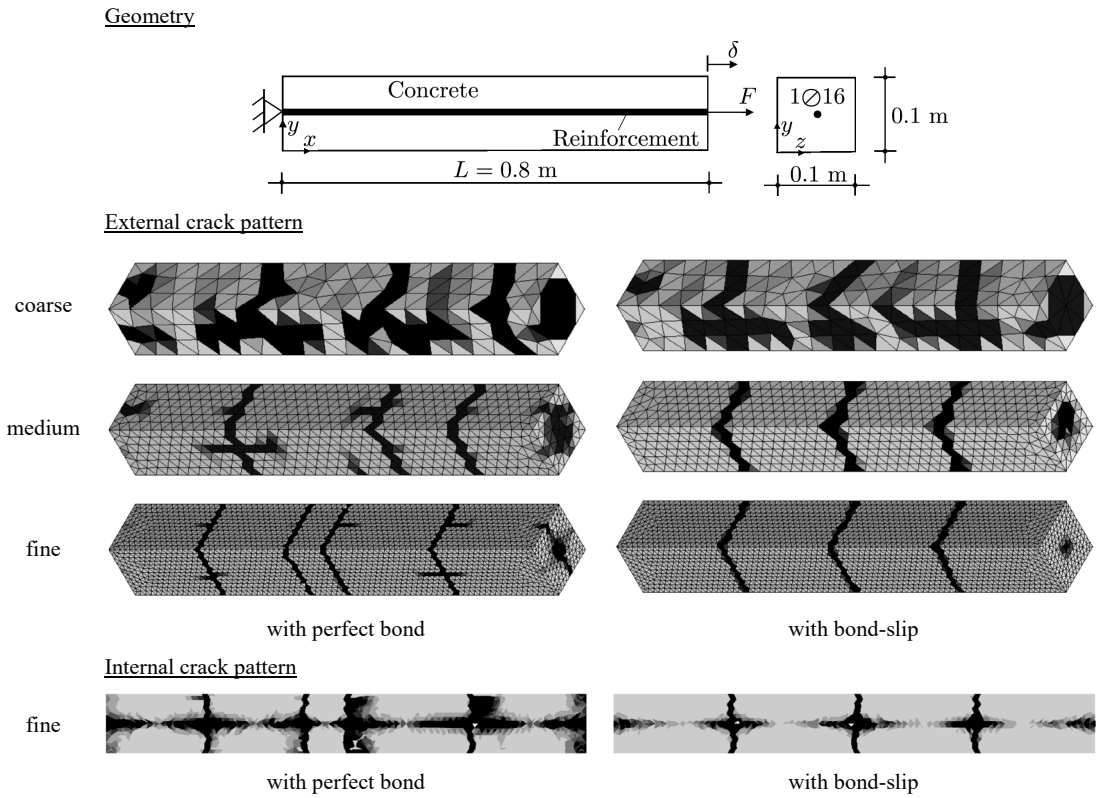

Figure 3.10 External and internal crack pattern in reinforced concrete prism subjected to a tensile load; effect of mesh density when assuming perfect bond or a bond-slip relation. Based on Grassl et al. (2018).

If using structural elements, i.e. beam or shell elements, to model the concrete structure so called *embedded reinforcement* (single bars or layers) are normally used, see Section 3.3.5. Hence, a crack situation similar to that illustrated in Figure 3.9c will be the case. However, in such elements, different zones, near and far away from the reinforcement bar, will not show radically different response since the reinforcement affects the whole element. Therefore, partial localisation within an element will not occur, and for such cases it is recommended to use $l_{cr} = s_{rm}$.

From the discussion above it might seem that there may only be problems with localisation when assuming perfect bond. However, this is not true. Depending on, for instance, the size and orientation of the elements used and what load case is studied, one cannot be sure that the cracks will localise within one element even though accurately modelling the bond-slip relation; see e.g. Lundgren (1999). I.e., even though a bond-slip relation is modelled it is possible that a localisation appears in e.g. two element rows next to each other. In such a case it would be more correct to use $l_{cr} = 2 \cdot l_{element}$ since the element crack formed now is based on the length of two elements.

To summarise, if the crack band width is assumed as the mean crack spacing and this length is larger than the length of the elements used, the results obtained will probably be somewhat too brittle. On the other hand, by approximating the crack band width as the element length, the response will most likely be somewhat too ductile, even though the interaction between concrete and reinforcement is accurately dealt with. Hence, it may be important to carry out a sensitivity study to more thoroughly

examine what influence the stress-strain relation used has on the response of the structure studied. A quite approximate way to do this is to vary the crack band width used by a factor of two: halved when using perfect bond and doubled when modelling the bond-slip. If this change has little effect on the result, then the analysis is also more likely to be trusted. However, if such a change has large impact on the structural response one should probably be careful when interpreting the results. A correct approach would then be to modify the crack band width originally used in those parts where the assumptions of it proved to be incorrect. A new analysis is then carried out and the validity of the assumptions checked. Evidently, this may lead to a cumbersome iteration process that may be quite time-consuming. However, if the post-peak ductility in tension proves to be vital, it may be the only way to obtain correct results.

In a cracked reinforced concrete member, the concrete in-between the cracks will contribute to the stiffness of the structure, see Figure 3.11. This is called the tension-stiffening effect. For a concrete slab subjected to bending, the concrete in the tension zones will contribute to the bending stiffness but its contribution to the bending capacity is negligible. An approximate way to account for the tension-stiffening effect on the stiffness in service state is to modify the stress-strain relation for concrete in tension. However, such a modification will also influence the ultimate capacity of the cross-section and may lead to unconservative results and over-estimation of the load carrying capacity. Further, this effect will also at least partly be automatically taken into account in a model using continuum elements (Levels IV and V); compare with the crack patterns in Figure 3.10. Consequently, a modification of the stress-strain relation to account for the tension-stiffening effect is not recommended.

3.3.3 Concrete in compression

Like concrete in tension, the softening branch of concrete in compression is also subjected to localisation, see e.g. van Mier (1984) and Hillerborg (1988). Van Mier showed that the post-peak ductility in compression tests depends on e.g. the height of the concrete specimen used. Figure 3.12a shows the normalised stress-strain relation for uniaxial compressive tests on concrete prisms of height 50, 100 and 200 mm.

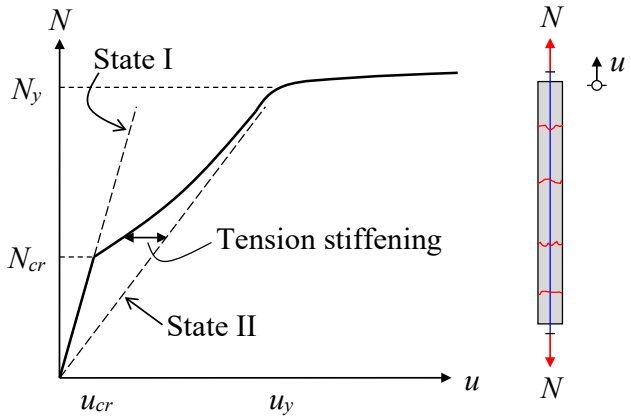

Figure 3.11 Tension stiffening effects in a concrete prism subjected to a tensile load N. State I corresponds to stiffness of uncracked prism and state II corresponds to fully cracked prism without influence of concrete (i.e. bare bar).

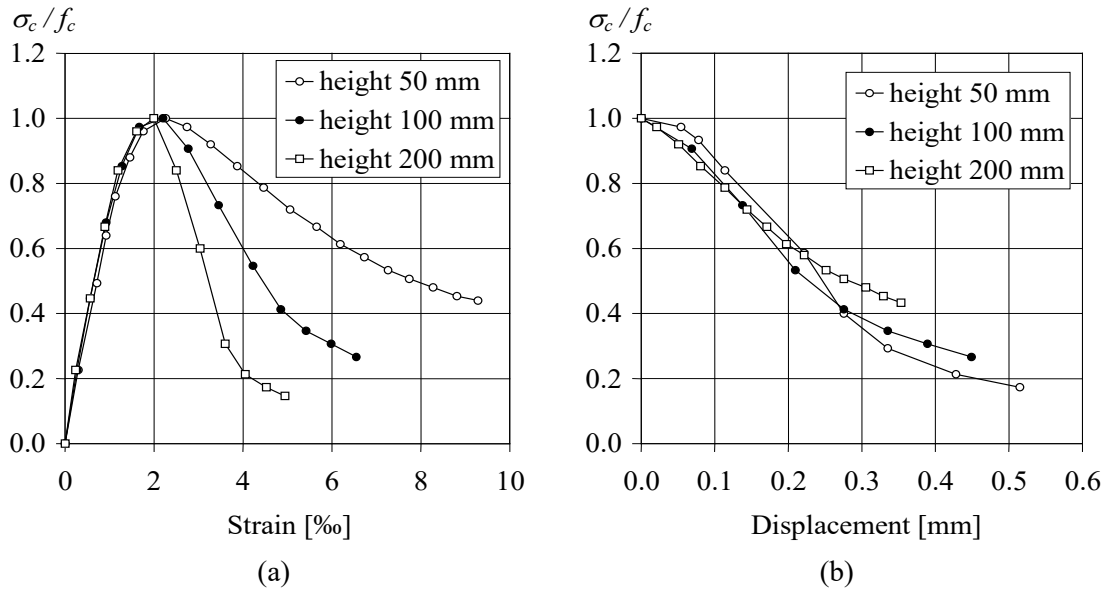

Figure 3.12 Post-peak behaviour of concrete prisms subjected to uniaxial compression: (a) normalised stress-strain relation; (b) normalised stress-displacement relation. Based on van Mier (1984).

According to this, a specimen with smaller height results in greater ductility. However, if instead comparing the displacement in the same specimens, the relations shown in Figure 3.12b are obtained. Consequently, it can be concluded that the stress-strain relations in Figure 3.12a do not correctly represent the concrete material behaviour and that the difference between them rather is due to a structural effect.

As in tension, information is needed about the softening zone width, in which the localisation in compression may occur. The stress-strain relations for concrete in compression given in the literature, see Appendix A, normally use the mean strain over the whole specimen and are therefore not suitable to be used as input data for FE analyses in which the softening of concrete is to be simulated. Such relations, i.e. the displacement measured divided by the height of the specimen, do not account for that a localisation occurs inside the specimen. Nevertheless, up to the compressive strength the stress-strain relation given is an appropriate approximation since the strain in the concrete thus far is quite homogeneous distributed. However, to correctly simulate the post-peak response, it is necessary to also consider the length of the softening zone. In e.g. Zandi *et al.* (2011b) and Shu *et al.* (2015) this softening zone were approximated using the length of the element used and related to the length of the height of the compression test cylinders used, see Figure 3.13. However, a more detailed approach may also be used in which the effect of the assumed softening zone is compared to the results obtained; see e.g. Mathern and Yang (2021).

Consequently, this is the same concept as used for concrete in tension when a localised crack is obtained. Hence, the concept described in both Figure 3.12 and Figure 3.13 is equivalent to that of fracture energy in compression; used by e.g. Markeset (1993) and Feenstra (1993). Also, see Hendriks *et al.* (2017) for a detailed description of alternative ways to make use of fracture energy in compression.

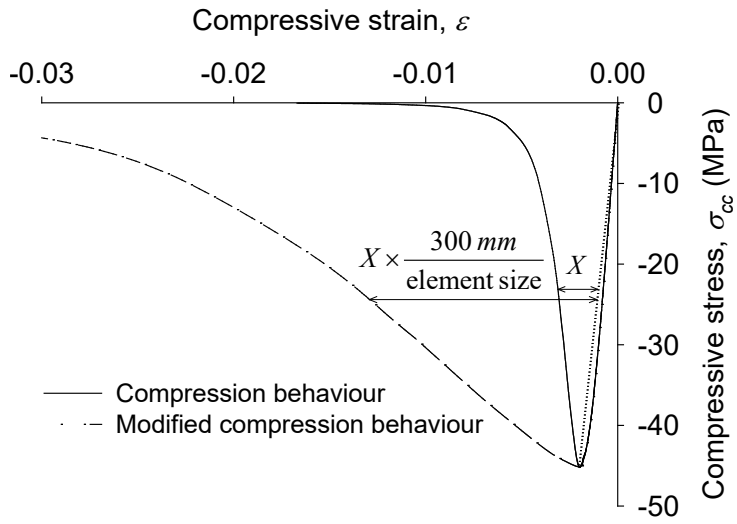

Figure 3.13 Illustration of how to modify the descending branch of the stress-strain relation in compression with respect to the concrete element size in the FE model; here, h_{cyl} = 300 mm. From Zandi et al. (2011b).

For bi-axial or tri-axial compression, the compression strength and ductility of concrete is increased, Similarly, compressed concrete subjected to tensile strains (or cracks) in the direction perpendicular to that of the compression, is softer and weaker than concrete subjected to uniaxial compression only. Consequently, depending on final failure mode, it may be important that the material model used is able to correctly describe this effect. In some software it may not be possible to combine a compressive-softening curve, adjusted for the size of the compression zone as shown in Figure 3.13, with the reduction of compressive strength due to perpendicular tensile strains. If the effect of reduced compressive strength is more important than the need to capture a concrete compression failure in order to simulate the failure response (e.g. a shear failure), an incorrect localization can be avoided by modelling the concrete in compression with an elastic-ideal plastic relationship instead. However, doing so, compression failure is avoided and there is hence also a risk of overestimating the structure´s plastic deformation capacity.

3.3.4 Concrete in shear

In Section 3.3.2 it is discussed how concrete in tension can be handled. The description is valid for cracks obtained due to a combination of a tensile force and bending, where the response of the crack, and its fracture energy, corresponds to that of a so called Mode I failure. However, for a shear crack, the failure mode is different, and therefore the crack band width should not necessarily be determined in the same way as for a bending crack.

If using a fixed crack model, the shear behaviour should be described by an adequate shear retention model. Alternatively, if using a rotating crack model shear retention is omitted since the selection of a shear retention model is only relevant for fixed crack models, see Section 3.3.2. In a conservative variable shear retention model, the secant shear stiffness degrades at the same pace as the secant tensile stiffness due to cracking. Alternatively, a variable shear retention model can be used in which the

shear stiffness gradually reduces to zero as a function of the average aggregate size. There are also software in which it is possible to combine a fixed and rotating crack model; i.e. a model in which the rotating crack model is used initially, and then it is transformed into a fixed crack model once a given criterion is reached. Such a criterion could be when the crack width w reaches a value $\alpha \cdot w_u$, where α is a constant set by the user. In structures where the shear response is important constant shear retention models are not recommended, see Shu *et al.* (2016), or should at least be accompanied with thorough post-analysis checks of spurious principal tensile stresses. However, if the structural response is dominated by bending the effect of shear retention will probably be small or even negligible.

To model the contribution of the dowel effect of bent bars in a reinforced structure, the reinforcement must be modelled using elements with a bending stiffness, e.g. beam elements. Even so, though, a fine mesh is probably needed in the zone of interest to correctly describe such a response. Incorrectly modelled, there is risk that the dowel contribution may be overestimated.

3.3.5 Steel reinforcement

In the type of FE models discussed here it will be sufficient to limit the contribution from the reinforcement to its uni-axial response, i.e. to model the reinforcement bars as one-dimensional and using a uni-axial stress-strain relationship. Reinforcing steel exhibits an elasto-plastic behaviour where the elastic limit is equal to the yield strength of the steel. The post-yield behaviour is known as hardening and may be important to include in the analysis together with an ultimate strain (modelled using a rapid drop to zero strength). Thereby, it is possible to make use of the entire tensile resistance of the reinforcement and to identify a failure govern by reinforcement rupture. For old reinforcement qualities the tension hardening and ultimate strain are often substantially more pronounced compared to modern reinforcement types. Including the tension hardening also makes the analysis more stable and facilitates the development of yield line failure in the analysis of slabs; this often makes it possible to follow the failure process longer. If, for some reason, it is decided to omit a correct strain hardening in the analysis, it is nevertheless recommended to still include a weak hardening (e.g. $E_{sh} = 0.1$ GPa) in the model. This may improve the stability of the analysis and hence help avoid potential numerical convergence issues related to the steel hardening being zero. To model reinforcement rupture it is also necessary to include an ultimate strain for the steel reinforcement. This value is set to represent the strain at ultimate strength, see Appendix A for further details.

Depending on the software used the modelling of the reinforcement may differ. However, in many software it is possible to include the effect of reinforcement defining specific reinforcement layers or separate bars. This method is often referred to as *embedded reinforcement* since no specific elements are added to the model; just their effect on stiffness in the direction of the reinforcement layers/bars. Another common method is to model the reinforcement using truss or beam elements. Which method to use depends on the magnitude of detail used and whether the interactions with the surrounding concrete is accounted for or not, see Section 3.3.6 for modelling of bond interaction.

3.3.6 Interaction between reinforcement and concrete

The interaction between reinforcement and the surrounding concrete is usually referred to as the bond between the two materials; see Figure 3.14 for schematic illustration. In conventional (Level I and II) calculations, the strain in the reinforcement bar and the concrete interacting with the bar is assumed to be the same. However, in reality, for stresses to be transferred between the materials a certain slip between the materials is required. When the reinforcement is modelled to fully interact with the surrounding concrete, i.e. no slip between reinforcement and concrete nodes, this is often referred to as "perfect bond". This is also the method used in assessment Level III and IV.

Often it may be sufficient to limit the Level of detailing by making use of a perfect bond assumption. One advantage of this approach is that it is easier to make the FE model in such a case. However, by including the effect of bond interaction in the model (i.e. assessment Level V) the following advantages will be obtained.

- Effect of anchorage is automatically included in the model, making the need for explicit check of anchorage unnecessary. In a case when anchorage is critical for the structure studied this may be an essential addition to the model.
- The crack pattern obtained in the FE analysis will be less dispersed since cracks will more easily localise within a limited region. This will also affect the choice of crack band width l_{cr}, see Section 3.3.2, and may also make it easier to reach convergence.

When the interaction between reinforcement and concrete is modelled using a bond-slip relation (Level V), see Appendix A for possible relations to use, the influence of anchorage is automatically accounted for in the analysis. However, even if perfect bond is assumed (Levels III and IV) it is still possible to approximately take into account the risk of anchorage failure in the analysis. Figure 3.15 shows schematically how the FE model can be adapted to achieve this. Here, the effective reinforcement area, i.e. the area corresponding to the tensile force the reinforcement can carry with respect to yield strength f_y and anchorage capacity, has been determined in a concrete slab with curtailed reinforcement based on required anchorage length l_b. Based on this it is possible to approximately model an effective reinforcement amount using $A_{s,mod}$. In what detail this is done depends on the element mesh; the finer the mesh the better approximation is possible.

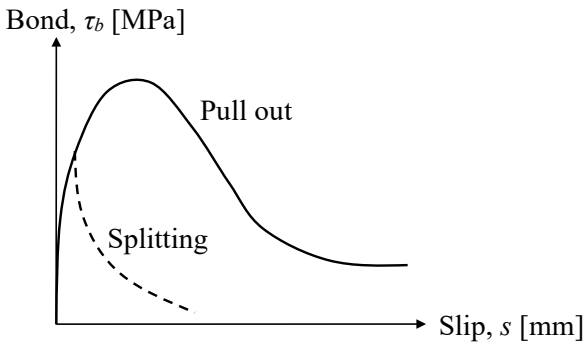

Figure 3.14 Schematic bond-slip relation between reinforcement and concrete.

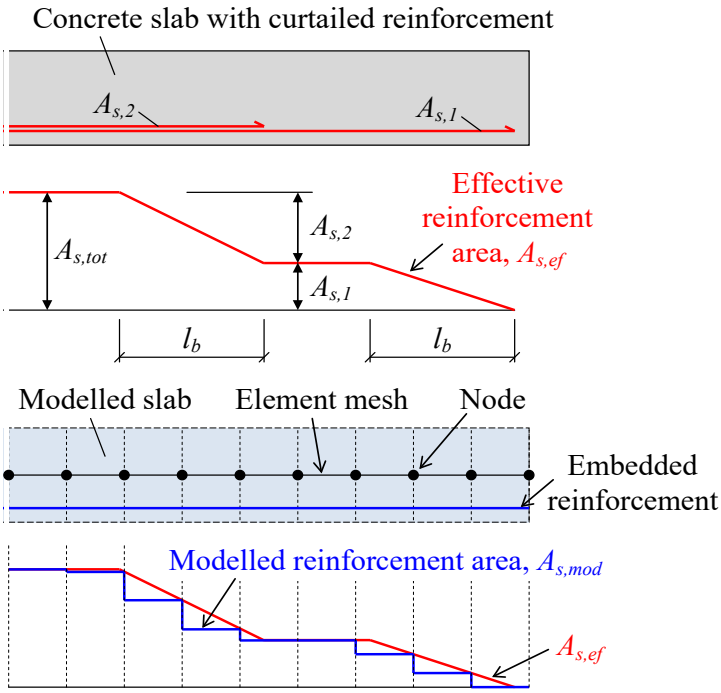

Figure 3.15 Illustration of how the effect of bond approximately can be taken into account in a Level II-IV analysis. Based on anchorage length l_b, the effective reinforcement amount can be determined and approximately modelled.

The effective reinforcement area can be defined as

$$A_{s,ef} = \frac{\sigma_{s,anchored}}{f_y} \cdot A_s \tag{3.4}$$

where $\sigma_{s,anchored}$ is anchored stress and A_s is the nominal reinforcement area.

If the reinforcement is modelled with gradually reduced cross-sectional area along the anchorage length in anchorage and splice regions, as schematically illustrated Figure 3.15, the anchorage capacity do not need to be checked separately. An anchorage failure will instead appear in the analysis as a bending failure in the anchorage region. However, if the anchorage failure is connected with splitting of the concrete cover, the analysis may show a more ductile response than if the anchorage failure had been modelled in detail. Consequently, as a conservative estimate, the load carrying capacity is suggested to be limited to the onset of reinforcement yielding in the anchorage zone.

Modelling of the bond-slip relation requires that an independent connection between the reinforcement and the surrounding concrete is provided for. This may be done in various ways of which two are schematically illustrated in Figure 3.16. Here, special interface elements or non-linear spring elements are used to connect the reinforcement with the concrete. The figures shown here are based on connection to 2D continuum (solid) elements but the same concept holds true also for 3D continuum elements. If the bond-slip response is included in the model, the mesh density used is important

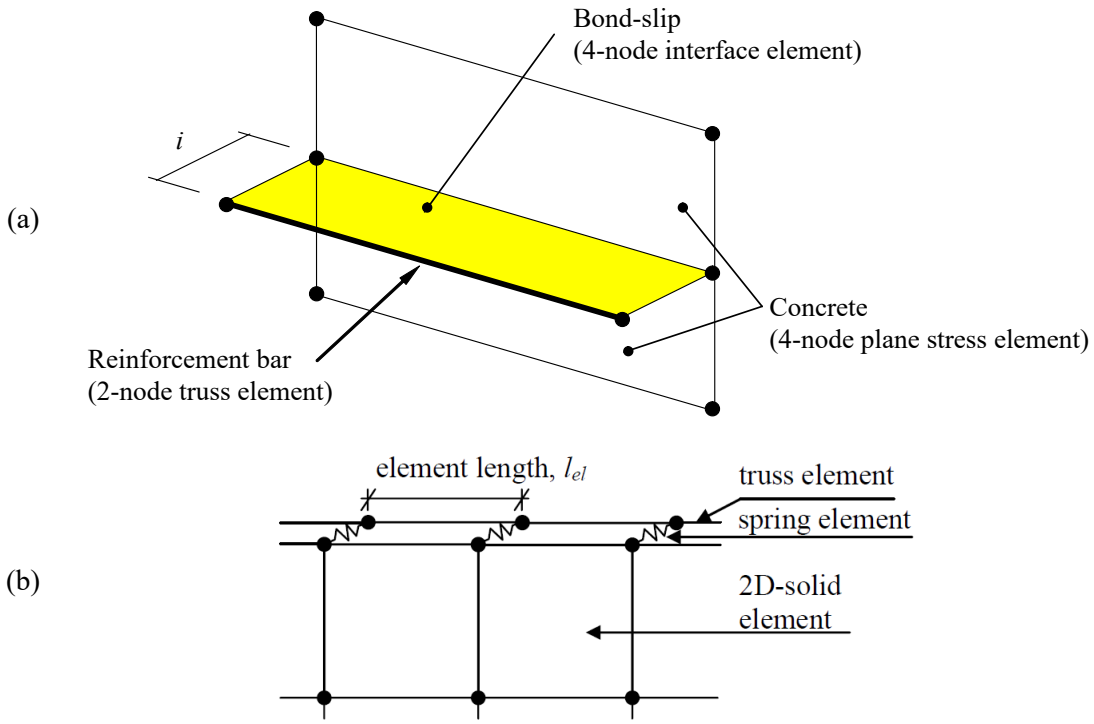

Figure 3.16 Examples of how to model the interaction between reinforcement and concrete using (a) interface elements, or (b) non-linear spring elements. From Johansson (1996) and Nesset and Skoglund (2007).

since there has to be a certain number of integration points between cracks to correctly describe localised cracking. Consequently, if the mesh is too coarse, it is not worthwhile to include bond in the model.

Note, that when using spring elements to model the bond interaction, stiffness need to be provided for each direction in a given node; i.e. the bond-slip relation is used in the bar´s longitudinal direction but stiffness also needs to be provided in the perpendicular directions (e,g, using constraints or springs). For an interface element, though, this is not needed since the perpendicular stiffness in such elements is provided automatically. Further, non-linear spring elements are often non-linear elastic, see Figure 3.2a, which means that the response will be incorrect at unloading if the slip is large. Hence, when using this technique to model the bond one should be attentive for such possible effects when large slip values are obtained.

Often the inclusion of bond-slip relations in the model requires that individual bars (or group of bars) are modelled using separate elements. However, depending on the software used, it may also be possible to include the effect of bond-slip relation when using embedded reinforcement.

3.4 Modelling recommendations

3.4.1 Element order

In linear FE analyses it is often recommended to use elements of higher order since they are more effective in describing the response, Hughes (1987). However, in non-

linear FE analyses this is not necessarily the case; this depends on the type of response that is to be described. For concrete, where localisation of deformations occurs when concrete cracks, and in compression if maximum strength is reached, elements of first order may be preferred. The reason for this is that low-order elements more easily can describe a local and sudden change of displacement, i.e. a crack, within an element.

It should be noted, though, that the concept of choosing element order in a non-linear FE analysis of a reinforced concrete structure is complex. In (Shams-Hakimi, 2012) it was found that using higher order elements was preferred in a Level III (shell elements) analysis, Further, in Hendriks *et al.* (2017) it is stated that higher order elements should be used (quadratic 8-node quadrilateral elements in 2D and 20-node hexahedron in 3D) when using continuum elements (Level IV and V); if necessary also quadratic triangle (2D) or tetrahedral (3D) may be used. It is argued that quadratic elements are better suited since they can describe more complex failure modes such as shear failure. On the other hand, if using an explicit solution method, using higher order elements is not an option and first-order elements with a reduced integration scheme must instead be used.

Hence, the recommendations given above at least partly contradict each other and are not suitable or even possible to use in all situations. What element order to use can also be much influenced on what software is used, see Broo *et al.* (2008), and therefore it is difficult to give too general advice of what element type should be used. The recommendations in the first paragraph are based on the authors' experience running non-linear FE analyses using the software DIANA. Nevertheless, to minimize compatibility problems, the shape functions of the elements used to model the reinforcement should be as similar as possible to that of the elements used for the concrete; i.e. elements used to model reinforcement bars in concrete should be of the same order as the concrete elements used.

3.4.2 Integration points

The stresses obtained in an element are based on the displacement of the element´s nodes and are determined in the integration points. In the post-processing, e.g. for contour plotting, these results may, by the software, be interpolated and extrapolated to other parts of the element as well. However, the response of the element depends on what happens in the integration points of the element. This means that the location of the integration points will influence the response of a concrete cross section; e.g. whether an element will crack or not, or which compressive stress that will be reached in an element in the compressive zone of a section subjected to bending.

In linear FE analyses it is common to use a Gauss integration scheme (often the default choice), with positioning of the integration points as indicated in Figure 3.17. This works well in a linear analysis, but in a non-linear analysis of a concrete structure it may not be as suitable. In Figure 3.17 it can be seen that the integration points in Gauss integration is located within the element; i.e. not at its edges. This means that if such an element is subjected to bending the integration points will not be able to correctly describe the maximum stress in the element. Consequently, if it is important to correctly describe when e.g. the cracking of the structure is initiated it may not be adequate to use Gauss integration. This problem may perhaps be

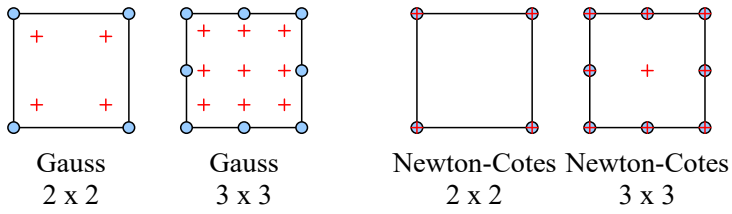

Figure 3.17 Location of integration points in Gauss integration and Newton-Cotes integration schemes. Based on Bathe (2016).

adequately solved using smaller elements, i.e. reducing the difference in stress at the element edge and in the integration point. Another way could be to change the integration scheme to e.g. Newton-Cotes; thereby, changing the location of the integration points from the interior to the element edges. If using reduced integration in a first order element, only one integration point (1x1), located in the centre of the element, is used. Hence, to counter unwanted effects of not having integration points at the element edge, the element size used must be reduced.

In a section subjected to bending, the number of integration points used will determine how well the material response is captured in the model. In Figure 3.18 this is exemplified using a shell element with 3 or 7 integration points in the element´s thickness direction. For this, Simpson integration is often used. To describe a linear elastic response (assessment Level II), 3 integration points in the thickness direction would be enough. To describe the non-linear response of cracked concrete or concrete in compression, though, a larger amount of integration points would be needed. Depending on software, there may be an upper limitation of what number of integration points may be used; in a Level III assessment, though, it is recommended not to use less than 7 integration points in the thickness direction. If few integration points are used and the compressive zone in the bent section is small, this might cause problems for the model since the correct response of the concrete in compression might not be adequately described.

As pointed out in Section 3.3.2 the number of integration points may, depending on the material model used, affect the crack band width l_{cr} when determining the stress-strain relation of the crack's softening branch. Note that for a shell element this refers to the integration points in the element plane, i.e. the crack band width refers to the localisation in the plane of the element.

If using an explicit solution method, see Section 3.2.2, elements of the first order with reduced integration will be used. In such a case special measures need to be taken to avoid so called hour-glass modes; see e.g. Malm (2016) for more information.

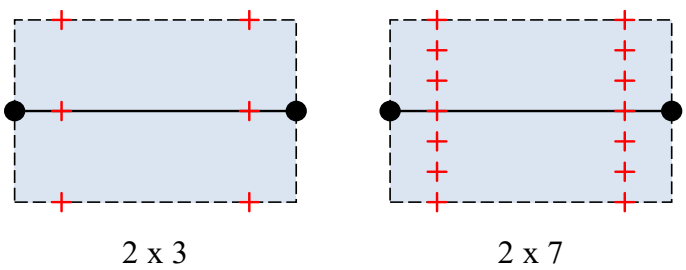

Figure 3.18 Integration points in shell element in thickness direction.

3.4.3 Mesh influence on crack pattern

In a non-linear analysis cracks tend to follow the direction of the element edges (Rots, 1988; Shu *et al.*, 2014; Slobbe *et al.*, 2013; Gottsäter *et al.*, 2019), see Figure 3.19 for an example of effect of crack propagation. Consequently, the crack pattern experiences a certain degree of locking effects that may cause it to become incorrect, which in turn may affect the total structural response. One way to counter this effect is to use triangular or tetrahedral elements rather than rectangular or quadrilateral elements for 2D and 3D models, respectively. Thereby, it will be easier for the cracks to form in the diagonal direction and a more correct crack pattern may be obtained.

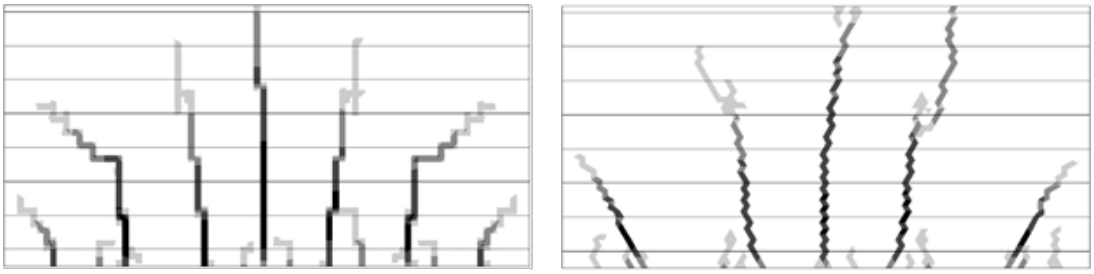

(a) (b)

Figure 3.19 Effect on diagonal crack cracking in a base restrained wall subjected to restraint loading when using a (a) rectangular, or (b) triangular mesh. Based on Gottsäter et al. (2019).

3.4.4 General advices

In this Section general advices of running nonlinear FE analysis of reinforced concrete structures are provided. These advices are based on the authors' personal experiences and are sorted in separate parts:

Model size and load application

- To save computational time there is an advantage if the size (i.e. amount of degree of freedom) of the model used can be restricted as much as possible. Often, it is possible to make use of symmetry lines or making geometrical simplifications to minimize the model size. It may also be possible to model parts of the structure using a detailed mesh (e.g. shell or continuum elements) and adjoining parts using a less detailed mesh (e.g. beam elements).
- To avoid unrealistic stress concentrations, distributed loads and boundary conditions can be used.

Default values and settings

- Make sure to understand the default settings used in the software, i.e. do not assume that all default settings are optimal for the problem presently studied.
- Make sure you understand what different settings in the software used mean and what effect they have on the analysis; it is easy to misunderstand the information given in the manual. Also be aware that the manual might be incomplete or that there may be bugs in the software.

Iteration and tolerances

- Be aware of what iteration method, tolerance type(s) and tolerance value(s) are used in the analysis.
- Make sure to know how to get tolerance information of iterations within a load increment, i.e. to find out how close/far from reaching convergence the iteration is.
- Increasing the number of iterations allowed may help. Often the default value is set to a low number (e.g. 10 iterations) but based on experience it may sometimes take more than 100 iterations to reach convergence.
- It can be worthwhile both increasing and decreasing the value of the tolerance used. Using a smaller tolerance (i.e. tougher demand) may decrease the amount of potential convergence problems later in the analysis. Using a larger tolerance may make it possible to get through a local convergence problem. However, if using a concept of an increased value, a return to a normal tolerance value is recommended when this is possible. Further, when increased tolerances are used, the quality control of the analysis results and the structural response achieved becomes even more important.
- Iteration methods based on the secant stiffness, see Figure 3.4, has often proven to be more robust to reach convergence.

Sensitivity checks

- Be aware of what effect the element mesh used have on your results; make at least one check with a different element mesh, e.g. divide or multiply element size with two in all directions. If applicable, it is important to adjust the material parameters for the adjusted model with respect to the element size dependency of the stress-strain relationship for concrete in tension and compression,
- Make simplified checks of your results. Often it may be difficult to correctly interpret exactly what a certain material model does. In such cases it is advised to make a very simple model (of just one or a few elements) in which the concept of interest may be tested. Performing such tests is often very effective to better understand the material model used.

Convergence problems

- Changing size of the load increment used may help to avoid convergence problems. Both a decrease and an increase of the load increment may have positive effects.
- Last successful increment may not always be fully trusted. If restarting an analysis to continue from a successful increment, do not start from the last one.
- Strive to find a physical explanation in the analysis of why convergence is not reached; looking at the incremental deformation in the last successful increment may help. It may also be helpful to change one model parameter at a time, e.g. fracture energy or compressive strength, to find a physical explanation of why convergence is not reached.

3.5 Quality control

The analyses should be verified in various aspects, i.e. both the capability of the FE program and the modelling method used to describe the behaviour, and that the actual FE model is correct should be verified. The description below is to a large extent based on Broo *et al.* (2008).

The FE software, including its element types and material models should be documented and verified by the software developer. However, in addition to that, the capability to simulate different types of responses should be verified. The modelling method used, made up of a specific combination of elements, material models, modelling of reinforcement etc. on a chosen level of detailing also need to be verified by comparison to experiments. Such verifications can either be done by the user or be based on relevant comparisons found in the literature, see e.g. Broo (2008), Belletti *et al.* (2018a, b) or Veganzones *et al.* (2019).

The verification of the actual FE model is recommended to be done in three steps:

- Graphically examine the model before any analysis is done. The following are examples of what is recommended to be checked:
  - Geometry
  - Boundary conditions (including possible rigid links and constraints)
  - Element mesh
  - Applied loads
  - Reinforcement (location, orientation, amount)
  - Material properties
  - Global and local orientations in elements used
- Analyse simplified cases to simplify comparisons to hand calculations, e.g.:
  - Linear analysis
  - Applying only the self-weight
  - Applying only concentrated load
- When performing the actual analysis, the results should be verified in different ways. Make sure that the results appear to be reasonable; if possible, compare with results from hand calculation and lower assessment levels or real measurements:
  - Deformations (shape and magnitude)
  - Support reactions
  - Cracking load
  - Crack pattern
  - Distribution of stresses, moments etc.
  - Ultimate capacity [4]

When choosing what results to look at, it is important that the whole response of the structure is studied, from initial loading and cracking to failure. By comparing different results, such as the load versus deformation response with crack pattern and stress in the reinforcement, the structural behaviour can be better understood. Sometimes, this can provide necessary information to make it possible to use analytical methods more correctly.

[4] Using an upper and a lower bound plastic analysis (i.e. yield line method and strip method, respectively), a good idea of the ultimate capacity of a RC slab can be obtained.

For the ultimate limit state, both the load-carrying capacity and the failure mode are important. For the serviceability limit state, the following items are examples of what can be of interest:

- Deformation
- Crack width
- Concrete compressive stress
- Reinforcement steel stress

4 Simplified and linear analysis (Levels I & II)

4.1 General.

A structural assessment is commonly started by an initial assessment based on existing documents, including inspection protocols and possibly a site visit, see Figure 2.1. Here, the structural assessment of a concrete slab is made using simplified analysis methods corresponding to **Level I** in *the Multi-Level Assessment Strategy*, see Figure 2.3. Traditionally, this has been the common level used for structural assessment. Today, this level is suited for rough calculations in the initial stage, aimed to indicate whether a more thorough assessment is needed. For this purpose, the assessment is preferably made for a limited number of load combinations that are considered critical. In this report, assessment on Level I is recommended for such an initial assessment with the aim to judge if there are doubts regarding a structures' safety, capacity, function or condition.

If sufficient load-carrying capacity cannot be shown, a continued structural assessment is needed. The next step is to perform a complete assessment, including all possible actions (loads) and combinations of actions. This is preferably made using a 3D linear analysis; with a three-dimensional model, the geometry of the structure is sufficiently well captured, and a linear analysis allows combination of loads to find critical load cases in a rational manner. For concrete slabs, 3D linear shell FE analysis corresponding to **Level II** in *the Multi-Level Assessment Strategy* is recommended.

In both Level I and II, the analysis of the structure is used to determine the action effects in the slab, normally expressed as cross-sectional forces and moments. The action effects are then compared to corresponding local cross-sectional resistances, determined according to common engineering practice. In a linear analysis, the action effects can be combined after the analysis is made, in the same way as the actions are combined, since the relation between an action and its action effect is linear. This makes it possible to first make an analysis for each action separately. The maximum action effects (together with simultaneously occurring other action effects) are then determined for all cross-sections and possible failure modes by combining the separate action effects in accordance with the design combinations of actions.

For assessment of existing structures, the actions acting on the structure and the design combinations of actions are commonly specified in national codes. The corresponding cross-sectional resistances are generally determined according to standards for design of structures, like e.g. the Eurocode 2 (CEN, 2004a). National standards or codes may also give specific demands or specify alternative resistance models for assessment. The partial safety factor (PSF) method is used to secure the required reliability level.

It should be noted that a linear 3D analysis on Level II will not always result in a higher demonstrated load carrying capacity than an analysis on Level I. If the structure originally was designed assuming a different stiffness relation between the main directions (due to different reinforcement amounts in the different directions) than the one given by the linear analysis, an analysis based on plasticity on Level I may very well show a higher load carrying capacity than a linear Level II analysis. This shows the importance of taking into consideration how the structure originally was designed when making a structural assessment.

When the structure is deteriorated due to, for instance, reinforcement corrosion or frost damage, the structural effect of the deterioration needs to be counted for in structural analyses and local resistance models. At analysis Levels I and II, the action effects will only be affected if the (concrete) material stiffness is affected. In the cross-sectional resistance models, reduced material strength as well as concrete spalling and reduced reinforcement cross-section area can also be taken into account. The reduction of bond between concrete and reinforcement can be accounted for in the calculation of anchorage capacity. Directions and references are given in Section 2.5 and Appendix B – E.

4.2 Simplified analysis methods (Level I).

To evaluate the action effects in ultimate limit state (ULS), analysis methods based on the lower bound theorem of plasticity can be used for assessment on Level I. A common such method is to simplify the load-carrying system by 2D linear beam or frame models with a pre-assumed load distribution between the main directions. For a reinforced concrete slab, this can be generalised to the strip method, see Hillerborg (1996). In both cases, the structural model is based on the lower bound theorem of plasticity, which means that it provides a conservative estimate of the load-carrying capacity, provided that the slab has sufficient plastic deformation capacity. The need for plastic deformations puts limits on how the load distribution can be made and how the strip (or load distribution) widths can be chosen. Recommendations on load distribution and strip widths are provided in handbooks like e.g. Hillerborg (1996) and in BBK 04 (Boverket, 2004). If such recommendations are followed, preliminary estimations of crack widths in serviceability limit state (SLS) can also be made using the same structural model.

The lower bound analysis can be complemented with an analysis based on the upper bound theorem of plasticity. For analysis of existing slabs, where the reinforcement content is known, the yield line method is well suited, Johansen (1972). Provided that the most critical yield line geometry is used, it gives a good indication of which load-carrying capacity that may be demonstrated with enhanced analysis methods with respect to bending. For two-way spanning slabs with distributed loads, there are also tabulated solutions based on linear slab analysis available in textbooks and handbooks for the distribution of load effects, e.g. Timoshenko and Woinowsky-Krieger (1959) and Betonghandboken Konstruktion (Svensk Byggtjänst, 1990). There are also influence surface diagrams available for concentrated loads on slabs, so called Pucher diagrams, Pucher (1973).

The cross-sectional resistances are determined by local models for bending, shear, punching and anchorage of reinforcement. Normally, standards like Eurocode 2 (CEN, 2004a) are used, but national codes may specify alternative resistance models. Similarly, crack widths are determined as action effects given the reinforcement available in the cross-sections and compared to crack width limitations in the standards or national codes. The calculations are normally made with material parameters specified in the standards or codes, based on material qualities specified in the documentation of the structure. If there are doubts regarding the material qualities, material parameters can be determined through standard tests on samples taken from the structure.

4.3 3D linear shell FE analysis (Level II)

4.3.1 General

For assessment on Level II in *the Multi-Level Assessment Strategy,* 3D linear FE analysis is used. The structural analysis is made with 3D FE models, most often based on shell or bending plate theory. Since the analysis is linear, the action affect from different loads can be superimposed, and the assessment can be made for all possible load combination with respect to all relevant failure modes throughout the structure.

Like the simplified lower bound methods described for Level I, a 3D linear FE analysis is theoretically based on the lower bound theorem of plasticity. The analysis provides a moment (and force) distribution that fulfils equilibrium. This means that, if the resistance is sufficient throughout the structure and the structure has sufficient plastic deformation capacity, the structure will have the required load-carrying capacity in ULS. In SLS, the use of linear elastic analysis is based on the assumption that the redistribution of moments (and forces) is limited.

In this report, for Level II analysis, it is recommended to follow Pacoste *et al.* (2012) regarding modelling, evaluation of results and distribution widths. The recommendations in Pacoste *et al.* (2012) are formulated for the design situation but are based on general principles and can be used also for assessment of existing reinforced concrete slabs.

Since both geometrical simplifications and the assumption of linear material response result in unrealistic stress concentrations, and since the reinforcement normally are arranged in strips with equal bar diameter and spacing, redistribution of the linear cross-sectional forces and moments are necessary. In Pacoste *et al.* (2012) recommendations are given on:

- Modelling of support conditions in a simplified, yet rational way,
- Choice of result sections to get representative action effects, and
- Choice of distribution widths over which the action effects can be distributed (averaged).

It also provides a special chapter on cantilever slabs, a common type of slab member in composite or concrete beam bridges.

4.3.2 Structural model

In the structural model, the concrete slab is commonly modelled by shell or bending plate finite elements, positioned in the system plane of the slab. In similar way, connecting structural elements and supports are recommended to be represented by elements or boundary conditions in their system planes or lines. It is important to ensure that support conditions are introduced in the model at their correct locations, acting in correct directions. In many cases, it is necessary to include connecting structural elements in the model in order to get correct action effects. The stiffness of the supports may also have a considerable influence on the results and need to be modelled with sufficient accuracy. More detailed recommendations for modelling of supports can be found in Pacoste *et al.* (2012).

To get sufficiently accurate results in support regions, or regions with dominating concentrated loads, the finite element mesh needs to be sufficiently dense here. In general, it is recommended that the mesh in this part of the slab should be dense

enough to provide at least one shell element (regardless of order) between the supported point or line and the critical *result cross-sections* for which the results are evaluated, further described in Section 4.3.3, see Pacoste *et al.* (2012).

4.3.3 Evaluation of load effects

For a slab modelled by shell (or bending plate) elements and supported along lines or in single support points, the FE analysis results will overestimate the action effects at the supports due to the simplification in geometry modelling. Instead, moments and shear forces must be evaluated in well-chosen *result sections* to get representative action effects. For example, if a column or abutment is supporting a slab in a single point, the slab moments and shear forces in this point will tend to infinity upon mesh refinement, see e.g. Sustainable Bridges (2007) or Hallbjörn (2019). In Pacoste *et al.* (2012) recommendations for choice of result sections are given. In Figure 4.1 some examples of recommended result sections are shown. As long as the results from these critical sections are used, and the finite element mesh is dense enough according to Section 4.3.2, the simplified way of modelling support conditions in discrete points or lines will not influence the design cross-sectional moments and shear forces.

However, not even the high stresses obtained at the critical sections do normally exist in reality. The concrete will crack already for service loads, and for higher loads the reinforcement will yield before maximum load is reached. This enables redistributions of the action effects in concrete structures, and the moments as well as the shear forces in a slab will redistribute over a certain width. The redistribution width that can be used to redistribute the sectional moment and shear force obtained from a linear analysis is in ULS limited by the slab's plastic deformation capacity, and in SLS by the redistribution occurring due to cracking. Recommendations on how to determine redistribution widths are given in Pacoste *et al.* (2012). Within the redistribution

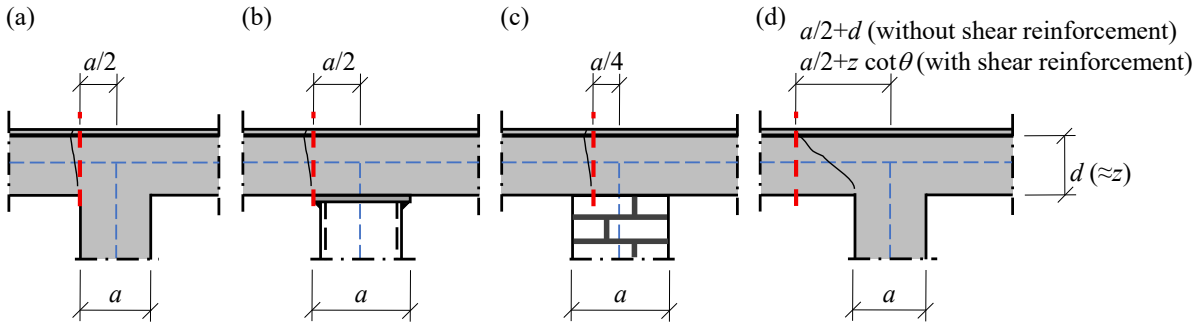

Figure 4.1 *Examples of result sections for Level II analysis:(a) bending moments for monolithic connection, (b) bending moments for rigid [5] simple support, (c) bending moments for weak[5] simple support (conservative approximation) and (d) shear force (independent of design and stiffness of the slab-support connection). From Pacoste et al. (2012).*

[5] Rigid and weak support, respectively, refers to the distribution of support pressure between the slab and the column head; a high stiffness of the column head in relation to the bending stiffness of the slab over the column (rigid support) will give high pressure at the column edge while the opposite (weak support) will result in a more equally distributed pressure over the support.

width, the average value of reinforcement moment and one-way shear force, respectively, can be used to assess if the slab provides sufficient resistance.

The recommendations in Pacoste *et al.* (2012) are written with design of new concrete slabs in mind, and the redistribution widths are typically used to design strips with constant reinforcement spacing. In the assessment situation, on the other hand, the amount and distribution of reinforcement is given. Here, the redistribution widths can instead be chosen based on the actual reinforcement layout, but within the limits given in Pacoste *et al.* (2012). To be rational, the areas with constant reinforcement spacings are chosen as redistribution widths.

4.3.4 Resistance models and load carrying capacity

As for Level I assessment, local resistance models are used for comparison with the action effects for possible failure modes. For slabs, the load-carrying capacity in ULS normally need to be evaluated with respect to bending, shear, punching and anchorage of reinforcement. The load carrying capacity is determined as the lowest load level for which the action effect equals the resistance for these failure modes. In SLS, it may be required to evaluate the response with respect to deflections and crack widths. Normally, the same resistance models as for Level I are used following Eurocode 2 (CEN, 2004a) or national standards or codes.

The bending moment resistance and the one-way shear resistance are compared to corresponding cross-sectional action effects, averaged over the chosen distribution width. The punching resistance is determined as the total resistance along a control perimeter representing the punching failure and is compared to the total shear force from the action that is transferred across the same perimeter. The tensile force capacity of the reinforcement, with respect to anchorage, is compared to the tensile force in the reinforcement caused by the action, in support and end zones of the slab and where the reinforcement is spliced or curtailed. The tensile reinforcement force caused by action is determined from the averaged moments and shear forces.

The resistance is normally determined with material parameters specified in the standards or regulations, based on material qualities specified in the documentation of the structure, or determined through standard tests on samples taken from the structure.

Bending crack widths can be evaluated by calculating reinforcement stresses for cracked cross-sections using the linear bending moment distribution from the linear analysis. Action effects in terms of crack widths are then calculated and compared to crack width limitations in the standards or national regulations. It should be noted that deflections cannot be obtained from the linear analysis since the stiffness reduction due to cracking is not taken into account. Rough estimates of the deflection can be made on one-way slab strips in the main directions, assuming a load distribution based on the distribution of load effects in the slab.

5 3D non-linear shell FE analysis (Level III)

5.1 General

Non-linear FE analysis has the potential to reveal higher load-carrying capacity in many cases where an assessment with conventional analysis methods on Levels I or II shows insufficient performance. A non-linear analysis might also give a deeper insight into the structural behaviour and can help in choosing a more correct simplified analysis model. For assessment of reinforced concrete slabs, it is recommended to start non-linear analysis with 3D shell FE analysis corresponding to **Level III** in *the Multi-Level Assessment Strategy*, see Section 2.3.

Like in Level II analysis, shell (or bending plate) finite elements are used. The reinforcement is included in the FE model but is assumed to have perfect bond to the concrete. With such an analysis, failure due to bending and in-plane forces will govern the maximum load-carrying capacity shown by the analysis. Consequently, out-of-plane shear, punching and anchorage failures must be checked by local resistance models. This can be made using higher *Level-of-Approximation* according to the Model Code 2010, fib (2013), based on the load distribution and deformations from the non-linear analysis.

A non-linear analysis is made for one particular combination of loads and simulates the response under successively increased loading. At the same time, a non-linear FE analysis is considerably more demanding to perform compared to a linear one. Consequently, the load-carrying capacity and structural response cannot be assessed for all possible load combinations. Instead, only the most critical load cases, identified at lower assessment levels, can be analysed with non-linear FE analysis. Which, and how many load cases that are to be evaluated through non-linear analysis need to be decided for each structure. The maximum utility ratios for different failure modes in different structural parts, determined at lower assessment levels, can be indicative for which critical cases that should be assessed through non-linear analysis.

Due to the increased effort to make non-linear analysis, it is important to evaluate if a more enhanced analysis is motivated. This is done by comparing the possible benefits of such an analysis, times the judged likelihood that the benefits will be reached, with the cost for the enhanced assessment. It is also important to compare the alternative of enhanced structural analysis with the gains from improved information, e.g. through inspections, monitoring and testing, and from improved safety verification, see Section 2.2. Often, improvement in all these three “dimensions” are needed to fully benefit from a non-linear analysis. For example, material tests may be needed to get sufficient input data for the non-linear analysis and a global safety factor method is needed to evaluate the load-carrying capacity.

For assessment on Level III according to *the Multi-Level Assessment Strategy*, the ECOV global safety factor method is recommended. To determine the global safety factor for the different failure modes, two non-linear analyses are performed with mean and characteristic material parameters, respectively.

Non-linear structural analysis has proven to be capable of describing the behaviour of deteriorated reinforced concrete structures in a comprehensive way, provided that appropriate constitutive models are adopted, see e.g. Zandi (2010). When the structure is deteriorated due to, for instance, reinforcement corrosion or frost damage, the structural effect of the deterioration can be directly accounted for in structural

analyses. In an analysis on Level III, the deterioration effect can be modelled as a change in:

- material properties of concrete,
- cross-sectional area of the structural member,
- material properties of the reinforcement steel, and
- cross-sectional area of the steel reinforcement.

Detailed recommendations are given in:

- Appendix B: Material properties of frost-damaged concrete
- Appendix C: Bond of reinforcement in frost-damaged concrete
- Appendix D: Material properties of concrete with corrosion cracking
- Appendix E: Bond for corroded reinforcement

5.2 Structural model and non-linear analysis

5.2.1 General

In a Level III analysis, the concrete slab is modelled by shell finite elements, similarly as for Level II. The main difference is that the reinforcement is included in the FE model and that non-linear material models are used for concrete and reinforcement. Generally, it is also recommended to include geometric non-linearity in the analysis since the out-of-plane deformation can become large in relation to the slab thickness, and the internal membrane forces are often not negligible.

5.2.2 Idealisation of the structure

In the same way as in a linear analysis on Level II, the slab is represented by elements that normally are positioned in the system plane of the slab. Adjacent structural parts, connected to the slab, are represented by elements modelled in their system planes or lines, respectively.

The reinforcement is preferably modelled as reinforcement layers within the shell elements of the slab, so called *embedded reinforcement* layers, see Section 3.3.5. Each layer of parallel reinforcement bars is represented by a reinforcement layer positioned in the centre-of-gravity plane of the reinforcement bars. Each reinforcement layer provides stiffness in the direction of the bars only, while its contribution to the stiffness in the perpendicular direction is zero.

In order to take the risk of anchorage and splice failure into account in the non-linear analysis, the *embedded reinforcement* can be modelled with gradually reduced cross-sectional area along the anchorage length, as described in Section 3.3.6. With this modelling method, an anchorage or splice failure will, in the non-linear analysis, appear as a bending failure in the anchorage or splice zone.

Modelling the reinforcement as *embedded reinforcement* means that the bars do not have degrees of freedom of their own and thus cannot be subjected to external loads, such as pre-stressing forces. However, prestressing may be specified explicitly as initial stress; the analysis must then start with iterations to find equilibrium. This means that this modelling option will much resemble pre-tensioning. However, some FE software have special options to resemble post-tensioning, (Broo *et al.*, 2008)

The boundary conditions often have a large influence on the response. Boundary conditions are also generally modelled in a simplified way, as free or fixed degrees of freedom in different directions. The simplifications introduced have largest influence locally, in the vicinity of the boundary condition. Consequently, it is important to include a sufficiently large part of the structure in the structural model. It is often not enough to just include the slab to be assessed itself. The stiffness of supporting structures and foundations are also often important to include but can often be represented by linear or non-linear springs.

Also, it is important that support conditions are specified at correct locations, acting in correct directions. For example, if a bearing provides a horizontal support for a slab, the boundary condition should generally act at the level of the bearing and not at the centre of the slab. To connect the boundary conditions to the slab, rigid links or stiff beam elements with no density can be used, see Figure 5.1. In some FE software it is also possible to specify an eccentricity to a boundary condition defined in a node of the slab.

In contrast to a linear analysis, it is important to model supports and connections so that singularities are avoided. Since non-linear material models are used in the analysis, local material failure will otherwise occur before a realistic failure load is reached. Figure 5.2 shows two alternatives of how a roller bearing support with a stiff

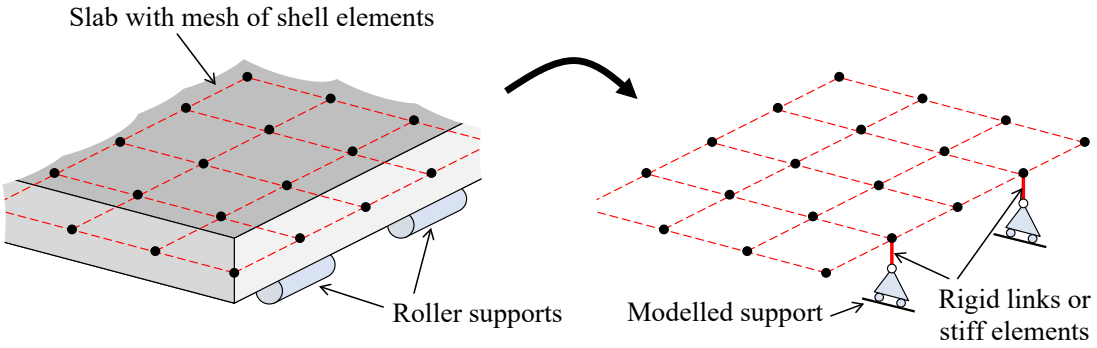

Figure 5.1 *Example showing how rigid links or stiff elements can be used to model boundary conditions at correct positions (and acting in correct direction).*

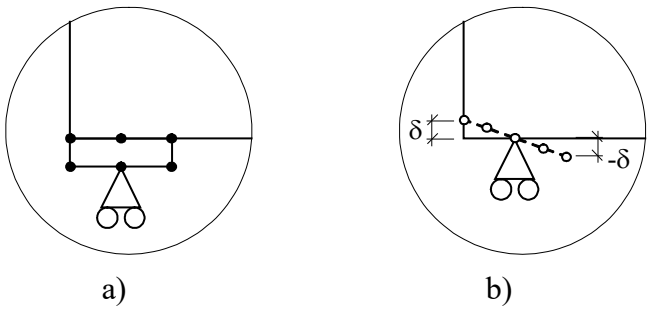

Figure 5.2 *Modelling of a roller bearing with a load-distributing support plate. (a) The support plate is modelled with FE elements. (b) The support plate is modelled by forcing the nodes on each side of the support plate to have the same vertical displacement but in the opposite direction. From Broo et al. (2008).*

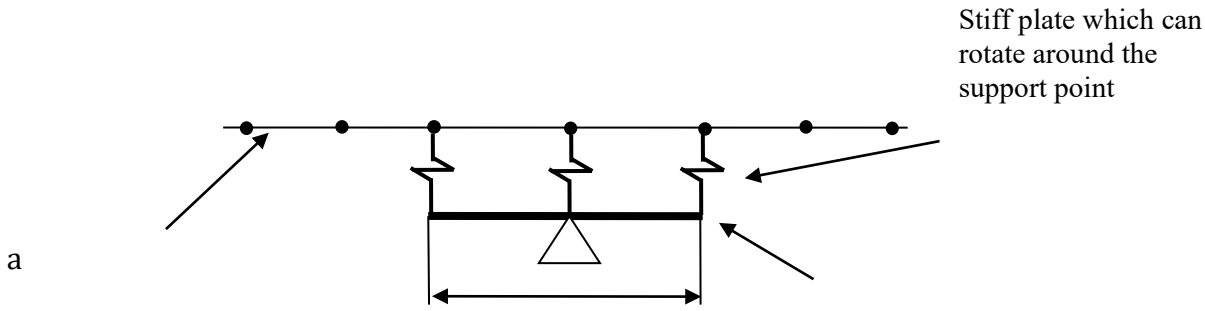

Figure 5.3 Elastomeric bearing support modelled with spring elements. Adapted from Pacoste et al. (2012).

support plate can be modelled. Figure 5.3 shows an alternative of how to model an elastomeric bearing using springs representing the stiffness of the bearing. In all of these cases, unrealistic high support pressure leading to premature crushing of the concrete is avoided.

5.2.3 Material models

In a structural model for Level III, the bending response must be realistically simulated throughout the analysis. Deformations and the overall cracking response must be captured so that the extension of the cracked regions and crack directions are reflected, even if individual cracks cannot be identified. Furthermore, the bending failure possibly limiting the load carrying capacity of the slab must be reflected. A bending failure is typically developing gradually through evolution of yield lines, and the load-carrying capacity is typically limited by concrete crushing or reinforcement rupture in the critical part of the yield line. Consequently, it must be possible to follow the local cross-sectional response well beyond yielding through the hardening of the reinforcement, and throughout the crushing of concrete in the compression zone. Furthermore, the distribution of shear forces in the structure must be reflected in a realistic way, even if a shear failure cannot be captured. This brings certain requirements on the material models used for concrete and reinforcement.

For concrete in tension the material model needs to describe the crack response in the normal crack direction, while the response in shear is of less interest on Level III, see also Section 3.3.2. This means that fixed as well as rotating and plasticity-based crack models may be suitable. However, fixed crack models assuming orthogonal crack directions have shown limited capacity in reflecting typical yield line patterns for two-way slabs and are consequently not recommended. The use of *embedded reinforcement* layers with perfect bond to surrounding concrete will result in a diffuse crack pattern where individual cracks are not reflected; instead all elements in the regions where cracking occur will generally be cracked. Consequently, it is recommended to approximate the crack band width to be equal to the mean crack spacing, $l_{cr} = s_{rm}$, see Section 3.3.2.

For concrete in compression the material model should describe the non-linear response up to maximum concrete compressive strength as well as the softening behaviour due to concrete crushing. To avoid mesh sensitivity at compression failure localisation, it is recommended to base the softening response on the fracture energy

in compression, as described in Section 3.3.3. For bi-axial compression, the compression strength of concrete is increased, and it is beneficial if this is included in the material model. It is important that the reduced compressive strength and stiffness of concrete cracked due to tensile strains perpendicular to the compression is accounted for in the material model, see Section 3.3.3. There is otherwise a risk for un-conservative results overestimating the load-carrying capacity in the analysis.

The reinforcement has a uni-axial response in the analysis, and it is sufficiently to specify the uni-axial stress-strain relationship properly for the reinforcement. The tension hardening of the reinforcement after yield initiation is important to include in the analysis, together with the maximum hardening strain, see Section 3.3.5. A softening branch for even higher strains can be beneficial to include, to be able identify reinforcement rupture.

It is recommended to not include the so-called tension stiffening effect in cracked concrete by modifying the stress-strain relation for concrete in tension, see Section 3.3.2.

For the cracked reinforced concrete, the overall Poisson's effect will be very small. Consequently, it is important to include a reduction of Poisson's ratio for concrete due to cracking. It is recommended to set the Poisson's ratio to $\nu = 0$ after cracking, see Appendix A. If the FE software do not provide the possibility for reduction of Poisson's ratio at cracking, it is recommended to use $\nu = 0$ throughout an analysis on Level III used to determine the load-carrying capacity.

5.2.4 Material parameters

As discussed in Chapter 3, a non-linear analysis, with non-linear material models for concrete and reinforcement steel, requires that many material parameters are specified as input data to the analysis. In addition to the material stiffness parameters, used also in linear analysis, and the material strength and strain limit parameters, used in common resistance models, additional material parameters are needed to describe e.g. the entire stress-strain response including material failure and the multi-axial response.

Recommendations for determination of material parameters are given in Appendix A. Here, it is described how material parameters can be estimated based on the given material quality based on standards, codes and handbooks like e.g. Eurocode 2 (CEN, 2004a) and Model Code 2010, fib (2013).

In many cases, it is motivated to determine the key material properties through material tests on samples from the structure to be evaluated, before doing a non-linear analysis. In-situ values for material parameters such as stiffness and uni-axial strengths can be evaluated through standard tests. It may also be motivated to determine the strain hardening response and ultimate strain for the reinforcement and the fracture energy for the concrete from material tests. Based on the material parameters determined through tests, the additional material parameters can be determined using the relations given in Appendix A.

5.2.5 FE modelling

Non-linear shell elements are used to model the slab, while non-linear or linear shell or beam elements can be used for adjacent parts included in the model, depending on their geometry and response. Both first and second order shell elements may be feasible for analysis on Level III. In the examples in Chapter 7, 8-node second order elements were used. Second order elements are generally good in capturing the bending behaviour also after concrete cracking. Furthermore, since the slab reinforcement is modelled as reinforcement layers on this level of analysis, no crack localisation is expected in the analysis.

Depending on the geometry of the structure and the expected crack pattern, quadratic or triangular elements may be feasible. In the examples in Chapter 7, quadratic elements were used. However, even though a Level III analysis results in a diffuse crack pattern, regular quadratic element meshes has a tendency to influence the crack pattern, and subsequently also the yield lines, to follow the element orientation, see also Section 3.4.3.

To reflect the bending behaviour of the concrete slab after cracking, it is important that the compression zone of the concrete cross-section is well represented in the analysis. Consequently, an integration scheme with integration points at the surface of the shell element should be used, with a sufficient number of integration points in the thickness direction, see also Section 3.4.2. In general, a lower reinforcement ratio gives a smaller compression zone, and hence more integration points are needed. It is recommended to use a minimum of 7 integration points over the slab thickness.

The size of the finite elements must be sufficiently small (or, in other words, the FE mesh must be sufficiently dense) in order to get correct results from the analysis. A general recommendation is that the element sizes should be chosen such that a relatively smooth stress (or sectional moment) field is achieved, Hendriks *et al.* (2017). Stress concentrations may particularly occur at support regions, sharp corners and other irregularities. However, compared to a linear analysis, the stress concentrations will be less pronounced in a non-linear analysis. Due to the non-linear response with concrete cracking and reinforcement yielding, stresses will be redistributed in the analysis. However, in a non-linear analysis on Level III, the moment capacity is evaluated directly from the FE analysis, without any redistribution of the action effect as in a linear analysis on Level II. Consequently, the recommendations on element sizes given in Pacoste *et al.* (2012) are not applicable in a non-linear analysis.

It is recommended to verify the chosen FE mesh by comparison to a corresponding model with higher mesh density, see Section 3.4.4. For a Level III analysis, it is recommended to compare deflections, moment distribution and failure mode in such a verification.

5.2.6 FE analysis

In a non-linear analysis for assessment of the load-carrying capacity, the structure is typically subjected to successively increasing static loads until structural failure is reached. Generally, the non-linear geometrical response needs to be taken into account for slabs; this is normally specified as a part of the definition of the analysis procedure.

In Section 3.2, the analysis procedure for non-linear analysis is described. In the analysis, the loads of the load combination studied are applied in steps to describe the loading history of the structure, see Section 2.4.7. For example, the permanent loads are applied first in one or several steps to simulate the construction, followed by the variable loads in one or several steps. Within each step, the load is applied in increments. In the ultimate analysis step, where structural failure is reached, it is recommended to use displacement-controlled loading, see Section 3.2.3.

As described in Section 3.2.2, equilibrium can be controlled in the analysis using an implicit or an explicit solution method. When an implicit solution method is used, it must be ensured that the number of increments in each step is sufficient to capture the non-linear response of the structure with the successive development of cracking and failure mechanism in the slab. In Sections 3.2.2 and 3.4.4, recommendations are given on iteration methods, number of iterations allowed and tolerances for the FE analysis.

5.3 Evaluation of structural response

To evaluate the load-carrying capacity and structural response of a concrete slab, it is important to study the whole response of the structure. For a Level III analysis, the response from initial loading, through the cracking and development of reinforcement yielding to the final failure is of interest. By comparing different results, such as the load versus deformation response with crack pattern and stress in the reinforcement, the structural behaviour can be understood. The evaluation of structural response is also an important part of the quality control, further described in Section 3.5.

It is recommended that a detailed description of the structural behaviour, evaluated from the non-linear analysis results, is reported as a part of the assessment. For an analysis on Level III, such a description could typically include:

- A load-displacement relation that describes the overall response of the slab. For slabs with several spans, several diagrams may be needed to explain the structural behaviour.
- Figures showing the deformation of the slab at different stages of loading, including the deformation at maximum load.
- A description of the cracking development in the slab, illustrated by figures showing the crack pattern.
- A description of the development of reinforcement yielding, illustrated by figures showing plastic strains in the reinforcement.

The failure load is determined in two consecutive analyses with mean and characteristic material parameters, respectively, for evaluation of design load carrying capacity using the ECOV global safety method, see Section 5.4.1.

To assess the load-carrying capacity with respect to bending, it is necessary to be able to follow the response up to failure of the structure. For a reinforced concrete slab, a bending failure is typically preceded by development and expansion of yield lines. The bending failure is then governed by crushing of concrete or reinforcement rupture in the critical part of the yield line. The final result needed from the non-linear analysis is the failure load. Evaluation of design load-carrying capacity with respect to bending is treated in Section 5.4.2.

To assess the load-carrying capacity with respect to shear failure, the resistance is determined according to Model Code 2010, fib (2013). Here, the shear capacity is

expressed as a function of the longitudinal mid-depth strain, ε_x. Consequently, the relationship between shear force from the external load and the longitudinal mid-depth strain, ε_x, must be determined from the non-linear FE analysis. The total shear force transferred perpendicular across the control section for shear is determined as a function of the average mid-depth strain perpendicular to the same control section, for the analysis history. This relation must be determined from the non-linear FE analyses with mean and characteristic material parameters, respectively. The procedure of assessing the shear capacity is described in detail in Section 5.4.3.

In a similar way, the load-carrying capacity with respect to punching failure is determined using a resistance model from Model Code 2010, fib (2013). Here, the punching capacity is expressed as a function of the rotation of the slab, ψ, instead. Consequently, corresponding relationship between total shear force from external load, transferred across the basic control perimeter for punching, and the slab rotation, ψ, must be determined for the analysis history of the non-linear FE analysis. Also, this relation must be determined with mean and characteristic material parameters, respectively, in the analysis. Model Code 2010 don't give any detailed advices on how or where the rotation should be determined from the non-linear analysis, but it refers to the slab rotation over the region with a critical punching shear crack. The procedure of assessing the punching capacity is described in detail in Section 5.4.4.

The risk of anchorage or splice failure do not need to be checked separately if the reinforcement is modelled with gradually reduced cross-sectional area along the anchorage length, as described in Section 3.3.6. Instead, reinforcement yielding occurring in anchorage or splice zones can be interpreted as an indication of risk for anchorage failure. However, if the reinforcement is modelled with full cross-sectional area along its entire length, the risk for anchorage or splice failure must be checked separately. For this purpose, the cross-sectional moments and forces, or the force in the reinforcement, from the non-linear analysis is used. Assessment of anchorage capacity is treated in Section 5.4.5.

To assess the response in serviceability limit state (SLS), deformations and cross-sectional forces and moments from the non-linear analysis can be used. Non-linear shear related deformations are not correctly reflected in the analysis but are in general negligible in SLS and can be ignored. Assessment of response in SLS including crack widths is treated in Section 5.5.

5.4 Load-carrying capacity

5.4.1 Safety format

To evaluate the load-carrying capacity based on 3D non-linear shell FE analysis on Level III, the ECOV global safety factor method is recommended, see Section 2.4.4, with a model uncertainty factor according to Section 2.4.6.

To determine the global resistance factors, two non-linear analyses are performed: one analysis with mean material parameters as input to the analysis and one with characteristic material parameters. The global resistance factor with respect to bending failure is determined directly from the failure loads obtained from the non-linear analyses. The load-carrying capacity with respect to other failure modes are determined using separate resistance models on higher *Level-of-Approximation* (LoA) according to the Model Code 2010, fib (2013). Here, the global resistance factors are

determined separately for each failure mode based on the load-carrying capacity determined with input from the non-linear analyses with mean and characteristic material parameters, respectively. This is further described in following sections.

Independently of the failure mode, the coefficient of variation is estimated based on the mean and characteristic global structural resistances, R_m and R_k, determined based on the non-linear analyses, and in case of shear and punching, also the local resistance models. The coefficient of variation is calculated using Equation (2.4) and the global resistance factor is determined using Equation (2.5), with the sensitivity factor and the target reliability according to Model Code 2010, fib (2013):

$$V_R = \frac{1}{1.65}\ln\left(\frac{R_m}{R_k}\right)$$

$$\gamma_R^* = \exp\left(\alpha_R \beta V_R\right) = \exp\left(0.8 \cdot 3.8 \cdot V_R\right)$$

Finally, the design load-carrying capacity is calculated according to Equation (2.1) for each failure mode studied, with the model uncertainty for Level III analysis according to Equation (2.6)

$$R_d = \frac{R_m}{\gamma_R^* \cdot \gamma_{Rd}} = \frac{R_m}{\gamma_R^* \cdot 1.1}$$

As discussed in Section 2.4.7, the design load-carrying capacity will have different meaning depending on how the loading to failure is applied in the analyses. However, regardless of how the design load-carrying capacity is defined in the particular assessment performed, it is important that the failures in the analyses with mean and characteristic material properties, respectively, are reached under the same loading scheme (i.e. in the same loading step according to Section 2.4.7). If different failure modes are obtained, the ECOV method may result in an unconservative load-carrying capacity; in such cases, the safety format according to Schlune *et al.* (2011, 2012) need to be used instead.

5.4.2 Bending

To determine the design load-carrying capacity with respect to bending, the global resistance factor is determined based on the failure loads from the non-linear analyses:

- R_m is determined as the failure load in a non-linear analysis with mean material parameters, Equation (2.2), and
- R_k is determined as the failure load in a non-linear analysis with characteristic material parameters, Equation (2.3).

The global resistance factor and the design load-carrying capacity is then calculated following the ECOV safety format, as described in Section 5.4.1

It is important that the failure loads from the two analyses are comparable and determined in the same way. The failure mode should be similar, and the same failure criterions should be used. If it is not possible to follow the response up to failure in one of the analyses, the global safety factor will become wrong, and it will not be possible to determine the design load correctly. This can occur, for example, if convergence difficulties make one of the analysis stop too early.

5.4.3 Shear

For slabs without shear reinforcement, it is recommended to determine the design load-carrying capacity with respect to (one-way) shear failure using the *Level-of-Approximation* II (LoA II) for shear, according to Model Code 2010, Section 7.3.3, fib (2013). This resistance model is based on the Simplified Modified Compression Field Theory (Bentz et al., 2006). According to this model, the design shear resistance can be expressed as a function of the longitudinal mid-depth strain, ε_x (positive in tension) perpendicular to the control section for shear. For cracked sections without stirrups:

$$V_{Rd,c} = k_v \frac{\sqrt{f_{ck}}}{\gamma_c} \cdot z b_w \tag{5.1}$$

$$k_v = \frac{0.4}{1+1500\varepsilon_x} \cdot \frac{1300}{1000 + k_{dg} z} \tag{5.2}$$

$$k_{dg} = \frac{32}{16 + d_g} \geq 0.75 \tag{5.3}$$

Here, z is the internal level arm of the section,
b_w is the width of the control section studied,
f_{ck} is the characteristic concrete compression strength in MPa,
γ_c is the partial factor for concrete,
k_v is a factor for the mid-depth strain dependency,
k_{dg} is a factor to take the aggregate size into account and
d_g is the aggregate size in mm.

The control section is determined according to Model Code 2010. For a cantilevering slab with a line support, the position and width of the control section is shown in Figure 5.4. For determination of mean and characteristic shear resistances, the partial factor for concrete in Equation (5.1) is omitted ($\gamma_c = 1$), and for mean shear strength the mean concrete compression strength is used:

$$V_{Rm,c} = k_v \cdot \sqrt{f_{cm}} \cdot z b_w \tag{5.4}$$

$$V_{Rk,c} = k_v \cdot \sqrt{f_{ck}} \cdot z b_w \tag{5.5}$$

The shear force-mid-depth strain relation expressing the shear resistance is compared to the relationship between shear force and mid-depth strain determined from a corresponding non-linear FE analysis on Level III, expressing the action effect from

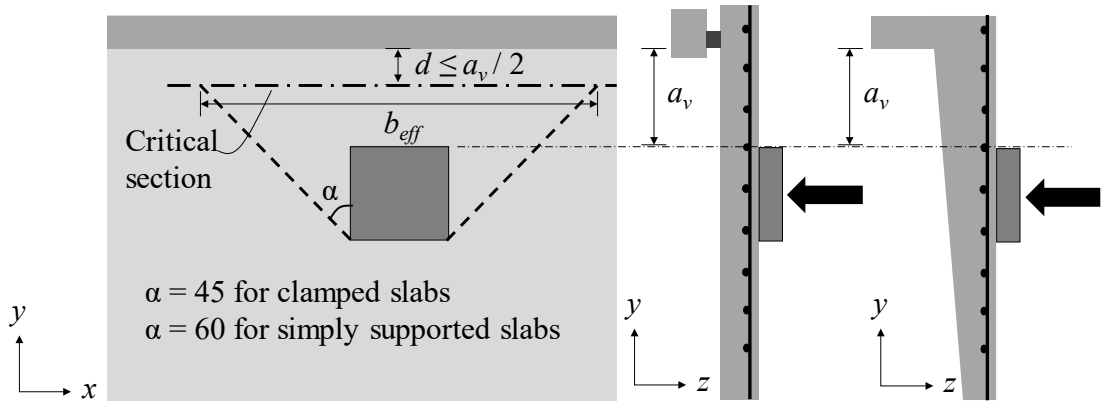

Figure 5.4 *Control section for a slab with a concentrated load, supported by a line support. Adapted from Model Code 2010, fib (2013). (The width of the control section, b_w, is here denoted b_{eff}.)*

external load as described in Section 5.3. The mid-depth strain from the non-linear analysis is evaluated for the mid-surface of the shell element. This comparison is exemplified in Figure 5.5. The shear force at the intersection between the curves represents the shear capacity, and the load applied on the slab at this shear force level represents the (global) structural resistance with respect to shear, R:

- The mean shear resistance, $V_{Rm,c}(\varepsilon_x)$, is compared to the shear force from an FE analysis with mean material properties, $V_{Em}(\varepsilon_x)$, to determine the mean structural resistance, R_m.
- The characteristic shear resistance, $V_{Rk,c}(\varepsilon_x)$, is compared to the shear force from an FE analysis with characteristic material properties, $V_{Ek}(\varepsilon_x)$, to determine the characteristic structural resistance, R_k.

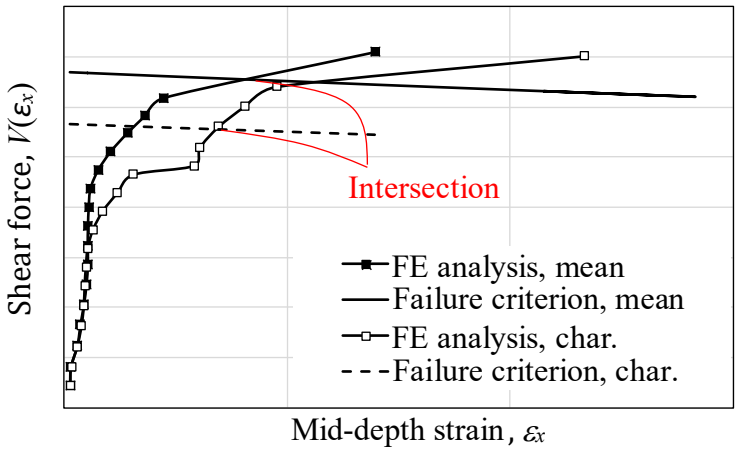

Figure 5.5 *Example of shear force - mid-depth strain relations describing the resistance and load effect, respectively, using mean and characteristic material parameters. The resistance (failure criterion) is obtained from Model Code 2010, fib (2013), and the load effect from a non-linear FE analysis on Level III. The intersections of the curves determine the mean and characteristic load-carrying capacity with respect to shear.*

If the shear force response never reaches up to the shear resistance curve, and an intersection point cannot be determined, this is an indication of that bending failure is reached before a shear failure occur.

Following the ECOV global safety format, the global resistance factor is calculated as described in Section 5.4.1, using Equations (2.4) and (2.5)**.**. The design load-carrying capacity is finally calculated according to Equation (2.1).

5.4.4 Punching

It is recommended to determine the design load-carrying capacity with respect to punching failure using the *Level-of-Approximation* IV (LoA IV) for punching, according to Model Code 2010, Section 7.3.5, fib (2013). This resistance model is based on the Critical Shear Crack Theory (Muttoni, 2008). According to this model, the design shear resistance can be expressed as a as a function of the rotation ψ of the slab. For cracked sections without stirrups:

$$V_{Rd,c} = k_{\psi} \frac{\sqrt{f_{ck}}}{\gamma_c} \cdot db_0 \tag{5.6}$$

$$k_{\psi} = \frac{1}{1.5 + 0.9 k_{dg} \psi d} \tag{5.7}$$

$$k_{dg} = \frac{32}{16 + d_g} \geq 0.75 \tag{5.8}$$

Here, d is the effective height of the section,
b_o is the length of the shear resisting control perimeter,
f_{ck} is the characteristic concrete compression strength in MPa,
γ_c is the partial factor for concrete,
k_{ψ} is a factor for the slab rotation around the support (or concentrated load) region,
k_{dg} is a factor to take the aggregate size into account and
d_g is the aggregate size in mm.

The effective height and the shear resisting control perimeter are determined according to Model Code 2010. The shear resisting control perimeter is based on the basic control perimeter, but accounts also for non-uniform shear distribution. The basic control perimeter is situated a distance $d/2$ outside the outer edges of a column or concentrated load and is constructed so that its length is minimised.

In the same way as for (one-way) shear, the mean and characteristic punching shear resistances are calculated from the mean and characteristic concrete compression strength, respectively, without including the partial factor for concrete ($\gamma_c = 1$):

$$V_{Rm,c} = k_{\psi} \cdot \sqrt{f_{cm}} \cdot db_0 \tag{5.9}$$

$$V_{Rk,c} = k_{\psi} \cdot \sqrt{f_{ck}} \cdot db_0 \tag{5.10}$$

Similar to (one-way) shear, the shear force-rotation relation expressing the shear resistance is compared to the relationship between shear force and rotation determined from a corresponding non-linear FE analysis on Level III, expressing the action effect.

The determination of this action effect from external loads is described in Section 5.3. This comparison is exemplified in Figure 5.6 The shear force at the intersection between the curves represents the punching shear capacity, and the load applied on the slab at this shear force level represents the (global) structural resistance with respect to punching, R:

- The mean punching shear resistance, $V_{Rm,c}(\psi)$, is compared to the shear force transferred across the basic control perimeter for punching, from an FE analysis with mean material properties, $V_{Em}(\psi)$, to determine the mean structural resistance, R_m.
- The characteristic punching shear resistance, $V_{Rk,c}(\psi)$, is compared to the shear force transferred across the basic control perimeter for punching, from an FE analysis with mean material properties, $V_{Ek}(\psi)$, to determine the characteristic structural resistance, R_k.

If the punching shear force from the non-linear analysis never reaches the shear resistance curve, an intersection point cannot be determined; this is an indication of that bending failure is reached before a punching failure occur.

Following the ECOV global safety format, the global resistance factor is calculated in the same way as for bending and shear failures using Equations (2.4) and (2.5), see Section 5.4.1. The design load-carrying capacity is finally calculated according to Equation (2.1).

5.4.5 Anchorage

There are two ways to check the risk of anchorage or splice failure based on a non-linear analysis on Level III:

If the reinforcement is modelled with gradually reduced cross-sectional area along the anchorage length in anchorage and splice regions, as described in Section 3.3.6, the

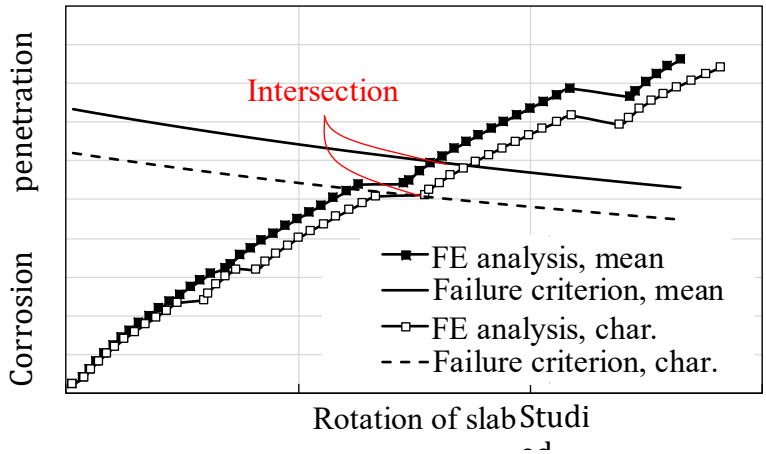

Figure 5.6 *Example of punching shear force-rotation relations describing the load effect and resistance, respectively, using mean and characteristic material parameters. The resistance (failure criterion) is obtained from Model Code 2010, fib (2013), and the load effect from a non-linear FE analysis on Level III. The intersection of the curves determines the punching shear force at punching failure.*

anchorage capacity does not need to be checked separately. An anchorage failure will instead appear in the analysis as a bending failure in the anchorage region. However, if the anchorage failure is connected with cover splitting, the analysis may show a more ductile response than if the anchorage failure had been modelled in detail. Consequently, as a conservative estimate, the load carrying capacity should be limited to the onset of reinforcement yielding in the anchorage zone.

If the reinforcement is modelled with full cross-sectional area along its entire length, the risk for anchorage or splice failure must be checked separately, in the same way as for a linear analysis. The force in the reinforcement from external loads can be obtained from the analysis directly or determined based on the moments and normal forces obtained in the non-linear analysis. As a conservative simplification, the design anchorage length from Eurocode 2 (CEN, 2004a) or national standards or codes can be used

5.5 Response under service conditions

A non-linear analysis on Level III can give a good overall representation of the response in serviceability limit state. Deflections due to bending are generally realistically reflected in the analysis. However, individual cracks and their crack widths cannot be directly evaluated from an analysis on this level of detailing. Also, local stress values from the analysis should be used with caution for checking of stress limitations.

However, the action effects in terms of sectional moments and forces can be used as a basis for checking of crack width limitations and stress limits. In this way the redistribution of moments and forces due to concrete cracking caused by bending is taken into account. Furthermore, in a partly cracked two-way concrete slab, the uncracked parts are often restraining the cracked parts of the slab, causing compression normal sectional forces here. These will cause an arch action that contributes to limiting the crack widths. A similar effect is obtained if the boundaries prevents expansion of the slab after cracking.

Crack widths and stresses are calculated from the sectional moments and forces in the same way as for a linear analysis on Level II. An alternative would be to use the stresses obtained in the FE analysis directly. However, the stresses may show larger fluctuations than the sectional forces and moments and should be used with caution. This may particularly be the case with the concrete stresses if the model does not represent the compression zone accurately enough.

6 3D non-linear FE analysis with continuum elements (Levels IV and V)

6.1 General

In cases where further enhancements of the assessment are motivated, a more detailed non-linear FE analysis can be made, where the volume of the structure is represented by 3D continuum (solid) finite elements. The reinforcement is also included in the FE model. With fully bonded reinforcement, such an analysis corresponds to **Level IV** in *the Multi-Level Assessment Strategy*, see Section 2.3. Here, not only bending but also shear-type failures are reflected by the analysis. If the bond and slip between the reinforcement and surrounding concrete is included too, the analysis corresponds to **Level V** in *the Multi-Level Assessment Strategy*; here also anchorage failure is reflected. A non-linear analysis on Levels IV or V can give a deeper understanding of the structural behaviour of the slab and by this facilitate a better utilisation of the structure. It also has the potential of revealing an even higher load-carrying capacity, compared to the lower levels of assessment.

In a **Level IV** analysis, the reinforcement is modelled with perfect bond to the concrete and *embedded reinforcement* layers or bars can be used. In the analysis, bending as well as shear cracking is reflected. If individual bars are used in dense meshes with small elements, the crack pattern is better reflected, and with sufficiently small elements individual cracks can be identified. Bending, shear or punching failure will govern the maximum load-carrying capacity shown by the analysis. However, anchorage failure needs to be checked using local resistance models, similarly to Level III.

In an analysis on **Level V**, the reinforcement is modelled as individual bars and the bond-slip behaviour of the interface between the reinforcement and the concrete is included. Separate truss or beam elements may be used for the reinforcement, with non-linear connections between the reinforcement and concrete elements to describe the bond-slip behaviour, see Section 3.3.6. In this type of analysis, the crack pattern is realistically reflected, and anchorage failure is captured by the analysis. Consequently, no major failure modes need to be checked with separate resistance models, and the load-carrying capacity can be evaluated from the analysis results directly. For even more detailed analysis, reflecting the local failure mechanism of anchorage including concrete splitting, the reinforcement can be modelled with continuum elements with a 3D bond model generating radial stresses from the reinforcement bars when they slip, see Lundgren and Gylltoft (2000).

As described in Section 5.1, only the most critical load cases identified at lower assessment levels are analysed with non-linear FE analysis at higher assessment levels. As for Level III analysis, an analysis on Level IV (or finally on Level V) simulates the response under successively increased loading for one particular load combination and loading history. Such an analysis may particularly be motivated to gain improved insight into the structural response and failure mechanism, but it may also show a higher load carrying capacity as demonstrated by the examples in Chapter 7. However, it will also require increased effort, and improved information on the structure and its actions is generally needed. Consequently, it is motivated to first evaluate and compare the possible gains and costs of a more enhanced analysis.

For assessment on Level IV and V, the safety format based on a global safety factor according to Schlune *et al.* is recommended, see Section 2.4.5. To determine the global safety factor, two or more non-linear analyses need to be performed using mean and characteristic material parameters. The model uncertainty for a Level IV or V analysis depends on the certain modelling method used to analyse the particular type of structure and failure mode assessed, see Section 2.4.6. Since the basis to determine the correct model uncertainty is insufficient for many cases, it might be necessary to use conservative general values on the uncertainty parameters. Consequently, it may in practice be hard to determine a reliable design capacity level that is not over-conservative for practical engineering cases. However, assessment on Level IV and V may be very valuable to get improved understanding of the structural behaviour and may assist in choosing correct structural models for lower assessment levels.

The structural effect of deterioration can be accounted for in similar way as described in Section 5.1. In an analysis on Level IV, the deterioration effect can be modelled as a change in:

- material properties of concrete and cross-sectional area of the structural member,
- material properties and cross-sectional area of steel reinforcement, and
- bond properties between reinforcement and concrete.

Detailed recommendations are given in Appendix B to E.

In structural assessment, an analysis on Level IV or V is always assumed to preceded by an analysis on Level III. Consequently, Chapter 6 do not go into detail on matters already treated in Chapter 5, that are valid to non-linear analyses on all levels. Instead, references are generally given to corresponding sections in Chapter 5.

6.2 Structural model and non-linear analysis

6.2.1 General

In Level IV and V analyses, a concrete slab is modelled by 3D continuum (solid) finite elements. As in an analysis on Level III, the reinforcement is included in the FE model, non-linear material models are used for concrete and reinforcement and geometric non-linearity is included, see Section 5.2.1.

The main difference between Level IV and Level V analyses concerns how the reinforcement and its interaction with concrete is described. In Level IV, perfect bond, i.e. a full interaction between the reinforcement and concrete, is assumed, and thus anchorage failures must be checked by local resistance models. However, in Level V analysis the interaction is described by a bond-slip relation, and anchorage failure is reflected in the model if an appropriate bond-slip relation is adopted.

6.2.2 Idealization of the structure

On Level IV and V a slab is represented by 3D continuum elements, providing is a more realistic geometrical representation of the structure compared to models at lower analysis levels. This leads to a model with large number of elements, which is computationally expensive. Consequently, it is crucially important to minimize the

model size by, e.g. using symmetry lines and avoiding unnecessarily small element sizes. At the same time it is most often important to include structural parts such as columns, edge beams and transversal beams in the model to get a good estimation of the support reaction distribution, and hence the stress distribution in the slab, Shu *et al.* (2015, 2016, 2017). However, adjacent structural parts connected to the slab can usually be modelled using structural finite elements on a detailing level corresponding to Levels II or III. Yet, the analysis is considered to be on Level IV even if adjacent parts are modelled with structural elements.

In analyses on Level IV, reinforcement is modelled either as reinforcement layers or discrete reinforcement bars, both embedded in the solid elements of the slab, providing stiffness in the direction of the bars only, see also Section 3.3.5. Similar to analysis at Level III, in order to take the risk of anchorage and splice failure into account in the analysis, the embedded reinforcement layer or bar can be modelled with gradually reduced cross-sectional area along the anchorage length, as described in Section 3.3.6. With this modelling method, an anchorage or splice failure will, in the non-linear analysis, appear as a bending failure in the anchorage or splice zone. Prestressing may be specified as initial stress in the reinforcement. See also Section 5.2.2 regarding different aspects of *embedded reinforcement*.

In analyses at Level V, the reinforcement is modelled as discrete reinforcement bars using truss or beam elements, and its interaction with concrete is described by a bond-slip relation, see Figure 6.1. The interaction can be modelled by separate interface or spring elements, but different software may provide different possibilities to include the bond-slip relation, see Section 3.3.6. In truss elements, the only deformation is the axial elongation; there is neither bending nor shear deformation. Therefore, dowel action of bars cannot be described using truss elements. Beam elements, on the other hand may have axial deformation, shear deformation and torsion; therefore, they can describe axial force, shear force and moment. Consequently, dowel action of bars can be included in the analysis if reinforcement is modelled using beam elements.

Similar to analysis at Level III, the boundary conditions have a large influence on the response. Detail considerations regarding boundary conditions at correct locations, support and loading places can be found in Section 5.2.2.

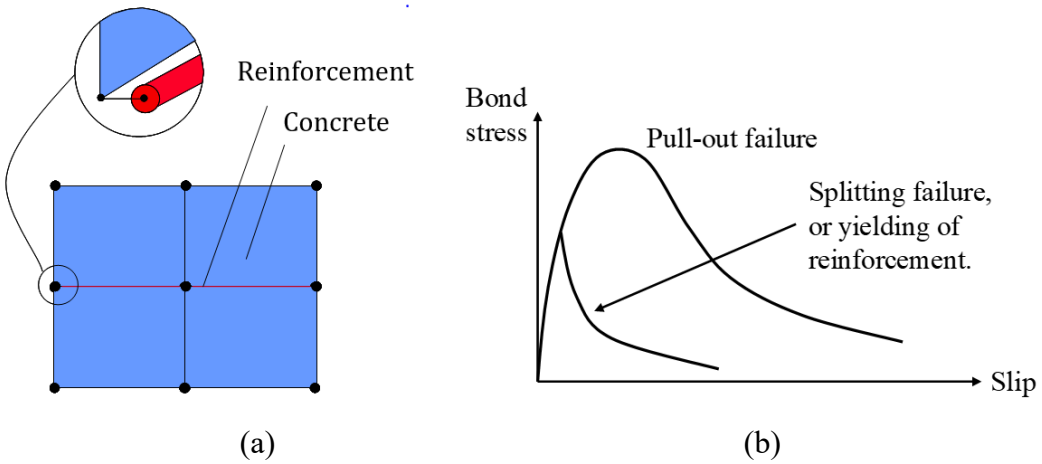

Figure 6.1 *Reinforcing steel can be modelled with truss elements with interface elements using a predefined bond stress-slip relationship to describe the interaction between the concrete and the steel; Broo et al. (2008)*

6.2.3 Material models

In a structural model for Level IV, not only bending but also the shear response must be realistically simulated throughout the analysis. Deformations as well as overall cracking response must be captured. Often it is sufficient to capture the extension of the cracked regions and crack directions correctly, while a very detailed FE mesh is needed to identify individual cracks. Nevertheless, not only bending but also shear cracking must be reflected. Irrespective of if bending or shear governs the failure, the failure of a concrete slab is normally preceded by the evolution of bending cracking and possibly by yield lines due to bending. The load-carrying capacity is then limited by either bending failure in the yield lines or by shear or punching failure preceded by inclined shear cracks in the critical regions. Consequently, it must be possible to follow both:

- the local bending cross-sectional response, with reinforcement hardening and rupture and crushing of concrete in the compression zone.
- the local shear response during development of one-way shear or punching failure. This includes the development of inclined shear cracking, and failure of the shear cracked regions.

This brings certain requirements on the material models used for concrete and reinforcement.

For concrete in tension the material model needs not only to describe the crack response in the normal crack direction, as described for Level III, see Section 5.2.3; the response in shear is also very important in Level IV and V analyses. Fixed as well as rotating and plasticity-based crack models may still be suitable, but in a fixed crack model the requirements on how the shear response in the crack is described is of much higher importance. In order to correctly reflect the shear response and shear failure, it is of great importance that the shear retention factor in the fixed crack model is properly defined, see Section 3.3.2. In rotating crack models, this difficulty is avoided. Nevertheless, rotating crack models have shown a good capability in describing also the shear response, as shown in the examples in Chapter 7. Fixed crack models with orthogonal cracks have shown inability to reflect shear response and should be avoided.

Similar to analysis at Level III, the use of embedded reinforcement bars with perfect bond to surrounding concrete in analysis at Level IV will in most cases result in a diffuse crack pattern where individual cracks are not reflected; instead all elements in the regions where cracking occur will generally be cracked. Consequently, if not a very dense FE mesh is used, it is recommended to approximate the crack band width to be equal to the mean crack spacing, $l_{cr} = s_{rm}$, for more details see Section 3.3.2.

For analysis at Levels IV and V, the requirements on the concrete material model regarding the response in compression is similar as for Level III, See Section 5.2.3. Also here it is important that the response up to and beyond concrete crushing is reflected, with the softening response based on fracture energy in compression, see Section 3.3.3. The multi-axial response of concrete should be reflected, including both reduced strength in case of perpendicular cracking and increased strength in case of multi-axial compression. It is recommended to not include the tension stiffening effect in cracked concrete by modifying the stress-strain relation for concrete in tension, see Section 3.3.2. As for Level III, it is recommended to set the Poisson's ratio to $\nu = 0$ after cracking of concrete.

For analysis at Levels IV and V, it is sufficiently to specify the uni-axial response for the reinforcement steel, in the same way as for Level III, see Section 5.2.3. Also, when the reinforcement bars are modelled as beam elements to include their dowel action, the uni-axial response will govern the bending response and the effect of multi-axial response will be negligible.

6.2.4 Material parameters

Recommendations for determination of material parameters for the non-linear material models are given in Appendix A. In the Appendix, it is described how material parameters can be estimated based on the given material quality based on standards, codes and handbooks like e.g. Eurocode 2 (CEN, 2004a) and Model Code 2010, fib (2013).

Compared to analysis on Level III, it is even more motivated to determine the key material properties through material tests on samples from the structure to be evaluated. On the contrary, it can be questioned if an analysis on Level IV or V is worth to perform without determining at least the in-situ uni-axial strength properties through tests. Often, the in-situ strength properties of old structures can differ substantially from code values based on specified material qualities. Furthermore, the analysis results may heavily influence by the material in-data given. Also, in-situ values for material parameters such as Young´s modulus, reinforcement strain hardening response and the fracture energy for the concrete can be motivated to be determined through tests.

6.2.5 Bond-slip relation for reinforcement-concrete interaction

For analyses at Level V, a bond-slip relation must be defined for the interaction between the reinforcement and surrounding concrete, see Figure 6.1. For monotonic loading it is recommended to use the relations provided by Model Code 2010, fib (2013). Figure 6.2 shows schematically these bond-slip relations, for pull-out and splitting failure, respectively. Recommendations for determination of the parameters governing the relations are given in Appendix A.

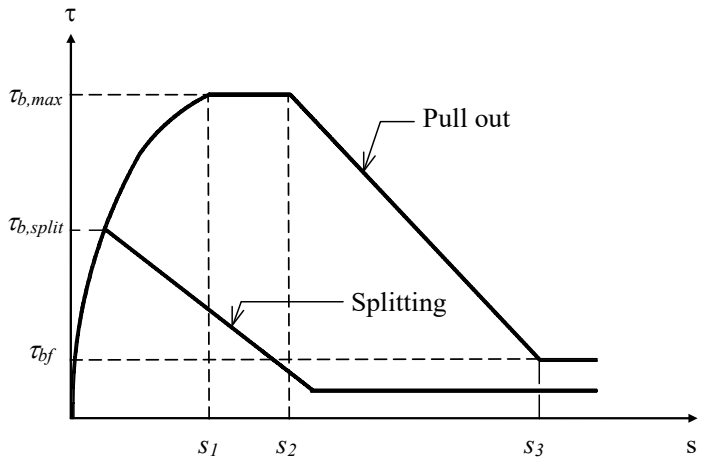

Figure 6.2 Bond-slip relation for interaction between reinforcement and surrounding concrete, for pull-out and splitting failure, respectively. Based on Model Code 2010, fib (2013).

6.2.6 FE modelling

In analysis on Levels IV and V, three-dimensional continuum elements are used to model the slab, while non-linear or linear shell or beam elements can be used for adjacent parts included in the model, depending on their geometry and response. Depending on the geometry of the structure and the expected crack pattern, tetrahedral (pyramid) or hexahedral (brick) elements, possibly complemented with pentahedral (wedge) elements, may be feasible, Shu (2015, 2016, 2017).

Both first and second order elements may be feasible, where second order elements generally give a less clear picture of the crack pattern. In the examples in Chapter 7, first or second order hexahedral elements were used. However, regular hexahedral element meshes has a tendency to influence the crack pattern, and subsequently also the yield lines, to follow the element orientation, see also Section 3.4.3.

To reflect the bending behaviour of the concrete slab after cracking, but also the possible failure mechanisms, it is important to use sufficiently many elements over the section height. This is important to describe the bending deformation, but also the compression zone of the concrete cross-section and the failure associated with inclined shear cracking. In Shu (2017) it was found that first order 8-node brick elements with at least 7 element layers over the section height was sufficient to reflect both the bending and shear response, but also first order tetrahedral elements were an applicable alternative. In Level IV analysis, 20-node brick elements with 3 layers of elements also gave satisfactory results. The use of higher order elements may be considered since they reduce the number of elements and the size of the FE model.

For an analysis of a slab, the limitations on aspect ratios of finite elements in combination with the number of elements needed over the section height most often governs the element size in the slab plane. This normally gives a sufficiently dense element mesh. It is recommended to verify the chosen FE mesh by comparison to a corresponding model with higher mesh density, see Section 3.4.4. In such a verification, it is recommended to compare deflections, crack load and crack distribution, yield load and yield line distribution, failure mode and failure load in such a verification.

6.2.7 FE analysis

A non-linear analysis at Levels IV and V is made in a similar way as for Level III; see Section 5.2.5. The non-linear geometrical response cannot be neglected and needs to be taken into account. The loading procedure is similar, see Section 2.4.7, and resembles how the load is applied to the structure in succeeding analysis steps. Within each such step, the load is applied through a number of increments for which equilibrium is controlled. For the analysis step in which the failure is reached, it is recommended to use displacement-controlled loading, see Section 3.2.3. With an implicit solution method, the equilibrium is controlled using an iteration method with prescribed tolerances. Recommendations for this is given in Sections 3.2.2 and 3.4.4.

6.3 Evaluation of structural response

An FE analysis at Levels IV or V is most often made to obtain an improved understanding of the structural behaviour. Consequently, the evaluation of the

structural response is of even greater importance compared than for a Level III analysis. For a Level IV and V analysis, the response from initial loading, through the cracking and development of reinforcement yielding to the final failure is of interest. By comparing different results, such as the load versus deformation response with crack pattern and stress in the reinforcement, the structural behaviour can be understood. As for a Level III analysis, the evaluation of structural response is also an important part of the quality control, see also Section 3.5.

A detailed description of the structural behaviour is recommended as a part of the assessment report, and could typically include:

- A load-displacement relation that describes the overall response of the slab. For slabs with several spans, several curves may be needed to explain the structural behaviour.
- Figures showing the deformation of the slab at different stages of loading, including the deformation at maximum load.
- A description of the cracking development in the slab, illustrated by figures showing the crack pattern. For a 3D model, it is important to include crack patterns in critical sections to identify the mode of cracking (bending or shear).
- A description of the development of reinforcement yielding, illustrated by figures showing plastic strains in the reinforcement.
- A description of the failure mode illustrated by figures showing concrete cracking and crushing, and reinforcement yielding and rupture.
- In analysis at Level V, the bond stress versus slip as well as bond stress versus total load can be shown in graphs. Anchorage failure can be identified in an 6.4.3analysis if slip increases for increasing deformation, after reaching the peak load.

For evaluation of design load-carrying capacity, the failure load is determined in two or more consecutive analyses with mean and characteristic material parameters, depending on the safety format used. The evaluation using the global safety format is treated in Section 6.4.1.

In Level IV and V analysis, bending, shear and punching failures are described in the model. In Level V analysis, anchorage failure is described in the analysis, provided that appropriate bond-slip relation is used. In Level IV analysis, the risk of anchorage or splice failure is described in a simplified way if the reinforcement is modelled with gradually reduced cross-sectional area along the anchorage length, as described in Section 3.3.6. Otherwise, the risk for anchorage or splice failure must be checked separately. Assessment of anchorage capacity is treated in Section 6.4.3.

For serviceability limit state (SLS) verifications of stress state and deflection, the values of stress and deflection can be directly read from the nonlinear finite element analysis and compared with the limit values imposed by the current codes. The procedures to calculate the crack opening, to be compared with the limit values imposed by the codes, is presented in Section 6.5.

6.4 Load-carrying capacity

6.4.1 Safety format

To evaluate the load-carrying capacity based on 3D non-linear continuum FE analysis on Levels IV and V, the safety format according to Schlune et al. (2011, 2012) is recommended, see Section 2.4.5. Here, one non-linear analysis is made with mean values on the material parameters, and one analysis each with characteristic values related to concrete compression, concrete tension and reinforcement failure, respectively. From the non-linear analyses, the design load-carrying capacity can be determined with respect to all failure modes that are reflected in the analysis, i.e. with respect to bending, shear and punching failure for Level IV analysis, and also anchorage failure in Level V analysis.

The coefficient of variation for modelling uncertainty, V_θ, and the model bias, θ_m, can be determined *a priori* for the modelling method used and the failure mode studied, see Section 2.4.6. If they are not determined for the specific modelling method used, conservative values according to Table 2.1 can be adopted. The coefficient of variation for geometrical uncertainty, V_g, can be assumed to be 5%, see Section 2.4.5.

The coefficient of variation for material uncertainty, V_f, is estimated based on the mean and characteristic global structural resistances, R_m and R_{ki}, determined based on the non-linear analyses. In general, the structural resistance from three analyses with characteristic values related to concrete compression (R_{kc}), concrete tension (R_{kct}) and reinforcement (R_{ks}) failure, respectively, is needed. The coefficient of variation is determined from the non-linear analyses with mean and characteristic values according to Equation (2.13):

$$V_f = \frac{1}{R_m}\sqrt{\left(\frac{R_m - R_{kc}}{f_{cm} - f_{ck}}\right)^2 \left(V_{fc}\cdot f_{cm}\right)^2 + \left(\frac{R_m - R_{kct}}{f_{ctm} - f_{ctk}}\right)^2 \left(V_{fc}\cdot f_{ctm}\right)^2 + \left(\frac{R_m - R_{ks}}{f_{sm} - f_{sk}}\right)^2 \left(V_{fs}\cdot f_{sm}\right)^2}$$

or (2.16):

$$V_f \cong \frac{1}{R_m}\max\left\{\frac{R_m - R_{kc}}{f_{cm} - f_{ck}}\cdot\left(V_{fc}\cdot f_{cm}\right),\quad \frac{R_m - R_{kct}}{f_{ctm} - f_{ctk}}\cdot\left(V_{fc}\cdot f_{ctm}\right),\quad \frac{R_m - R_{ks}}{f_{sm} - f_{sk}}\cdot\left(V_{fs}\cdot f_{sm}\right)\right\}$$

Recommendations for mean and characteristic material parameters are given in Appendix A and for the coefficients of variation for material parameters in section 2.4.5. If the failure mode is obvious and it is possible to see directly which of the terms in Equation (2.13) or (2.16) that will be critical, the number of analyses may be reduced and only the critical analysis with characteristic values need to be performed. This implies that the same failure mode is critical irrespective of which material parameters that are set to characteristic values.

The coefficient of variation for the resistance is then calculated using Equation (2.8) and the global resistance safety factor using Equation (2.7), with the sensitivity factor and the target reliability according to Model Code 2010, fib (2013):

$$V_R = \sqrt{V_\theta^2 + V_g^2 + V_f^2}$$

$$\gamma_R^* \cdot \gamma_{Rd} = \frac{\exp\left(\alpha_R \beta V_R\right)}{\theta_m} = \frac{\exp\left(0.8 \cdot 3.8 \cdot V_R\right)}{\theta_m}$$

Finally, the design load-carrying capacity is calculated according to Equation (2.1):

$$R_d = \frac{R_m}{\gamma_R^* \cdot \gamma_{Rd}}$$

In the same way as for a Level III analysis, the design load-carrying capacity must be interpreted differently depending on the load scheme in the final load step for which failure is reached, see Section 2.4.7. However, regardless of how the design load-carrying capacity is expressed, the failure should be reached under the same loading step in the analyses with mean and characteristic material properties, respectively, see Section 2.4.7.

6.4.2 Failure modes reflected in the non-linear analysis

To determine the design load-carrying capacity with respect to bending, shear and punching, and the global resistance factor is determined based on the failure loads from the non-linear analyses. The same applies to anchorage failure for Level V analysis. When the safety format according to Schlune *et al.* (2011, 2012), Section 2.4.5, it used, the following global resistance values are determined from the non-linear analysis:

- R_m is determined as the failure load in a non-linear analysis with mean material parameters, Equation (2.6),
- R_{kc} is determined as the failure load in a non-linear analysis with characteristic material parameters related to concrete compression, Equation (2.10),
- R_{kct} is determined as the failure load in a non-linear analysis with characteristic material parameters related to concrete tension, Equation (2.11), and
- R_{ks} is determined as the failure load in a non-linear analysis with characteristic material parameters for the reinforcement steel, Equation (2.12).

The coefficient of variation for material uncertainty and for the structural resistance is then calculated, as described in Section 6.4.1. Finally, the global resistance factor and the design load-carrying capacity is calculated.

As for Level III analysis, it is important to emphasize that the failure loads from all the analyses are comparable and that the failure load is determined in the same way. If it is not possible to follow the response up to failure in one of the analyses, the coefficient of variation for material uncertainty will become wrong, resulting in a false global safety factor. Consequently, and it will not be possible to determine the design load correctly. This can occur, for example, if convergence difficulties make one of the analysis stop too early.

6.4.3 Anchorage

In a Level IV analysis, the risk of anchorage or splice failure can be checked in the same way as for a Level III analysis, described in Section 5.4.5:

- If the reinforcement cross-sectional area is gradually reduced in anchorage and splice regions, as described in Section 3.3.6, a bending failure in these region will indicate anchorage failure. The load carrying capacity should then be limited to the onset of yielding in these regions, as a conservative estimate.
- If the reinforcement has full cross-sectional area along its entire length, the risk for anchorage or splice failure must be checked separately. The design anchorage length from Eurocode 2 (CEN, 2004a) or national standards or codes can be used as a conservative estimate.

In a Level V analysis, anchorage failure is reflected in the analysis and need not be checked separately.

6.5 Response under service conditions

As described in Section 6.3 deflections and stresses can be directly evaluated from a Level IV or V analysis. In a Level V analysis, individual cracks and their crack widths are also realistically reflected in the analysis. However, in a Level IV analysis, individual cracks and crack widths cannot be directly determined. Here, averaged reinforcement stresses in the cracked regions can be used to estimate crack widths using the models for crack widths in e.g. Eurocode 2, similarly as for a linear analysis on Level II. In this way the non-linear response of the slab is taken into account, including stress redistributions and possible arch effects. (See also Section 5.5)

7 Examples

In this chapter, examples are provided to show the feasibility to use the proposed recommendations for assessment of reinforced concrete slabs. The first two examples are on rather simple structural elements tested in laboratory. These examples show the applicability of the assessment strategy, but also that it results in conservative estimates of the load-carrying capacity. The third example shows the application on a real bridge example with hypothetic (future) deterioration. This example shows how the assessment strategy can be applied on a real deteriorated structure.

Other examples with applications of non-linear FE analyses can be found in literature. Some examples of modelling strategies developed for different applications that may be useful are given below. Mathern *et al.* (2021) developed a FE modelling strategy for cracking and crushing behaviour in reinforced concrete structures subjected to bending. The strategy is applied to reinforced concrete beams strengthened with fibre reinforced polymer laminates. Bagge *et al.* (2019) extended the *Multi-Level Assessment Strategy* in Plos *et al.* (2017) for analysis of a prestressed concrete bridge. In Hendriks *et al.* (2017), guidelines for analysis of reinforced concrete structures with non-linear FEM are given. In Belletti *et al.* (2017a, b), examples for validation of these guidelines are provided. Engen *et al.* (2019) developed a solution strategy for non-linear FE analyses af large reinforced concrete structures. In Broo *et al.* (2008) recommendations are given for non-linear finite element modelling of shear and torsion in concrete bridges.

7.1 Example 1: application to two-way slabs subjected to bending failure

In the first example, the recommended assessment strategy is applied to two-way slabs, previously experimentally tested to bending failure. No safety format is adopted, and the design load-carrying capacity is not evaluated since the objective in this example rather was to compare the calculated mean load-carrying capacity on different assessment levels to the test results. Consequently, mean values of material properties are used in the entire assessment procedure. This case study has previously been reported in Plos *et al.* (2017).

7.1.1 Experiment

Fall *et al.* (2014) carried out a series of tests on two-way slabs. As a part of a larger test series, three specimens with the same dimensions were tested, see Figure 7.1. The specimens were octagonal, 80 mm thick slabs, supported on four edges by five rollers along each edge, and subjected to a point-load at the centre. The loading was deformation-controlled, and the reaction forces were measured by strain gangues on the rollers supporting the slab. The compressive and tensile strength of the concrete and the tensile strength of the steel reinforcement were determined through material tests. The reinforcement, consisting of 6 mm bars, was twice as dense at the first bottom layer (s = 98 mm) compared to the second layer (s = 196 mm). The concrete cover for the dense reinforcement layer was 20 mm.

The three slabs tested showed very similar results, see Figure 7.2. In the tests, cracking started when the load was 26 kN on the average, followed by bending

hardening. The slabs failed at the ultimate load of $P_{u.exp}$ = 70 kN on the average, with a rupture of reinforcement bars; the tests were aborted when two bars had ruptured (Fall et al., 2014). Later, the results from one of the slabs, CR1, will be used for comparison with FE analyses.

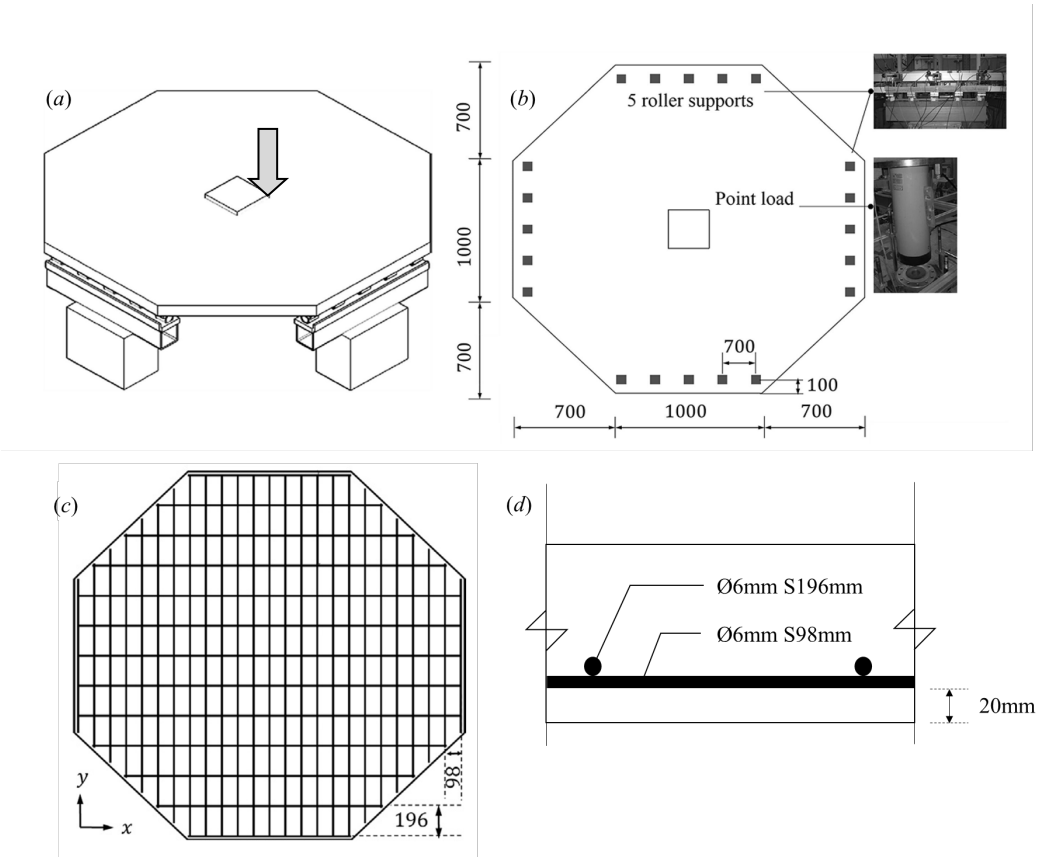

Figure 7.1 *(a) Set-up of the test, (b) dimension of tested slab, dimensions in mm, (c) layout of reinforcement bar in plan (d) layout and concrete cover of reinforcement bar in vertical directions.*

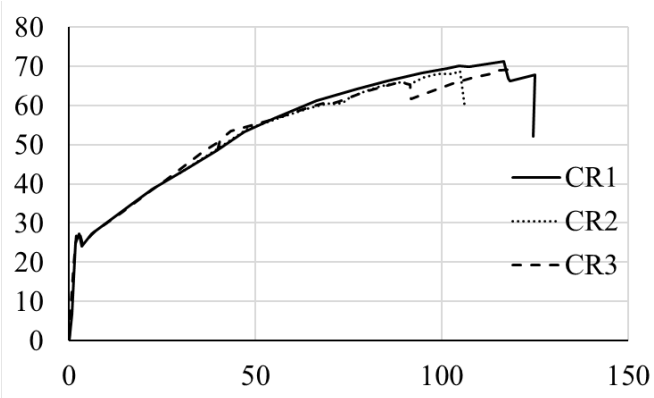

Figure 7.2 *Load-deformation relations from the tests of the three slabs.*

7.1.2 Analysis at different assessment levels

In this section, the two-way slab was assessed at different levels according to the *the Multi-Level Assessment Strategy* described in Section 2.2. For the FE analyses, the finite element software DIANA 9.4.4 (TNO, 2015) was used. In the following sub-sections, the material models and properties used for the analysis on all levels of assessment are described. The methods used and the results obtained are then presented individually for the different levels of assessment. The results are compared to each other and to the test results in Section 7.1.3.

7.1.2.1 Material models and material parameters

In all calculations, mean material parameters from the tests were used, see Table 7.1.

For the non-linear FE analysis at Levels III–V, concrete was modelled using a fracture energy based total strain crack model (TNO, 2015). In tension, a smeared rotating crack model (Rots, 1988) was used. In this approach, the crack width w is related to the crack strain ε_{cr} perpendicular to the crack via a characteristic length, the crack band width l_{cr}, see Section 3.3.2. The crack band width was determined differently depending on the bond-model for reinforcement (see Section 3.3.2) and an example of the tension softening curve can be found in Figure 7.3 (a).

The behaviour of concrete in compression was described by an isotropic damage constitutive law. When the stress-strain relationship was used in numerical analyses, the localization of deformation in compressive failure needs to be taken into account, see Section 3.3.3. As explained there, the compression softening behaviour is related to the boundary conditions and the size of the specimen. Consequently, the stress-

Table 7.1 Material parameters for the two-way slabs. Plos et al. (2017).

Parameter of concrete		Parameter of reinforcement steel	
Young´s modulus	E_c = 24.5 GPa	Young´s modulus	E_s = 210 GPa
Poisson's ratio	ν = 0.15	Poisson's ratio	ν = 0.2
Compressive strength	f_{cm} = 50.9 MPa	Yield strength	f_y = 550 MPa
Tensile strength	f_{ctm} = 2.7 MPa	Ultimate strength	f_u = 666 MPa

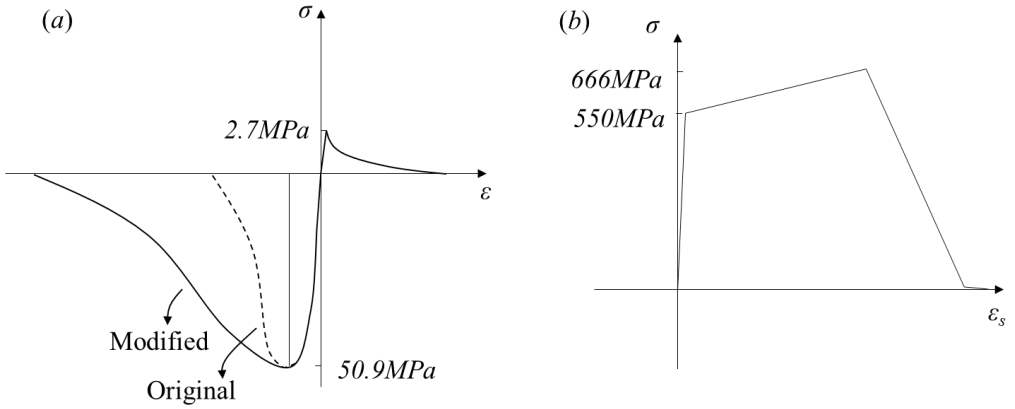

Figure 7.3 Stress–strain relations used for the uniaxial response of concrete in tension and compression (a); and of reinforcement steel (b). From Plos et al. (2017).

strain relation used has been calibrated by measurements of compression tests on 300 mm long cylinders. The softening branch needs to be modified for the concrete element size used in the FE model. Thus, the stress-strain curve according to Thorenfeldt (1987) was modified to fit the concrete element size (see Section 3.3.3), resulting in a uniaxial stress versus strain response as shown in Figure 7.3 (a).

The behaviour of the reinforcement was described by a Von Mises plasticity model, including strain hardening, using values as obtained from material tests, see Figure 7.3 (b).

7.1.2.2 Level I: simplified analysis methods

At the initial level of structural assessment, the load-carrying capacity with respect to bending failure was estimated using the strip method (Hillerborg, 1996) for a lower bound value and the yield line method (Johansen, 1972) for an upper bound value; see Figure 7.4. One-way shear, punching shear and anchorage failure modes were not checked here because the slab was designed to avoid them; see (Fall et al., 2014). The results of this calculation are displayed in Table 7.2. The anchorage was also checked according to Eurocode 2 (CEN, 2004a) and proven to be non-critical to this case.

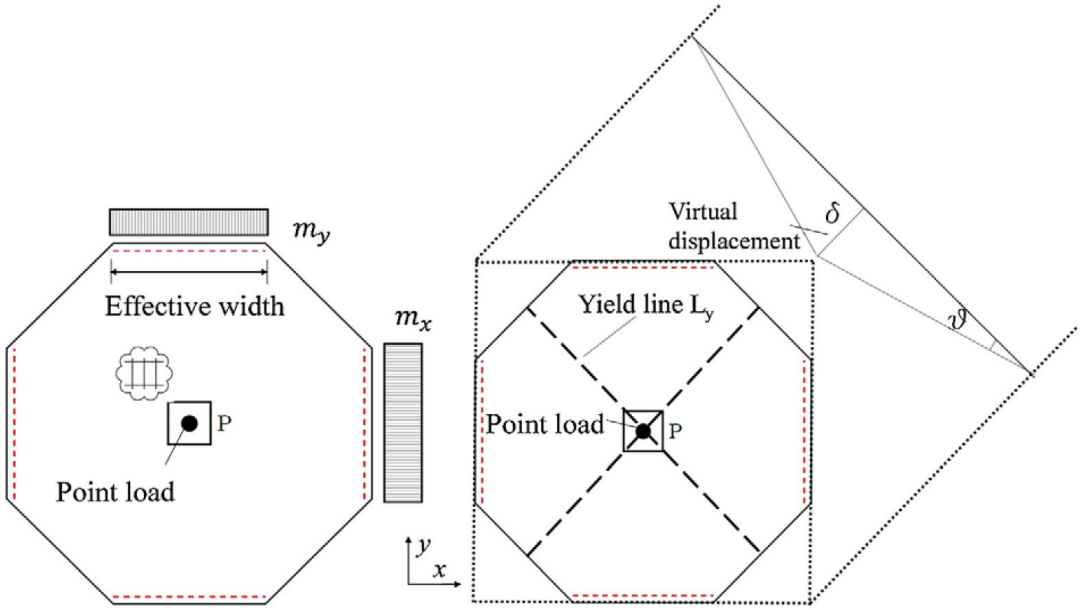

Figure 7.4 Calculation models for the two-way slabs using strip method (a) and yield line method (b). From Plos et al. (2017).

Table 7.2 Calculated load-carrying capacity for bending, one-way shear and punching shear. From Plos et al. (2017).

Resistance with respect to:	Load-carrying capacity Q_u (kN)
Bending capacity (Strip method)	29.8
Bending capacity (yield line theory)	37.9

7.1.2.3 Level II: 3D linear shell FE analysis

At level II, a 3D linear FE model of a quarter of the slab was defined, as seen in Figure 7.5 (*a*). The concrete slab was modelled with 8-noded rectangular shell elements of size 40 mm × 40 mm. Symmetry boundary conditions were applied to the symmetry lines and the rollers supports were modelled by preventing translations in vertical direction and horizontally along the rollers. A unit pressure load equal to 1 kN was applied to the centre area of the slab, at the position of the loading plate.

The linear FE analysis results in a moment field consisting of bending and torsional moments. The entire moment field, caused by the actions on the slab, must in the ultimate limit state be balanced by bending moment resistances provided by the forces in the main reinforcement layers times their inner level arms. Consequently, reinforcement moments from the load, m_{rx} and m_{ry}, in the two perpendicular reinforcement directions x and y, was calculated (see e.g. Pacoste *et al.,* 2012):

$$\begin{cases} m_{rx} = m_x + \mu \left| m_{xy} \right| \\ m_{ry} = m_y + \mu \left| m_{xy} \right| \end{cases} \tag{7.1}$$

Here, m_x and m_y are the bending moments in the x and y directions, respectively, and m_{xy} is the torsional moment. The factor μ can be chosen, but a value close to 1 is generally recommended. In assessment of an existing structure it can be chosen with respect to the actual reinforcement distribution in the slab. Here it was chosen to 1.

Figure 7.5 (*b*) shows schematically the distribution of reinforcement moment m_{rx} along line L_2 in a direction orthogonal to the reinforcement direction (in this case, parallel to line L_1). Owing to the plastic redistributions capacity of the concrete slab, the reinforcement moments can be redistributed over a certain width, here denoted w.

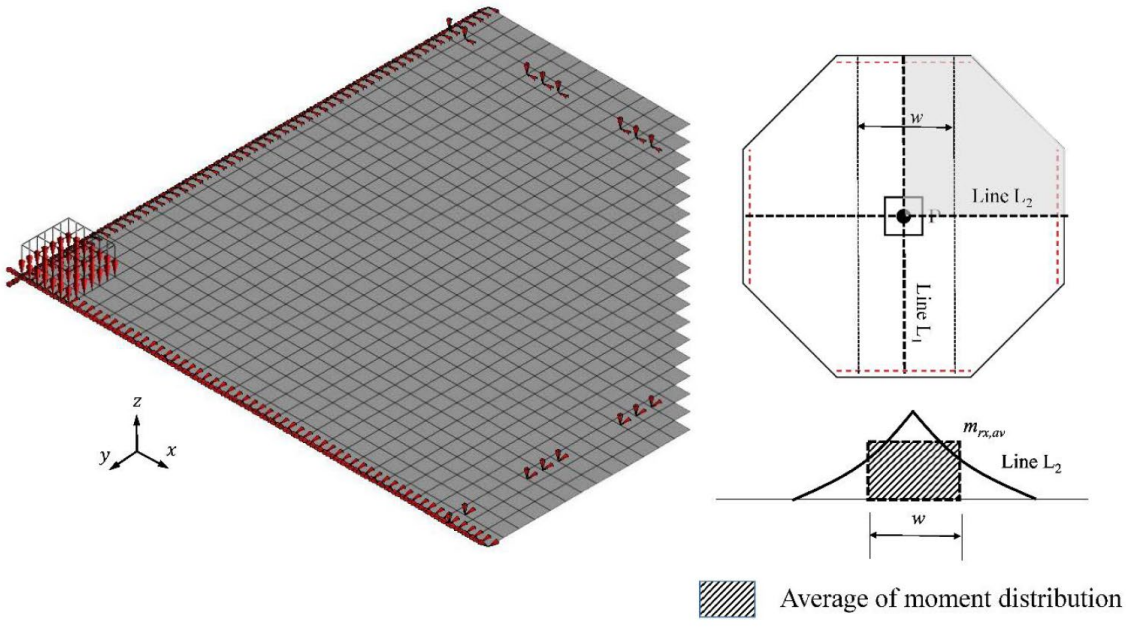

Figure 7.5 Linear shell element model of the two-way slabs, for Level II analysis (a) and schematic moment distribution along a section through the slab (b). From Plos et al. (2017).

Within the redistribution width w, the linear moment distribution m_{rx} along line L_2 is replaced by a constant moment with the average value $m_{rx,av}$, computed as:

$$m_{rx,av} = \frac{1}{w}\int_0^w m_{rx} d_y \tag{7.2}$$

The redistribution width is affected by the rotation capacity of the slab, which can be represented by the ratio between the compression zone height, x_u, over the effective depth of the cross-section, d. Here, the recommendations in Pacoste *et al.* (2012) was followed, and the redistribution width for the slab studied calculated by interpolation between the equations:

$$w = \begin{cases} \frac{L_c}{2}, for \frac{x_u}{d} = 0.15 \\ \min(5h, \frac{L_c}{5}), for \frac{x_u}{d} = 0.0 \end{cases} \tag{7.3}$$

In the equations above, h is the height of the section and L_c is the characteristic span width, in this case $h = 80$ mm, $L_c = 2200$ mm and $x_u/d = 0.05$ which yields $w = 638$ mm by interpolation. The capacity of the slab for concentrated loading, with respect to bending, was calculated to be

$$P_u = \frac{m_{Rx}}{m_{rx,av}} \cdot 1 \text{ kN} = 44.3 \text{ kN} \tag{7.4}$$

7.1.2.4 Level III: 3D non-linear shell FE analysis

For a non-linear structural analysis at Level III, the slab was modelled with shell elements using the same mesh as for Level II, see Figure 7.6. In this model, the

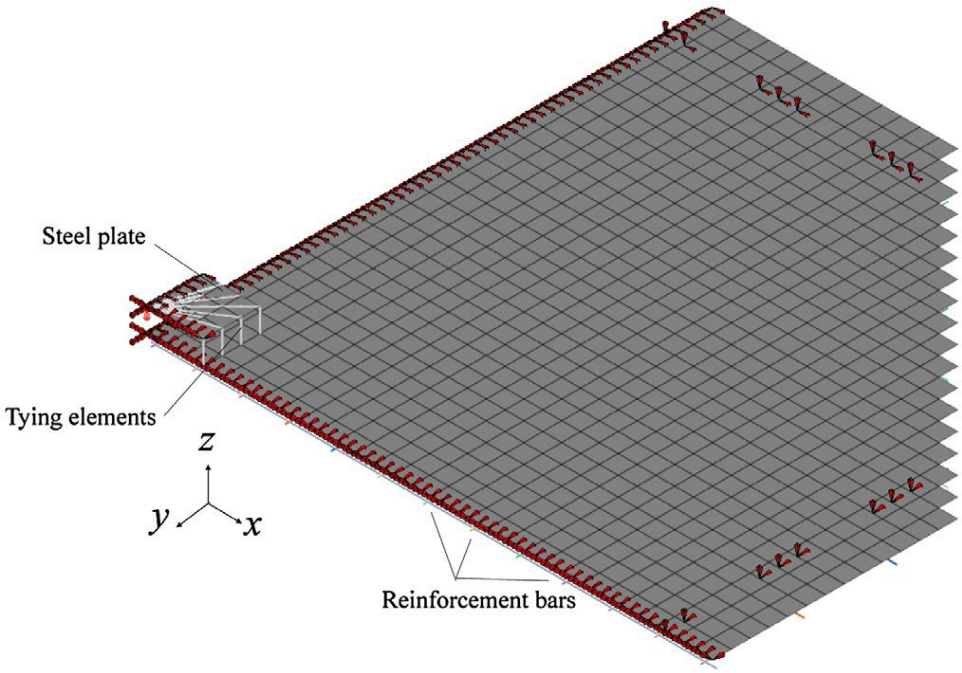

Figure 7.6 Non-linear shell element model of the two-way slabs, for Level III. From Plos et al. (2017).

geometric non-linearity with Total Lagrange description was included because a large deflection (120 mm) of the tested slab was observed. A Simpson integration scheme was used with 9 integration points over the thickness together with Gauss integration with 2×2 integration points over the shell area. The reinforcement was included in the model as fully bonded *embedded reinforcement*, in this case as individual rebars with the same layout as in reality[6]. Instead of applying an equally distributed load, as in Level II, a steel plate was added to the model. All nodes of the steel plate were tied to the centre node using rigid links so that they all had the same displacement in z direction. In this way displacement control could be used for the node at the centre of the slab in the loading procedure.

The analysis was carried out using a regular Newton-Raphson iteration method based on force and energy convergence criteria, with a tolerance of 0.01. The analysis finished when the analysis could not achieve convergence due to reinforcement rupture. The load-carrying capacity obtained was P_u = 60.7 kN. The risk of shear and punching failures, as well as anchorage failure, were checked separately based on a Level I analysis and found not to be critical.

7.1.2.5 Level IV: 3D Non-linear FE analysis with continuum elements and fully bonded reinforcement

For Level IV, a detailed 3D model with continuum elements was defined, as displayed in Figure 7.7. In (Shu *et al.*, 2014) such a model proved capable of predicting the load-carrying capacity of the same two-way slab reasonably well. In the

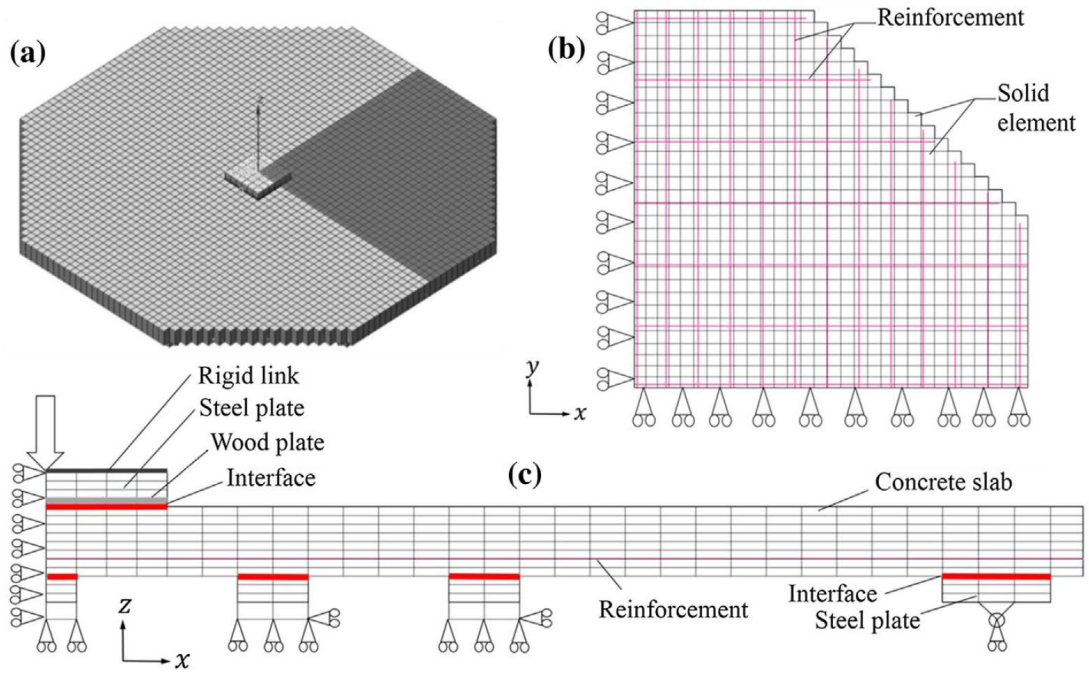

Figure 7.7 Non-linear continuum element model of the two-way slabs for level IV and V; (a) isometric view with the modelled quarter of the slab marked; (b) top view; (c) side view. From Plos et al. (2017).

[6] Compared to using embedded reinforcement layers, this means that not all concrete elements include reinforcement.

predicting the load-carrying capacity of the same two-way slab reasonably well. In the FE model, the steel plates at the supports were included and interface elements were used between the concrete and the steel plates to describe contact and friction. To model the boundary conditions provided by the roller supports, the translation of the nodes representing the centre of the rollers under the steel plates were fixed in both vertical direction and along the rollers. The translation of all nodes at the symmetry faces were fixed in the perpendicular direction. In this model, the geometric non-linearity with Total Lagrange description was also included. First order 8-noded brick elements, 40×40×10 mm (length×width×height) were used. The analysis was carried out using a regular Newton-Raphson iteration method based on force and energy convergence criteria. Since continuum elements were used, a tolerance of 0.02 was used since it is more difficult to achieve convergence than with the model at Level III.

The analysis finished when convergence could not be achieved due to bending failure limited by reinforcement rupture. The load-carrying capacity obtained was P_u = 66.7 kN. Shear or punching failure was not expected in this analysis (based on previous checks), and therefore a large aspect ratio (a value of 4) of the brick elements was considered acceptable. Since perfect bond was assumed for the interaction between the reinforcement and the concrete, the anchorage failure was also checked according to Eurocode 2 (CEN, 2004a) and found to be non-critical.

7.1.2.6 Level V: 3D Non-linear FE analysis with continuum elements including reinforcement bond

The models at Level IV and V were identical except for the bond of reinforcement. Instead of using fully bonded reinforcement, as at Level IV, a bond-slip behaviour was included in Level V to better describe the interaction between reinforcement and concrete. When the bond-slip model was used, 2-noded truss elements for the reinforcement were connected to the concrete elements by line interface elements; this was done automatically by the FE-program during pre-processing. These interface elements described a bond-slip behaviour in terms of a relation between the traction and the relative displacement along the bars. The analytical bond-slip relation given in Model Code 1990 (CEB-FIP, 1993) was used, see Figure 7.8. Unconfined concrete

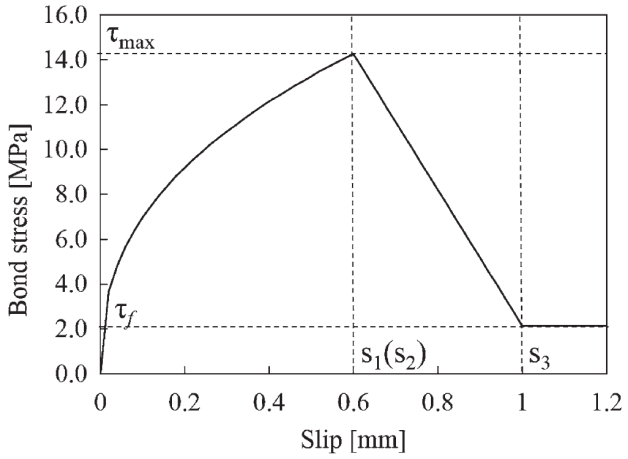

Figure 7.8 Bond–slip relation used for the interaction between concrete and the ribbed reinforcement bars for two-way slabs (CEB-FIP, 1993). From Plos et al. (2017).

under “good” bond conditions was assumed i.e., with the notation used in Model Code 1990, $s_1 = s_2 = 0.6$ mm, $s_3 = 1.0$ mm, $\tau_{max} = 14.26$ MPa and $\tau_f = 2.14$ MPa. The difference to Model Code 2010 (fib, 2013), as recommended in Section 6.2.5 and Appendix A, is on the descending branch of the bond-slip relation and is judged to have negligible influence on the results. The analysis finished after reinforcement rupture. The load-carrying capacity obtained was $P_u = 62.5$ kN.

7.1.3 Results and discussion

7.1.3.1 Structural behaviour

The load-carrying capacity of the two-way slab at Level I-II and the load-deflection curves from non-linear FE analyses at Level III-V are compared to the experimental result from test CR1 (see Figure 7.2) in Figure 7.9. Figure 7.10 shows crack patterns from the same test and the non-linear analyses. It is evident that the load-deflection behaviour in the non-linear analyses well reflected the experimental tests. In the experiments, the slabs failed at an average ultimate load of 70 kN with rupture of reinforcement bars. Several flexural cracks propagated from the centre in the diagonal direction, see Figure 7.10. The crack pattern was well predicted by the models at Levels III-V, and coincides with the failure mechanism assumed in the yield line method at Level I.

The yielding and rupture of reinforcement was influenced by the bond-slip property. Figure 7.11 (top) presents the yielding pattern of reinforcement from the analyses at Levels III, IV and V. Two of the reinforcement bars, located at the centre of the slab, started to yield when the load in all analyses reached around 40 kN. Then, the number of elements in which the reinforcement yielded gradually increased at Levels III and IV but not at Level V. In all analyses, the stress in the reinforcement bars continuously increased until the descending branch, indicating reinforcement rupture, was reached.

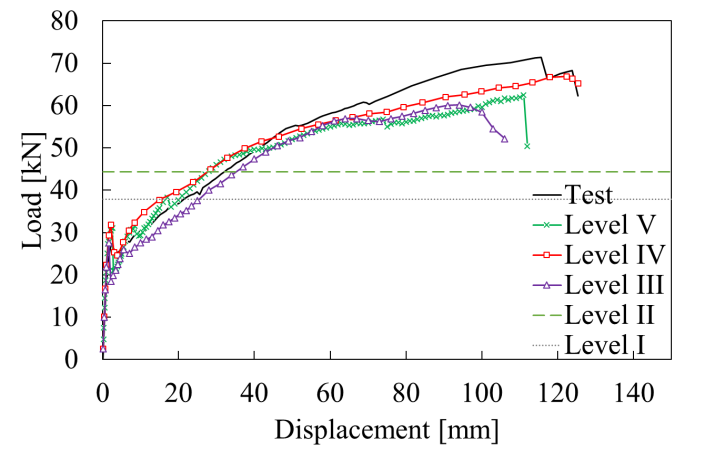

Figure 7.9 Load–deflection response and bending resistance of the two-way slabs. From Plos et al. (2017).

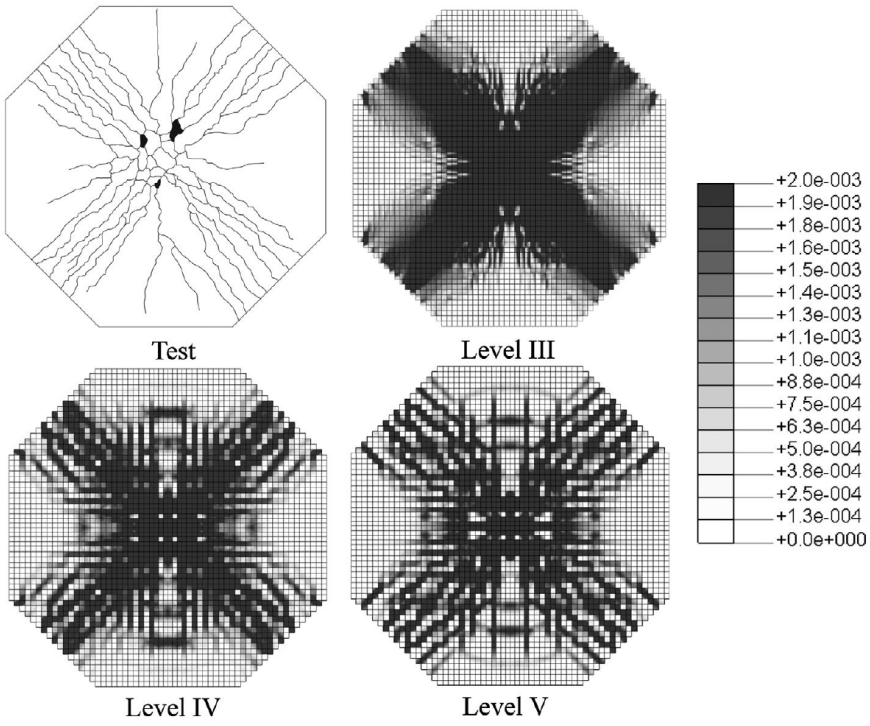

Figure 7.10 Crack pattern from experiment (CR1) and the strain-based crack pattern from analysis of the two-way slabs at 95% of the ultimate load (ε = 0.002 indicates fully open cracks), at the top surface of the slab from (a) experiment (b) analysis at Level III; (c) analysis at Level IV; (d) analysis at Level V. From Plos et al. (2017).

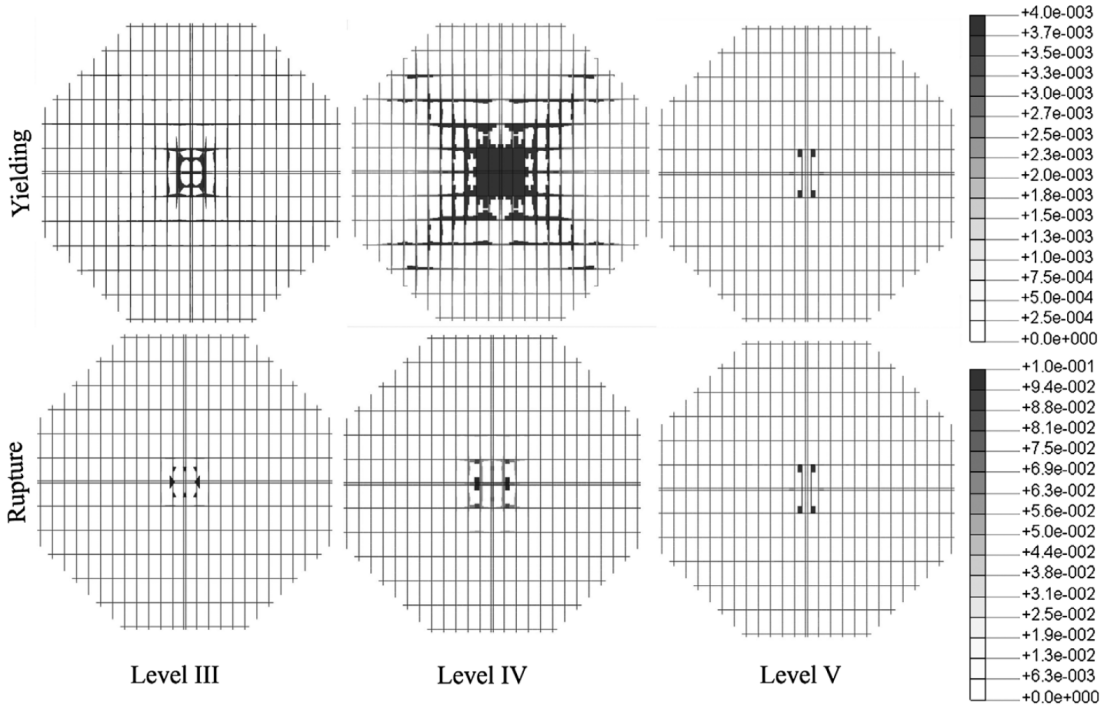

Figure 7.11 The strain-based yielding pattern from analysis of the two-way slabs at 95% of the ultimate load ($\varepsilon_y = 0.004$ indicates yielding) of reinforcement (top) and rupture pattern ($\varepsilon_y = 0.100$ indicates rupture) of reinforcement (bottom). From Plos et al. (2017).

7.1.3.2 Load-carrying capacity

Figure 7.12 summarizes the load-carrying capacity from the analyses on different assessment levels and the experimental tests of the slabs. It is obvious that the detectable load-carrying capacity increased for higher levels of assessment. However, the capacity detected was always lower than the experimental value. The lowest resistance obtained was from analytical calculations according to the yield line theory (Level I). The linear FE model (Level II) resulted in a higher capacity than Level I. On this level, the reinforcement moments obtained from the linear analysis were redistributed over an effective width. However, the redistribution widths according to Pacoste *et al.* (2012) are intended to be conservative estimates. In this case, the slab had the same reinforcement spacing over the entire width. In other cases, for assessment of existing structures, it can be important to adopt the redistribution widths to how the reinforcement is distributed in the slab.

A lower load-carrying capacity was estimated at Levels I and II than Levels III-V, largely because neither the hardening of reinforcement steel nor membrane action of the slab was included in the structural analysis. Compared to linear FE shell analysis (Level II), non-linear FE shell analysis (Level III) increase the capacity considerably since it includes material non-linearity. In addition, the load-deflection response can be studied with this level of analysis. The crack pattern was also visible, showing where and how the slab gets damaged and fails. Compared to the non-linear FE shell model, the non-linear FE continuum element models (Levels IV-V) predicted the capacity more accurately. One reason for this is probably because the geometric non-linearity was included in the continuum element model of the slab. The slab had a significant deflection during the test, arriving at 120 mm, greater than the thickness itself. By including the geometric non-linearity, the membrane action was accounted for more correctly at large deflections. It would have been beneficial to include geometric non-linearity also for the Level III analysis, as recommended in Section 5.2.6.

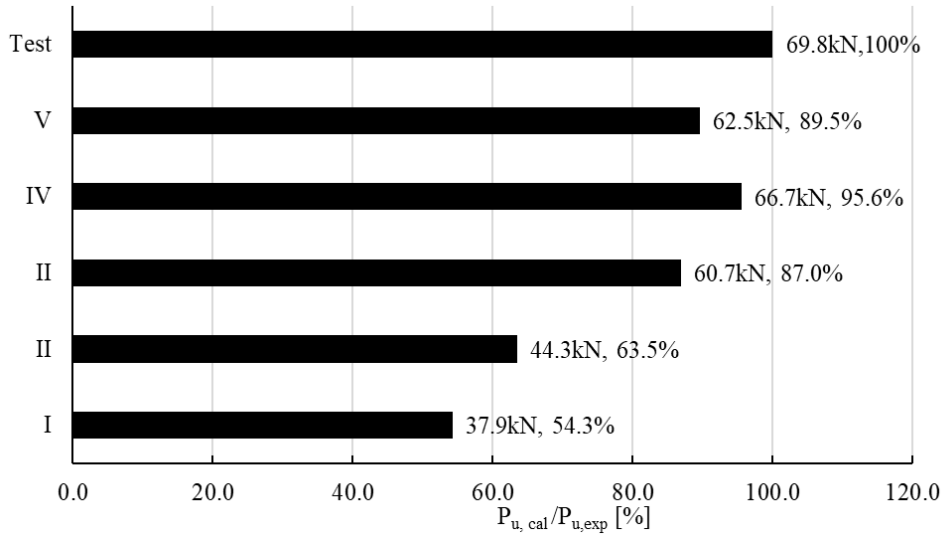

Figure 7.12 Load-carrying capacity, limited by bending failure, of the two-way slabs with assessment at different levels, compared with experimental results. From Plos et al. (2017).

7.2 Example 2: Application to a cantilever slab test subjected to one-way shear failure

In the second example, the recommended assessment strategy was applied to an experimental test of a cantilever slab subjected to shear failure. No safety format was adopted and the design load-carrying capacity was not evaluated. Instead, mean values of material properties were used in the entire assessment procedure to be able to compare the calculated results to that from tests. This case study has previously been reported in Plos *et al.* (2017).

7.2.1 Experiment

To investigate the structural behaviour and failure mode of cantilever bridge deck slabs, several experiments have been performed (Vaz Rodrigues *et al.*, 2008). The experimental work involved six experiments on two specimens, representing the cantilever deck slab of a box girder bridge in 3/4 scale, without shear reinforcement in the slab. A slab with four concentrated loads, slab DR1-a, was chosen for the study in this example, see Figure 7.13 (a). The cantilever had a span of 2.78 m and a length of 10 m. The slab thickness varied from 0.38 m at the supported end to 0.19 m at the cantilever tip as shown in Figure 7.13 (b, c), with a concrete cover of 0.03 m. The fixed end support was clamped by means of vertical pre-stressing. The reinforcement layout is displayed. The specimen was subjected to four concentrated forces simulating traffic loads. The concentrated loads were applied on the top of the slab using steel plates with dimensions 300 × 300 × 30 mm. The deflection at point *p* was measured.

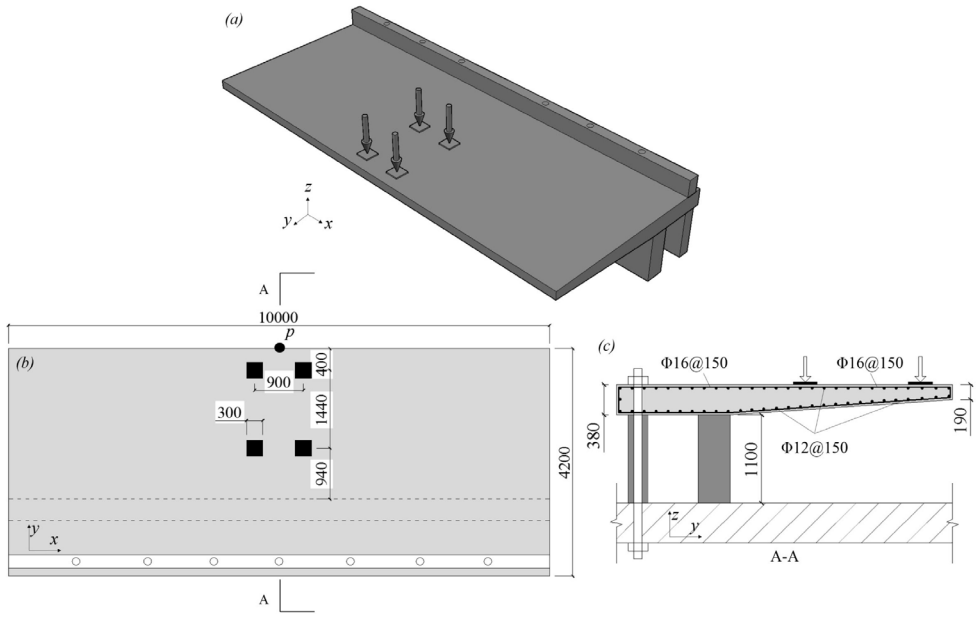

Figure 7.13 The experiment set-up, dimensions and reinforcement layout for cantilever slab DR1-a, adapted from (Vaz Rodrigues, 2007); (a) isometric view (b) top view and (c) cross-section; all dimensions are in mm. From Plos et al. (2017).

The specimen failed in a brittle manner at a total load of $Q_{u.exp}$ = 1396 kN by the development of a curved shear failure surface around the concentrated loads. The crack pattern at ULS included flexural cracks at the top and bottom surface, and inclined shear cracks from the top towards the bottom of the cantilever slab (Vaz Rodrigues *et al.*, 2008).

7.2.2 Analysis at different assessment levels

In the same way as in Example 1, the cantilever slab in Example 2 was assessed at the different levels of assessment according to Section 2.2. To analyse the response, the finite element software DIANA 9.4.4 (TNO, 2015) was used.

7.2.2.1 Material models and material parameters

In all calculations, mean material parameters from the tests were used, see Table 7.3. The non-linear material models used in the analyses of the cantilever slab were the same as for the two-way slab, previously described in Section 7.1.2.1. A total strain rotating crack model was used for the concrete and a Von Mises yield criterion was used for the reinforcement. The material properties available from the experiment were used and complemented with some assumptions regarding the non-linear material response. For example, linear tension softening after cracking and the Thorenfeldt (1987) compressive behaviour were used for concrete, while bi-linear hardening plasticity behaviour was adopted for reinforcement, see Figure 7.14.

Table 7.3 Material parameters for the cantilever slab (Vaz Rodrigues, 2007).

Parameter of concrete		Parameter of reinforcement steel	
Young´s modulus	E_c = 36.0 GPa	Young´s modulus	E_s = 210 GPa
Poisson's ratio	ν = 0.15	Poisson's ratio	ν = 0.2
Compressive strength	f_{cm} = 39.1 MPa	Yield strength	f_y = 499 MPa
Tensile strength	f_{ctm} = 2.9 MPa	Ultimate strength	f_u = 600 MPa

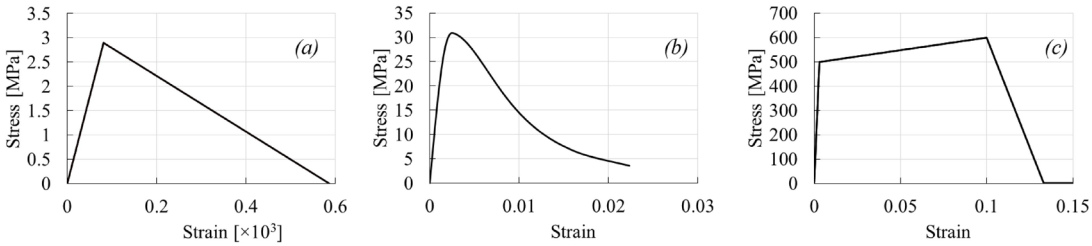

Figure 7.14 Examples of stress–strain relations used for material response in the cantilever slab, for (a) concrete in tension, (b) concrete in compression and (c) reinforcement steel. From Plos et al. (2017).

7.2.2.2 Level I: simplified analysis method

To assess the load-carrying capacity in the ultimate limit state, several possible failure mechanisms was evaluated such as (a) flexural failure, (b) one-way shear failure and (c) punching shear failure. The anchorage capacity, checked according to Eurocode 2 (CEN, 2004a), was found to be non-critical to this case. The flexural load-carrying capacity was checked using the yield line theory (Vaz Rodrigues, 2007), see Figure 7.15 (a). Resistance models for one-way shear and punching shear resistance of flat slabs were checked according to Eurocode 2 (CEN, 2004a), see Figure 7.15 (b, c).

The design punching shear strength V_R is determined by multiplying a shear strength per unit length (nominal shear strength v_R) by a control perimeter (b_0). For a group of four loads, simulating vehicle loads, the critical control perimeter may be in section 1 or 2, Figure 7.15 (c). Calculation results show that the outer section 1 was more critical due to shorter perimeter and smaller effective depth.

The resistance for bending, one-way shear and punching shear can be found in Table 7.4. It was found that the governing failure mode was punching shear at section 1 and the load-carrying capacity Q_u = 906 kN at this level of assessment.

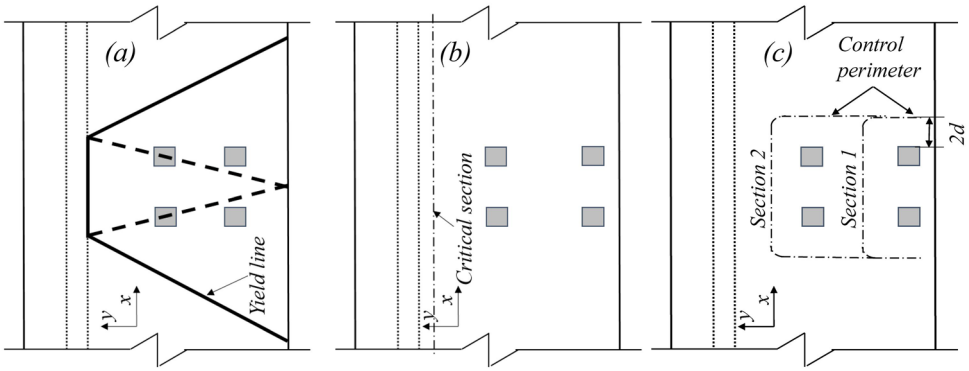

Figure 7.15 Resistance models used for the cantilever slab at Level I: (a) yield line figure used for bending resistance, (b) critical section for one-way shear and (c) critical sections for punching shear. From Plos et al. (2017).

Table 7.4 Calculated load-carrying capacity for bending, one-way shear and punching shear. (Plos et al., 2016)

Resistance	Load-carrying capacity Q_u (kN)
Bending capacity	1600
One-way shear	1650
Punching shear	906

7.2.2.3 Level II: 3D linear shell (FE) analysis

To determine the load effects by linear FE analysis in the cantilever slab, a 3D shell element model was created, see Figure 7.16. The dimensions in the FE model were

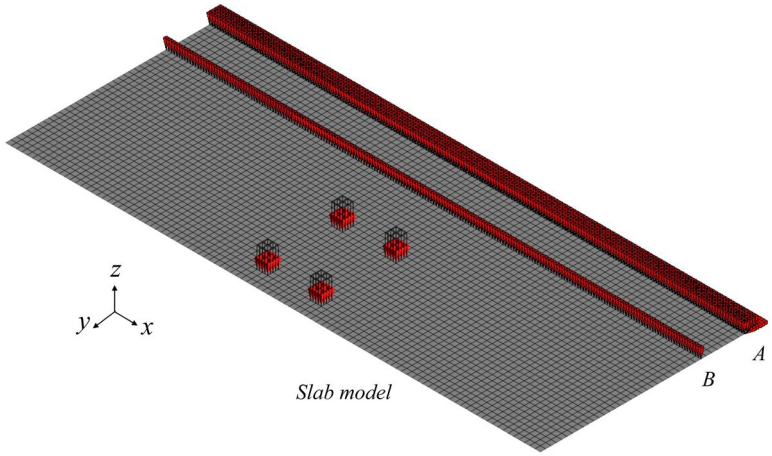

Figure 7.16 Linear shell element model of the cantilever RC slab, for Level II. From Plos et al. (2017).

identical to the experiment. The concrete slab was modelled with 8-noded rectangular shell elements at 100 mm × 100 mm size. The boundary conditions were chosen to simulate the experimental conditions, with all translations fixed along edge A, and the vertical translations constrained along the simply supported edge B. A unit load of 1 kN was equally distributed over the four loading plates.

To analyse the one-way shear capacity, the shear force field from the linear FE analysis was used. According to Pacoste *et al.* (2012), the critical cross-section for shear forces is situated at a distance $y_{cs} = (c+d)/2$ from the centre of the loading plate, where d is the effective depth of the slab and c is shown in Figure 7.17. For the slab test studied, this results in two possible critical cross sections as shown in Figure 7.17 (left). In Figure 7.17 (right), a typical shear force distribution obtained from linear FE analysis, for one of the critical sections, is shown. The distribution width w_x can be determined according to Equation (7.5) and (7.6), see details in Pacoste *et al.* (2012).

$$w_{\max} = \max \begin{cases} 7d + b + t \\ 10d + 1.3y_{cs} \end{cases} \text{ for } y = 0 \tag{7.5}$$

$$w_{\min} = \min \begin{cases} 7d + b + t \\ 10d + 1.3y_{cs} \end{cases} \text{ for } y = y_{max} \tag{7.6}$$

where d is the effective depth at the critical section, t is the thickness of the surface and b and c are the dimensions of the loading plates, as shown in Figure 7.17. The distance y is measured from the support edge to the critical cross-section. The shear resistance for sections 1 and 2 were calculated to be 967 kN and 1015 kN, respectively.

The punching shear capacity was calculated according to Model Code 2010 (fib, 2013), using a higher *Level-of-Approximation*. (Consequently, the recommendations in Section 4.3.4 to use Eurocode 2 (CEN, 2004a) is not followed here). The shear resistance was calculated as:

$$V_{Rm,c} = k_{\psi} \cdot \sqrt{f_{cm}} \cdot db_0 \tag{7.7}$$

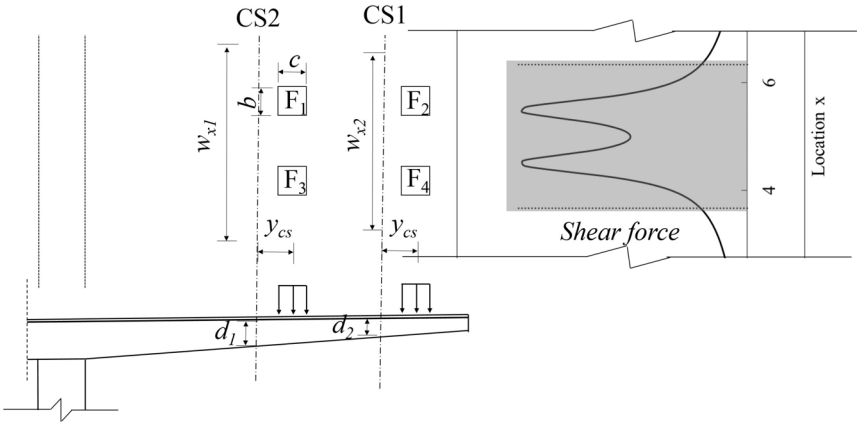

Figure 7.17 Schematic illustration of one-way shear assessment for the cantilever RC slab, using linear shell FE analysis at Level II; (a) top view of cantilever slab, layout of loads, critical sections and shear distribution width w; (b) cross-section of cantilever slab; (c) shear force distribution along critical sections. From Plos et al. (2017).

The parameter k_ψ depends on the rotations ψ of the slab, which was calculated according to Model Code 2010 (fib, 2013). d is the effective depth of the slab and b_0 is the shear-resisting control perimeter. The total load carrying capacity of the slab with respect to one-way and punching shear are summarized in Table 7.5.

The bending capacity was also calculated and proved to be non-critical. Thus, the governing failure mode at this assessment level was punching shear at section 2 and the load-carrying capacity Q_u = 1009 kN at this level of assessment.

Table 7.5 Load-carrying shear capacity of cantilever slab at Level II. Plos et al. (2017).

Load-carrying capacity (kN)	One-way shear	Punching shear
Section 1	1077	1167
Section 2	1055	1009

7.2.2.4 Level III: 3D non-linear shell FE analysis

At Level III, the slab was modelled with shell elements using the same FE mesh as in the Level II analysis; see Figure 7.18, but with non-linear material response. The integration scheme was identical to Level III in Section 0, i.e., Simpson integration with 9 integration points in the thickness direction. Furthermore, the boundary condition at support B was modelled differently than Level II; instead of using simply supports along a line, the supports, consisting of concrete blocks, was included and modelled using non-linear springs, representing the stiffness of the concrete blocks in compression and with negligible stiffness in tension to allow uplifting. The reinforcement was modelled as fully bonded *embedded reinforcement* grids in both x and y directions.

To enable deformation control of the four concentrated loads on steel plates, a loading sub-structure was used in the model, see Figure 7.18. The loading sub-structure was

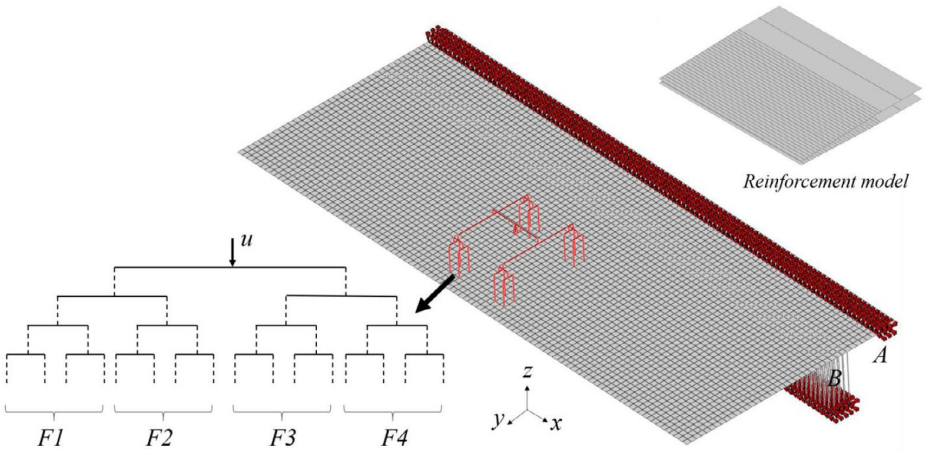

Figure 7.18 Non-linear shell element model of the cantilever RC slab, for Level III. From Plos et al. (2017).

modelled with very stiff beam elements and was designed to be statically determinate. The stiff beams were connected by tying some of the nodes to each other, (the dashed lines in Figure 7.18), so that they had the same translation in z-direction. This way, the load was distributed equally on 16 nodes, each concentred load in the test represented by four node loads. The analysis was carried out using a regular Newton-Raphson iteration method based on force and energy convergence criteria, with a tolerance of 0.01. The analysis finished when it could not reach convergence due to reinforcement rupture, indicating a bending failure, at a load level of 1683kN.

Since shear type failures are not reflected in the analysis at this level, the resistance with respect to one-way shear and punching was separately evaluated according to Section 5.4.4. The governing punching capacity was calculated using the results from the non-linear FE analysis by applying the critical shear crack theory (CSCT) by Muttoni, according to Model Code 2010 (fib, 2013), *Level-of-Approximation* IV (LoA IV). In this method, the punching shear strength V_R depends on the rotation ψ of the slab. The punching capacity for both critical sections 1 and 2 were checked, see Figure 7.19 (a).

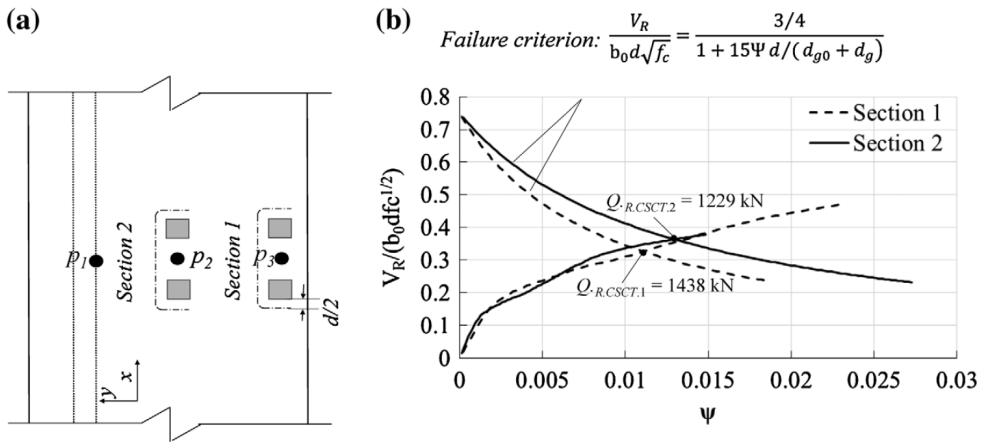

Figure 7.19 Determination of shear punching resistance based on the critical shear crack theory (CSCT) (Muttoni, 2008) for the cantilever RC slab; (a) location of points p1, p2, p3 and critical sections and (b) load–rotation curve and failure criterion. From Plos et al. (2017).

The rotation ψ was determined from the non-linear analysis as the difference in inclination between points p_1 and p_2 for critical section 2; and between points p_2 and p_3 for critical section 1. The failure loads were determined as the intersection point between the relation for the relative shear force versus rotation obtained from the non-linear FE analysis and the corresponding failure criterion according to Figure 7.19 (b). The results show that the punching capacity, instead of bending and one-way shear, was found to limit the load-carrying capacity of the slab to Q_u = 1229 kN.

7.2.2.5 Level IV: 3D Non-linear FE analysis with continuum elements and fully bonded reinforcement

In order to capture inclined cracking and shear failure, a detailed 3D model of half of the slab was created for assessment Level IV using continuum elements, as displayed in Figure 7.20. In this FE model, the steel plates along edge A under the hydraulic jacks of the loading system, used in the test, were included in the model. The supporting concrete blocks along line B were also included, with interface elements between the blocks and the slab to describe contact and friction. Second-order 20-noded brick elements, 150×150×60 mm (length×width×height) were used. In contrast to Example 1, first order elements were not used to prevent the analysis from becoming too time consuming (Shu *et al.*, 2014a; Hendriks *et al.*, 2017); Three elements instead of eight was used over the height since 2nd order elements were used, resulting in approximate 1/10 of the number of elements. The translations of all nodes at the symmetry faces were fixed in the direction perpendicular to the face. The steel plates along edge A had fixed translation for vertical direction, and the concrete block at position B was simply supported at its lower face. A loading sub-structure, as described at Level III, was included also in this model. Each reinforcement bar of the slab was modelled as a fully bonded *embedded reinforcement* bar. The analysis was carried out using a regular Newton-Raphson iteration method based on force and energy convergence criteria, with a tolerance of 0.01. The analysis finished when a shear type failure with an inclined shear surface was formed. The response and failure are further discussed in Section 7.2.3. The load-carrying capacity obtained was Q_u = 1260 kN.

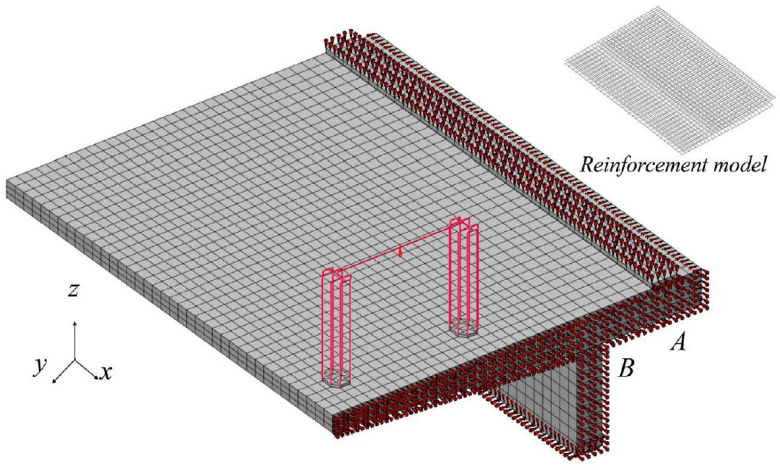

Figure 7.20 Non-linear continuum element model of cantilever RC slab, for Level IV. From Plos et al. (2017).

7.2.2.6 Level V: 3D non-linear FE analysis with continuum elements including reinforcement bond

The model at Levels V & IV were identical except for the reinforcement. Instead of using fully bonded reinforcement, a bond-slip relation was included to describe the interaction between the reinforcement and surrounding concrete more in detail. The bond-slip property used was based on Model Code 1990 (CEB-FIP, 1993); see the example in Figure 7.8. The analysis finished when a shear type failure with an inclined shear surface was formed and the load-carrying capacity obtained at this level was Q_u = 1269 kN.

7.2.3 Results and discussion

7.2.3.1 Structural behaviour

The load-carrying capacity of the cantilever slab at assessment Levels I-II and the load-deflection curves from the non-linear FE analyses at Levels III-V are compared to the experimental result in Figure 7.22.

Figure 7.22 shows the crack pattern from both the experiment and the non-linear FE analyses at 95% of ultimate load. It is evident that the load-deflection behaviour from the analyses at Levels III-V are in good agreement with experimental results, except for deflections smaller than around 20 mm. In the experiment, the slab was subjected to 100 loading cycles up to 410 kN to investigate the behaviour at service limit state before loaded up to failure; this cyclic loading was not included in the analyses explaining the discrepancy in deflection for smaller loads. The cracks at the top

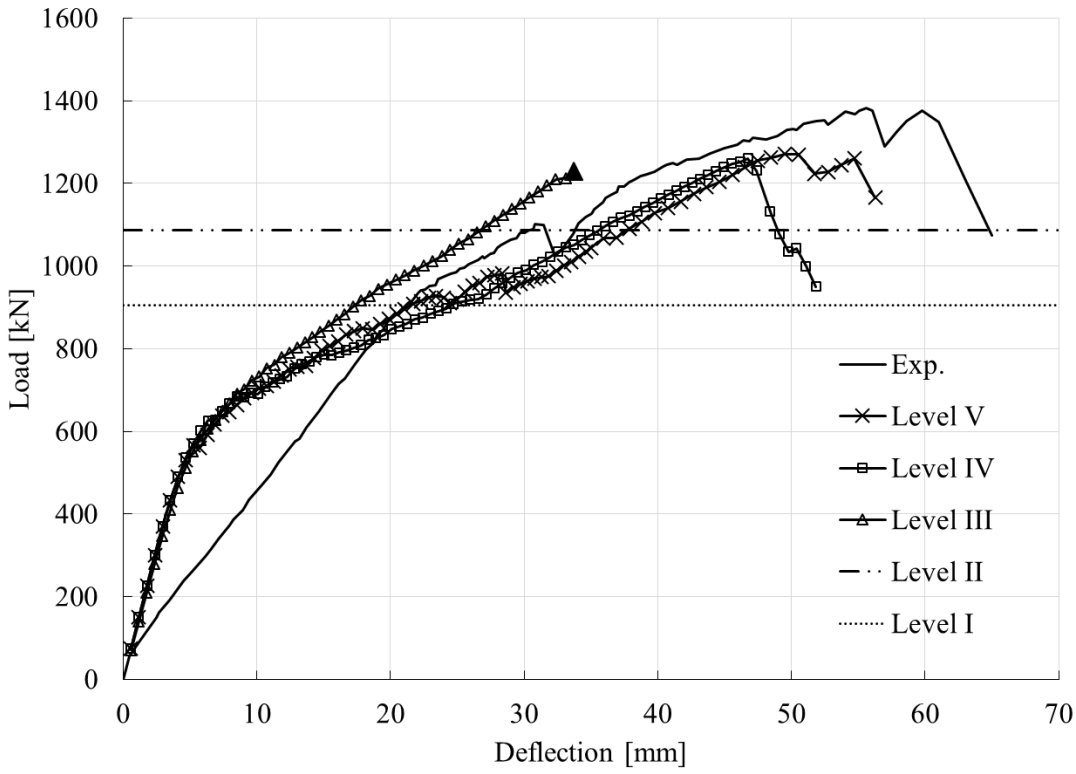

Figure 7.21. Load–deflection response and load-carrying capacity for cantilever RC slab. Adapted from Plos et al. (2017).

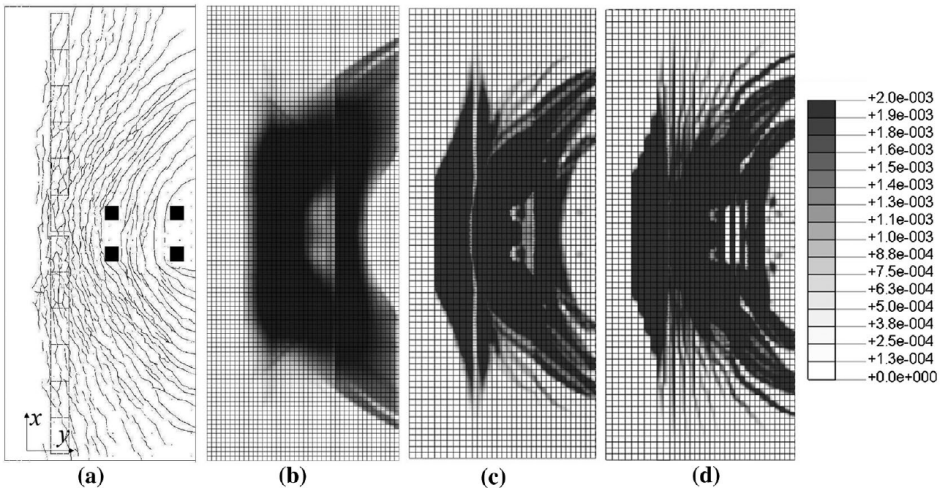

Figure 7.22 Crack pattern from experiment and strain-based crack pattern from analysis of the cantilever RC slab at 95% of the ultimate load (ε = 0.002 indicates elements with fully open cracks), at the top surface of the slab from (a) experiment, adapted from (Vaz Rodrigues, 2007), (b) analysis at Level III; (c) analysis at Level IV; (d) analysis at Level V. From Plos et al. (2017).

surfaces developed as a semi-circular shape around the load, resembling the crack pattern expected by the yield line theory mechanism at the ultimate load stage, see Figure 7.22. This indicates that the slab displayed bending behaviour at this stage. Figure 7.22 (b) (c) and (d) show contour plots of the largest principal strain indicating the crack pattern at 95% of the ultimate load from the non-linear FE analyses at Levels III - V.

Meanwhile, an inclined shear crack developed around the two concentrated loads closest to the tip of the cantilever at a load level of about Q = 825kN (approximately 60% of ultimate capacity), corresponding well with the experiment results. This provoked the failure of the slab in a way similar to the experiment, see Figure 7.23.

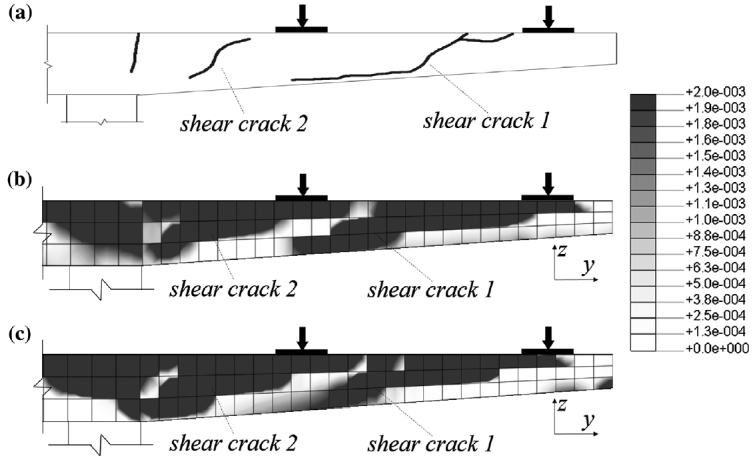

Figure 7.23 Strain-based crack pattern at section A-A from analysis of the cantilever RC slab at 95% of the ultimate load (ε = 0.002 indicates fully open crack) from (a) experiment, adapted from (Vaz Rodrigues 2007), (b) analysis at Level IV and (c) analysis at Level V. From Plos et al. (2017).

Another shear crack developed in the region between the clamped edge and the concentrated loads. This latter crack, however, did not develop to a complete failure surface. The shear cracks did not occur at Level III as shell elements cannot describe shear cracking in the cross-section. Compared to Level IV, the analysis at Level V displayed a clearer crack pattern, but a similar structural behaviour. The experiment failed at a load of $Q_{u.exp}$ = 1396kN, in a shear manner, which is higher than in the analyses at Levels IV – V, but much lower than the ultimate load (1600kN) estimated based on the yield-line theory.

The influence of flexural cracks on the shear force distribution was also observed when shifting from linear to non-linear FE analysis. The initial flexural crack started at the mid region, which forced the shear force to be redistributed away from the cracked region, i.e., to be moved outwards from the middle. Since the non-linear redistribution can reduce the shear force in the most critical region from what is predicted from linear analysis, it is beneficial if structures sensitive to shear are assessed taking this redistribution into account. Based on the measured crack widths in the experiment, yielding occurred both in the top and in the bottom reinforcement before punching failure occurred (Vaz Rodrigues, 2007). Consequently, the load was redistributed, as the slab was capable of carrying increasing loads after yielding of the reinforcement. However, in the non-linear analyses, yielding of the reinforcement was observed only in the analysis at Level V, but not in the Level III and IV analyses. The reason was that at Level III and IV, the strain of the reinforcement was limited by the full bond to surrounding concrete. However, in the non-linear FE analysis at Level V, this restriction did not exist.

7.2.3.2 Load-carrying capacity

Figure 7.24 summarizes the ultimate loads from all assessment levels and the experiment of the bridge cantilever slab. Generally, the predicted capacity increased for higher levels, but was always smaller than the experimental value. The lowest resistance was obtained from analytical calculations according to Eurocode 2 (Level I). The linear FE analysis (Level II) resulted in a slightly higher prediction. At this level, a distribution of the shear force from linear FE model was made by assuming a

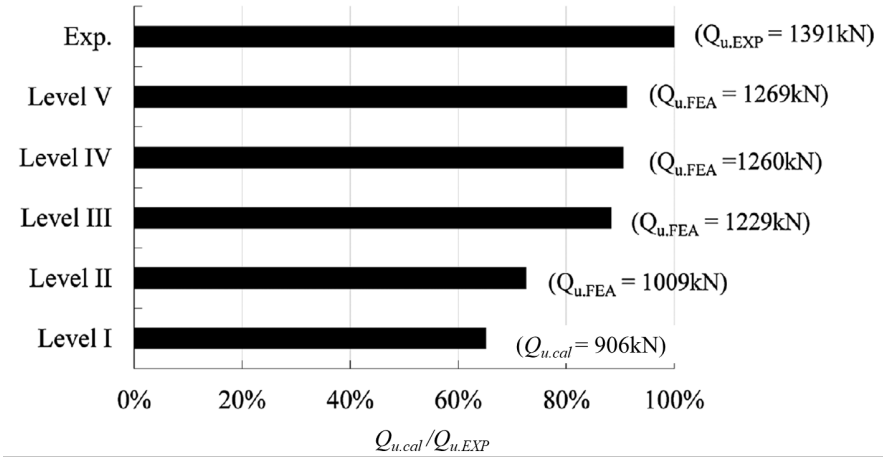

Figure 7.24 Load-carrying capacity, limited by punching shear, of the cantilever RC slab DR1-a with assessment at different levels, compared with experimental results. From Plos et al. (2017).

redistribution width according to Pacoste *et al.* (2012). The assessment at Levels I and II underestimated the load-carrying capacity partly because the redistribution of shear forces due to cracking was not included in the structural analysis. However, a major reason that the non-linear shell FE analysis (Level III) estimated the punching capacity better than the linear shell FE analysis (Level II) is that the non-linear response from the structural analysis is included in the resistance model. However, it is important to note that even though the flexural crack pattern was reflected in analyses at Level III, shear cracking in the cross-sections cannot be reflected. Therefore, the non-linear FE continuum element analyses (Level IV and Level V), which were capable of simulating punching failure and shear crack pattern, offered enhanced opportunity to accurately assess the RC slab subjected to shear. When the bond-slip properties of the reinforcement bars were included in the continuum element model (Level V), the deformation of the structure and the interaction between the reinforcement and surrounding concrete could be reproduced closer to the reality.

7.3 Example 3: Application to a real bridge with hypothetic (future) deterioration

This example was used to demonstrate and validate *the Multi-Level Assessment Strategy* according to Section 2.3 through a case study on a real bridge. The bridge is located in Sweden, is in reality relatively new and in good condition. However, for the case study, it was assumed to be deteriorated in a hypothetic future scenario. This case study has previously been reported in Shu *et al.* (2019).

7.3.1 Bridge description and definition of study scenarios

The bridge is, according to the as-built drawings and design report, a simply supported, 47.2 m long composite bridge consisting of three steel girders and a reinforced concrete deck slab. The free span of the bridge is 35 m. Further information of the dimensions can be found in Figure 7.25. The characteristic cylinder

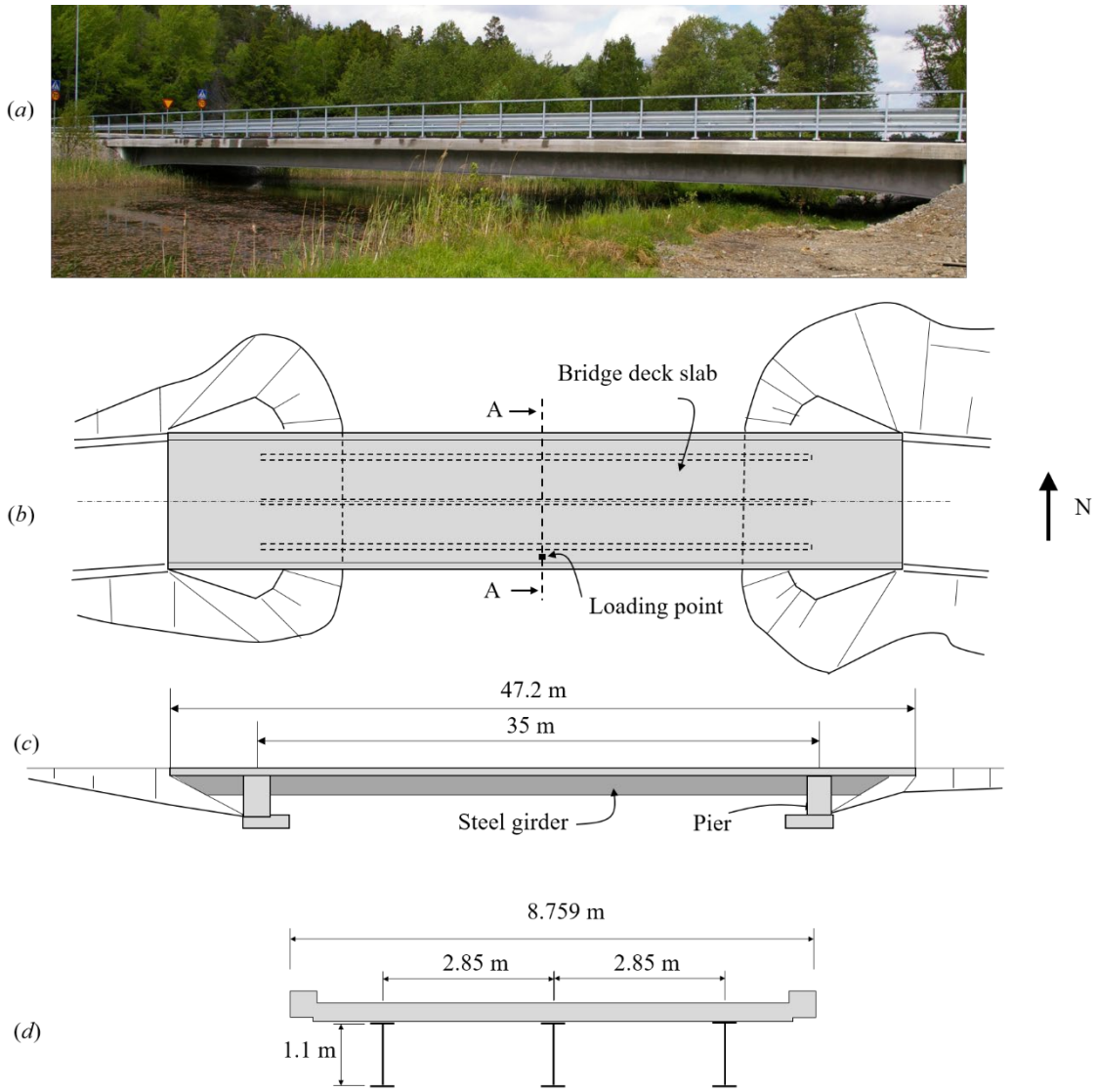

Figure 7.25 (a) Photo of the bridge used for example 3, (b) plan view of the bridge, (c) side view of the bridge; section A-A is subjected to the concentrated load; (d) cross-section of the bridge. From Shu et al. (2019).

compressive strength of the concrete is 40 MPa and the characteristic yield strength for the reinforcement is 500 MPa. The concrete cover is 45 mm. The characteristic yield strength for the girder steel is 460 MPa.

Since the bridge is relatively new, no extensive deterioration has been observed. However, this might become the case in the future, after several decades in service. Moreover, requirements might also change with time e.g. due to changes in use or in relevant specifications. Because of this, a fictitious deterioration scenario was defined to demonstrate the assessment strategy. In the chosen scenario, it was assumed that the bridge deck is deteriorated due to a combination of frost, alkali–silica reaction and corrosion. The assessment strategy was then tested by performing a simulated safety assessment of the shear capacity of the cantilever slab. The cantilever slab, at section A-A, was loaded with a single wheel load close to the edge beam, according to Swedish regulations for assessment of bridges (Swedish Traffic Administration, 2018); see Figure 7.26. The hypothetic future minimum requirement for the design axle load was assumed to be 200×1.3 kN = 260 kN.

The thickness of the bridge deck slab is 250 mm. However, the assumed material deterioration, i.e. the deterioration due to frost and alkali–silica reaction (ASR) damages, as well as due to corrosion of reinforcement leading to concrete cracking, may cause a significant reduction in concrete strength. In this study, a reduction of 50% in compressive strength was assumed as a result of such damage mechanisms, according to the research by Zandi *et al.* (2011a, b). Furthermore, it was assumed that the bridge deck slab had experienced severe reinforcement corrosion leading to spalling of concrete cover; a reduced cross-sectional height of 50 mm was assumed for parts of the slab. Based on the assumption above, a stepwise assessment procedure according to *the Multi-Level Assessment Strategy,* Plos *et al.* (2017)*,* outlined in Chapter 2, was carried out.

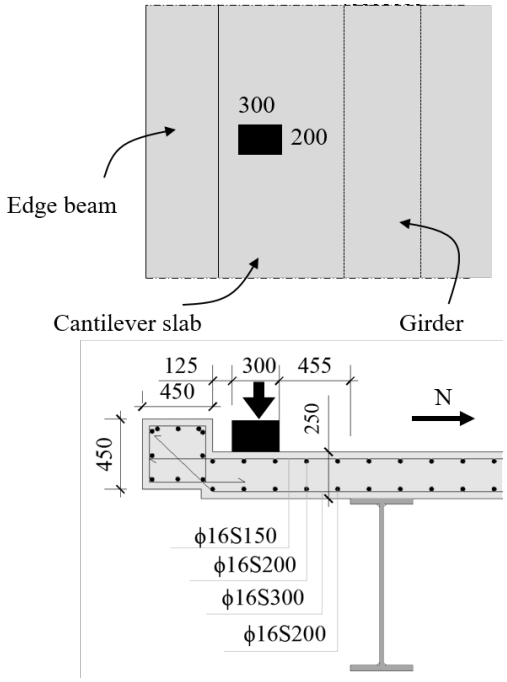

Figure 7.26 Loaded section A-A: load position, the dimension of the bridge deck slab and the layout of the reinforcement bars. All dimensions are in mm. From Shu et al. (2019).

7.3.2 Analysis at different assessment levels

Following *the Multi-Level Assessment Strategy*, Section 2.3, and the recommended safety formats in Section 2.4.3, the successively improved assessment of the bridge deck slab was carried out on the following levels:

- Level I analysis + PSF + Tested material properties
- Level II analysis + PSF + Tested material properties
- Level III analysis + ECOV + Tested material properties
- Level IV analysis + Schlune *et al.*+ Tested material properties

7.3.2.1 Level I analysis

As an initial level of structural assessment, the load-carrying capacity was calculated according to Eurocode 2 (CEN, 2004a) using the partial safety factor (PSF) method. For one-way shear, the entire concentrated load was assumed to be carried by the cantilever slab and distributed over an effective width according to French Annex (Chauvel *et al.*, 2007), i.e. corresponding to the principal of a 45 degree distribution of the load. Since the shear span $a_v \geq 2d$ from the edge of a support, the arching action was not taken into account, according to Eurocode 2 (CEN, 2004a). The shear resistance for one-way as well as punching shear was calculated as:

$$V_{Rd,c} = C_{Rd,c} k (100 \rho f_{ck})^{\frac{1}{3}} bd \tag{7.8}$$

$$k = 1 + \sqrt{\frac{200}{d}} \tag{7.9}$$

Here, $C_{Rd,c} = 0.18/\gamma_c$; ρ is the main reinforcement ratio (in the transversal direction of the bridge deck slab) for one-way shear and average reinforcement ratio in two directions for punching shear; f_{ck} is characteristic compressive strength based on tests of concrete; d = 200mm-45mm-16/2mm = 147mm is effective depth of the RC slab; k is a parameter considering size effect; b refers to the effective width (b_w = 1710 mm) for one-way shear and to the control perimeter (b_0 = 1724 mm) for punching shear. The length of the effective width b_w for one-way shear is shown in Figure 7.27 (*a*).

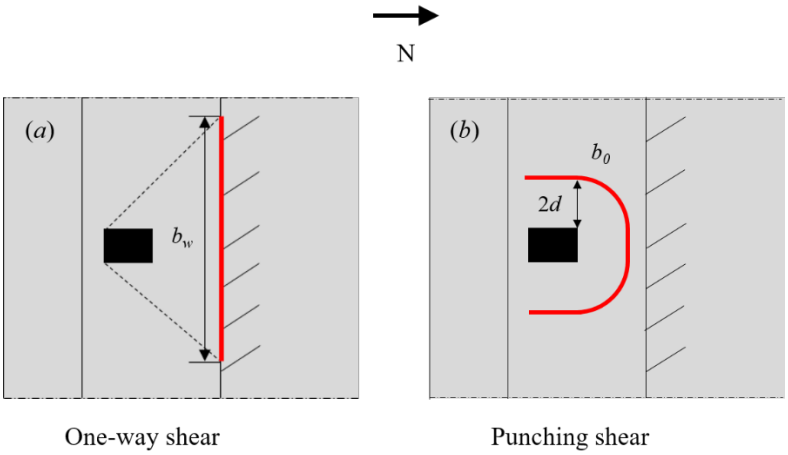

Figure 7.27 (a) Effective width for calculation of one-way shear resistance and (b) control perimeter b_0 for calculation of punching shear resistance. From Shu et al. (2019).

For punching shear, the critical section is located 2*d* from the boundary of the load in Eurocode 2 (CEN, 2004a). The critical sections for calculation of punching shear resistance are shown in Figure 7.27 (*b*). Considering the existence of the edge beam, the control perimeter is unsymmetrical to remain inside the edge beam due to the conservative assumption.

The bending capacity was calculated using the strip method (Hillerborg, 1996). The strip width was taken the same as for one-way shear, i.e. b_w = 1710 mm. At this step, load-carrying capacity calculated for one-way shear, punching shear and bending failure was obtained as 153 kN, 159 kN and 192 kN, respectively. Consequently, the governing failure mode for load-carrying capacity at this level of assessment was one-way shear and the capacity was lower than the minimum required design load capacity of 260 kN. If the actual condition of the bridge had been unknown, and the concrete compressive strength had not been determined through tests, there would have been a substantial risk that the load-carrying capacity had been severely over-estimated.

7.3.2.2 Level II analysis

In this step, a 3D shell element model in TNO DIANA (TNO, 2015) was created and a linear FE analysis (Level II analysis) was made to determine the load effects; see Figure 7.28. The bridge was modelled using 8-node 50×50 mm rectangular shell elements for the bridge deck in the area close to the load and 100 mm to 400 mm rectangular shell elements for other parts of the slab and the I-shaped steel beams. For the shell elements, a Simpson integration scheme was used over the thickness together with Gauss integration of 2×2 integration points over the shell area. Reinforcement bars were not included in the linear FE model. The connection between the concrete deck slab and steel girders was assumed to be fully bonded. The bridge was simply supported at the end abutments.

The resistance for shear was determined using resistance models in Model Code 2010 (fib 2013). Consequently, the recommendations in Section 4.3.4 regarding resistance models for Level II was not fully followed in this case study, but resistance models on

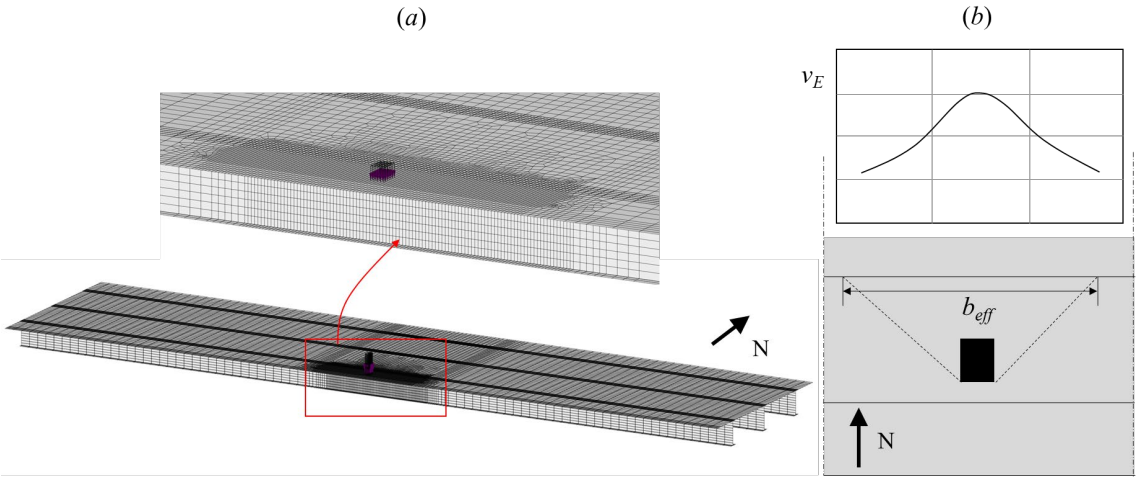

Figure 7.28 (a) Linear shell FE model of the tested slab, (b) Average of shear force at the critical sections within effective b_w for one-way shear. From Shu et al. (2019).

higher *Level-of-Approximation* was used. The one-way shear resistance was determined as a shear force-strain relation according to Equation (7.10) from Model Code 2010 (fib, 2013), based on the Simplified Modified Compression Field Theory (Bentz, Vecchio, & Collins, 2006). k_v was given by Equation (7.11) (using LoA II (fib, 2013)). The parameter k_{dg} depends on the maximum aggregate size d_g and may be calculated using Equation (7.12). The resistance shear force-strain relation was compared to the corresponding linear shear force-strain relation evaluated from the FE analysis, and the load carrying capacity was obtained from the intersection between these curves. An estimation of the reference longitudinal strain at mid-depth of the effective shear depth ε_x was obtained from the results of FE analysis as the strain averaged along and perpendicular to the control section according to Model Code 2010 (fib, 2013).

$$V_{Rd,c} = k_v \frac{\sqrt{f_{ck}}}{\gamma_c} \cdot z b_w \tag{7.10}$$

$$k_v = \frac{0.4}{1+1500\varepsilon_x} \cdot \frac{1300}{1000 + k_{dg} z} \tag{7.11}$$

$$k_{dg} = \frac{32}{16 + d_g} \geq 0.75 \tag{7.12}$$

For punching shear, the applied load was compared to the punching shear resistance calculated according to Equation (7.13) from Model Code 2010 (LoA II) (fib, 2013):

$$V_{Rd,c} = k_\psi \frac{\sqrt{f_{ck}}}{\gamma_c} \cdot d b_0 \tag{7.13}$$

$$k_\psi = \frac{1}{1.5 + 0.9 k_{dg} \psi d} \tag{7.14}$$

where f_{ck} is tested characteristic value of concrete compressive strength, d is the effective depth of the slab and b_0 is the length of the basic control perimeter according to Model Code 2010. The parameter k_ψ and, hence, the punching resistance depend on the rotations ψ of the slab. Rotations ψ = 0.0026 was obtained from the results of FE analysis according to Model Code 2010.

The bending capacity was calculated by evaluating the linear FE analysis of the slab according to the recommendations in Pacoste *et al.* (2012). The load effect within the range of effective width w was determined by the FE analysis and averaged as m_E. The unit moment resistance at the critical section was calculated as m_R and the total load-carrying capacity Q_R was calculated according to.

$$Q_R = \frac{m_R}{m_E} \times Q_E \tag{7.15}$$

At this assessment step, the design resistances for one-way shear, punching shear and bending failure were obtained as 200 kN, 407 kN and 888 kN, respectively. Therefore, the governing failure mode for load carrying capacity also at this level was one-way shear with 200 kN, and even if a higher load carrying capacity was demonstrated, the capacity was still smaller than the minimum required design capacity of 260 kN. The benefit of complementing analytical methods with FE

analysis, compared to hand calculations, was that more influencing factors, such as geometry detailing and load distribution could be taken into account in the structural analysis.

7.3.2.3 Level III analysis

At this level of analysis, the slab was modelled with shell elements using the same FE mesh as in the Level II analysis; see Figure 7.28 (*a*). A Simpson integration scheme with nine integration points over the thickness was used together with Gauss integration of 2×2 integration points over the shell area. However, non-linear behaviour of the materials determined through laboratory tests was also included in the analysis.

For the tensile behaviour of concrete, a constitutive model based on non-linear fracture mechanics using a smeared rotating crack model based on total strain was adopted (TNO, 2015). In this approach, the crack width w is related to the crack strain ε_{cr} perpendicular to the crack via a characteristic length called crack band width l_{cr}, see Section 3.3.2. The advantage of this method is that the formulation remains local and the algorithmic structure of the FE code would require only minor adjustments, limited to the part of the code responsible for evaluations of the stress (and stiffness) corresponding to a given strain increment (Jirásek, 2012). The crack band width was assumed to be equal to the mean crack distance since the reinforcement was modelled as fully bonded (Shu et al., 2015). A tension softening curve according to Hordijk (1991) was used; see Figure 7.29 (*a*).

The behaviour of concrete in compression was described by an elastic continuum damage constitutive law. For the stress-strain relationship used in numerical analyses, the localization of deformation in compressive failure needs to be taken into account. The compression softening behaviour is related to the boundary conditions and size of the specimen (Mier, 1984). The stress-strain relationship used was based on Thorenfeldt *et al.* (1987) which was calibrated by measurements of compression tests on 300 mm long cylinders. Consequently, the softening branch needed to be modified for the concrete element size used in the FE model. Thus, the stress-strain curve according to Thorenfeldt *et al.* (1987) was modified to fit the concrete element size (Zandi *et al.*, 2011b), resulting in a uniaxial stress versus strain response as shown in

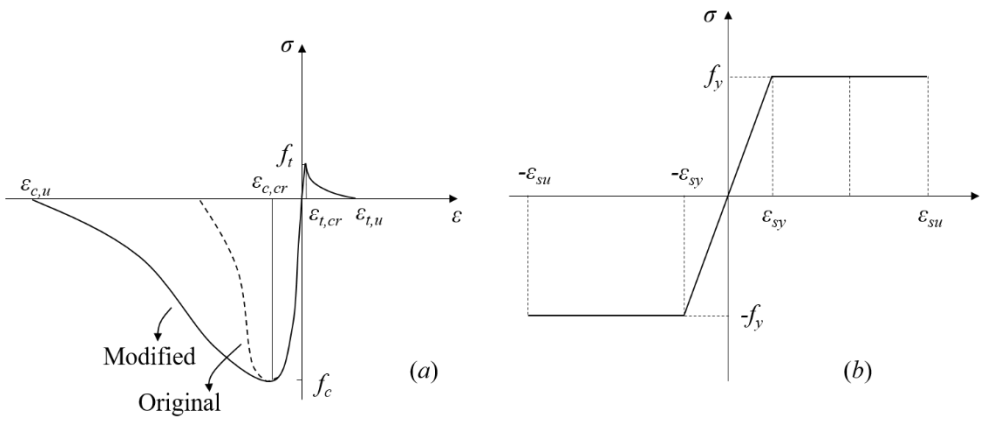

Figure 7.29 Material property adopted in the non-linear FE model: (a) concrete and (b) reinforcing steel. From Shu et al. (2019).

Figure 7.29 (*a*). This was done by assuming that the compressive failure would take place in one element row; an assumption that was later found to be correct. The main difficulty with this method of compression behaviour modelling is that the number of elements in which the compressive region will localize is not known in advance. Thus, this assumption needs to be checked when the analysis is finished.

The behaviour of the reinforcement was described by a von Mises plasticity model, including strain hardening in a bilinear stress-strain relationship, using values obtained from material tests; see Figure 7.29 (*b*). The reinforcement was included in the model as fully-bonded *embedded reinforcement* bars, in accordance with the layout in the original drawings. The reinforcement adds stiffness to the concrete finite elements but does not have independent degrees of freedom. The space occupied by the reinforcement is ignored and does not contribute to the weight of the element.

The analysis was carried out using a regular Quasi-Newton iteration method based on force and energy convergence criteria, with an error tolerance of 0.001.

The one-way shear resistance was obtained at the intersection between the relationship between load and longitudinal mid-depth strain, determined from the FE analysis and corresponding load-strain failure criterion from Model Code 2010 (fib, 2013), see Equations (7.10) to (7.12); see Figure 7.30. The longitudinal strain at mid-depth of the effective shear depth ε_x was obtained from results of FE analysis in the control section.

The punching shear resistance $V_{R,C}$ was expressed as a function of the rotation ψ of the slab according to Model Code 2010 (fib, 2013), see Equations (7.13) and (7.14); see Figure 7.31 (*a*). The load-carrying capacity was determined as the intersection between this function and the corresponding relation between the shear force from the applied load versus slab rotation obtained from the non-linear FE analysis.

At this level of assessment, the global resistance factor with Estimation of Coefficient of Variation of Resistance Method (ECOV) was used. With this method, an estimate of mean and characteristic values of the load carrying capacity was calculated through FE analysis using mean and characteristic values of material parameters as indata, see Section 2.4.4. The results obtained are given in Table 7.6.

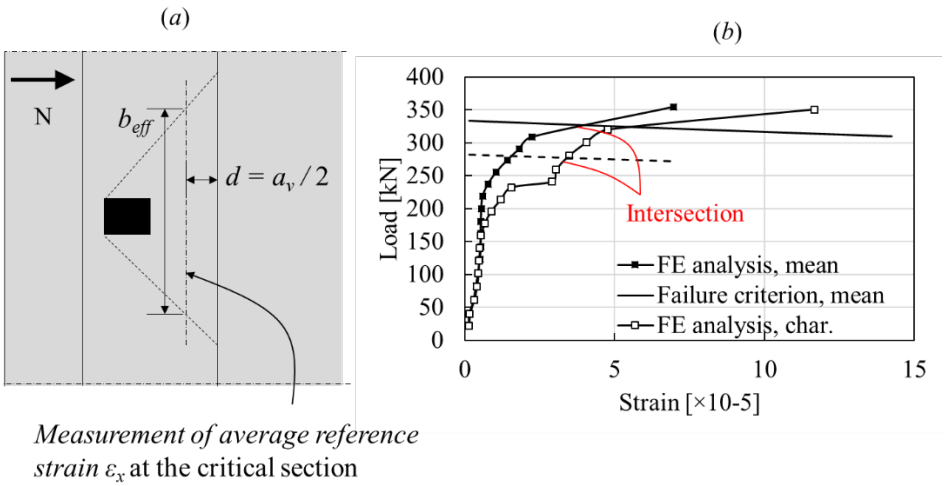

Figure 7.30 Level III analysis: non-linear FE analysis coupled with Model Code 2010 (LoA II) for one-way shear failure. From Shu et al. (2019).

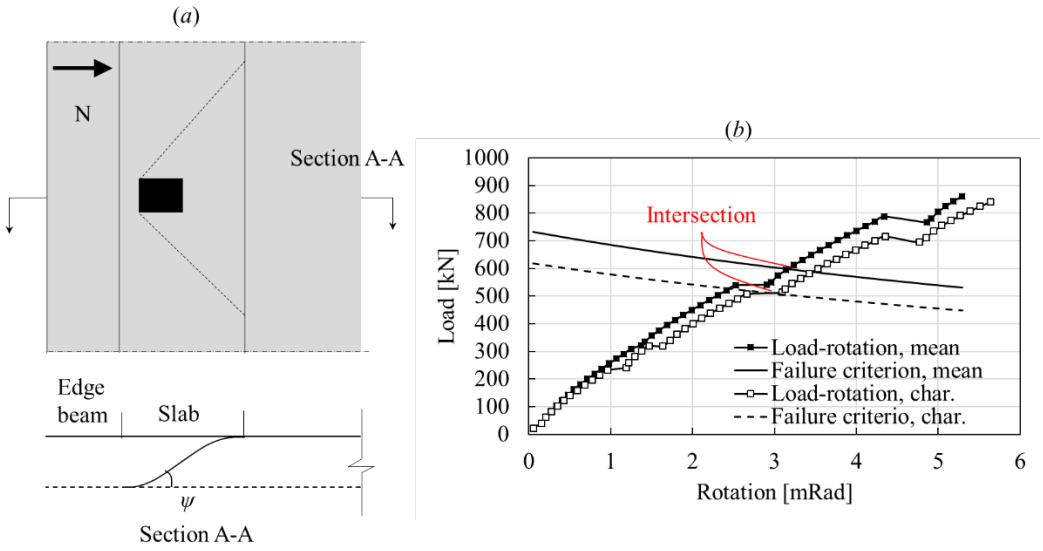

Figure 7.31 Level III analysis: non-linear FE analysis coupled with Model Code 2010 (LoA II) for punching shear failure. From Shu et al. (2019).

Table 7.6 Input parameters and estimation of the load-carrying capacity of the cantilever slab at assessment Level III using ECOV. Based on Shu et al. (2019).

Input parameters				Estimation of load-carrying capacity			
					One-way shear	Punching shear	Bending
f_{ctk} [MPa]	1.55	f_{ctm} [MPa]	2.21	Mean value [kN]	336	595	861
f_{ck} [MPa]	20	f_{cm} [MPa]	28	Char. value [kN]	282	511	840
G_{Fk} [MPa]	125	G_{Fm} [MPa]	133	V_R	0.10	0.09	0.01
$f_{yk.rebar}$ [MPa]	500	$f_{ym.rebar}$ [MPa]	550	γ_R	1.37	1.31	1.05
$f_{yk.girder}$ [MPa]	460	$f_{ym.girder}$ [MPa]	506	γ_{Rd}	1.06	1.06	1.06
h_b [mm]	323	h_b [mm]	323	Q_R [kN]	230	424	776

At this level, the design load-carrying capacity with respect to one-way shear, punching shear and bending failure was obtained as 230 kN, 424 kN and 776 kN, respectively. Therefore, the governing failure mode also at level III was one-way shear and the maximum design load was found to be 230 kN. Consequently, even if the load carrying capacity demonstrated was higher, it did still not meet the required 260 kN.

7.3.2.4 Level IV analysis

At Level IV, the bridge was modelled through a detailed 8-node brick element model for concrete deck slabs and steel girders, as shown in Figure 7.32. The size of brick elements was 50×50×35.7 mm (length×width×height) for the loaded area of the slab, and maximum 400×200×35.7 mm for the remaining part of the slab modelled with brick elements. The connection between the concrete deck slab and steel girders was

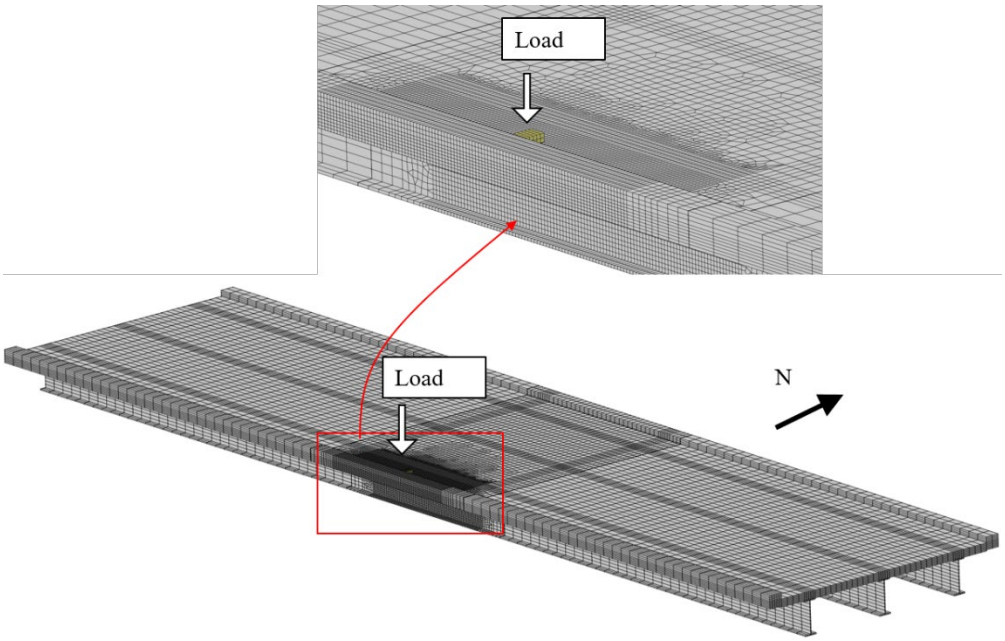

Figure 7.32 Level IV analysis: non-linear continuum FE model of the tested bridge. From Shu et al. (2019).

assumed to be fully bonded. At least seven elements were used for the entire deck slab in the thickness direction to sufficiently reflect the flexural behaviour (Shu *et al.*, 2015). The reinforcement was modelled the same way as in Level III analysis.

Boundary conditions were defined in the same way as for the model at level III. Between the top flange of the steel beams and the concrete slab, interface elements were used to describe contact (Shu *et al.*, 2015). The load was added using displacement control: 0.1 mm for the first 10 steps and 1 mm per step thereafter.

The analysis was carried out using a Quasi-Newton iteration method based on force and energy convergence criteria, with a tolerance of 0.01. Compared to shell FE analysis at Level III, continuum FE analysis at Level IV required larger tolerance to achieve convergence due to larger model size. The analysis stopped when convergence could not be achieved due to shear failure.

At this step, the safety format according to Schlune *et al.* (2011, 2012) was adopted, see Section 2.4.5. According to this safety format, the resistance of, at least, three cases is needed to be calculated:

- $R_{m.is}$: when mean values of in-situ material parameters are used
- $R_{fc.red}$: when the reduced value of concrete material strength is used
- $R_{fy.red}$: when the reduced value of steel material strength is used

Non-linear FE analyses were carried out for the 3 cases and the load-deflection relationship and the crack pattern in the loaded cross-section at the ultimate limit state are presented in Figure 7.33. The deflection was measured right at the point under the centre of the concentrated load. It was observed that the global behaviour of the structure was generally in the elastic stage before a sudden drop of load-carrying capacity. The principal strain based crack pattern is presented at the loaded mid cross-section A-A (see Figure 7.33). Before the failure of the slab, only a few minor cracks

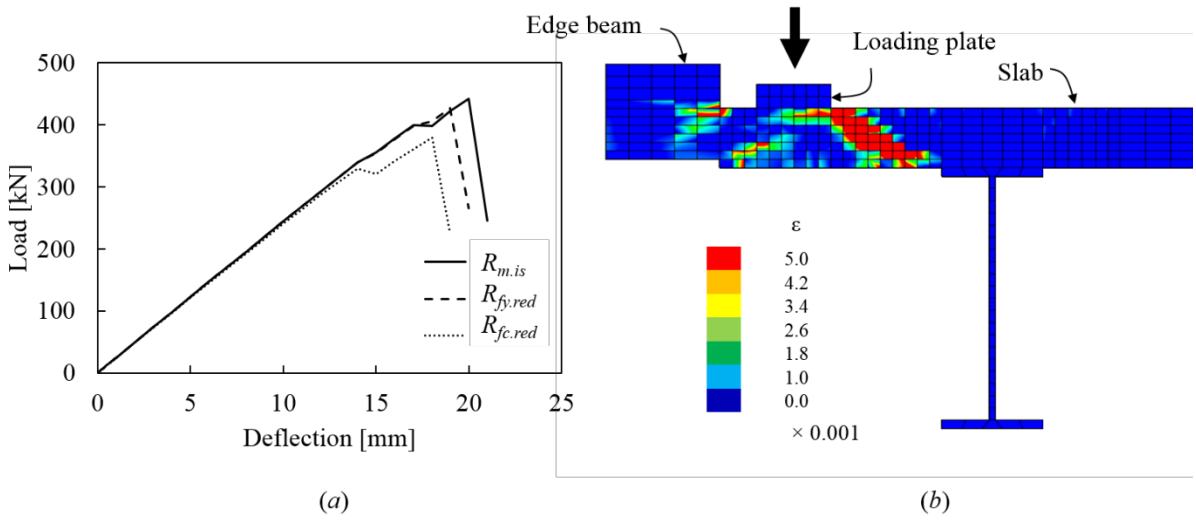

Figure 7.33 (a) Load-deflection (global) relationship for level IV analysis and (b) corresponding crack pattern at the ultimate limit stage at cross-section A-A. From Shu et al. (2019).

were observed. At failure, a sudden inclined large crack occurred from the bottom edge of the loading plate to the top edge of the main girder, forming an approximate 45-degree inclination. The concrete elements at the compressive top side, under the load, were crushed at the same time. The crack pattern indicates that the final failure mode was predominantly a one-way shear failure. The failure crack started to developed parallel to the girder and propagated then around the loading plate, forming a U shape failure surface.

The main contribution to the deflection was from the main girder, rather than from the slab. In Figure 7.34, the local deflection of the cantilever slab is shown as the difference in displacement between the loading point on the cantilever slab and the closest point on the girder. It clearly shows that also the slab followed a nearly elastic behaviour until the shear failure occurred.

The load-carrying capacity was calculated according to Section 2.4.5. Given the difficulties in reproducing brittle shear failures with continuum elements, the

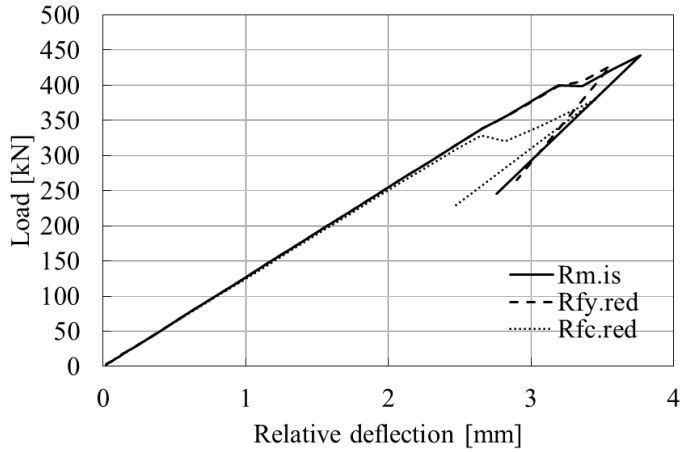

Figure 7.34 Load-deflection (local) relationship for Level IV analysis. From Shu et al. (2019).

Table 7.7 Estimation of the load-carrying capacity of the cantilever slab at Level IV using enhanced safety format by Schlune et al. (2011, 2012)*. Based on Shu et al. (2019).*

V_{fc}	16.2%	V_{fy}	5.4%	$R_{m.is}$	442
$f_{cm.is}$ [MPa]	28.0	$f_{ym.is}$ [MPa]	550.0	V_g	5%
d_{fc}	8.2	d_{fy}	60.3	V_m	10%
$f_{c.red}$ [MPa]	20	$f_{y.red}$ [MPa]	489.7	α_R	0.80
$\sigma_{fc.is}$	4.5	σ_{fy}	29.7	β	3.80
$R_{fc.red}$ [kN]	380	$R_{fy.red}$ [kN]	427	θ_m	1.00
				V_f	0.08
				γ_R	1.52
				Q [kN]	292

coefficient of variation regarding modelling uncertainty was assumed to be 10%, as recommended by the study of Pimentel *et al.* (2014). For the case of shear type failure in slabs, the relative importance of the model uncertainty is larger than any other variable (material uncertainty or geometrical uncertainty), according to the study of Belletti *et al.* (2015) and Engen *et al.* (2017). In Table 7.7, indata and failure loads for the three analyses are given together with parameters for calculation of the load-carrying capacity, which was found to be Q_R = 292 kN.

7.3.3 Results

The load-carrying capacity was calculated at different levels of assessment according to *the Multi-Level Assessment Strategy*. The results are summarized and compared in Figure 7.35. The failure mode was one-way shear failure for all steps. The one-way shear capacity increased using improved structural assessment, and the detectable load-carrying capacity became significantly higher. With the result from Level IV, it was finally shown that the bridge had sufficient capacity to meet the minimum required load-carrying capacity of 260 kN.

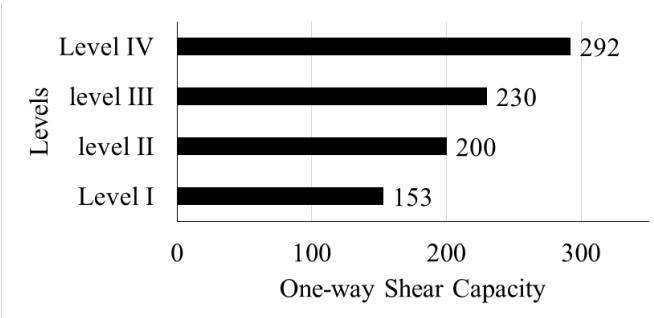

Figure 7.35 Load-carrying capacity calculated at different steps within the assessment framework based on the Multi-Level Assessment Strategy. Based on Shu et al. (2019).

8 References

ACI (2011). Building Code Requirements for Structural Concrete and Commentary. Farmington Hills, Mich: ACI American Concrete Institute, Committee 318.

Bagge N., Plos M., Popescu C. (2019): A multi-level strategy for successively improved structural analysis of existing concrete bridges: examination using a prestressed concrete bridge tested to failure, *Structure and Infrastructure Engineering*, 15:1, pp. 27-53

Bathe K-J. (2016): *Finite Element Procedures*. 2nd Edition. K.J. Bathe, Watertown, MA, USA.

Bažant, Z.P., Oh, B.H. (1983): Crack band theory for fracture of concrete. *Mat. Constr.* 16, 155–177.

Bentz, E.C., Vecchio, F.J., Collins, M.P. (2006): Simplified modified compression field theory for calculating shear strength of reinforced concrete elements. *ACI Structural Journal*, 103(4), pp. 614–624[12]

Belletti B, Scolari M, Muttoni A, Cantone R. (2015): Shear strength evaluation of RC bridge deck slabs according to CSCT with multi-layered shell elements and PARC_CL Crack Model. *IABSE Conf. Geneva* 2015,1158–65.

Belletti, B., Damoni C., Hendriks, M. A. N., de Boer, A., (2017a). *Validation of the Guidelines for Nonlinear Finite Element Analysis of Concrete Structures, Part: Reinforced beams.* (Version 1.0). Rijkswaterstaat Centre for Infrastructure, Report RTD:1016-3A:2017, 2017.

Belletti, B., Damoni C., Hendriks, M. A. N., de Boer, A., (2017b). *Validation of the Guidelines for Nonlinear Finite Element Analysis of Concrete Structures, Part: Slabs.* (Version 1.0). Rijkswaterstaat Centre for Infrastructure, Report RTD:1016-3C:2017, 2017.

Björnsson Í., Larsson Ivanov O., Honfi D., and Leander J. (2017): Decision support framework for bridge condition assessment, *Structural Safety*, Vol. 81, No. 101874

Blaauwendraad, J. (2010). Plates and FEM: Surprises and Pitfalls (ISBN 978-9.). Springer Science, Business Media B.V.

Blomfors M., Coronelli D., Lundgren K., Zandi K. (2018): Engineering Bond Model for Corroded Reinforcement. *Engineering Structures*. Vol. 156, p. 394-410.

Boverket (2004). Boverkets handbok om betongkonstruktioner, *BBK 04* (In Swedish). Vällingby, Sweden, ISBN 91-7147-816-7.

Boverket (2019): *Boverkets konstruktionsregler, EKS 11. BFS 2011:10 med ändringar till och med BFS 2019:1* (In Swedish). Boverket, Karlskrona, Sweden.

Broo H. (2008): *Shear and Torsion in Concrete Structures – Non-Linear Finite Element Analysis in Design and Assessment*. Division of Structural Engineering, Concrete Structures, Chalmers University of Technology, Ph.D. Thesis, Göteborg, Sweden.

Broo H., Lundgren K., Plos M. (2008): *A guide to non-linear finite element modelling of shear and torsion in concrete bridges*. Division of Structural Engineering, Concrete Structures, Chalmers University of Technology, Report 2008:18,

Göteborg, Sweden.

CEB-FIP (1993). *Model Code for Concrete Structures 1990*. Lausanne: International Federation for Structural Concrete (fib).

CEN (2002a). *EN 1990 Eurocode - Basis of structural Design*. Brussels, Belgium: CEN European Committee for Standardization.

CEN (2002b). *EN 1991 Eurocode 1 - Actions on structures*. Brussels, Belgium: CEN European Committee for Standardization.

CEN (2003). *EN 1991-2 Eurocode 1 - Actions on structures - Part 2 - Traffic loads on bridges*. Brussels, Belgium: CEN European Committee for Standardization.

CEN (2004a). *EN 1992-1-1 Eurocode 2: Design of concrete structures - part 1-1: General rules and rules for buildings*. Brussels, Belgium: CEN European Committee for Standardization.

CEN (2004b). *EN 1992-2 Eurocode 2: Design of concrete structures - part 2: Concrete bridges. Design and detailing rules*. Brussels, Belgium: CEN European Committee for Standardization.

Cervenka V., Cervenka J. and Pukl R. (2007): Safety in fracture analysis of concrete structures. *Proceedings of the 6th International Conference on Fracture Mechanics of Concrete and Concrete Structures*, Catania, Italy, pp. 1043-1049.

Chauvel D, Thonier H, Coin A, Ile N. Shear resistance of slabs not provided with shear reinforcement. France; 2007.

Chen, E., Berrocal, C.G., Fernandez, I., Löfgren, I., Lundgren, K. (2020). Corrigendum to "Assessment of the mechanical behaviour of reinforcement bars with localised pitting corrosion by Digital Image Correlation". *Engineering Structures*, 2021, 231, 111634.

Du, Y. G., Clark, L. A. and Chan, A. H. C. (2005). Effect of corrosion on ductility of reinforcing bars. Magazine of Concrete Research, Vol. 57, No. 7, pp. 407–419.

Engen, M., Hendriks, M.A.N., Köhler, J., Øverli, J.A., Åldstedt, E. (2017): A quantification of the modelling uncertainty of non-linear finite element analyses of large concrete structures. *Structural Safety*, 2017, 64, pp. 1–8.

Engen, M., Hendriks, M.A.N., Øverli, J.A., Åldstedt, E. (2019): Nonlinear finite element analyses applicable for the design of large reinforced concrete structures, *European Journal of Environmental and Civil Engineering*, 23:11, pp. 1381-1403,

Engström B. (1992): *Ductility of Tie Connections in Precast Structures*. Division of Concrete Structures, Chalmers University of Technology, Ph.D. Thesis, Publication 92:1, Göteborg, Sweden.

European Concrete Platform ASBL (2008): *Eurocode 2 Commentary*, Brussels.

Fall, D., Shu, J., Rempling, R., Lundgren, K., & Zandi, K. (2014). Two-way slabs: Experimental investigation of load redistributions in steel fibre reinforced concrete. *Engineering Structures*, *80*, 61–74.

Feenstra P.H. (1993): *Computational aspects of biaxial stress in plain and reinforced concrete.* Delft University, Delft University Press, Delft, The Netherlands.

Fernandez, I., Bairán, J.M., Marí, A.R. (2015) Corrosion effects on the mechanical properties of reinforcing steel bars. Fatigue and σ-ε behavior. *Construction and Building Materials*, 2015, 101, pp. 772–783

fib (2013). *Model Code for Concrete Structures 2010*. Lausanne: International Federation for Structural Concrete (fib).

fib (2018). *Safety and performance concepts: Reliability assessment of concrete structures*. International Federation for Structural Concrete (fib), Bulletin 86.

Gottsäter E., Johansson M, Plos M, Larsson Ivanov O. (2019): Crack widths in base restrained walls subjected to restraint loading. *Engineering Structures*, Vol. 189, pp. 272-285.

Grassl P., Johansson M, Leppänen J (2018): On the numerical modelling of bond for the failure analysis of reinforced concrete, Eng. Fract. Mech. 189 (2018) 13–26.

Gylltoft K. (1983): *Fracture Mechanics Models for Fatigue in Concrete Structures*. Division of Structural Engineering, Luleå University of Technology, Doctoral Thesis 1983:25D, Luleå, Sweden.

Hakimi, P. S. (2012). *Distribution of shear force in concrete slabs*. Master Thesis, Chalmers University of Technology, Gothenburg.

Hallbjörn, L. (2019): *Betongplattor, beräkning och dimensionering vid koncentrerade upplagsreaktioner och fria kanter*, (in Swedish). Rapport ACE / Institutionen för arkitektur och samhällsbyggnadsteknik, Chalmers tekniska högskola: 2019:8, Göteborg, Sweden.

Hendriks, M. A. N., den Uijl, J. A., de Boer, A., Feenstr, P. H., Belletti, B., & Damoni, C. (2012). *Guidelines for nonlinear finite element analysis of concrete structures.* (1st ed.). Delft: Rijkswaterstaat Centre for Infrastructure.

Hendriks, M. A. N., de Boer, A., Belletti, B. (2017). G*uidelines for Nonlinear Finite Element Analysis of Concrete Structures.* (Version 2.1). Rijkswaterstaat Centre for Infrastructure, Report RTD:1016-1:2017, 2017.

Hillerborg A., Modéer M. and Petersson P-E. (1976): Analysis of Crack Formation and Crack Growth in Concrete by means of Fracture Mechanics and Finite Elements. *Cement and Concrete Research*, Vol. 6, No. 6, pp. 773-782.

Hillerborg A. (1988): Rotational Capacity of Reinforced Concree Beams. *Nordic Concrete Research*, No. 7, Oslo, Norway, pp. 121-134.

Hillerborg, A. (1996). *Strip method design handbook*. London, Great Britain: Technology & Engineering.

Hughes, T.J.R. (1987): *The Finite Element Method, Linear Static and Dynamic Finite Element Analyses*. Prentice-Hall, Englewood Cliffs, New Jersey, USA.

JCSS (2001): Probabilistic Model Code. Joint Committee on Structural Safety, 12th draft, Zurich.

Jirásek M and Zimmerman T. (1998): Rotating Crack Model with Transition to Scalar Damage. *J. Eng. Mech.*, 124(3): pp. 277-284.

Jirásek M and Bazant Z.P. (2001): *Inelastic Analysis of Structures*. Wiley, 758 pp.

Jirásek, M. (2012). *Modeling of localized inelastic deformation*. Prague: Czech Technical University in Prague.

Johansen, K. W. (1972). *Yield-Line formulae for slabs.* (ISBN 0-721). London: Cement and Concrete Association.

Johansson, M. (1996). *New Reinforcement Detailing in Concrete Frame Corners of Civil Defence Shelters: Non-linear Finite Element Analyses and Experiments.* Division of Concrete Structures, Chalmers University of Technology, Licentiate Thesis, Publication 96:1, Göteborg, Sweden.

Johansson M. (1997): *Armeringsseghetens inverkan på deformationsförmågan hos betong-konstruktioner* (Influence of Reinforcement Ductility on the Deformation Capacity of Concrete Structures. In Swedish). Division of Concrete Structures, Chalmers University of Technology, Report 97:1, Göteborg, Sweden.

Johansson M. (2000): *Structural Behaviour in Concrete Frame Corners of Civil Defence Shelters: Non-linear Finite Element Analyses and Experiments.* Division of Concrete Structures, Chalmers University of Technology, Ph.D. Thesis, Publication 00:2, Göteborg, Sweden.

König G, Nguyen T. and Ahner C. (1997): Consistent safety format. Non-linear Analysis: Discussion Papers from the Working Party in Commission 1, Comité Euro-International du Béton (CEB), Bulletin d' Information 239, Lausanne, 1-16.

Lundgren K. (1999): *Three-Dimensional Modelling of Bond in Reinforced Concrete: Theoretical Model, Experiments and Applications.* Division of Concrete Structures, Chalmers University of Technology, Ph.D. Thesis, Publication 99:1, Göteborg, Sweden.

Lundgren K. and Gylltoft K. (2000): A model for the bond between concrete and reinforcement. *Magazine of Concrete Research*, Vol. 52 No. 1 pp. 53-63.

Malm, R. (2016): *Guideline for FE analyses of concrete dams*. Energiforsk, Report 2016:270.

Markeset G. (1993): *Failure of Concrete under Compressive Strain Gradients.* Department of Structural Engineering, The Norwegian Institute of Technology, Ph.D. Thesis, Trondheim, Norway.

Mathern A., Yang J. (2021): A practical finite element modelling strategy to capture cracking and crushing behaviour of reinforced concrete structures. *Materials*. 14(3), p. 506. doi: 10.3390/ma14030506

van Mier J.G.M. (1984): *Strain Softening of Concrete Under Multiaxial Loading Conditions.* Eindhoven University of Technology, Ph.D. Thesis, Eindhoven, The Netherlands.

Muttoni, A. (2008): Punching shear strength of reinforced concrete slabs without transverse reinforcement. *ACI Structural Journal*, Vol. 105 (4), pp. 440-450.

Nesset J. and Skoglund S. (2007): *Reinforced Concrete Subjected to Restraint Forces: Analytical and Non-Linear Finite Element Analysis.* Division of Structural Engineering, Chalmers University of Technology, Master's Thesis 2007:23, Göteborg, Sweden.

Pacoste, C., Plos, M., & Johansson, M. (2012). *Recommendations for finite element analysis for the design of reinforced concrete slabs*. Stockholm: TRITA-BKN Rapport 114.

Pimentel M, Brühwiler E, Figueiras J. (2014) Safety examination of existing concrete structures using the global resistance safety factor concept. *Engineering Structures*. Vol. 70, p. 130–143.

Plos M. (1995): *Application of Fracture Mechanics to Concrete Bridges - Finite Element Analyses and Experiments.* Division of Concrete Structures, Chalmers University of Technology, Ph.D. Thesis, Publication 95:3, Göteborg, Sweden.

Plos M., Gylltoft K. (2006): Evaluation of Shear Capacity of a Prestressed Concrete Box Girder Bridge using Non-Linear FEM. *Structural Engineering International*, Vol. 16, No. 3, August 2006, IABSE, pp. 213-221

Plos, M., Shu, J., Zandi, K., & Lundgren, K. (2017). A multi-level structural assessment strategy for reinforced concrete bridge deck slabs. *Structure and Infrastructure Engineering*, vol. 13(2), pp. 223-241.

Pucher A (1973) *Influence surfaces of elastic plates*. 4th edition. Springer, Wien.

Rombach, G. A. (2004). Finite element design of concrete structures. Thomas Telford.

Rots, J. G. (1988). *Computational modeling of concrete fracture*. Doctoral Thesis, Delft University of Technology, Delft.

Rots J.G. (1989): *Fracture Mechanics of Concrete Structures: From theory to applications.* RILEM Technical Committee 90-FMA, Edited by Elfgren L., Chapman and Hall, London, England, pp. 138-145.

Schlune H. (2011): *Safety Evaluation of Concrete Structures with Nonlinear Analysis.* Ph.D. Thesis, Division of Structural Engineering, Chalmers University of Technology, ISBN 978-91-7385-551-8, Göteborg, Sweden.

Schlune H., Plos M., Gylltoft K. (2011): Safety formats for nonlinear analysis tested on concrete beams subjected to shear forces and bending moments. *Engineering Structures*. Vol. 33 (8), p. 2350-2356.

Schlune H., Plos M., Gylltoft K. (2012): Safety formats for non-linear analysis of concrete structures. *Magazine of Concrete Research*. Vol. 64 (7), p. 563-574.

Shams-Hakimi P. (2012): *Distribution of Shear Force in Concrete Slabs – A study of how to distribute shear force from linear FE analyses in bridge decks.* Division of Structural Engineering, Chalmers University of Technology, Master's thesis 2012:148, Göteborg, Sweden.

Shu, J., Fall, D., & Plos, M. (2014). Finite Element Modelling of Two-way RC Slabs with Varying Modelling Choices. *The 10th Fib International PhD Symposium in Civil Engineering*, 589–594. Quebec, Canada.

Shu, J., Fall, D., Plos, M., Zandi, K., Lundgren, K. (2015). Development of modelling strategies for two-way RC slabs. *Engineering Structures*, *101*, 439–449.

Shu, J., Plos, M., Johansson, M., Zandi, K., Nilenius, F. (2016). Prediction of punching behaviour of RC slabs using continuum non-linear FE analysis. *Engineering Structures*, Vol. 200 art. nr 109666.

Shu, J., Belletti, B.; Muttoni, A., Scolari, M., Plos, M. (2017): Internal force distribution in RC slabssubjected to punching shear. *Engineering Structures*, Vol. 153 pp. 766-781

Shu J. (2017): *Structural Analysis Methods for the Assessment of Reinforced Concrete Slabs.* Ph.D. Thesis, Division of Structural Engineering, Chalmers University of Technology, ISBN 978-91-7597-584-9, Göteborg, Sweden.

Shu, J., Bagge, N., Plos, M., Johansson, M., Yang, Y., Zandi, K. (2018) Shear Capacity of a RC Bridge Deck Slab: Comparison between Multilevel Assessment and Field Test. *Journal of Structural Engineering*, Vol. 144 (7), No. 04018081.

Shu, J., Honfi, D., Plos, M., Zandi, K., Magnusson, J. (2019). Assessment of a cantilever bridge deck slab using multi-level assessment strategy and decision support framework. *Engineering Structures*, 125, 15-25.

Slobbe A.T., Hendriks M.A.N., Rots J.G. (2013): Systematic assessment of directional mesh bias with periodic boundary conditions: Applied to the crack band model. *Eng. Fract. Mech.* 109 (2013) 186-208.

Sustainable Bridges (2007): *Non-Linear Analysis and Remaining Fatigue Life of Reinforced Concrete Bridges.* Prepared by Sustainable Bridges- a project within EU FP6.

Swedish Traffic Administration. (2018). *TDOK 2013:0267 KRAV: Bärighetsberäkning av broar (Load-Carrying Capacity of Bridges)*. In Swedish, Stockholm.

Svensk Byggtjänst (1990): *Betonghandboken Konstruktion*, Utgåva 2. In Swedish. Svensk Byggtjänst, ISBN: 9789173325332, 791 pp

Tahershamsi M., Fernandez I., Zandi K., Lundgren K. (2017). Four levels to assess anchorage capacity of corroded reinforcement in Concrete, *Engineering Structures*, Vol. 147, p. 434–447.

Thorenfeldt, E., Tomaszewicz, A., & Jensen, J. J. (1987). Mechanical properties of high-strength concrete and applications in design. *In Proc. Symp. Utilization of High-Strength Concrete*. Stavanger.

Timoshenko, S. and Woinowsky-Krieger, S. (1959): *Theory of plates and shells*, 2nd edition, McGraw-Hill, ISBN 0-07-064779-8

TNO. (2015). Diana finite element analysis, User's Manual -- Release 9.6. In *TNO DIANA BV.* Delft.

Vaz Rodrigues, R. (2007). *Shear strength of reinforced concrete bridge deck slabs*. PhD Thesis, École Polytechnique Fédérale de Lausanne, Lausanne.

Vaz Rodrigues, R., Fernández Ruiz, M., & Muttoni, A. (2008). Shear strength of R/C bridge cantilever slabs. *Engineering Structures*, *30*(11), 3024–3033.

Veganzones, J.J., Pacoste C., Karoumi, R. (2019): Width and Edge Beam Effects on the Ultimate Behaviour of RC Bridge Overhangs. *Nordic Concrete Research*, Publ. No. NCR 61 – Issue 2. p. 131-152.

Zandi K. (2010): *Structural Behaviour of Deteriorated Concrete Structures.* Ph.D. Thesis, Division of Structural Engineering, Chalmers University of Technology, ISBN 978-91-7385-461-0, Göteborg, Sweden.

Zandi Hanjari, K. ; Kettil, P. ; Lundgren, K. (2011a) Analysis of Mechanical Behavior of Corroded Reinforced Concrete Structures. *ACI Structural Journal*, vol. 108(5), pp. 532-541.

Zandi Hanjari, K.; Kettil, P.; Lundgren, K. (2011b). Modeling the structural behavior of frost-damaged reinforced concrete structures, *Structure and Infrastructure Engineering*, Vol. 9, No. 5, pp 416–431.

Zandi Hanjari, K., Utgenannt, P., & Lundgren, K. (2011c). Experimental study of the material and bond properties of frost-damaged concrete. *Cement and Concrete Research*, *41*(3), 244–254. https://doi.org/10.1016/j.cemconres.2010.11.007.

Zandi K., Lundgren K., Plos M., Coronelli D. (2013). Three-dimensional modelling of structural effects of corroding steel reinforcement in concrete. *Structure and Infrastructure Engineering*, Vol. *9* (7), 702-718.

Appendices

A Material properties for non-linear analysis of reinforced concrete

In Table A.1 recommendations for determination of material parameters for non-linear analysis of reinforced concrete slabs are presented. If results from material tests are available, they should be used instead of the expressions given below. It is also possible to use a combination of material tests and these expressions, e.g. to determine an approximate value of the Young's modulus or fracture energy based on the tested compressive strength determined in tests.

Table A.1 Recommendations for material parameters in non-linear analysis of reinforced concrete.

Parameter	Expression	Reference
Young's modulus [GPa]	$E_{ck} = E_{cm} = 22 \cdot \left(0.1 \cdot f_{cm}\right)^{0.3}$	CEN (2004a)
Poisson's ratio [-]	$\nu_{uncracked} = 0.2$ $\nu_{cracked} = 0$ [1)]	CEN (2004a)
Density [kg/m^3]	$\rho_{PC} = 2400$ (plain concrete) $\rho_{RC} = 2500$ (reinforced concrete)	CEN (2002b)
Compressive strength [MPa]	$f_{ck} = 0.8 \cdot f_{ck,cube}$ $f_{cm} = f_{ck} + 8$	CEN (2004a), fib (2013)
Compressive strains [%]	$\varepsilon_{c1} = 0.7 \cdot f_{cm}^{0.31} \le 2.8$ $\varepsilon_{cu1} = 3.5$ $f_{ck} \le 50$ MPa $\varepsilon_{cu1} = 2.8 + 27 \cdot \left(0.98 - 0.01 \cdot f_{cm}\right)^4$ $f_{ck} > 50$ MPa	CEN (2004a) [2)]
Tensile strength [MPa]	$f_{ctm} = 0.30 \cdot f_{ck}^{2/3}$ $f_{ck} \le 50$ MPa $f_{ctm} = 2.12 \cdot \ln\left(1 + 0.1 \cdot f_{cm}\right)$ $f_{ck} > 50$ MPa $f_{ctk,\min} = 0.7 \cdot f_{ctm}$, $f_{ctk,\max} = 1.3 \cdot f_{ctm}$	CEN (2004a), fib (2013)
Fracture energy in tension [N/m]	$G_{Fk} = \frac{f_{ctk}}{f_{ctm}} \cdot G_{Fm}$ [3)] $G_{Fm} = 73 \cdot f_{cm}^{0.18}$	fib (2013), Authors
Fracture energy in compression [N/m]	$G_{Ck} = \frac{f_{ck}}{f_{cm}} \cdot G_{Cm}$ [3)] $G_{Cm} = 250 \cdot G_{Fm}$	Hendriks *et al.* (2017), Authors

1) Upon cracking, it is advantageous if the material model used could include an apparent decrease of the Poisson effect; as an approximation Poisson's ratio can be assumed to be zero after cracking. However, if this is not possible with the material model used, the concrete in a slab that will be predominantly cracked may be approximately modelled setting Poisson's ratio to zero.

2) In Model Code 2010, similar values of ε_{c1} and ε_{cu1} are listed for different concrete strengths; these values can be used as well.

3) This expression is not presented in the reference mentioned but is a suggestion by the authors. Using this relation, the shape of the descending stress-strain relation is kept intact.

The expressions given in Table A.1 for concrete relations in compression, tension and bond are based on mean values. However, if a non-linear FE analysis instead is to be made using characteristic values (i.e. to follow the Global safety factor methods described in Section 2.4) a modification is needed. In such cases the characteristic relations can be obtained by replacing the mean value used with the corresponding characteristic value.

The stress-strain relation for concrete in compression, see Figure A.1, can be expressed as

$$\sigma_c = \left[\frac{k\cdot\eta-\eta^2}{1+(k-2)\cdot\eta}\right]\cdot f_{cm} \tag{A.1}$$

where

$$k = 1.05\cdot E_{cm}\cdot\frac{\varepsilon_{c1}}{f_{cm}} \tag{A.2}$$

and $\eta = \varepsilon_c / \varepsilon_{c1}$.

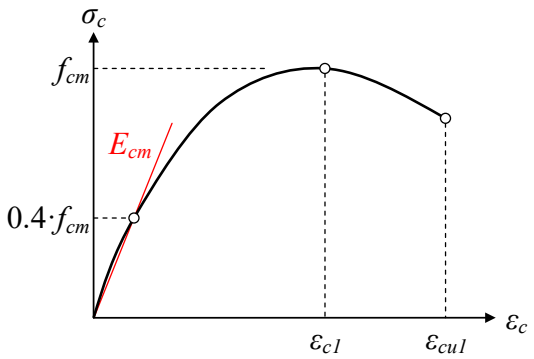

Figure A.1 Stress-strain relation for concrete in compression. Based on Eurocode 2, CEN (2004a).

The expression in Equation (A.1) is given in both Eurocode 2 and Model Code 2010. However, a disadvantage with this relation is that it lacks information of how the stress is affected by strains $\varepsilon_c > \varepsilon_{cu1}$. Therefore, another relation is needed to cover this part; e.g. that suggested by Thorenfeldt *et al.* (1987):

$$\sigma_c = f_c\cdot\frac{\varepsilon}{\varepsilon_{c1}}\left(\frac{n}{n-1+\left(\frac{\varepsilon}{\varepsilon_{c1}}\right)^{n\cdot k}}\right) \tag{A.3}$$

where n and k are factors determined as

$$n = 0.80 + \frac{f_c}{17} \tag{A.4}$$

$$k = \begin{cases} 1 & 0 \le \varepsilon \le \varepsilon_{c1} \\ 0.67 + \dfrac{f_c}{63} & \varepsilon > \varepsilon_{c1} \end{cases} \tag{A.5}$$

and the strain at maximum stress is defined as

$$\varepsilon_{c1} = \frac{n}{n-1} \cdot \frac{f_c}{E_c} \tag{A.6}$$

Note that when $\varepsilon_c > \varepsilon_{c1}$, i.e. when the descending branch is reached, the strain value should be extended to account for localised compression failure as described in Section 3.3.3. If using expression in Equation (A.3) to describe the descending branch, the height of the cylinders used to derive this expression were 300 mm.

For the stress-strain relation for concrete in tension, there exists many different suggestions of how this can be approximated and in Figure A.2 some common relations are presented. However, if possible, in the software used, it is recommended to use a bi-linear or continuous relation since these relations better correspond to the real response in plain concrete. Using this type of relations will also result in more localised cracking; thus, help avoiding areas of diffuse cracking (Hendriks et al., 2017).

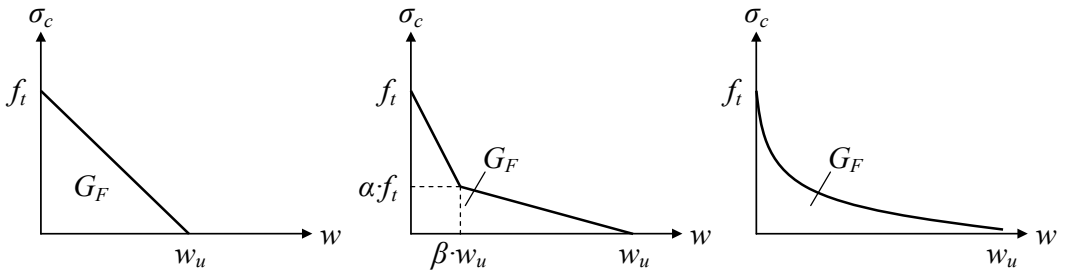

Figure A.2 Schematic illustrations of possible stress-crack opening relations for cracked concrete: (a) linear, (b) bi-linear, (c) exponential. The area under the curve corresponds to the fracture energy G_F.

For the bi-linear relation in Figure A.2b, the crack opening w_u at a fully opened crack (i.e. $\sigma_c = 0$) can be determined as

$$w_u = \frac{2}{\alpha + \beta} \cdot \frac{G_F}{f_{ct}} \tag{A.7}$$

Some recommendations of α and β, found in the literature, are listed in Table A.2. The linear relation in Figure A.2a is a special case of the bi-linear relation and is obtained when $\alpha = 0$ and $\beta = 1$.

$$\sigma_c = f_t \cdot \left[1 + \left(c_1 \cdot \frac{w}{w_u} \right)^3 \cdot e^{-c_2 \cdot w/w_u} - \frac{w}{w_u} \cdot \left(1 + c_1^3 \right) \cdot e^{-c_2} \right] \tag{A.8}$$

This expression is valid for $0 \le w \le w_u$; for $w > w_u$ the concrete stress $\sigma_c = 0$. Parameters commonly used in this expression are $c_1 = 3.0$ and $c_2 = 6.93$ and the crack opening w_u at a fully open crack can then be determined as (Hendriks *et al.*, 2017)

Table A.2 Examples of values for factors α and β found in the literature.

Reference	α [-]	β [-]	$2 / (\alpha + \beta)$ [-]
Gylltoft (1983)	0.33	0.67	4.00
Model Code 2010, fib (2013)	0.20	0.20	5.00
Jirásek and Zimmermann (1998)	0.30	0.15	4.44

For the exponential relation, an expression based on e.g. Hordijk (1991) may be used:

$$w_u = 5.136 \cdot \frac{G_F}{f_{ct}} \tag{A.9}$$

Reinforcement

In Figure A.3, examples of typical stress-strain relations for different types of steel reinforcement bars are illustrated. Modern reinforcement bars that are hot-rolled and heat-treated correspond to reinforcement of class B to D while cold-worked bars correspond to class A[7]. The idealised stress-strain relation in Figure A.3 may be used as an approximation for all type of bars. In Table A.3, recommendations for material parameters for steel reinforcement bars are presented.

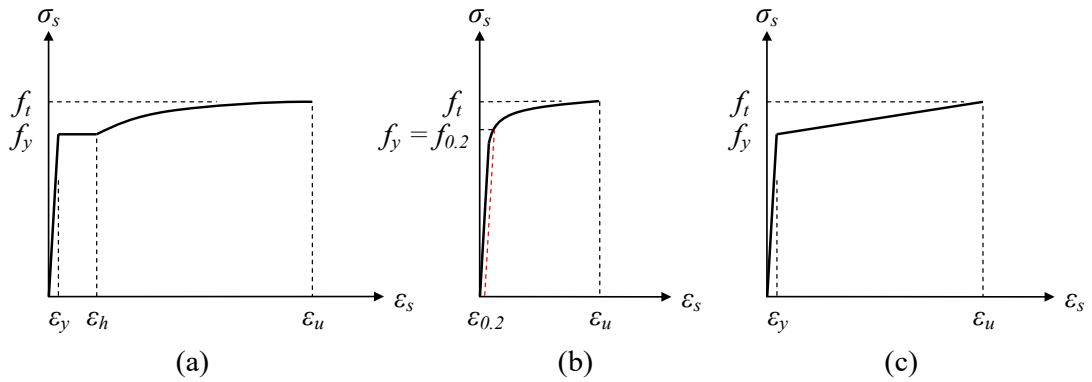

Figure A.3 Stress-strain relation for steel reinforcement: (a) hot-rolled or heat-treated bars; (b) cold-worked bars; (c)idealised stress-strain relation.

Bond

The bond-slip relation for interaction between reinforcement and surrounding concrete can for ribbed bars be described as schematically shown in Figure A.4 (fib, 2013) using the following expressions:

[7] For older type of reinforcement there may not be a suitable reinforcement class defined. However, generally, older reinforcement types usually have a more ductile response and therefore class D may be a good approximation. This is e.g. the case for the, in Sweden, commonly used bar type Ks40.

Table A.3 Recommendations for material parameters in non-linear analysis of steel reinforcement.

Parameter	Expression	Reference
Young's modulus [GPa]	$E_{sk} = E_{sm} = 200$	CEN (2004a)
Poisson's ratio [-] [1)]	$\upsilon = 0.3$	CEN (2004a)
Density [kg/m^3]	$\rho = 7850$	CEN (2002b)
Yield strength [MPa]	$f_{ym} = 1.1 \cdot f_{yk}$	Hendriks et al. (2017), Authors [2)]
Ultimate strength [MPa]	$f_{tk} = k_{class} \cdot f_{yk}$ [k_A =1.05; k_B = 1.08; 1,15; k_C = 1.15; k_D = 1.25 [4)]] $f_{tm} = 1.1 \cdot f_{tk}$	CEN (2004a), fib (2013), Authors [2)]
Yield strain [‰]	$\varepsilon_y = \frac{f_y}{E_s}$	-
Strain at hardening [‰]	$\varepsilon_{hk} = \varepsilon_{hm} = 15 - 30$	Authors [3)]
Strain at ultimate strength [‰]	$\varepsilon_{uk,A} = 25$; $\varepsilon_{uk,B} = 50$; $\varepsilon_{uk,C} = 75$; $\varepsilon_{uk,D} = 80$ [4)] $\varepsilon_{um} = 1.2 \cdot \varepsilon_{uk}$ [2)]	fib (2013), Authors [2)]

1) The value of Poisson's ratio has only an influence if the bars are modelled using 3D continuum elements.

2) No specific values are given in the codes for the relation between characteristic and mean values. Hence, the values given are estimates based on the authors' experience of real stress-strain relations observed in tests.

3) No specific values are given in the codes for strain at start of hardening. Hence, the values given are estimates based on the authors' experience of real stress-strain relations observed in tests. The value of ε_h increase with an increased value of ε_u. For coiled reinforcement there is no yield plateau, i.e. $\varepsilon_h = \varepsilon_y$.

4) Reinforcement of Class D is not included in Eurocode 2 but introduced in Model Code 2010. It is included here to be used for very ductile reinforcement, e.g. type Ks40 used in Sweden until the mid-1990s.

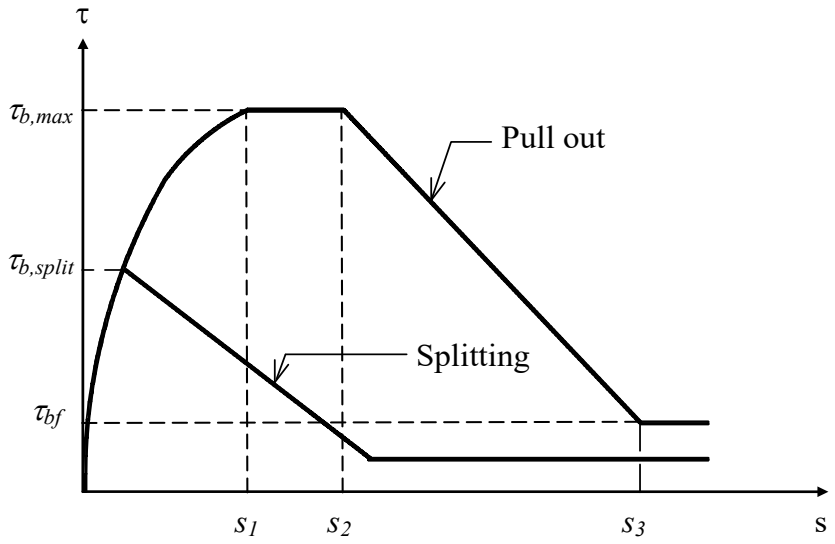

Figure A.4 Bond-slip relation for interaction between reinforcement and surrounding concrete. Based on Model Code 2010, fib (2013).

$$\tau_b = \tau_{b,\max} \cdot \left(\frac{s}{s_1}\right)^{0.4} \quad \text{for } 0 \le s \le s_1 \tag{A.10}$$

$$\tau_b = \tau_{b,\max} \quad \text{for } s_1 \le s \le s_2 \tag{A.11}$$

$$\tau_b = \tau_{b,\max} - \left(\tau_{b,\max} - \tau_{bf}\right) \cdot \left(\frac{s - s_2}{s_3 - s_2}\right) \quad \text{for } s_2 \le s \le s_3 \tag{A.12}$$

$$\tau_b = \tau_{bf} \quad \text{for } s_3 < s \tag{A.13}$$

where s_1, s_2 and s_3 are parameters listed in Table A.4. The parameters used depend on whether the failure mode is due to pull-out or splitting, what type of bond condition is valid and (for splitting failure mode) whether the bars are unconfined or confined. The values in Table A.4 under the column "Pull-out" are valid for well-confined concrete (concrete cover $\geq 5\phi$, clear spacing between bars $\geq 10\phi$) or suitable confining reinforcement. The values under the column "Splitting" are valid for other cases, which are calculated based upon the splitting strength, $\tau_{bu.split}$, given in Model Code 2010 as:

$$\tau_{bu,split} = \eta_2 \cdot 6.5 \cdot \left(\frac{f_{cm}}{25}\right)^{0.25} \cdot \left(\frac{25}{\phi_m}\right)^{0.2} \left[\left(\frac{c_{min}}{\phi_m}\right)^{0.25} \left(\frac{c_{max}}{c_{min}}\right)^{0.1} + k_m \cdot K_{tr}\right] \tag{A.14}$$

where η_2 is 1.0 and 0.7 for "good" and "all other" bond conditions respectively, f_{cm} is the mean cylinder compressive strength in MPa, ϕ_m is the diameter of the anchored bar in mm, and c_{min} and c_{max} are defined as

$$c_{min} = \min\left(c_s/2\,, c_x, c_y\right) \tag{A.15}$$

$$c_{max} = \max(c_s/2\,, c_x) \tag{A.16}$$

where c_s is the clear spacing between main bars, c_x is the cover in x-direction and c_y is the cover in y-direction. k_m and K_{tr} are the confinement coefficient and the amount of the transverse reinforcement, respectively, defined as

$k_m = 12$ for bars located within $5\phi_m \le 125$ mm from a stirrup corner

$k_m = 6$ if $c_s \ge 8c_y$

$k_m = 0$ if $c_s < 8c_y$, or if a crack can propagate to the concrete surface without crossing transverse reinforcement

The transverse reinforcement is quantified as:

$$K_{tr} = n_t A_{st}/(n_b \phi_m s_t) \le 0.05 \tag{A.17}$$

where n_t the number of legs of confining reinforcement crossing a potential splitting-failure surface at a section, A_{st} is the cross-sectional area of one leg of a transverse bar, s_t is the longitudinal spacing of confining reinforcement and n_b is the number of anchored bars or pairs of lapped bars in the potential splitting surface.

If the reinforcement bar yields, the bond stress will decrease considerably (Engström, 1992). In Engström (1992), no explicit bond-slip relation is proposed but depends on when the bonded bar yields. Further, the principal bond-slip relation for this yield case is similar to the relation used in Model Code 2010 when splitting failure is obtained. Therefore, it is suggested to assume a bond-slip relation based on splitting failure in regions where yielding of the reinforcement is likely to occur.

Table A.4 Parameters defining bond-slip parameters defined in Figure A.4. Based on Model Code 2010, fib (2013).

	Pull-out		**Splitting**			
	"Good"	**"All other"**	**"Good"**		**"All other"**	
			Unconfined	**Stirrups**	**Unconfined**	**Stirrups**
τ_{bmax}	$2.5\sqrt{f_{cm}}$	$1.25\sqrt{f_{cm}}$	$2.5\sqrt{f_{cm}}$	$2.5\sqrt{f_{cm}}$	$1.25\sqrt{f_{cm}}$	$1.25\sqrt{f_{cm}}$
$\tau_{bu,split}$	-	-	Eq. (A.14)	Eq. (A.14)	Eq. (A.14)	Eq. (A.14)
s_1	$1.0\ mm$	$1.8\ mm$	$s(\tau_{bu,split})$	$s(\tau_{bu,split})$	$s(\tau_{bu,split})$	$s(\tau_{bu,split})$
s_2	$2.0\ mm$	$3.6\ mm$	s_1	s_1	s_1	s_1
s_3	$c_{clear}{}^{\star}$	$c_{clear}{}^{\star}$	$1.2s_1$	$0.5c_{clear}{}^{\star}$	$1.2s_1$	$0.5c_{clear}{}^{\star}$
τ_{bf}	$0.4\tau_{bmax}$	$0.4\tau_{bmax}$	$0^{\dagger}$	$0.4\tau_{bu,split}{}^{\dagger}$	$0^{\dagger}$	$0.4\tau_{bu,split}{}^{\dagger}$

* c_{clear} is the clear distance between ribs.
† residual capacity modified in the local bond-slip model.

It should be noted that the bond-slip relations presented here are valid for one single bar. Hence, if the reinforcement amount used in the FE model represents more than one bar this has to be accounted for by increasing the bond with regard to the number of bars represented. If the bars are bundled, the bond-slip relation should be applied to a surface area corresponding to that of the effective bar diameter ϕ_e, i.e.

$$\phi_{ef} = \sqrt{\phi_1^2 + \phi_2^2} \tag{A.18}$$

where ϕ_1 and ϕ_2 are the diameters of the two bundled bars.

References

References are included in the main reference list

B Material properties of frost-damaged concrete

Frost damage in concrete is caused by a) the differing thermal expansion of ice and concrete and b) by the volume expansion of freezing water in the concrete pore system, Chatterji (1999). The former mechanism is involved when the structure is subjected to cold climates in the presence of saline water. The stress arises from the difference in thermal expansion of ice and concrete, which leaves the ice in tension as the temperature drops. Therefore, a crack in saline ice penetrates into the substrate and causes the superficial damage known as surface scaling, Valenza and Scherer (2006). This damage usually results in spalling of the concrete surface, while the remaining concrete is mostly unaffected; see Wiberg (1993), Gudmundsson and Wallevik (1999) and Fagerlund (2004). The latter mechanism is involved when the volume expansion of the freezing water, restrained by the surrounding concrete, cannot be accommodated in the pore system. Thereby, tensile stresses are initiated, and micro and macro cracks are introduced into the concrete body, which leads to the type of severe damage known as internal frost damage. This mechanism affects the compressive strength, tensile strength, Young´s modulus, fracture energy, and the bond between the reinforcing bar and surrounding concrete in damaged regions; see Powers (1945), Shih *et al.* (1988) and Fagerlund *et al.* (2001).

A methodology to analyse the mechanical behaviour and to determine the remaining load-carrying capacity of reinforced concrete structures affected by frost damage is presented. The methodology is based on the premise that the effect of internal frost damage can be modelled as changes in material and bond properties. Moreover, the effect of surface scaling can be taken into account as a change in geometry, such as a reduction in concrete cross-section when surface scaling leads to cover spalling while the remaining concrete is assumed to be unaffected, Wiberg (1993). The methodology is restricted to the prediction of the mechanical behaviour of a structure with an observed amount of damage at a given time; hence, the formation of the damage over time is not included.

In the assessment of the damaged structures, the compressive strength and the dynamic modulus of elasticity, as indicators of damage, must be measured in each individual case. The compressive strength can be evaluated by compression tests on a few drilled cores, supplemented with non-destructive tests to determine the extent of the damaged region. The dynamic modulus of elasticity (dynamic Young´s modulus) can be evaluated using either ultrasonic transit time measurement or fundamental transverse frequency test. Frost damage changes the internal structure of concrete, by introducing micro and macro cracks, which lengthens the travel time of an ultrasonic wave through the damaged concrete. It is believed that there is a strong correlation between the level of frost damage and the dynamic modulus of elasticity; see Petersen *et al.* (2007) and Zandi *et al.* (2011). Such a correlation can be suggested using the available test data in the literature; see Figure B.1. Thereafter, the effect of frost damage on material properties, such as the stress-strain response in compression, the stress-crack opening relation in tension and the bond-slip behaviour, is estimated using the damage indicators. Finally, the behaviour of the damaged structure can be studied in the finite element (FE) analysis. Within this context, suggestions are given on how the effect of frost can be considered as changes in the effective material and bond properties. Reference is made to several tests performed and models developed by other authors, in order to clarify different aspects of the methodology.

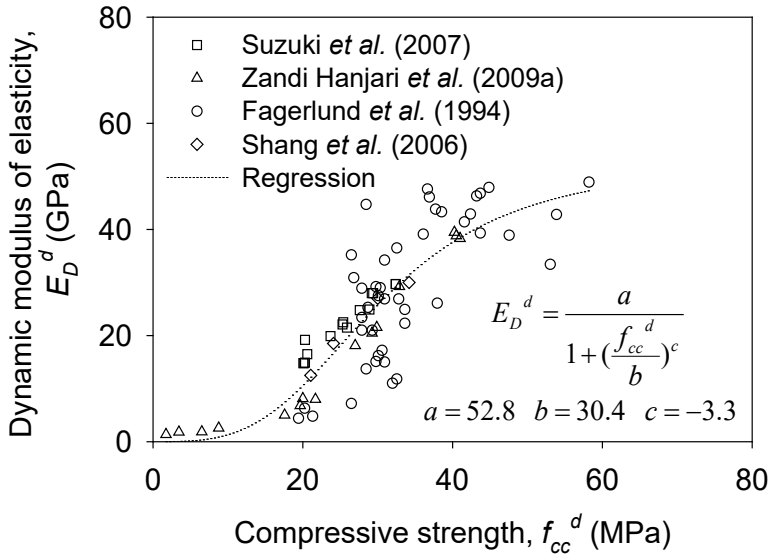

Figure B.1 Correlation between compressive strength and dynamic modulus of elasticity for frost-damaged concrete.

Relation between Compressive and Tensile Strength

For undamaged concrete, the relation between compressive strength and tensile strength is well-established and widely used, e.g. see Model Code 2010, fib (2013) and EuroCode 2. For practical reasons, to reduce the number of tests required to compression tests only, it would be useful if similar relations could be found for frost-damaged concrete. Test results for the tensile strength of undamaged and frost-damaged concrete were adapted and plotted versus the corresponding compressive strength and compared with relations for undamaged concrete, Figure B.2 (a). In the study carried out by Fagerlund *et al.* (1994), specimens have been cast from eleven concrete batches with different water/cement ratios of 0.5, 0.65 and 0.8. The pre-dried specimens have been evacuated to different residual pressures of 2, 20 and 50 mmHg. Then water has been introduced in the vacuum chamber and the specimens have been reached different degrees of saturation. Finally, the specimens have been exposed to seven freeze-thaw cycles, each cycle with a duration of two days and a minimum temperature of -18˚C. The higher the degree of vacuum was, the higher the degree of saturation and the more severe damage was reached.

In Figure B.2 (a), the compressive strength was recalculated from a dry 100 mm cube to a 150 mm cube by multiplying it by 0.96; see Neville (1996), and then to the standard wet 150 × 300 mm cylinder which is commonly used in codes by multiplying it by 0.85 according to Model Code 2010, fib (2013). The tensile strength was obtained from the measured splitting tensile strength by multiplying it by 0.9. As can be seen, the relations for the undamaged concrete cannot be used directly for the frost-damaged concrete. The tensile strength of the damaged concrete is markedly lower than if it was estimated from the relations for undamaged concrete. By curve fitting, although the scatter is large, the following relation for the damaged concrete is found:

$$f_{ct}^{\,d} = 0.027 \cdot \left(f_{cc}^{\,d}\right)^{1.2} \tag{B.1}$$

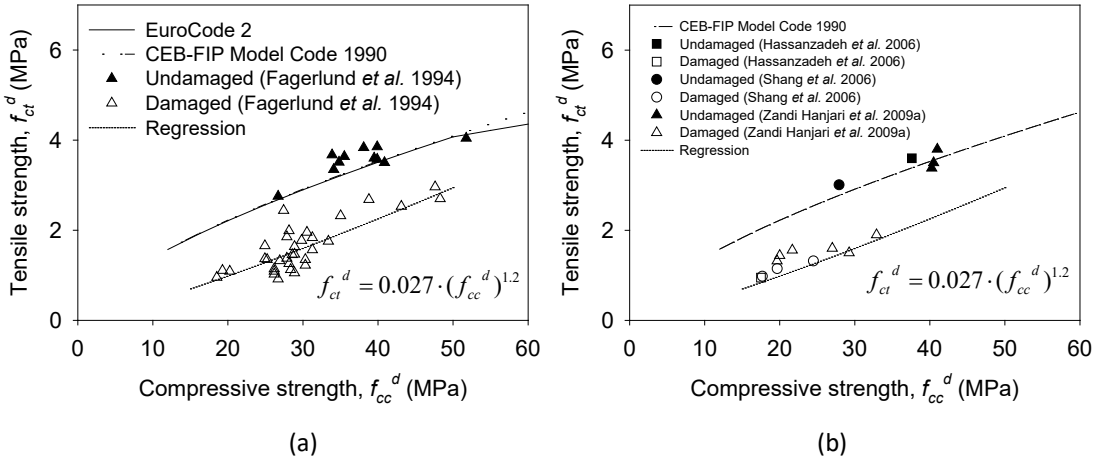

Figure B.2 Compressive strength versus tensile strength of frost-damaged concrete from (a) Fagerlund et al. (1994) and (b) other experimental investigations.

where f_{ct}^{d} is the tensile strength of the damaged concrete, and f_{cc}^{d} is the measured compressive strength of the damaged concrete in MPa using a standard 150 × 300 mm cylinder.

Subsequently, the proposed relationship was compared with experimental work carried out by other researchers; see Hassanzadeh and Fagerlund (2006), Shang and Song (2006) and Zandi *et al.* (2011). It should be noted that the proposed relation is independent of environmental conditions and only considers the observed amount of damage, i.e. compressive strength of the damaged concrete, at a given time. As shown in Figure B.2 (b), the tensile strength of the damaged concrete was reasonably well estimated by Equation (B.1), and the deviation from experimental results remained less than 18%.

Behaviour in Compression

The cracks caused by the internal frost damage influence the response of the concrete in compression, Suzuki and Ohtsu (2004). The damaged concrete exhibits a considerably lower initial elastic modulus, a relatively larger strain at the peak stress and a more ductile response in the post-peak behaviour compared to the undamaged concrete; see Shang and Song (2006) and Hasan *et al.* (2008). In an earlier work, concrete cylinders with two levels of frost damage corresponding to approximately 25 and 50% reduction in compressive strength were tested in compression, Zandi *et al.* (2011). It was observed that the ascending branch of the stress-strain relation is subjected to a change of the stiffness. This is believed to be caused by the randomly oriented cracks in the concrete due to the damage before the specimens were subjected to loading. Consequently, loading starts on a concrete specimen of low stiffness before the cracks are closed, and then the loading continues with a stiffer concrete, Ueda *et al.* (2009). However, the stiffness never fully recovers, and a permanent stiffness loss is observed, Zandi *et al.* (2011). These effects are here considered by adapting the stress-strain relation of the undamaged concrete according to the model by Thorenfeldt *et al.* (1987), see Equation (B.2), to make it work for the damaged concrete.

$$\sigma_{cc} = f_{cc}^{\ d}\left(\frac{\varepsilon}{\varepsilon_{cc}^{\ d}}\right)\cdot\left(\frac{n}{n-1+\left(\frac{\varepsilon}{\varepsilon_{cc}^{\ d}}\right)^{n\cdot k}}\right) \tag{B.2}$$

where σ_{cc} and ε are the stress and strain in the concrete, respectively, and $\varepsilon_{cc}^{\ d}$ is the strain at the maximum stress. The correction factors, n and k, are calculated as follows:

$$n = \frac{E_c^{\ d}}{E_c^{\ d} - E_0^{\ d}} \tag{B.3}$$

$$k = \begin{cases} 1 & \text{for} \quad 0 < \varepsilon < \varepsilon_{cc}^{\ d} \\ 0.67 + \dfrac{f_{cc}^{\ d}}{62} & \text{for} \quad \varepsilon > \varepsilon_{cc}^{\ d} \end{cases} \tag{B.4}$$

where $E_c^{\ d}$ and $E_0^{\ d}$ are the secant and tangential elastic modulus of the damaged concrete, respectively. The strain at the maximum stress, $\varepsilon_{cc}^{\ d}$, can be estimated by means of the experimental data, Figure B.3 (a), and the secant elastic modulus is calculated as $f_{cc}^{\ d}/\ \varepsilon_{cc}^{\ d}$. An approximation of the tangential elastic modulus of the damaged concrete based on the dynamic modulus of elasticity has been given by Petersen (2003); see Figure B.3 (b). Relatively good agreement is seen when the approximation is compared with the later experimental data; see Suzuki *et al.* (2007) and Zandi *et al.* (2011). The analytical stress-strain response of the damaged concrete from Equation (B.2) is compared with that of the experimental data from Zandi *et al.* (2011) in Figure B.4.

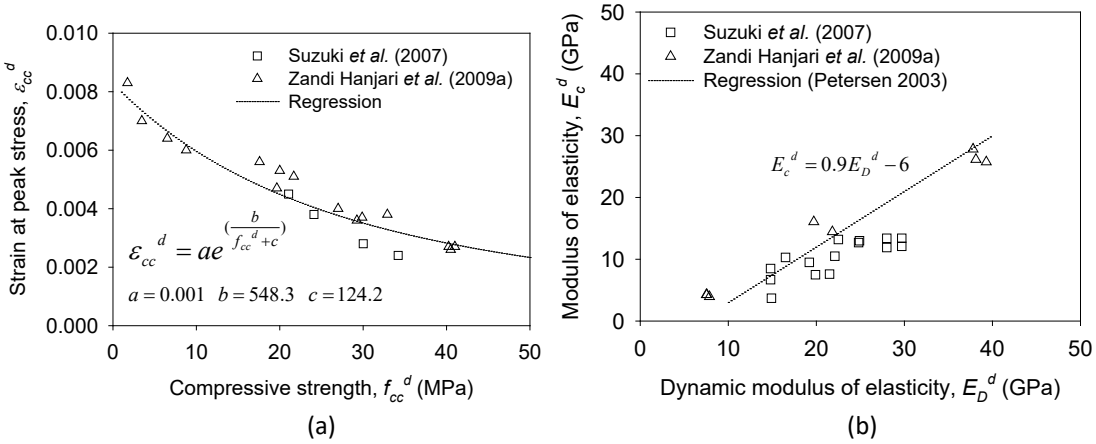

Figure B.3 Estimation of the (a) strain at peak stress and (b) tangential elastic modulus for the damaged concrete, using the damage indicators, $f_{cc}^{\ d}$ and $E_D^{\ d}$.

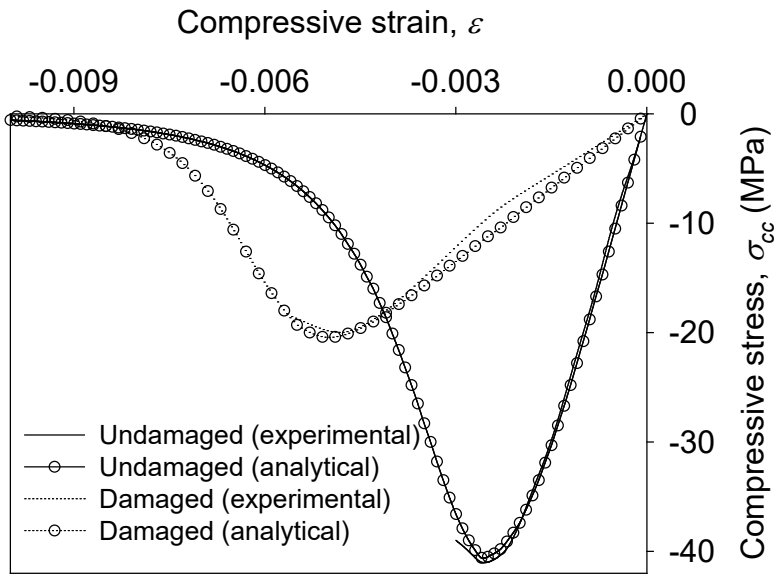

Figure B.4 Stress-strain response in compression; the level of frost-damage corresponds to 50% reduction in compressive strength, Zandi et al. 2011).

Behaviour in Tension

The tensile strength of the frost-damaged concrete has been investigated using splitting tensile tests, Fagerlund *et al.* (1994), Shang and Song 2006 and Zandi *et al.* (20011), and wedge splitting tests, Zandi *et al.* (2011). A slightly larger effect of frost damage on the tensile strength than on the compressive strength has been reported; see Figure B.5. However, there is very little information concerning the softening behaviour of the frost-damaged concrete. This is particularly important because of the direct application of such a relation in numerical analyses. In a recent study, Zandi *et al.* (2011), a bi-linear relation between tensile stress, σ_{ct}, and crack opening, w, of the frost-damaged concrete was estimated by using inverse analysis carried out on wedge splitting test results. The test was performed on cylinder specimens of 100 × 100 mm, damaged to two levels equivalent to 25 and 50% reduction in compressive strength, damage levels I and II in Figure B.5 (a).

It was found that the fracture energy and the critical crack opening, corresponding to zero tensile stress, significantly increased by the evolution of damage. Relatively large increase in fracture energy, up to approximately 170 Nm/m^2, was also reported by other researchers, e.g. Hassanzadeh and Fagerlund (2006); see Figure B.5 (b). To the best of knowledge of the authors, the bi-linear σ_{ct}-w relation given by Zandi *et al.* (2011) is the only data available in the literature which can be used as input in finite element analysis of frost-damaged concrete; see Figure B.5 (a).

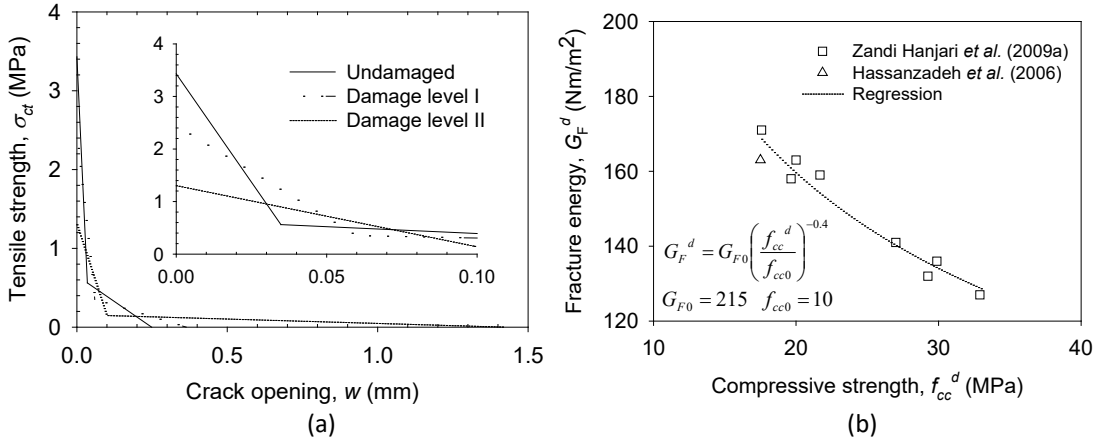

Figure B.5 *(a) Bi-linear σ_{ct}-w relation; damage levels I and II correspond to 25 and 50% reduction in compressive strength, Zandi et al. (2011); (b) the effect of frost damage on fracture energy.*

References

CEN (2004a). EN 1992-1-1 Eurocode 2: *Design of concrete structures - part 1-1: General rules and rules for buildings*. Brussels, Belgium: CEN European Committee for Standardization.

Chatterji, S., 1999b. Aspects of the freezing process in a porous material-water system Part 1. Freezing and the properties of water and ice. *Cement and Concrete Research*, 29 (4), 627–630.

Gudmundsson, G. and Wallevik, O., 1999. Concrete in an aggressive environment. In: J. Janssen, M.J. Setzer, M.B. Snyder, *ed. International RILEM Workshop on Frost Damage in Concrete*, Proceeding 25, 28-30 June 1999 Minneapolis, USA: RILEM Publications S.A.R.L, 87–102.

Fagerlund, G., *A Service Life Model for Internal Frost Damage in Concrete*, Division of Building Materials, Lund Institute of Technology, Lund, Sweden, 2004.

Fagerlund, G., Janz, M., Johannesson, B., *Effect of Frost Damage on the Bond between Reinforcement and Concrete*, Report, Division of Building Materials, Lund Institute of Technology, Lund, Sweden, 1994.

Fagerlund, G., Somerville, G., Jeppson, J., *Manual for Assessing Concrete Structures Affected by Frost*, Division of Building Materials, Lund Institute of Technology, Lund, Sweden, 2001.

fib (2013). *Model Code for Concrete Structures 2010*. Lausanne: International Federation for Structural Concrete (fib).

Hasan, M., Okuyama, H., Sato, Y., Ueda, T., Stress-strain model of concrete damaged by freezing and thawing cycles, *Journal of Advanced Concrete Technology* 2 (1) (2004) 89-99.

Hasan, M., Ueda, T., Sato, Y., Stress-Strain relationship of frost-damaged concrete subjected to fatigue loading, *J Mater Civ Eng* 20 (1) (2008) 37-45.

Hassanzadeh, M., Fagerlund, G., Residual strength of the frost-damaged reinforced concrete beams, *III European Conference on Computational Mechanics Solids,*

Structures and Coupled Problems in Engineering, Lisbon, Portugal, 5-8 June, 2006.

Neville, A.M., 1996. *Properties of concrete*. London: John Wiley & Sons.

Petersen, L. Lohaus, L., Polak, M. A., Influence of freezing-and-thawing damage on behavior of reinforced concrete elements, *ACI Mater J* 104 (4) (2007) 369-378.

Powers, T.C., 1945. A working hypothesis for further studies of frost resistance of concrete. *Journal of American Concrete Institute*, 16 (4), 245–271.

Petersen, L., 2003. *Einfluss baustofflicher schädigungsprozesse auf das tragverhalten von stahlbetonbauteilen*. Thesis (PhD). Universität Hannover.

Shang, H. S., Song, Y. P., Experimental study of strength and deformation of plain concrete under biaxial compression after freezing and thawing cycles, *Cem Concr Res* 36 (10) (2006) 1857-1864.

Shih, T. S., Lee, G. C. Chang, K. C. (1988) Effect of freezing cycles on bond strength of concrete, *J Struct Eng-ASCE* 114 (3) (1988) 717-726.

Suzuki, T. and Ohtsu, M., 2004. Quantitative damage evaluation of structural concrete by a compression test based on AE rate process analysis. *Construction and Building Materials*, 18 (3), 197–202.

Suzuki, T., Ohtsu, M. and Shigeishi, M., 2007. Relative damage evaluation of concrete in a road bridge by AE rate-process analysis. *Materials and Structures*, 40 (2), 221–227.

Thorenfeldt, E., Tomaszewicz, A. and Jensen, J.J., 1987. Mechanical properties of high-strength concrete and applications in designed. *Conference on Utilization of High-Strength Concrete*, Stavanger, Norway.

Ueda, T., Hasan, M., Nagai, K., Sato, Y. and Wang, L., 2009. Mesoscale simulation of influence of frost damage on mechanical properties of concrete. *Journal of Materials in Civil Engineering*, 21 (6), 244–252.

Valenza, J.J. and Scherer, G.W., 2006. Mechanism for salt scaling. *Journal of the American Ceramic Society*, 89 (4), 1161–1179.

Wiberg, U., 1993. *Material characterization and defect detection in concrete by quantitative ultrasonics*. Thesis (PhD). Kungl Tekniska Högskolan.

Zandi Hanjari, K., Utgenannt, P., & Lundgren, K. (2011). Experimental study of the material and bond properties of frost-damaged concrete. *Cement and Concrete Research*, 41(3), 244–254.

C Bond of reinforcement in frost-damaged concrete

Available experimental studies concerning the effect of frost damage on the bond between the reinforcement and concrete lead to the following three conclusions:

- In spite of a large scatter, the tests show an obvious influence of frost on the bond strength. Fagerlund *et al.* (1994) suggested lower and upper bound values for the reduction of the bond strength equal to 30 and 70%. Zandi *et al.* (2011) reported 15 and 50% bond deterioration for frost damage levels equivalent to 25 and 50% reduction in compressive strength. A linear decrease of the bond strength with the increase of damage was suggested by other researchers; see Petersen *et al.* (2007) and Ji *et al.* (2008).
- For a low level of damage, when the effect of frost is limited to the concrete cover, a small decrease of the slip at the maximum bond stress is observed, Petersen *et al.* (2007). For a large damage, when the effect of frost is extended to the interface between the concrete and the reinforcement, the bond capacity suddenly decreases and the slip slowly increases; see Shih *et al.* (1988), Petersen *et al.* (2007) and Zandi *et al.* (2011).
- The residual bond strength, represented by a constant stress after the descending branch of the bond stress-slip relationship, decreases with increased damage level, Zandi *et al.* (2009).

The bond stress-slip relation proposed by Model Code 2010, fib (2013), was modified by Zandi *et al.* (2013) to incorporate frost effects. In regions where the concrete cover is totally spalled off due to surface scaling, the bond strength is assumed to be zero. In other areas where the cover still remains (but may be cracked), the bond-slip properties are estimated based on the following approximations:

1) The relation between bond strength, τ_b, and slip, s, given in Model Code 2010, fib (2013), see Appendix A, are adopted for the undamaged concrete. To account for intermediate cases in between the extreme cases “confined” (i.e. ductile pull-out failure) and “unconfined” (i.e. brittle failure due to cover cracking induced by the radial tensile stress), the following interpolation formula was proposed by Lundgren *et al.* (2012):

$$\tau_b = k_{\text{int}} \cdot \tau_{b,confined} + (1 - k_{\text{int}}) \cdot \tau_{b,unconfined} \tag{C.1}$$

The interpolation factor is determined by

$$k_{\text{int}} = \max \begin{cases} k_{c/\phi} \\ k_{Asw} \end{cases} \tag{C.2}$$

where $k_{c/\phi}$ is a factor that depends on the ratio of cover to bar diameter, c/ϕ; k_{Asw} is a factor that depends on the amount of effective shear reinforcement, A_{sw}/s_w; and s_w is the shear reinforcement spacing. Factors $k_{c/\phi}$ and k_{Asw} are chosen according to Figure C.1.

2) The variation of the maximum bond stress in relation with the frost damage quantified with the relative dynamic modulus of elasticity (dynamic Yound’s modulus) was formulated by Petersen *et al.* (2007):

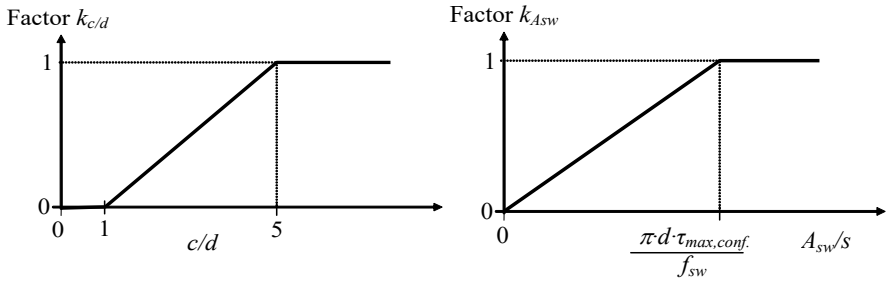

Figure C.1 Interpolation between "confined" and "unconfined" concrete.

$$\tau_{\max}{}^{d} = \left(0.17 + 0.007 \cdot E_{D,rel}{}^{d}\right) \cdot \tau_{\max} \tag{C.3}$$

where $\tau_{\max}{}^{d}$ and $\tau_{\max}$ are the bond strength for damaged and undamaged concrete, respectively, and $E_{D,rel}{}^{d}$ is the relative dynamic modulus of elasticity for the damaged concrete.

3) The residual bond strength is reduced proportionally to the reduction in the bond capacity, see Zandi *et al.* (2011).

$$\tau_{f}{}^{d} = \left(\frac{\tau_{\max}{}^{d}}{\tau_{\max}}\right) \cdot \tau_{f} \tag{C.4}$$

where $\tau_{f}{}^{d}$ and τ_{f} are the residual bond strength for damaged and undamaged concrete, respectively.

The analytical bond-slip relation for frost-damaged concrete, Equations (C.1) - (C.4), is compared with that of the experimental data from Zandi *et al.* (2011) in Figure C.2.

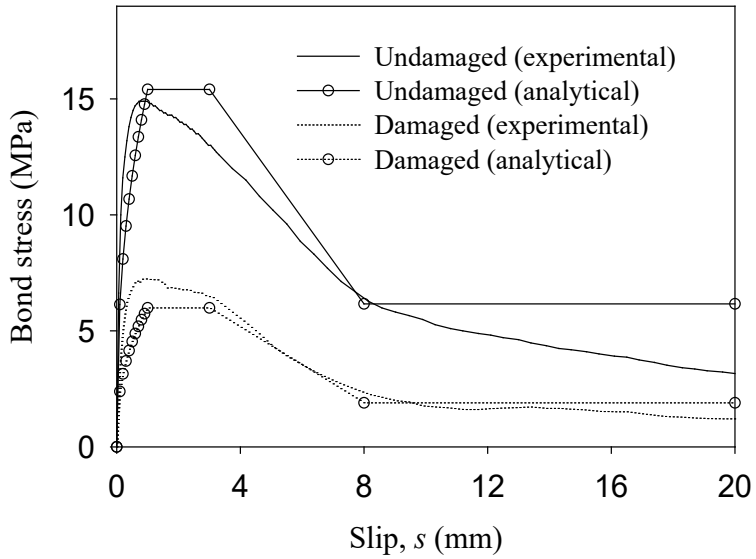

Figure C.2 Bond-slip relation for "Good" bond condition; the level of frost-damage corresponds to 50% reduction in compressive strength, Zandi et al. (2011).

References

Fagerlund, G., Janz, M. and Johannesson, B. (1994): *Effect of frost damage on the bond between reinforcement and concrete*. Report, Division of Building Materials, Lund Institute of Technology, Sweden.

fib (2013). *Model Code for Concrete Structures 2010*. Lausanne: International Federation for Structural Concrete (fib).

Ji, X., Song, Y. and Liu, Y. (2008). Effect of freeze-thaw cycles on bond strength between steel bars and concrete. *Journal Wuhan University of Technology, Materials Science Edition*, 23 (4), 584–588.

Lundgren K, Kettil P, Zandi Hanjari K, Schlune H, Roman ASS (2012): Analytical model for the bond-slip behaviour of corroded ribbed reinforcement. *Struct. Infrastruct Eng.*; 8: 157–69.

Petersen, L., Lohaus, L. and Polak, M.A. (2007). Influence of freezing-and-thawing damage on behavior of reinforced concrete elements. *ACI Materials Journal*, 104 (4), 369–378.

Shih, T.S., Lee, G.C. and Chang, K.C. (1988). Effect of freezing cycles on bond strength of concrete. *Journal of Structural Engineering*, 114 (3), 717–726.

Zandi Hanjari, K., Utgenannt, P., & Lundgren, K. (2011). Experimental study of the material and bond properties of frost-damaged concrete. *Cement and Concrete Research*, 41(3), 244–254.

Zandi Hanjari, K., Kettil, P. and Lundgren, K. (2013). Modeling the structural behavior of frost-damaged reinforced concrete structures, *Structure and Infrastructure Engineering*, Vol. 9, No. 5, pp 416–431.

D Material properties of concrete with corrosion cracking

The corrosion product expansion causes cracking of the concrete surrounding the reinforcement, reducing the concrete strength. High levels of corrosion can spall or delaminate the concrete, reducing the concrete cross section. The loss of concrete strength or residual concrete cross section must be considered for calculating the stiffness and ultimate bearing capacity of structures. Moreover, spalling and delamination affect the bond properties of the reinforcement; see appendix F.

Experimental observation

The most serious corrosion-induced damage occurs with a generalized spreading of corrosion over the surface of the reinforcement that is typical of high carbonation and the higher stages of chloride corrosion; the latter type of deterioration causes also pits with localized cross-section reduction. The crack patterns depend on many parameters, namely the position of the bar in the cross-section, cover depth, concrete porosity, the presence of other bars, different types of reinforcement, just to name a few.

The simplest types of corrosion-induced cracks, so called splitting cracks, develop parallel to the corroding longitudinal bars reaching to the outer surface of concrete. If longitudinal bars are closely spaced, in addition to cracks reaching to the surface, more cracks may originate from one bar reaching to an adjacent bar. In a layer including several closely spaced bars, cracks connecting the bars in a plane parallel to the outer cover of the member may form, making delamination possible. Additionally, the corrosion of transverse reinforcement can form more numerous cracks and complicate the patterns.

In porous concrete, the formation of cracks can be delayed because the expansive oxides fill the voids before developing pressure. If the oxides can leak out of the concrete, no pressure build up takes place and thus no cracking occurs. Reinforcement in the interior of a prestressed member can also corrode and cause cracks visible either on the exterior or, more dangerously, not visible at all.

Strength reduction due to corrosion-induced cracks

The following applies to the part of the section damaged by corrosion-induced cracking. To consider the reduction in compression strength of cracked concrete, the following equation may be used, according to Capè (1999):

$$f_c^{red} = f_c /(1 + 0.1\varepsilon_{cor} / 0.002) \tag{D.1}$$

$$\varepsilon_{cor} = \Sigma w_i^{cor} / b \tag{D.2}$$

with ε_{cor} is mean tensile strength in the concrete equivalent to corrosion cracks; b is the width of concrete cross-section; and w_i^{cor} is the width of the corrosion-induced crack for any number of cracks, i, that form around a corroding bar.

Equation (D.1) was proposed by Capè (1999), adapting the formulation of the Modified Compression Field Theory by Vecchio and Collins (1986) now included also in Model Code 2010, fib (2013). Coronelli and Gambarova (2004) and Zandi *et al.* (2013) used this equation modelling beams tested by and reported in Rodriguez *et al.* (1985).

Concrete cross section loss

The calculation of the capacity of a member requires considering the measured concrete cross-section counting for spalling and delamination. Different assumptions can be made to obtain approximations of, for instance, bending capacity for corroded reinforced concrete elements, Rodriguez *et al.* (1985) and Zandi *et al.* (2013), such as reducing the reinforcement cross-section and the top and bottom cover, or the whole cover; see Figure D.1.

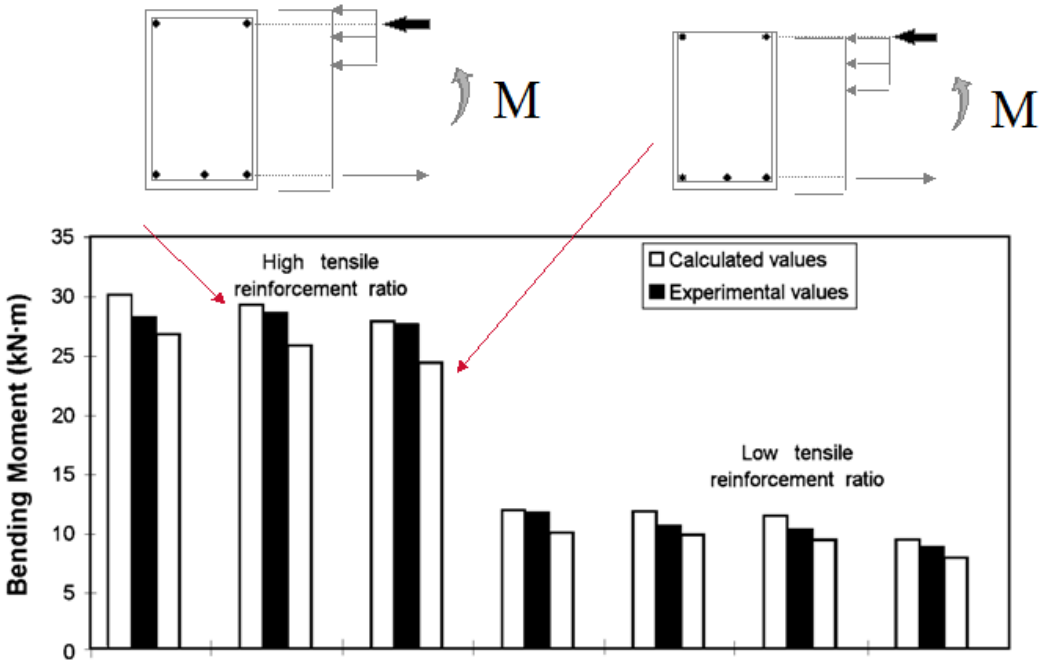

Figure D.1 Modelling concrete cross section loss for flexural capacity of beams; similar assumptions can be made for shear; see Rodriguez et al. (1985).

References

Capè, M. (1999). *Residual service-life assessment of existing R/C structures. Master Thesis*. Chalmers University of Technology (Sweden) and Milan University of Technology (Italy, Erasmus Program), 133

fib (2013). *Model Code for Concrete Structures 2010*. Lausanne: International Federation for Structural Concrete (fib).

Vecchio, F.J. and Collins, M.P. (1986) The Modified Compression Field Theory for Reinforced Concrete Elements Subjected to Shear. *ACI Journal*, Proceedings V.83, No. 2, Mar.-Apr., pp. 219-231.

Zandi Hanjari, K., Kettil, P. and Lundgren, K. (2013). Analysis of the Mechanical Behaviour of Corroded Reinforced Concrete Structures, *ACI Structural Journal*, 108 (5), 532.542.

Rodrigues J., Ortenga L.M., and Casal J. (1996): Load bearing capacity of concrete columns with corroded reinforcement, *4th Int. Symp. Corrosion of Reinforcement in Concrete*, Cambridge, UK, July.

E Bond for corroded reinforcement

The treatment of bond is differentiated in two parts: a local bond slip relationship for the analysis of bond problems, and a semi-empirical model for the prediction of anchorage capacity.

Bond-slip differential equation

The mathematical model is based on the differential equation governing the equilibrium condition along a bar, see Lundgren *et al.* (2009) and Blomfors *et al.* (2018) and Figure E.1:

$$A_s \cdot \frac{d\sigma_s}{dx} - \pi \cdot \phi_m \cdot \tau_b = 0 \tag{E.1}$$

where A_s is the cross-sectional area of the bar and ϕ_m is the bar diameter, σ_s is the stress in the bar and τ_b is the bond stress.

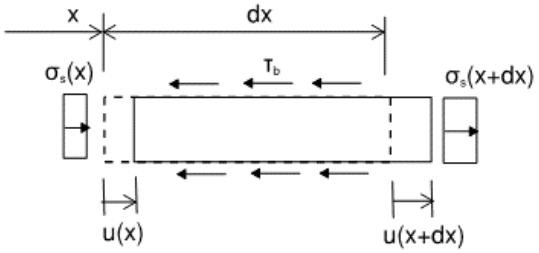

Figure E.1 Illustration of stresses acting on a bar segment with length dx and the resulting deformation; see Lundgren et al. (2009).

The reinforcement bar within the anchorage length is assumed to be in the elastic range, thus:

$$\sigma_s = E_s.\varepsilon_s, \quad \varepsilon_s = \frac{du}{dx} \tag{E.2}$$

where E_s is the elastic modulus, ε_s is the strain and u denote the displacement of the bar at point x. If the deformation of the surrounding concrete is neglected, the slip s between the reinforcement bar and the surrounding concrete equals the displacement of the bar:

$$u = s \tag{E.3}$$

When considering pull-out of a reinforcement bar with embedment length l_b and prescribed displacement, the boundary conditions are:

$$\sigma_s(0) = 0, \quad u(l_b) = u_{l_b} \tag{E.4}$$

where u_{l_b}, is the displacement at the end of the bar where the pull-out force is applied. The corresponding pull-out force F_{l_b}, can be obtained as:

$$F_{l_b} = A_s.\sigma_s(l_b) \tag{E.5}$$

where A_s is the area of the bar, and $\sigma_s(l_b)$ is the stress at the pulled end.

Local bond-slip model

The local bond-slip relation for an uncorroded bar can be described as given in Model Code 2010, fib (2013); see Appendix A.

Influence of corrosion

A model counting for the effect of corrosion on bond is described in the following; detailed description can be found in Blomfors *et al.* (2018). The model is referred to as "**ARC model**". Note that the ARC model is based on the local bond-slip model in in Model Code 2010, fib (2013).

It has been observed that the local bond stress-slip curve of corroded reinforcement can be approximated by shifting the uncorroded curve in the slip direction as shown in Figure E.2, see the details in Lundgren *et al.* (2009) .

This can be expressed as:

$$s_{eff} = s + s_{eq} \tag{E.6}$$

where s_{eff} is the effective slip, s is the mechanical slip and s_{eq} is the equivalent slip to account for the effect of corrosion. The equivalent slip can be estimated as:

$$s_{eq,nostir} = 2.9W_c \quad \text{without stirrups} \tag{E.7}$$

$$s_{eq,stir} = 13.6W_c \quad \text{with stirrups} \tag{E.8}$$

where W_c is the corrosion level (weight loss) in decimals and the equivalent slip is output in mm. For cases without stirrups there is data up to around 15% corrosion,

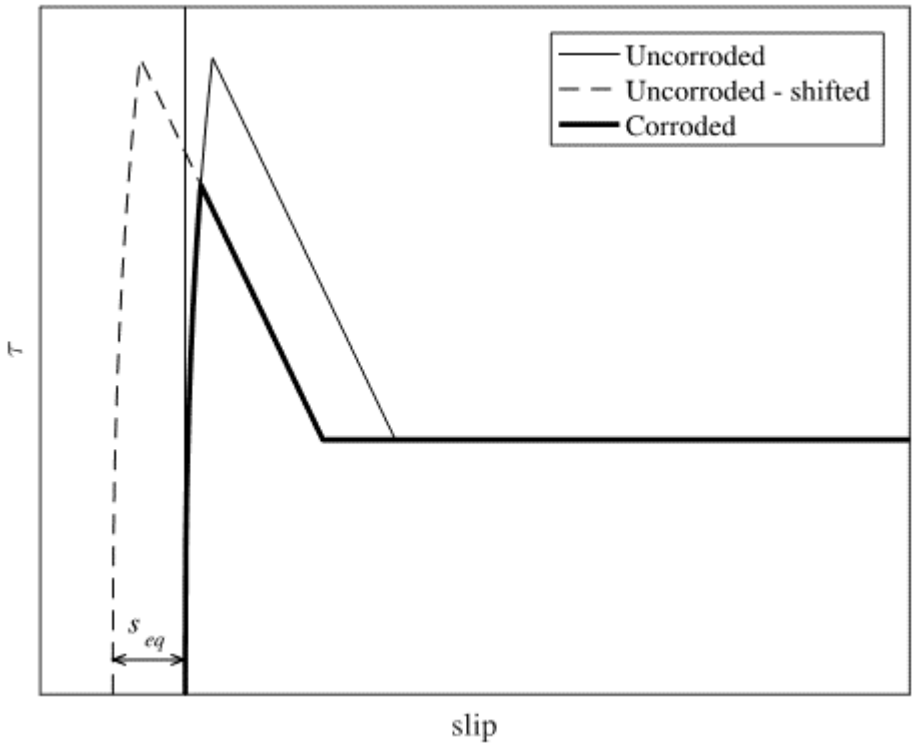

Figure E.2 Illustration of the equivalent slip, s_{eq}, to account for the effect of corrosion in a bond stress-slip curve, where splitting strength governs the maximum bond stress.

and for cases with stirrups up to approximately 20% corrosion. Therefore, the domains for Equation 17 and 18 are 0-15% and 0-20% corrosion weight loss, respectively.

Increasing corrosion levels will ultimately crack the concrete cover. The corrosion penetration leading to cracking can be estimated as:

$$x_{cr} = 11 \cdot \left(\frac{f_{cm}}{40}\right)^{0.8} \cdot \left(\frac{c}{\phi_m}\right)^{1.5} \cdot \left(\frac{\phi_m}{16}\right)^{0.5} \quad \text{(E.9)}$$

where f_{cm} is the mean cylinder compressive strength in MPa, ϕ_m is the diameter of the anchored bar in mm, and c is the concrete cover. The influence of corrosion on cracking of the cover is accounted for by using the reduced splitting strength:

$$\tau_{bu,split,red} = \eta_2 \cdot 6.5 \cdot \left(\frac{f_{cm}}{25}\right)^{0.25} \cdot \left(\frac{25}{\phi_m}\right)^{0.2} (1 + k_m \cdot K_{tr}) \quad \text{(E.10)}$$

where η_2 is 1.0 and 0.7 for "good" and "all other" bond conditions, respectively, f_{cm} is the mean cylinder compressive strength in MPa, ϕ_m is the diameter of the anchored bar in mm, and k_m and K_{tr} are the confinement coefficient and the amount of the transverse reinforcement, respectively, defined in the previous section.

A modified expression of the residual bond capacity for specimens with low stirrup content is proposed for both the corroded and uncorroded cases:

$$\tau_{res,mod}(K_{tr}) = \begin{cases} (0.16 + 12K_{tr}) \cdot \tau_{bu,split,red} & \text{for } 0 \le K_{tr} \le 0.02 \\ 0.4 \cdot \tau_{bu,split,red} & \text{for } 0.02 < K_{tr} \end{cases} \quad \text{(E.11)}$$

Model parameters

Reinforcement bar:

ϕ_m = bar diameter
E_s = elastic modulus

Concrete:

f_{cm} = mean cylinder compressive strength in MPa

Bond:

s_{eq} = equivalent slip, only dependent on
W_c = corrosion level (weight loss) in percent
τ_{bmax} defined by Table A-4, and is only dependent on f_{cm}
$\tau_{bu,split}$ for uncorroded bars and $\tau_{bu,split,red}$ for corroded bars are defined by Equation A.14 and E.10 respectively, and are dependent on:
η_2 = 1.0 and 0.7 for "good" and "all other" bond conditions, respectively
c_{min} and c_{max} according to Equation A.15 and A.16, defined by:
c_s = the clear spacing between main bars
c_x = cover in x-direction
c_y = cover in y-direction
k_m = confinement coefficient, depends on distance from stirrup corner
c_s = clear spacing between main bars

K_{tr} = coefficient amount of transverse reinforcement, as given by Equation A.17, depends on:
n_t = number of legs of confining reinforcement

A_{st} = cross-sectional area of one leg of a transverse bar
s_t = longitudinal spacing of confining reinforcement
n_b = the number of anchored bars
$\tau_{res,mod}$ = residual strength, as given by Equation E.11, and depends on
$\tau_{bu,split,red}$ = given by Equation E.10

Determination and selection of parameters

Reinforcement bar:

ϕ_m = bar diameter (original/uncorroded), obtained from drawing or measured on site
E_s = elastic modulus of rebar steel, may be set to 200 GPa

Concrete:

f_{cm} = mean cylinder compressive strength, obtained from drawing or measured by e.g. compression test on drilled cores

Bond:

η_2 = 0.7 - 1.0 dependent on bond conditions
$c_s = c_x = c_y$ = measured on site, see Figure E.3. If cover has spalled, a reduced splitting strength is used, see Equation E.10.

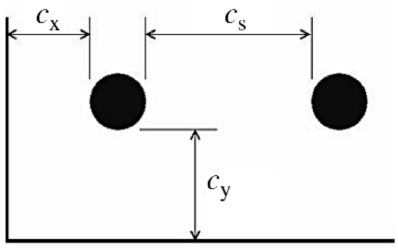

Figure E.3 Notations for bar spacing and cover, Model Code 2010, fib (2013).

Corrosion level:

W_c = corrosion level, weight loss in principle measured at one section of the bar)
$W_c = (A_s - A_{s,corr})/A_s$ corrosion level, weight loss (in principle measured at one section of the bar)
A_s = Area of uncorroded reinforcement, $\pi \phi_m^2/4$
A_{corr} = Area of corroded reinforcement, $\pi(\phi_m - 2x)^2/4$ if x is corrosion penetration

For cases without stirrups there is data up to around 15% corrosion, and for cases with stirrups up to approximately 20% corrosion. Bond strength is not significantly influenced by a varied corrosion distribution around a bar; see Figure E.4.

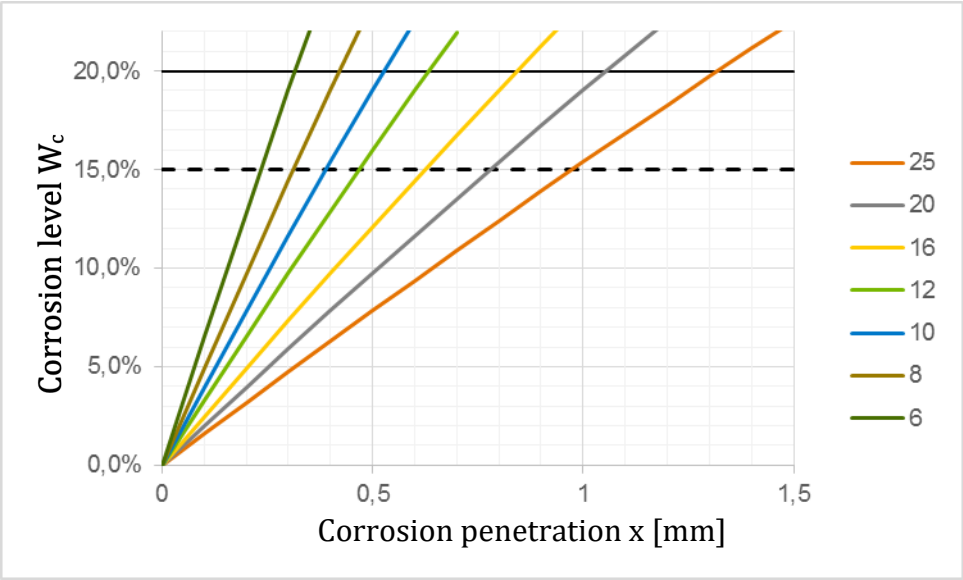

Figure E.4 Corrosion x [mm] versus corrosion level Wc [%] for reinforcement bars 6 mm to 25 mm; Blomfors et al. (2018).

Confinement:

Corrosion level W_c (see Figure E.4)
$k_m = 12$ for bars located within $5\phi_m \leq 125$ mm from a stirrup corner
$k_m = 6$ if $c_s \geq 8c_y$
$k_m = 0$ if $c_s < 8c_y$, or if a crack can propagate to the concrete surface without crossing transverse reinforcement
n_t, A_{st}, s_t, n_b = regarding transverse reinforcement, obtained from drawing or measured on site

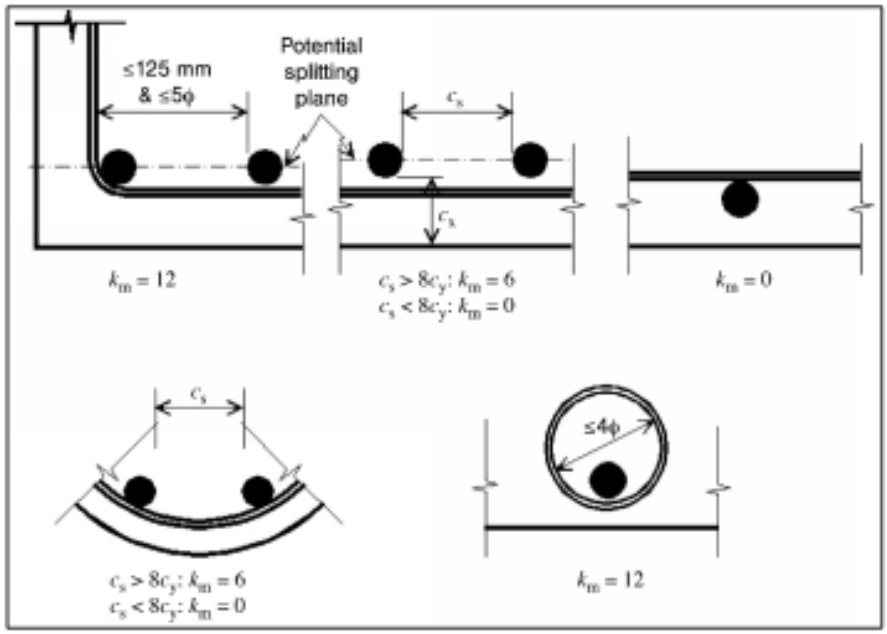

Figure E.5 Confinement coefficients for transverse reinforcement, Model Code 2010, fib (2013).

The influence of corroded stirrups on the bond capacity is not explicitly included in the model. However, based on the corrosion level of the stirrups their effective area can be used as input to the ARC model. When corrosion of the stirrups has caused the concrete cover to crack or spall off, this can be treated by using a reduced splitting strength as presented in Equation E.10.

Bundled reinforcement

For bundled reinforcement the area and perimeter are de-coupled, see Figure E.6 and Table E.1. A corrosion level is applied and the cross-sectional area is reduced. The equivalent area and perimeter after corrosion is:

$$A_{corr} = W_c \cdot A_e, \tag{E.12}$$

$$A_{e,corr} = (1 - W_c) \cdot A_e \tag{E.13}$$

$$\phi^e_{m,corr} = \sqrt{\frac{4A_{e,corr}}{\pi}} \tag{E.14}$$

$$p_{e,corr} = p_e(\phi_{corr}), \text{ where } \phi_{corr} = \sqrt{\phi^2 \cdot (1 - W_c)} \tag{E.15}$$

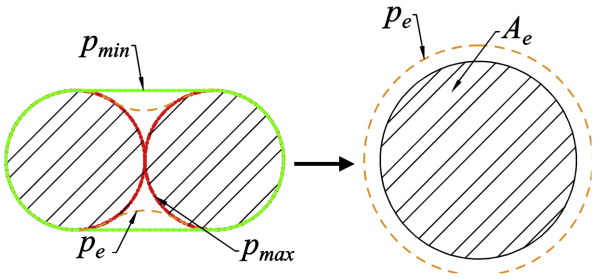

$A_s = A_e$ = equivalent area of bundled bars

p_e = bond perimeter of bundled bars, average value of upper bound p_{max} and lower bound p_{min}

Figure E.6 Scheme of the minimum, maximum and average perimeters and the equivalent area and perimeter for the bundled reinforcement bars.

Table E.1 Equivalent diameter and perimeter.

Uncorroded case (2 bars):	Uncorroded case (3 bars):	Uncorroded case (4 bars):
$A_e = 2 \cdot \pi \cdot \frac{\phi^2}{4}$ $\phi^e_m = \sqrt{\frac{4A_e}{\pi}}$ $p_e = \phi\left(1 + \frac{3\pi}{2}\right)$	$A_e = 3 \cdot \pi \cdot \frac{\phi^2}{4}$ $\phi^e_m = \sqrt{\frac{4A_e}{\pi}}$ $p_e = \phi\left(\frac{3}{2} + \frac{7\pi}{4}\right)$	$A_e = 4 \cdot \pi \cdot \frac{\phi^2}{4}$ $\phi^e_m = \sqrt{\frac{4A_e}{\pi}}$ $p_e = \phi(2 + 2\pi)$

Multi-layer reinforcement

Investigations has shown that the second (and higher) layer of reinforcement (seen from the bottom) has equal or greater capacity than the lower layer. This is also in accordance with Eurocode 2 (CEN, 2004), which does not differentiate capacity for one or several layers. Hence, calculations can be performed for the bottom layer, and

then the anchorage capacity for the second (and higher) layers can be set equal to the capacity of the bottom layer.

Evaluation of results

The design resistance for the anchored force R_d should be calculated as according to Blomfors *et al.* (2019):

$$R_{\mathrm{d}} = \frac{R_{\mathrm{ARC}}(f_{\mathrm{ck}}, f_{\mathrm{yk}}, \boldsymbol{x}_{\mathrm{nom}})}{\gamma_{\mathrm{M}}} \tag{E.16}$$

where R_{ARC} is the force calculated by the ARC model using characteristic values (95%) for strength parameters, and nominal (average) values for the rest of the parameters, and γ_M is a partial safety factor with proposed values according to Table E.2.

Table E.2 Proposed values for partial safety factor γ_M, Blomfors *et al.* (2019).

Corrosion level W_c	Without stirrups	With stirrups
0%	2.0	1.9
5%	-	4.7
10%	-	4.9
15%	3.4	5.2-6.4*
20%	-	5.2-7.6*

*For cases where n_{b} is 1-5, intermediate cases can be interpolated.

Remark: Due to high uncertainties associated with corrosion levels of 5 and 10% in case of no stirrups, it was chosen to not differentiate between different levels of corrosion for the partial factors. The partial factors are instead derived for an uncorroded case and a corroded case. For the corroded case 15% corrosion should be used as input to the ARC model.

Background for partial safety factors

The target reliability index is $\beta_{\mathrm{t}} = 3.7$ (one-year reference period) according to recommendations by the Joint Committee on Structural Safety. It should be noted that this β_{t} may not be used for new designs. When verifying the partial factors normal and Gumbel distributions were used for the permanent and variable loads respectively, with characteristic levels of 50 and 98%. For a detailed description of the derivation of the partial factors, see Blomfors *et al.* (2019).

Design anchorage length L_d is theoretically the anchorage length that fulfil the equality

$$R_{\mathrm{ARC}}\left(f_{\mathrm{ck}}, f_{\mathrm{yk}}, \boldsymbol{x}_{\mathrm{nom}}, L_d\right) = (F_{\mathrm{yk}}/\gamma_{\mathrm{s}}) * \gamma_{\mathrm{M}} \tag{E.17}$$

where F_{yk} is the rebar yield force for the actual level of corrosion. One should note that the force $F_{\mathrm{yk}}/\gamma_{\mathrm{s}} * \gamma_{\mathrm{M}}$ usually substantially exceeds the rebar yield force, which make the formula somewhat theoretical and not possible to be verified by experiment. Therefore, the formula is replaced by the following formula based on approximation by linearization:

$$R_{\mathrm{ARC}}\left(f_{\mathrm{ck}}, f_{\mathrm{yk}}, \boldsymbol{x}_{\mathrm{nom}}, L_k\right) = F_{\mathrm{yk}} \quad \text{(E.18)}$$

$$L_d = L_{\mathrm{k}} * (\gamma_{\mathrm{M}}/\gamma_{\mathrm{s}}) \quad \text{(E.19)}$$

Note that the approximation corresponds to the commonly used assumption/approximation of uniform bond stress along the anchorage length.

Lap lengths may be assumed equal to anchorage lengths. For several layers of reinforcement, it is assumed that maximum 50% of the reinforcement is spliced at the same position, otherwise a special investigation must be performed.

References

Blomfors M., Coronelli D., Lundgren K., Zandi K: "Engineering bond model for corroded reinforcement". *Engineering Structures*, 2018, Volume 156, pp. 394-410.

Blomfors, M., Larsson Ivanov, O., Honfi, D., Engen, M. "Partial safety factors for the anchorage capacity of corroded reinforcement bars in concrete". *Engineering Structures*, Volume 181, 15 February 2019, Pages 579-588.

fib (2013). *Model Code for Concrete Structures 2010*. Lausanne: International Federation for Structural Concrete (fib).

Lundgren, K., Kettil, P., Zandi Hanjari, K., Schlune, H., and Roman, ASS. "Analytical model for the bond-slip behaviour of corroded ribbed reinforcement". *Structure and Infrastructure Engineering*, 8(2), 2009, pp.157–169.

F Example – Anchorage capacity of a two-way slab

Reinforced concrete (RC) slabs are among the most exposed parts in quay structures and the reinforcing bars maybe subjected to corrosion damage since they are often within the splash zone of see water. Bending and punching shear are usually governing failure modes at the ultimate limit state for RC slabs subjected to concentrated loads. However, anchorage capacity may become critical, for instance at the curtailment and splicing region at the casting joints, if the reinforcing bars are subjected to extensive corrosion. While provisions in EC2 and Model Code can be used to calculate bending and punching shear capacities, calculation methods to estimate anchorage capacity, or the required anchorage length to prevent anchorage failure, of corroded RC slabs are not given in design codes. This example aims to demonstrate how the anchorage capacity in corroded RC slabs can be estimated.

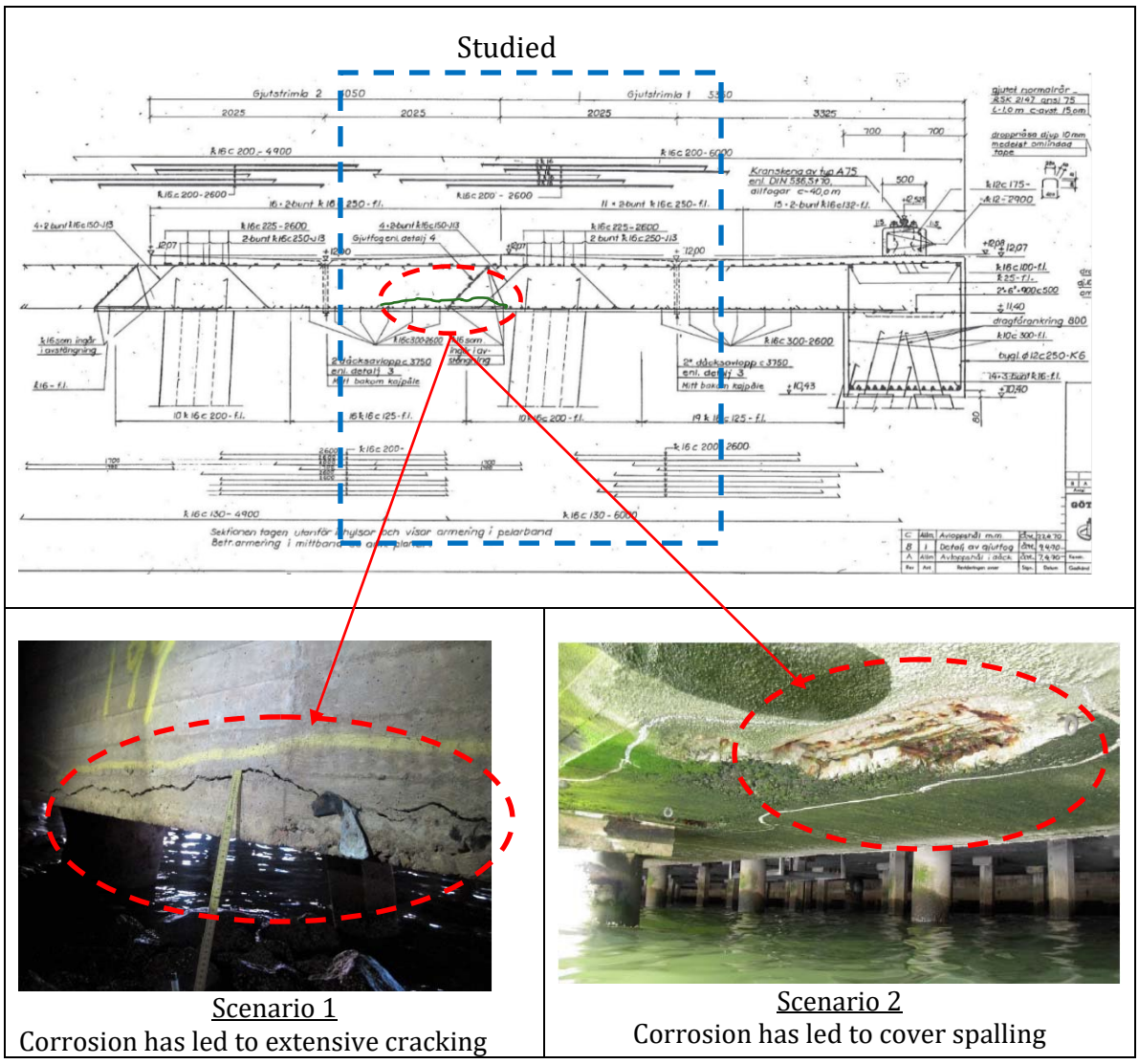

Figure F.1 An example quay structure in Gothenburg harbour with two damage scenarios (shown in red circle).

The principles of the method applied here are described in detail in Blomfors *et al.* (2018), and the model is implemented in a MATLAB code called ARC 2010 Program. The code, together with a user's manual, can be found here:

https://www.chalmers.se/en/staff/Pages/kamyab-zandi.aspx

In short, the program contains a model that describes the bond-slip response of corroded reinforcement which can be used in the assessment of the anchorage capacity in corrosion-damaged structures. The model is an extension of the bond-slip model given in the Model Code 2010 (fib, 2013) to account for the effect of corrosion.

In the example described above, two scenarios are studied, see Figure F.1, in which corrosion of bottom reinforcement in the RC slab has led to extensive cracking (scenario 1), and cover spalling (scenario 2). The geometry of the RC slab is summarised in Figure F.2, and the dimensions, reinforcement amounts and material properties are given in Table F.1.

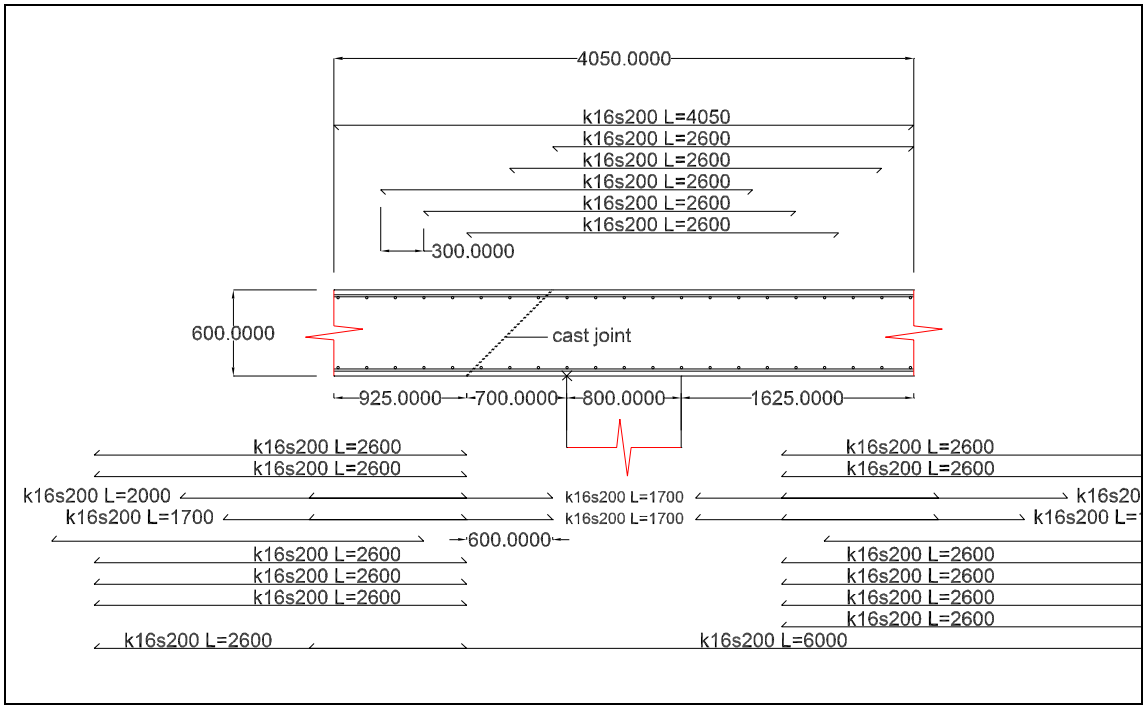

Figure F.2 The dimensions and rebar layout of the studied slab (inspired by a quay structure from Gothenburg harbour); all dimensions are in mm.

Table F.1 Dimensions, reinforcement amounts and the assumed material properties. d is effective height; f_c is the compressive strength of concrete; d_g is aggregate size; f_y and f_u are yield and ultimate strength of reinforcement steel.

Slab dimension [mm] B×B×*h*	Concrete			Reinforcing steel		
	TB [mm]	f_c [MPa]	d_g [mm]	reinforcement	f_y [MPa]	f_u [MPa]
4050×4050×600	40	30	16	Ø16 s200	400	450

The design load in ULS is 100 kN/m2, with 25% permanent load and 75% variable load.

The utilisation ratios and load capacity with respect to moment*, shear and bond failure is to be determined for different levels of reinforcement corrosion penetration 0 and 0.6 mm, corresponding to 0 and 15% corrosion weight loss for the main ϕ16 bars.

It is important to note that, the calculation here is limited to moment capacity with respect to the bottom reinforcement, which is most critical with respect to corrosion. The top reinforcement and punching shear capacities has not been checked in this example.

The shear force and maximum sagging moment are:

```
q = [25, 75]                          % Dead and live load [kN/m2]
L = 4                                 % Span length
x = [0:0.5:L/2]
V = sum(q)*(L/2-x)
M(1,:) = q(1)*L/2*x - q(1)*x.^2/2
M(1,:) = -M(1,end)*2/3+M(1,:)
M(2,:) = q(2)*L/2*x - q(2)*x.^2/2
M(2,:) = -M(2,end)*1/3+M(2,:)

M = M(1,:)+M(2,:)
```

The shear capacity is:

```
d = 0.55                              % [m]
fv = 0.45e3                           % estimated value, [kN/m2]
Vcr = d*fv = 247 kN/m
```

The utilisation ratio in shear is (checked at support, x ≈ 0.8/2 m):

```
ny = V(2)./Vcr*100 = 61 %
```

The moment capacity is:

```
d = 0.55                              % [m]
Asl = 5*[201, 170]*1e-6               % for 0 and 0.6 mm corrosion [m2]
fsl = 400e3/1.15                      % design value, [kN/m2]
Mr =0.9*d*Asl*fsl = [173, 146] kNm
```

The utilisation ratio for maximum moment is:

```
ny = M(end)./Mr*100 = [67, 80]    % for 0 and 0.6 mm corrosion, [%]
```

The total force in the main rebars due to bending moment and due to inclined cracking by shear is:

```
z = 0.9*d
Fsm = M/z                             % Due to bending
Fsv = V/2                             % Due to shear
```

```
Fsd = Fsm + Fsv
Fsd = min(Fsd,Fsm(end)*ones(1,5))
```

Plot total force:

```
figure(1); clf; hold on
plot(x,Fsd,'b-')
axis([0,2, 0,400])
```

The following input data is used to compute the required anchorage length by the ARC 2010 program:

ϕ =16 mm
c_clear = 6.4 mm
c_y = 40 mm
c_s = 200-16 = 184 mm
c_x = 184/2 = 92 mm
f_{ck} = 30 MPa
E_s = 200 GPa, f_{yk} = 400 MPa
$\eta 2$ = 1.0
k_m = 0, n_b = 1, n_t = 1, α = 0.4, ptr = 0, w_{cr} = 0
W_c = 15%

Partial safety factors of 2.0 and 3.4 are applied for the cases with 0 and 0.6 mm corrosion respectively, according to Blomfors *et al.* (2018). Table F.2 shows the computed anchorage lengths.

Table F.2 Computed design anchorage length for different corrosion levels.

Corrosion [mm]	**Corrosion Level W_c**	**Anchorage length L_{bk} [mm]**	**Design anchorage length L_{bd} [mm]**	**Rebar design yield force [kN]**
0	0%	174	160*(2.0/1.15) = **300**	200*347e-3 = 69.7
0.6	15% (1-20%)	1240	1240*(3.4/1.15) = **3700**	170*347e-3 = 59.0

Plot total force resistance of main bars, and compute utilisation:

No corrosion:

```
Lb = 0.3
Fsr = 69.7*5
xr=[0:0.1:2.0];

xr1 = [0, 2.0];
Fsr1= [1.0, 1.0]*0.5*Fsr;
Fsr1 = interp1(xr1, Fsr1,xr)

xr2 = [0, 0.4, 0.4+Lb, 2.0]
Fsr2 = [0, 0, 1.0, 1.0]*0.1*Fsr
```

```
Fsr2 = interp1(xr2, Fsr2,xr)

xr3 = [0, 0.7, 0.7+Lb, 2.0]
Fsr3 = [0, 0, 1.0, 1.0]*0.4*Fsr
Fsr3 = interp1(xr3, Fsr3,xr)

Fsr = Fsr1 + Fsr2 + Fsr3

plot(xr,Fsr,'b-')

xi = [0:0.01:1];
ny = interp1(x, Fsd,xi) ./interp1(xr,Fsr,xi)
max(ny) %= 60%
```

Corrosion 0.6 mm, for spans without laps:

```
Lb = 3.7
Fsr = 59.0*5
xr=[0:0.1:2.0];

xr1 = [0, 1.5, 2.0];
Fsr1= [1.0, 1.0, 1.0]*0.5*Fsr;
Fsr1 = interp1(xr1, Fsr1,xr)

xr2 = [0, 0.4, 0.4+Lb, 2.0]
Fsr2 = [0, 0, 1.0, 1.0]*0.1*Fsr
Fsr2 = interp1(xr2, Fsr2,xr)

xr3 = [0, 0.7, 0.7+Lb, 2.0]
Fsr3 = [0, 0, 1.0, 1.0]*0.4*Fsr
Fsr3 = interp1(xr3, Fsr3,xr)

Fsr = Fsr1 + Fsr2 + Fsr3

plot(xr,Fsr,'m-')

xi = [0:0.01:1];
ny = interp1(x, Fsd,xi) ./interp1(xr,Fsr,xi)
max(ny) %= 99%
```

Corrosion 0.6 mm, for spans with laps at mid-span:

```
Lb = 3.7
Fsr = 59.0*5
xr=[0:0.1:2.0];

xr1 = [0, 1.5, 2.0];
Fsr1= [2.5/3.7, 1.0/3.7, 2*0.5/3.7]*0.5*Fsr; % W.r.t. to the laps at midspan
Fsr1 = interp1(xr1, Fsr1,xr)
```

```
xr2 = [0, 0.4, 0.4+Lb, 2.0]
Fsr2 = [0, 0, 1.0, 1.0]*0.1*Fsr
Fsr2 = interp1(xr2, Fsr2,xr)

xr3 = [0, 0.7, 0.7+Lb, 2.0]
Fsr3 = [0, 0, 1.0, 1.0]*0.4*Fsr
Fsr3 = interp1(xr3, Fsr3,xr)

Fsr = Fsr1 + Fsr2 + Fsr3

plot(xr,Fsr,'r-')

xi = [0:0.01:1];
ny = interp1(x, Fsd,xi) ./interp1(xr,Fsr,xi)
max(ny) %= 188%

xlabel('Coordinate x [m]')
ylabel('Total force in main bars [kN]')
title('Force and resistance main bars')
grid on
```

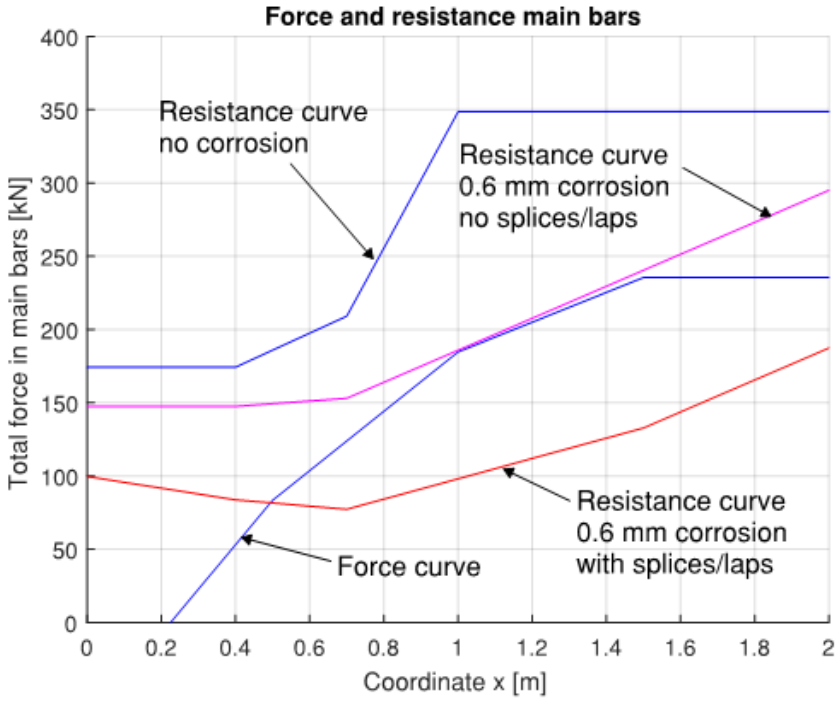

Figure F.3 Force and resistance, main bars.

The utilisation ratios and corresponding load capacities w.r.t. anchorage are:

ny = 60% for no corrosion
qrd ≥ 100 kN/m2

ny = 99% for 0.6 mm corrosion, for spans without reinforcement splices/laps

qrd = 100/0.99 ≈ 100 kN/m2

ny = 188% for 0.6 mm corrosion, for spans with reinforcement splices/laps
qrd = 100/1.88 ≈ 50 kN/m2

The example shows that the anchorage of the curtailed bars and reinforcement splices/laps are clearly most critical w.r.t. to corrosion.

In the example, the load capacity w.r.t. to the bottom reinforcement is 100 kN/m2 for up to 0.6 mm corrosion for spans having no laps. For spans with laps the load must be reduced to 50 kN/m2.

References:

Blomfors M., Coronelli D., Lundgren K., Zandi K. (2018): Engineering Bond Model for Corroded Reinforcement. *Engineering structures*. Vol. 156, p. 394-410.

fib (2013). *Model Code for Concrete Structures 2010*. Lausanne: International Federation for Structural Concrete (fib), pp. 152–189.

DEPARTMENT OF ARCHITECTURE AND CIVIL ENGINEERING
CHALMERS UNIVERSITY OF TECHNOLOGY
Gothenburg, Sweden
www.chalmers.se

CHALMERS
UNIVERSITY OF TECHNOLOGY